Nanoparticle Based Biosensors for Environmental and Clinical Analysis

THESIS

Submitted in partial fulfilment
of the requirements for the degree of
DOCTOR OF PHILOSOPHY

By

SOUVIK PAL

Under the Supervision of

Prof. Sunil Bhand

BITS Pilani
Pilani | Dubai | Goa | Hyderabad

BIRLA INSTITUTE OF TECHNOLOGY AND SCIENCE
PILANI (RAJASTHAN) INDIA
2015

BIRLA INSTITUTE OF TECHNOLOGY AND SCIENCE

PILANI (RAJASTHAN)

CERTIFICATE

This is to certify that the thesis entitled **"Nanoparticle Based Biosensors for Environmental and Clinical Analysis"** and submitted by **SOUVIK PAL,** ID No. **2010PHXF814G** for award of Ph.D. Degree of the Institute embodies original work done by him under my supervision.

Signature in full of the Supervisor: 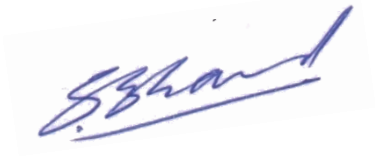

Name in capital block letters: **Prof. SUNIL BHAND**

Designation: Professor, Department of Chemistry

Date: 13.04.2015

ACKNOWLEDGEMENT

I wish to express my sincere appreciation to those who have contributed to this thesis and supported me in one way or the other during this amazing journey. It is my privilege to take this opportunity to humbly acknowledge and express my gratitude to them.

It will not be an exaggeration to say that possibly the only reason I am writing this Thesis, and this acknowledgement today, is because of my supervisor, Professor Sunil Bhand. He has been not only a mentor and an advisor, but also a friend and, often, a confidante. At the risk of stating the obvious, I would like to place on record my debt to him for my training in turbulence and for allowing me to work with others independent of him. Apart from being an example of how an academic should approach his work, he has shown me what it means to have infinite patience, propriety and encouragement for all. And always with a smile. I am thankful to my beloved supervisor Prof. Sunil Bhand for his avant-garde ideas and unyielding supports round the clock.

I am extremely grateful to Prof. B. N. Jain (Vice Chancellor, BITS, Pilani), Prof. Sasikumar Punnekkat (Director, BITS, Pilani - K. K. Birla Goa Campus), Prof. S. K. Verma (Dean, Academic Research, Ph. D. Programme, BITS, Pilani), Prof. Sunil Bhand (Dean, Sponsored Research and Consulting, BITS, Pilani- K. K. Birla Goa campus), and Prof. P. K. Das (Associate Dean, Academic Research, BITS, Pilani - K. K. Birla Goa Campus) for providing me with the facilities to conduct my research work at BITS, Pilani - K. K. Birla Goa Campus.

I express my gratitude to the members of the Doctoral Advisory Committee, Prof. N. N. Ghosh and Dr. Amrita Chatterjee, Department of Chemistry for their guidance and co-operation. I also express my sincere thanks to Prof. R. N. Behera, Head, Department of Chemistry, Prof. Bhavana P., Convener, Departmental Research Committee, and members Prof. Halan Prakash, Dr. Mainak Banerjee, and Prof. Anjan Chattopadhyay for their support.

I am thankful to Prof. A. P. Koley (Professor of Chemistry and Associate Dean, Instruction Division) for his valuable advice, motivation and support at various phases of my work.

A significant portion of my Ph.D. work was carried out in collaboration with Prof. Paul A. Millner (University of Leeds, UK), Prof. Ratnamala Chatterjee (Department of Physics, IIT-Delhi), Prof. Sudhir Chandra and Mr. Bhagaban Behera (CARE, IIT-Delhi), Dr. G. S. Lodha (ISUD, Raja Ramanna Centre for Advanced Technology, Indore), Dr. V. K. Suri (Bhabha

Atomic Research Centre, Mumbai, India), Prof. N. N. Ghosh and Mr. Subhenjit Hazra (BITS, Pilani-K.K. Birla Goa Campus). I have been fortunate to work with them, very fine collaborators in their respective areas, over the last five years. I am thankful to Dr. Mansi Thakur & Mr. Girish Pai from MGM, Mumbai, for their collaborative research work including joint patent in process. I am also thankful to Mr. Gautam Bacher from Department of EEE & I and Dr. Lizy Kanungo within Biosensor laboratory for their active collaboration.

My gratitude also extends to Prof. Bengt Danielsson, Acromed Invest Lund, Sweden, Prof. M. Willander, Linköping University, Sweden, Dr. S. F. D'Souza, Nuclear Agriculture and Biotechnology Division BARC, Mumbai, Prof. Chanchal K. Mitra, University of Hyderabad for scientific interaction and fruitful discussions.

I humbly express my sincere thanks again to Prof. Sunil Bhand, Mrs. Ujjwala Bhand and their son Saumya for the support and affection given by them and always considering me as a family member.

I also extend my thanks to my other lab mates Dr. Kanchanmala Deshpande, Dr. Rupesh Kumar Mishra, Mr. Geetesh Mishra, Mr. Atul Sharma, Mr. Arun Prusty, Miss. Aruna Singh.

I must say without financial support, it would not be possible for me to carry out my research study. Therefore, I take this opportunity to thank National Agricultural Innovation Project (Senior Research Fellowship from May 2009 - June 2011 and Research Associate Fellowship from July 2011-June 2014); BITS, Pilani-K.K. Birla Goa Campus (Institute fellowship from July 2014 – Nov 2014); NFBSFARA project (Senior Research Fellowship from Nov 2014 onwards) for their financial support.

It was the patience and silent sacrifice of my parents, Dr. Mohanpada Pal and Mrs. Bela Pal, which led me to complete this *sojourn*. My achievements are outcome of their dedication towards ensuring that I stand by myself with confidence. I also express my sincere thanks to all my family members for their moral support.

Words fail to express my appreciation to my wife, Gorima whose patience, inspiration, suggestion, constant encouragement and moral support have helped me realize my aspirations. Her endless love and patience kept me focused and always steered me in right direction.

Souvik Pal

CONTENTS

ABSTRACT

With the advancement of nanotechnology, the creation of functional materials, devices, and systems through the control of nano scale materials, have recently become one of the most influential fields at the forefront of analytical chemistry. In recent years, there has been a tremendous growth towards application of nanomaterials in biosensors. Nanomaterials like gold nanoparticles, nano magnetic beads, nanocomposites, metal oxide nanoparticles and porous materials have been widely used for biosensing. These materials are attractive biosensing probe candidates owing to their (i) small size (usually 1 to 100 nm) and correspondingly large surface area-to-volume ratio, (ii) chemically tailorable physical properties, which relate directly to size, composition, and shape, (iii) unusual target binding properties, (iv) overall structural robustness, (v) unique optical or electrical properties and (vi) minimum surface fouling of the sensing systems.

Advances in nanotechnology has affected existing technologies and led to the development of novel bioanalytical tools. These techniques facilitate improvement in speed of analysis, lower sample requirements and the ability to perform multiple detections in smaller devices. Novel biosensing systems that require less sample materials are being developed so as to perform sophisticated tests at the point of care and make possible the multiplex analysis. The comparable size of nanomaterials and biomolecules has allowed the integration of biological systems with nanometer sized structures, building novel hybrid nanobiosensors. Furthermore, there is tremendous growth and potential in employing such devices in the determination of environmental and clinical analytes with excellent properties and functions. Biosensor technology has become an important tool for high throughput analysis of biological systems. Specifically, optical biosensing systems provide portable, efficient and low-cost methods for monitoring of these analytes (Chapter 1).

Milk, which is usually contaminated with small amounts of aflatoxin M1 (AFM1), is a risk for human health, especially for children who are major milk consumers. Thus, AFM1 analysis and detection in milk is vital for ensuring food safety and quality. The maximum permissible limit of AFM1 in milk under European Union (EU) and Food Safety and Standards Authority of India (FSSAI) directives is 50 pg mL^{-1}. To date, aflatoxins are regulated in many countries because of the milk intake in infants is high and when they are young the vulnerability to toxins is higher. Thus, it is necessary to control and monitor AFM1

in milk at ultra low level. Therefore, development of analytical methods with ultra sensitive and lower limit of detection is paramount.

Chapter 2 of this thesis presents development of nanoparticles (NPs) based ultra-sensitive sandwich Enzyme-Linked Immunosorbent Assays (ELISA) for detection of AFM1 in milk. Recent trends in immunosensors report extensive use of NPs in combination with commonly used immunoassay techniques. Owing to their high surface area, nanomaterials can facilitate miniaturization; thereby provide enhanced number of binding sites. Herein, ultra sensitive Fe_3O_4 magnetic NPs (MNPs) and non-magnetic NPs (AuNPs, HfO_2NPs) have been exploited to develop hybrid ELISA by coupling with micro plate assay for analysis of AFM1 in milk. The NPs based probe have been constructed using self-assembled monolayers (SAMs) *e.g.,* silanization, thiolation and phosphonation. The monoclonal antibody (mAb) has been immobilized on NPs using cross-linking chemistry. The miniaturized hybrid column that has been developed using monoclonal antibody coupled NPs with microwell plate assay has enabled simultaneous measurement of low (0.5 pg mL^{-1}) as well as high AFM1 contamination (200 pg mL^{-1}) in milk. The most promising feature of these NPs-ELISA are the small column size, high capture efficiency and lower cost over other reported materials.

Zinc oxide (ZnO) nanostructures are good candidates because of their low toxicity, good thermal stability, good oxidation resistibility, good biocompatibility, large specific surface area and high electron mobility. Notably, the isoelectric point (IEP) of ZnO is as high as about 9.5, *i.e.* suitable for immobilization of the enzymes and proteins.

Chapter 3 of this thesis presents nanostructured ZnO in biosensing and bio-catalysis. Various nanostructure *e.g.,* nanorods (NRs), NPs and whiskers were exploited in choline biosensing, bio-analysis of organophosphate pesticide residues (OPs) and bio-catalysis of para-nitrophenol phosphate (*p*NPP). The covalent immobilization of the enzymes on the ZnO nanostructures has been achieved using 16-phosphonohexadecanoic acid (16-PHA) as SAMs. The phosphonation on ZnO nanostructures has imparted significant stability to the immobilized enzyme as compared to physisorbed enzyme. The ZnONR choline nanobiosensor has been constructed by co-immobilization of the enzymes choline oxidase and peroxidase. The ZnONR-choline biosensor has been investigated over a wide range of choline from 0.0005 – 2 mM. Using the developed biosensor, choline has been measurable even after 30 days with 60 repeated measurements. For bio-analysis of OPs, acetylcholinesterase (AchE) coupled 16-PHA modified ZnONPs have been exploited.

Developed bio-analysis technique provides multiple analyte detection in a single platform, a neurotransmitter (acetyl choline) in the range 0.01 – 10 mM and OPs in the range 0.01 – 5 ng mL^{-1}. It can save time, quantity of the sample and the cost of analysis. Furthermore, biochip based on ZnO-$ZnAl_2O_4$ composite whiskers has been successfully demonstrated for bio-catalysis of pNPP. The developed biosensors may easily be extended for routine environmental analysis.

Porous materials have attracted considerable attention since 1960s because of their wide variety of scientific and technological applications. Porous materials can range from highly ordered crystalline materials (*e.g.*, aluminosilicates or Metal-Organic Frameworks) to amorphous sol-gel compounds, polymers and fibers. There has been growing interest in the preparation of nanostructures of metal and metal oxides with controlled interior nanospace and they are currently subject to intensive research. The most relevant characteristic of porous materials is the highly effective surface to volume ratio of pores.

Chapter 4 of this thesis is based on the development of porous functional materials (PFM) for bio and chemical sensing. Of the reported macroporous materials, controlled pore glass (CPG), is a promising candidate for enzyme immobilisation. CPG exhibits a broad pore size ranging between 3 and 1000 nm, high thermal, mechanical and chemical stability and high resistance towards aggressive chemicals *e.g.* acids. A novel immobilized glucose oxidase (GOD) enzyme micro column based on the CPG support has been developed for continuous monitoring of glucose in serum. These GOD coupled CPG beads are further exploited to construct a novel PFM entrapment glucose sensing device. The sensing probe has been applied as duel read out system *i.e.* colorimetric and impedimetric. In both cases, glucose is measurable in the range from 0.001 mM to 10 mM. Well known mesoporous silica is the Santa Barbara Amorphous material (SBA-15) which is a structurally well ordered mesoporous material with a narrow pore-size distribution of 1.5 – 300 Å. SBA-15 with uniform tubular channels has been widely used for the construction of sensors. A novel fluorescent nanosensor based on fluorescein isothiocyanate (FITC) coupled within the nanosize pores of SBA-15 has been developed for selective detection of Pb^{2+} in water. This modified SBA-15 acts both as a molecular recognition module and signal reporter as a quencher. The remarkable feature of the developed sensor is its low detection limit of 0.01 ng mL^{-1} with short analysis time of 2 min. Further, in comparison to another divalent cation, Cd^{2+}, this chemically engineered sensing probe shows appreciably better selectivity and specificity towards Pb^{2+}.

Chapter 5 of this thesis deals with the development of a highthroughput novel hybrid miniaturized ELISA using antibody immobilized ZnONPs for the detection of carcinoma embryonic antigen (CEA) in serum. Due to lowering of IEP in biological pH, the surface of ZnO has a positive charge, the immobilization of protein with low IEP (in case of CEA is 4.7) is favourable. CEA in serum is considered as a biomarker related to the presence and progression of a tumour. It is used in clinical analyte as an indicator to detect recurrence of disease. Therefore, the sensitive determination of CEA in serum is very important in clinical research and early diagnosis. The reported concentrations of CEA are 2.5 ng mL^{-1} for non-smokers and 5.0 ng mL^{-1} for smokers. Thus, accurate determination of CEA is of significance for monitoring and screening disease recurrence. The construction of immunoassay is based on very specific monoclonal antibody of CEA on the 16-PHA modified ZnONPs. The developed ZnONPs coupled hybrid immunoassay has been compared with the conventional ELISA in the range 0.001 – 20 ng mL^{-1}. The miniaturized hybrid nano-immunoassay exhibits an excellent analytical performance in terms of sensitivity, with a much lower detection limit, good selectivity and reproducibility over the microwell plate ELISA. Furthermore, the hybrid immunosensor possesses high thermal stability as compared to microplate ELISA.

In conclusion, various magnetic and non-magnetic nanomaterials *e.g.* Fe_3O_4 MNPs, AuNPs, HfO_2NPs, nanostructured ZnO (NR, NPs, whiskers) and PFM (CPG, SBA-15) have been explored for biosensing applications in environmental and clinical analysis. The construction of the nanomaterial biosensor is based on efficient immobilization of bio-molecule *via* SAMs. Several SAMs procedures such as thiolation, silanization and phosphonation have been exploited to achieve better selectivity, stability and sensitivity over the conventional techniques. The biosensing applications are developed for the environmental analytes (AFM1, OPs, and heavy metals) and clinical analytes (choline, acetylcholine, glucose, CEA biomarker) under this thesis work. The major highlights of this work include development of

- Nanoparticles based high-throughput immunoassay for aflatoxin M1 in milk.
- Nanostructured ZnO in biosensing (choline, acetylcholine and organophosphate pesticide residues) and bio-catalysis (pNPP).
- Porous functional materials in bio (glucose) and chemical sensing (heavy metal).
- Development of nano-immunosensor for early stage cancer detection (CEA biomarker).

Table of Content for Chapters

List of Tables

List of Figures

List of Symbols & Abbreviations

Symbols	Description
°C	Degree centigrade
µg	Microgram
µL	Microliter
Å	Angstrom
cm	Centimetre
eV	Electron volt
g	Gram
h	Hours
H_c	Coercivity
Hz	Hertz
IC_{50}	Half maximal inhibitory concentration
K	Maxwell Turns/volt
K_B	Boltzmann constant
kg	kilogram
K_m	Michaelis–Menten constant
L	Liter
m	Meter
mg	Milligram
min	Minutes
mL	Milliliter
mL	Mililiter
mM	Millimolar
M_s	Saturation magnetization
ng	Nanogram
nm	Nanometer
Oe	Oersted
pg	Picogram

pH	Acidity measurement unit
ppb	Parts per billion
sec	Second (s)
η	Coefficient of viscosity
λ	Wavelength
λ_{em}	Emission wavelength
λ_{ex}	Excitation wavelength
μg	Microgram

Abbreviations	**Description**
AA	Ascorbic acid
AAS	Atomic Absorption Spectrometry
Ab	Antibody
1° Ab	Primary monoclonal antibody
2° Ab-FITC	Anti-rabbit (Rat) Fluorescein isothiocyanate conjugated secondary antibody
2° Ab-HRP	Anti AFM1 HRP conjugated secondary antibody
3° Ab – FITC	Goat F (ab) polyclonal secondary antibody to rabbit IgG – H&L FITC labelled
3° Ab – HRP	Goat polyclonal secondary antibody to rabbit IgG – H&L HRP labelled
AchCl	Acetyl choline chloride
AchE	Acetylcholinesterase
ACN	Acetonitrile
ADU	Arbitrary defined unit
AFB1	Aflatoxin B1
AFG1	Aflatoxin G1
AFM1	Aflatoxin M1
AFM2	Aflatoxin M2
ALP	Alkaline phosphatase

APTES	3-aminopropyl-triethoxysilane
ATR	Attenuated total reflectance
Au	Gold
BSA	Bovine serum albumin
CB	Carbonate buffer
CCD	Charged coupled device
CDI	N,N'-Carbonyl diimidazole
CEA	Carcino embryonic antigen
ChCl	Choline chloride
CL	Chemiluminescence
CMEA	Coil-microelectrode array
CNBr	Cyanogen bromide
CNTs	Carbon nanotubes
COD	Choline oxidase
CPG	Controlled Pore Glass
CR	Cross-reactivity
CRM	Certified reference materials
DA	Dopamine
DI	Deionized
DIC	Differential interference contrast
DLS	Dynamic light scattering
EC	European Comission
ECLIA	Electrochemiluminescnt immunoassay
EDC	1-ethyl-3-(3-dimethylaminopropyl) carbodiimide
EIS	Electrochemical impedance spectroscopy
ELISA	Enzyme-linked immunosorbent assays
EU	European Union
FRET	Fluorescence resonance energy transfer
FESEM	Field emission scanning electron micrograph

FITC	Fluorescein isothiocyanate
FL	Fluorescence
FSSAI	Food Safety and Standards Authority of India
FT-IR	Fourier Transform InfraRed
GA	Glutaraldehyde
GB	Glycine buffer
GOD	Glucose oxidase
HfO_2	Hafnia
HLT	Hysteresis Loop Tracer
HRP	Horseradish peroxidase
HRTEM	High-resolution Transmission Electron Microscopy
I %	Inhibition percentage
IARC	International Agency for the Research on Cancer
ICP-MS	Inductively coupled plasma – mass spectrometry
IEP	Isoelectric point
IUPAC	International Union of Pure and Applied Chemistry
LC-MS	Liquid chromatography – tandem mass spectrometry
LO	Longitudinal – optical
LOD	Limit of detection
LOQ	Limit of quantitation
LSCM	LASER scanning confocal microscopy
MCL	Maximum contaminant level
MCM-41	Mobil Composition of Matter No. 41
MNPs	Magnetic nanoparticles
MOF	Metal-organic frameworks
MPS	Mesoporous silica
11-MUA	11-mercaptoundecanoic acid
N_2-BET	Nitrogen Brunauer–Emmett–Teller adsorption–desorption isotherms

NHS	*N*-hydroxy succinimide
NMOs	Nanostructured metal oxides
NNI	National Nanotechnology Initiative
NPs	Nanoparticles
NPs-ELISA	Nanoparticle based enzyme-linked immunosorbent assay
NRs	Nanorods
NWs	Nanowires
OPD	*o*-Phenylenediamine
OPs	Organophosphate pesticide residues
OTA	Ochratoxin A
16-PHA	16-Phosphonohexadecanoic acid
PB	Phosphate buffer
PBS	Phosphate buffered saline
PBST	Phosphate buffered saline Tween20
PCB	Printed circuit board
PDI	Polydispersity index
PEG	Poly(ethylene glycol)
PFM	Porous functional materials
Pluronic P123	Poly(ethylene glycol)–poly(propylene glycol)–poly(ethylene glycol)
p-NP	*p*-nitrophenol
*p*NPP	*p*-nitrophenyl phosphate
PSA	Particle size analyzer
QCM	Quartz crystal microbalance
QDs	Quantum Dots
R.E. %	Relative error percentage
R.S.D.	Relative Standard Deviation
RIA	Radioimmunoassay
S.D.	Standard deviation

SAMs	Self-assembled monolayers
SBA-15	Santa Barbara Amorphous material
SEM	Scanning Electron Microscopy
SERS	Surface-enhanced Raman scattering
SPR	Surface plasmon resonance
TEM	Transmission electron microscopy
TEOS	Tetraethyl orthosilicate
TLC	Thin layer chromatography
TRFIA	Time-resolved fluoro-immunoassay
UA	Uric acid
UHPLC-MS	Ultra – high pressure liquid chromatography – tandem mass spectrometry
USEPA	United States Environmental Protection Agency
UV	Ultraviolet
XRD	X-ray diffraction
ZnO	Zinc oxide
ZnONR	Zinc oxide nanorod
ZnO-$ZnAl_2O_4$	Zinc oxide- Zinc aluminate composite

CHAPTER 1: INTRODUCTION

About the thesis

This thesis deals with the latest developments in the field of nanoparticles based optical biosensors to detect and analyse environmental contaminants and clinical analytes. Monitoring bio-molecular interactions has become a constituent element of various environmental and clinical applications. The importance of measuring the bio-molecular interaction, evident as a potpourri of sensing strategies, is currently and continuously devised. Nanoparticles based contaminants detection and clinical analytes diagnostics are becoming an increasingly relevant alternative to traditional techniques. The methods can easily be incorporated into low cost user friendly sensing platforms.

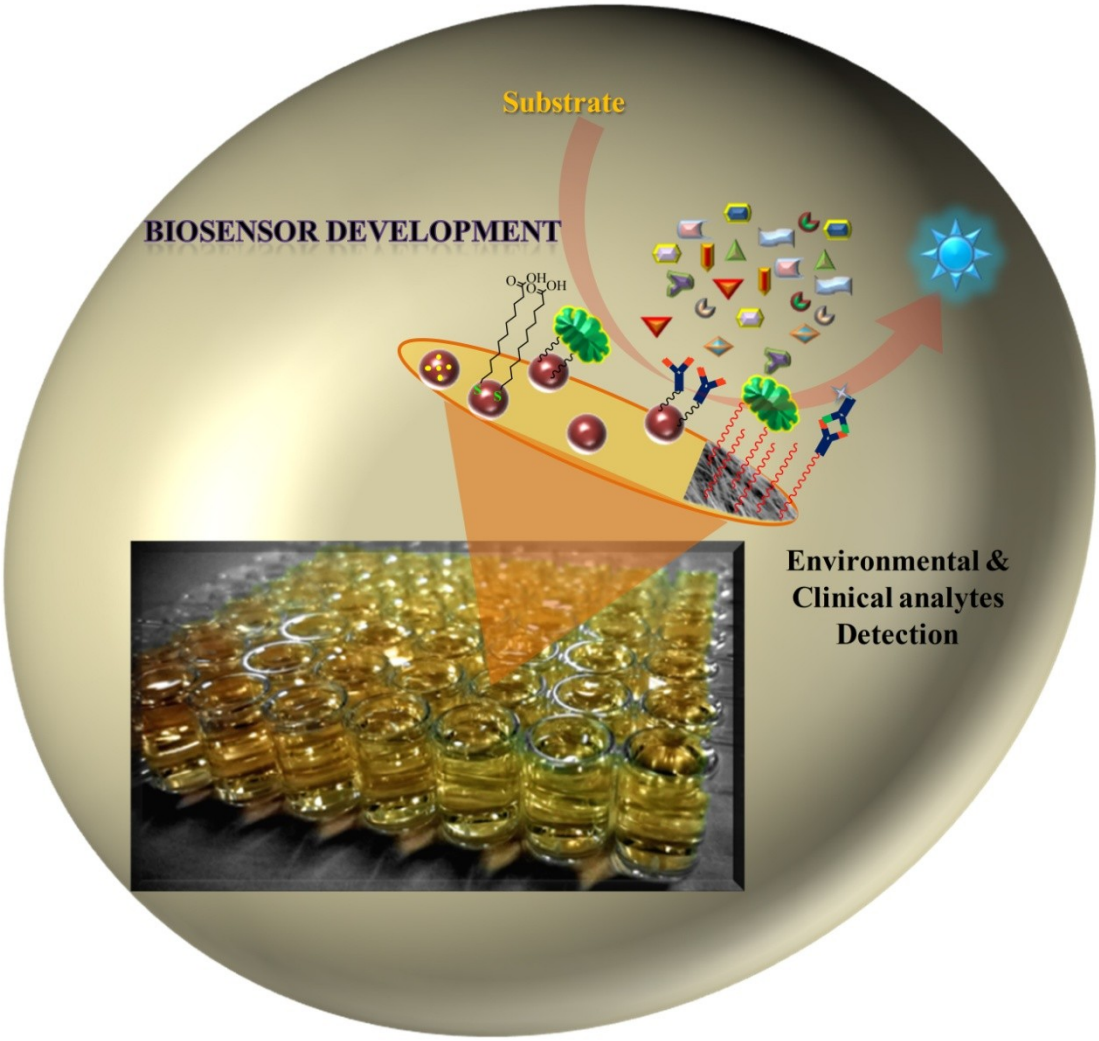

Graphical abstract of nanoparticles based biosensing techniques for environmental and clinical analysis

1.1 Introduction

Materials science explores the relationship between the structure and properties of materials. Borrowing techniques and practices from solid-state chemistry and physics for the synthesis and characterization of materials, it has been developed as a separate scientific area. Originally, it had no affinity with biology, but the advent and integration of nanoscience and nanotechnology into materials science has changed this dramatically (Niemeyer, 2001; Whitesides, 2005). Nanotechnology deals with the manipulation of matter at the atomic and molecular levels for the bottom-up synthesis of materials. The synthesis of supramolecular structures in nature is the archetypical example of such processes. Nanotechnology is considered by many as the next 'big revolution' (Sanvicens and Marco, 2008). In the past decade, this technological leap in controlling materials at the nanoscale has driven developments enabling the use of nanodevices and nanoparticles (NPs). These NPs have found applications in diverse fields ranging from electronics and communications, through to optics, chemistry, energy and of course biology. Due to the nature of nanoscale materials, astonishing advantages are being realized compared to the bulk-scale properties. Particularly, the powerful combination of nanotechnology and biotechnology can open a novel paradigm on human health care and well-being life care.

1.1.1 Scope of research

Fabrication of advanced nanomaterials with multiple components, complex structure, and integrated functionality has become a trend in materials design for nanotechnology. The use of biological materials is advantageous over traditional top-down processing to produce these advanced nanomaterials in terms of exquisite spatial control at the nanometer scale and parallel self-assembly of multiple components, generating hierarchical structures to provide multifunctionality. These remarkable features have stimulated investigation into bio-mimetic approaches for the design of materials recently. Bio-mimetic is the emerging field of nanotechnology that adopts problem-solving methods inspired by nature's functions and structures. Use of nature's approach for control over small dimensions is based on building structures from the molecular level as nature does, "from the bottom up" (Seeman and Belcher, 2002; Love *et al.,* 2005).

1.2 Nanomaterials and nanotechnology

The term "nano" is derived from the Greek word for "dwarf", "Nanos". This etymology and

placement on the metric scale (1 nm = 10^{-9} m), make it clear that tiny dimensions not visible to the naked eye, beyond the normal limits of our observation, are involved. Approaching it from familiar terrain may make the "nanoworld" more easily accessible (Figure 1.1). The diameters of hairs, cells (such as red blood cells), bacteria (such as *Escherichia coli*), viruses, or molecules (such as hemoglobin or the Buckminster fullerene C_{60}) can serve as path marks here. On this length scale, bodies with lateral dimensions less than 100 nm are typically termed nanomaterials. This classification is somewhat arbitrary, but it is largely established in the scientific literature and it also covers well the range in which specific properties of materials become size-dependent and differ from those of three-dimensional infinite solids.

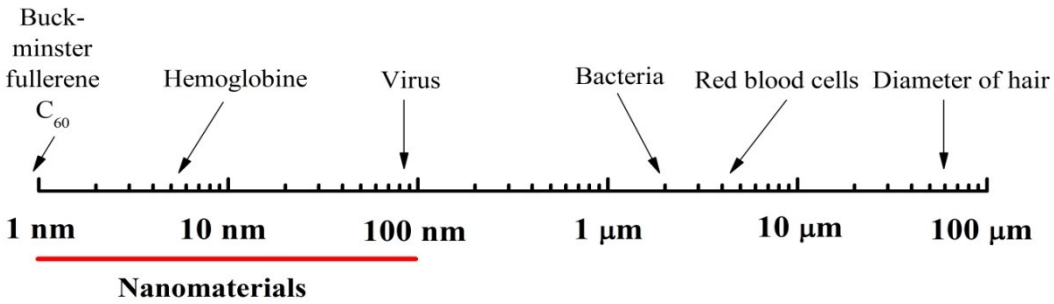

Figure 1.1 Length scale for classifying nanoparticles.

Nanotechnology is a research at the interface between chemistry, biology, material science, physics and engineering where ultra-precision engineering can be combined with nanostructured materials and molecular manipulation to produce novel devices. The National Nanotechnology Initiative (NNI) defines nanotechnology as "*Research and technology development at the atomic, molecular or macromolecular scale leading to the controlled creation and use of structures, devices and systems with a length scale of 1-100 nanometers (nM)"* (McNeil, 2005).

1.3 Nanomaterials in construction of biosensor

Nanometre-sized particles are in the same range of dimension as antibodies, membrane receptors, nucleic acids and proteins, among other biomolecules. These bio-mimetic features, together with their high surface to volume ratio and the possibility of modulating their properties, make NPs powerful tools for imaging, diagnosis and therapy (Pison *et al.,* 2006; Yezhelyev *et al.,* 2006). Thus, NPs offer significant improvements in performance compared to existing technologies. A combined effort in the field of nanotechnology, biology and advanced materials has resulted in the evolution of nano-biosensors as a diagnostic tool. A

biosensor is a device that uses specific biochemical reactions mediated by isolated enzymes, immunosystems, tissues, organelles, or whole cells to detect chemical compounds, usually by electrical, thermal, or optical signals (IUPAC, 1997). For a basic understanding, a biosensor usually comprises three structural elements: a recognition element, a transducer, and an amplifier (Figure 1.2).

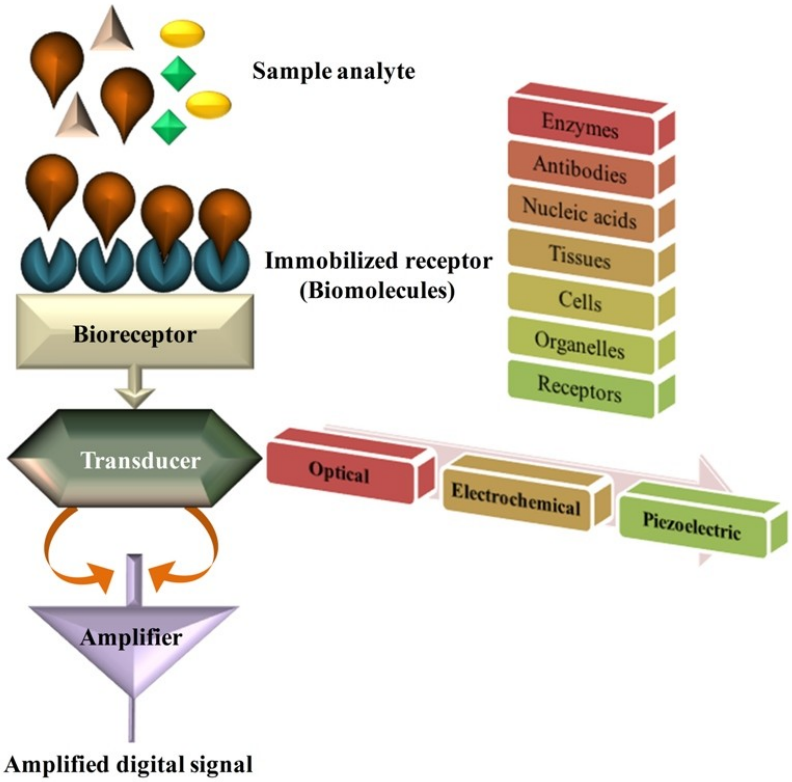

Figure 1.2 Schematic representation of biosensor and its components.

Ideally, a biosensor should have an optimal balance of specificity, stability, linearity, sensitivity, and reaction time. Additionally, a biosensor should be cheap, small, portable, and capable of being used by semi-skilled operators. Furthermore, biosensors used for invasive monitoring in clinical situations should be biocompatible, non-toxic, nonantigenic, portable, and stable under physiological conditions. Nanomaterials have promising roles in sensing and biochemical analysis due to their physicochemical properties, which are highly tuneable depending on their size and shape. Their unique surface chemistry, thermal stability, high surface area, and large pore volume per unit mass make them highly suitable for sensor fabrication. Nanomaterials can measure non-polar molecules that do not respond to most measurement devices. Immobilization systems are used in the fabrication of biosensors to amplify biomolecules specificity. Rapid and continuous monitoring of response signals can be performed using nanomaterials based biosensors. These unique properties have been

utilized in the fabrication of biosensors with elevated specificity and sensitivity (Tiwari and Turner, 2014).

1.4 Bio-functionalization of nanomaterials

The unique properties of nanoscale materials (1–200 nm) offer excellent platforms for electronic or optical signal transduction and the design of a new generation of bioelectronic and biosensing devices. However, the drawbacks of NPs in biocompatibility and biological recognition ability limit their application in analytical chemistry. The bio-functionalization of nanomaterials can endow them with good biocompatibility for the immobilization of biomolecules, tissue, or cells and high specificity for biological recognition (Goesmann and Feldmann 2010; Yin and Talapin 2013), which lead to stable biosensing systems with good selectivity and reproducibility.

Functional nanomaterials offer manifold perspectives for the increasing miniaturization, novel properties and functions, and complexity of technical developments. The conjugation of NPs with biomolecules could provide excellent signal transduction of biological phenomena in the development of electronic or optical biosensors (Wang *et al.,* 2004). Particularly, the bio-functional NPs can produce a synergic effect among catalytic activity, conductivity, and biocompatibility to accelerate signal transduction and achieve a rapid response to target with a very high sensitivity by signal amplification. The need for ultrasensitive bioassays and the trend toward miniaturized assays have made the bio-functionalization of nanomaterials one of the most recent fields (Wang *et al.,* 2009).

Two approaches for the functionalization of NPs have been involved: (i) non-covalent interaction, including physical adsorption and entrapment of biomolecules around the NPs, and (ii) covalent interaction by forming self-assembled monolayer on the NP's surface (Neouze and Schubert, 2008; Murray, 2008).

1.4.1 Non-covalent assembly

1.4.1.1 Physical adsorption

The simple adsorption of biomolecules on NPs has frequently been performed for the bio-functionalization of NPs with biomolecules, which range from small organic substances to large protein/enzyme molecules (Veiseh *et al.,* 2010). In the case of NPs that are stabilized by anionic ligands, such as carboxylic acid derivatives, citrate, tartrate, and lipoic acid, the

functional NPs allow effective binding to the positively charged amino acid side chains of the protein by the negatively charged anionic groups on their surface (Figure 1.3). For example, gold (Au) NPs produced by citrate reduction can be functionalized with anti-carcinoembryonic antibody molecules at pH values that lie slightly above the isoelectric point (IEP) of the citrate ligand (Lai *et al.*, 2009).

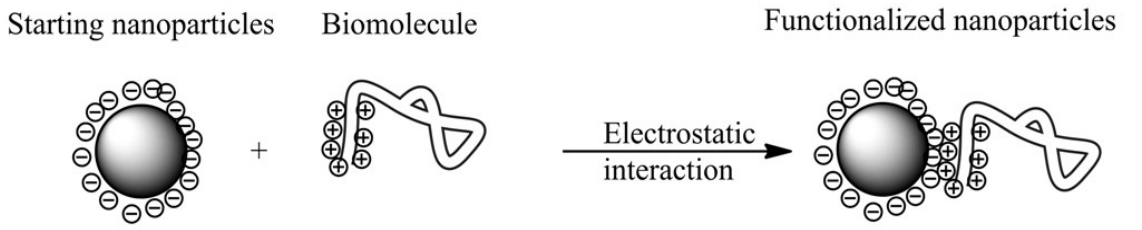

Figure 1.3 Bio-functionalization method of nanomaterials by non-covalent assembly.

The electrostatic deposition of biomolecules, particularly proteins or enzymes, may be extended to multilayer-level assemblies. This strategy permits the preparation of functional films on NPs with a high density of enzyme molecules (Zhao and Ju, 2006).

1.4.1.2 Entrapment of biomolecules

Another method for immobilizing biomolecules on NPs is to entrap them in a biocompatible polymer such as poly(ethylene glycol) (PEG), nafion, chitosan, and copolymer. The coating polymers not only prevent the aggregation of NPs, but also provide abundant positions for functionalization with second biomolecules. In particular, an electroactive polymer, which can generate a large number of electrons during electrochemical oxidation, can serve to amplify the electrochemical signal and therefore enhance the detection sensitivity. For example, polytyrosine has been used as an electroactive label for the detection of prostate-specific antigen (PSA) with the limit of detection of about 1 nM (Gao and Cranston, 2010).

1.4.1.3 Affinity interactions

Affinity interaction is efficient for the bio-conjugation of targeting ligands to NPs due to specific and strong complementary recognition interactions such as antigen – antibody, nucleic acid – DNA, lectin – glycan, streptavidin – biotin, aptamer – protein, aptamer – small biomolecules and hormone – receptor interactions. Moreover, various biomolecules contain several binding sites; for example, antibodies exhibit two antigen – binding sites, whereas streptavidin or concanavalinA each displays four binding domains. As shown in Figure 1.4,

the surfaces of NPs can be modified with streptavidin, which specifically binds biotinylated molecules. The linkage formed is highly stable and the strongest of all non-covalent linkages. Unlike hydrophobic and electrostatic interactions, affinity binding is not sensitive to environmental conditions such as changes in pH, salinity, or hydrophilicity (Meiser *et al.*, 2004).

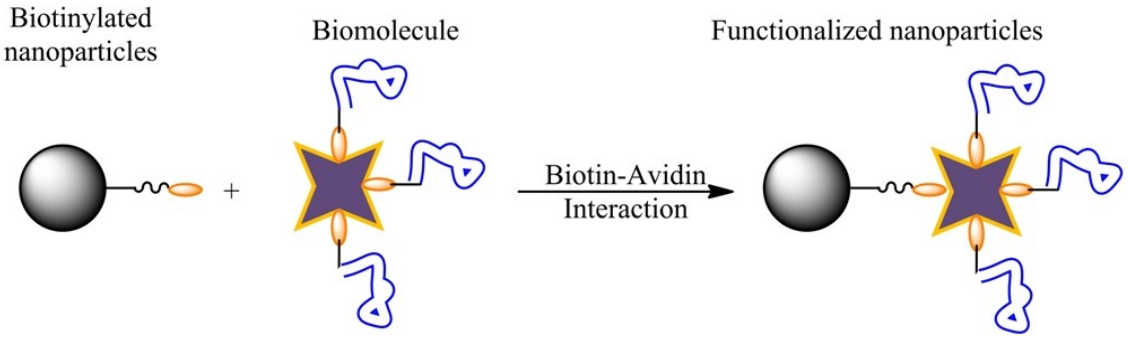

Figure 1.4 Affinity interactions between NPs and biomolecules.

1.4.2 Covalent interactions

Controlled chemisorption *via* covalent binding in general is preferable to unspecific physisorption in terms of the stability and reproducibility of the surface functionalization.

1.4.2.1 Immobilization *via* self-assembled monolayer

Self-assembly is the fundamental phenomenon that generates structural organization on all scales. Self-assembly is also a manufacturing method used to construct biosensors at the nanometer scale. Functional groups on the NP surfaces can be directly bonded to reactive self-assembled monolayers (SAMs) by a linkage reaction facilitated with the aid of catalysts. NPs surface functionalized with sulfhydryl, amine, aldehyde and carboxylic functional groups may be targeted (Zhang, 2003).

SAMs provide a convenient, flexible, and simple system with which one can mould the interfacial properties of metals, metal oxides, and semiconductors. SAMs are organic assemblies formed by the adsorption of molecular constituents from solution or the gas phase onto the surface of solids or in regular arrays on the surface of liquids (in the case of mercury and probably other liquid metals and alloys), where the adsorbates organize spontaneously (and sometimes epitaxially) into crystalline (or semicrystalline) structures. The molecules or ligands that form SAMs have a chemical functionality, or “head group”, with a specific affinity for a substrate; in many cases, the head group also has a high affinity for the surface

and displaces adsorbed adventitious organic materials from the surface. There are number of head groups that bind to specific metals, metal oxides, and semiconductors are shown in Table 1.1.

Table 1.1 Combinations of head groups and substrates used in forming SAMs on NPs

Ligands	**Substrate NPs**	**Ligands**	**Substrate NPs**
R-OH	Fe_xO_y, Si	R-S-S-R′, 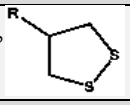	Ag, Au, CdS, Pd
R-COO^-/R-COOH	α-Al_2O_3, Fe_xO_y, Ti/TiO_2	R-CSSH	Au, CdSe
RCOO – OOCR	Si (111), Si (100)	R-$S_2O_3^-$ Na^+	Au, Cu
R-NH_2	Mica, Stainless steel (ss316L), CdSe	$RSiX_3$, X = H, Cl, OCH_2CH_3	SiO_2, TiO_2, ZrO_2, ITO, HfO_2, PtO
R-SH	Au, Ag, CdS, Cu, FePt, GaAs, Hg, Ni, Pd, Pt, ss316L, Zn, ZnS	R-PO_3^{2-}/ R-P(O)$(OH)_2$	Al-OH, GaAs, Mica, ITO, TiO_2, ZrO_2

Table1.1 adopted with permission from Love et al., 2005

The most extensively studied classes of SAMs are derived from the adsorption of alkanethiols on Au (Ulman, 1996; Biebuyck *et al.,* 1994), Ag and Cu (Laibinis *et al.,* 1991), Pd (Carvalho *et al.,* 2002), Pt (Li *et al.,* 2003) and Hg (Muskal *et al.,* 1996). The high affinity of thiols for the surfaces of noble and coinage metals makes it possible to generate well-defined organic surfaces with useful and highly alterable chemical functionalities displayed at the exposed interface (Love *et al.,* 2005).

The main compounds used for modifying metal oxide NPs are silanes, carboxylates and phosphonates. Silanes are the most frequently used modifiers for metal oxide surfaces, since silanes can bear numerous functionalities, including amino, cyano, carboxylic acid, epoxy groups, etc., for subsequent functionalization. On the other hand, it is one useful way to bio-functionalize the surface of metal oxide NPs with the binding of carboxylate ligands and

phosphonate groups of biomolecules via monodentate coordination, bridging chemisorption, or chelating chemisorption (Neouze and Schubert, 2008).

1.4.2.2 Linker chemical reaction

Biomolecules, especially for protein, in direct contact with an unprotected solid substrate are subject to denaturing of varying severity and resulting loss of their specific biochemical functionality. Low-molecular bi-functional linkers, which have anchor groups for their attachment to NP surfaces and functional groups for their further covalent coupling to the target biomolecules, have been extensively used in the generation of covalent-tethered conjugates of biomolecules with various NPs. A wide variety of terminal functional groups are available in different bi-functional linkers. The most common amine, active ester, isothiocyanate, and maleimide groups are used to couple biological compounds covalently by means of carbodiimide-mediated esterification and amidation reactions or through reactions with thiol groups (Liu *et al.,* 2010). The main role of the linker molecules is not only to provide a high density of docking sites for the specific attachment of biomolecules, but also to maintain a sufficiently low density of electronic defects at the NP's surface.

1.4.2.3 Activation of functionalized nanomaterials

When the NP surfaces are primarily functionalized with some groups, such as the sulfhydryl, amine, carboxylic, or hydroxyl groups, the further bio-functionalization of these NPs sometimes needs a step to activate these groups, which enables the groups to react with ligands of choice. The method selected for the activation of a functional NP surface must be compatible with both the ligand and the NPs. The general methods may be summarized as follows.

The amine reactive chemistry is the first method introduced to activate the NPs surface. Here cyanogen bromide (CNBr) is used universally for the activation of hydroxyl groups. It can react with the –OH group at a high pH to produce a very reactive cyanate ester, which then reacts directly with amine groups. The procedure is relatively simple to carry out and is very reproducible for coupling sensitive biomolecules such as enzymes and antibodies to NPs.

Another method of amine reactive chemistry is the use of *N*-hydroxy succinimide (NHS) esters as active groups to form amide bonds with primary amines. NHS can activate both -OH and -COOH groups. The produced NHS ester will react quite efficiently with primary amine-containing ligands to form a stable amide bond. For the activation of a –COOH group, *N*,*N*′-

carbonyl diimidazole (CDI) and 1-ethyl-3-(3-dimethylaminopropyl) carbodiimide (EDC) are highly reactive carbonylating reagents. NPs decorated with carboxylic acid groups can be covalently bonded to biomolecules bearing primary amines through EDC/ NHS linkers (Zhang *et al.,* 2010a). A reaction pathway towards enzyme coupling by activating –COOH group *via* EDC/NHS cross-linking is shown in Figure 1.5.

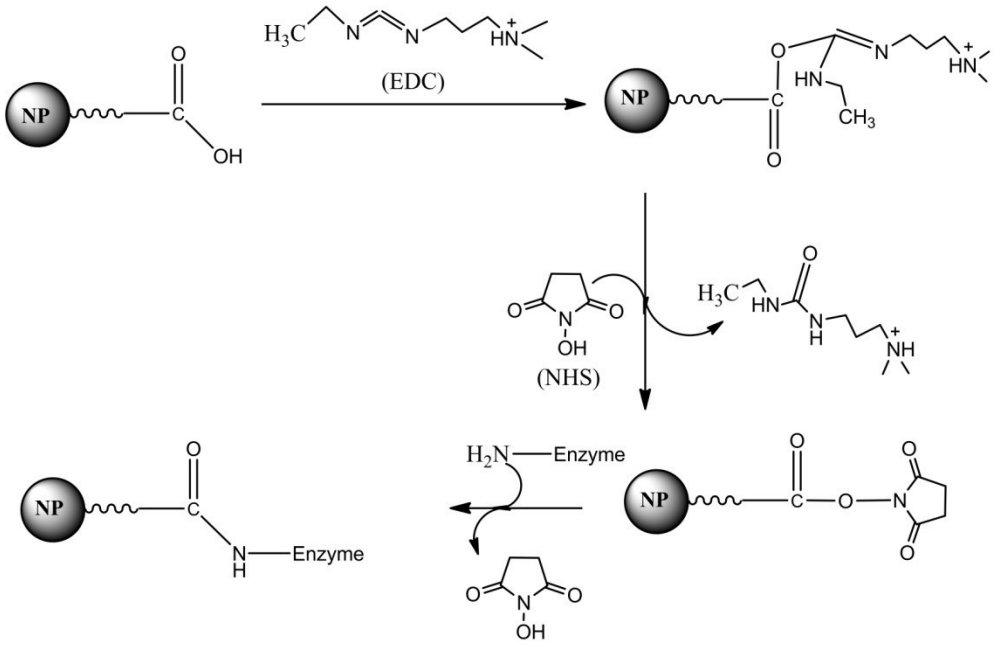

Figure 1.5 Reaction pathway towards enzyme coupling by activating –COOH group *via* EDC/NHS cross-linking.

Biosensors may also be constructed by immobilizing the proteins by adsorbing them onto the NPs, by crosslinking them with bi-functional agents such as glutaraldehyde, or by mixing them with the other components of composite NPs (Tang *et al.,* 2015).

1.5 Types of bio-functional nanoparticles

1.5.1 Metal nanoparticles

Metal NPs such as Au, Ag, Pd, and Pt NPs have mainly been modified with thiols, disulfides, amines, nitriles, carboxylic acids, and phosphines (Neouze and Schubert, 2008). Formation of SAMs is a straightforward way to fix functional molecules in the desired geometry. Carboxylic acid - amine coupling can be used to link any protein bearing a primary amine to metal NPs (Daniel and Astruc, 2004).

1.5.2 Magnetic nanoparticles

The surface functionalization and modification of magnetic NPs (MNPs) are widely studied and applied in various fields of biology and medicine (Lu *et al.,* 2007). Currently, there are two strategies to fabricate magnetic NP-based multifunctional nanostructures. The first one is molecular functionalization, which involves attaching antibodies, proteins, and dyes to the MNPs. The second method integrates the MNPs with other functional nanocomponents, such as QDs or metallic NPs. Because they can exhibit several features synergistically and deliver more than one function simultaneously, such multifunctional MNPs could have unique advantages in biomedical applications (Gao *et al.,* 2009).

1.5.3 Nanostructured metal oxides

Nanostructured metal oxides (NMOs) of metals such as Zn, Ce, Sn, Zr, Ti, and Mg have been found to exhibit interesting nanomorphological, functional biocompatible, non-toxic and catalytic properties. These materials also exhibit enhanced electron-transfer kinetics and strong adsorption capability, providing suitable microenvironments for the immobilization of biomolecules and resulting in enhanced electron transfer and improved biosensing characteristics. Various morphologies of NMOs have been reported using a variety of methods, including soft templating for the preparation of nanorods and nanofibers, sol–gel methods for the production of three-dimensional ordered rough nanostructures, radiofrequency sputtering for rough nanostructures and hydrothermal deposition for NPs with controlled shape. Recently, the optical, electrical and magnetic properties of NMOs have been reported to be enhanced through the incorporation of NPs of conducting or semiconducting materials such as carbon nanotubes (CNTs), graphene, Au and Ag, as well as quantum dots (QDs) of various semiconductors, with advantages for improved biosensor characteristics (Solanki *et al.,* 2011).

1.6 Nanoparticles for biosensing of environmental contaminants

Environmental security is one of the fundamental requirements of our well-being. However, it still remains a major global challenge. Therefore, in addition to reducing and/or eliminating the amounts of toxic discharges into the environment, there is need to develop techniques that can detect and monitor these environmental pollutants in a sensitive and selective manner to enable effective remediation. Because of their integrated nature, biosensors are ideal for environmental monitoring and detection as they are portable and provide selective and

sensitive rapid responses in real time. The combination of nanotechnology with modern biosensing techniques allows the introduction of powerful, reliable devices for effective process and pollution control. Although the NPs in general play different roles in different biosensors, with regard to environmental analysis using NPs-modified biosensors, they have several advantages: (1) effective catalysis; (2) fast mass transport; (3) large effective sensor surface area; and, (4) good control over electrode microenvironment (Campbell and Compton, 2010). Several NPs based biosensors that have been utilized to develop environmental applications are summed up in Table 1.2.

Table 1.2 Nanoparticles exploited in construction of biosensors for environmental contaminants

Nanoparticles	Biomolecules	Application	References
AuNPs	Aptamer to Ochratoxin A (OTA)	Aptasensor for using OTA	Yang *et al.*, 2011
Fe_3O_4	AFM1 antibody	Sandwich immunoassay for AFM1 in milk	Kanungo *et al.*, 2011
Fe_3O_4-graphene oxide	AFM1 antibody	Electrochemiluminescnt immunoassay (ECLIA) for AFM1 in milk	Gan *et al.*, 2013
AuNPs	uranyl-specific 39E DNAzyme	Uranyl Ion in Living Cells	Wu *et al.*, 2013
MNPs and AuNPs	Aflatoxin M1 (AFM1) antibody	Detection AFM1 of in milk by dynamic light scattering	Zhang *et al.*, 2013
Magnetic beads and AuNPs	Aflatoxin B1 (AFB1) antibodies	Colorimetric immunoassay for the detection of AFB1	Wang *et al.*, 2014
AuNPs	DNAzyme	Spectrophotometric biosensor for detection of Hg^{2+} ions	Mashhadizadeh and Talemi, 2014
IrO_2NPs	Tyrosinase and bovine serum albumin	Pesticides and phenolic compounds	Mayorga-Martinez *et al.*, 2014
Fe_3O_4 - Chitosan	Acetylcholinesterase enzyme	Determination of carbofuran pesticide	Jeyapragasam and Saraswathi, 2014

AuNPs	Phytochelatin-6 oligopeptide	Lead(II) ions in aqueous solutions	Politi *et al.*, 2015
Porous silicon	Urease and glucose oxidase	Low toxic metals (Cu^{2+}, Pb^{2+}, and Cd^{2+})	Syshchyk *et al.*, 2015
AuNPs-Graphene oxide	Acetylcholinesterase enzyme	Organophosphate residues	Zhao *et al.*, 2015

1.7 Nanoparticles for biosensing of clinical analytes

Technological platforms that provide the reliable, rapid, quantitative, cheap, and high-throughput identification of biomolecules play a significant role in the clinical deployment of personalized treatment (Hood *et al.*, 2004). Over the past decades, A tremendous amount of activity in the area of biosensors as well as their clinical applications (D'Orazio, 2003) especially for cancer diagnosis (Wu *et al.*, 2007; Pathak *et al.*, 2007) has been found due to their advantages of specificity, speed, portability, and low cost. The early diagnosis of disease is crucial for the successful treatment of the disease. The emergence of nanotechnology – the creation and utilization of materials, devices, and systems through the control of matter on the nanometer scale – is opening new horizons for the development of nanoprobes, nanosensors, and nanosystems with submicron-sized dimensions that are suitable for molecular diagnostics (Jain, 2005; Vo-Dinh, 2008). Some recent developments using various NPs based biosensors for clinical applications are summarized in Table 1.3.

Table 1.3 Nanoparticles exploited in construction of biosensors for clinical analysis

Nanoparticles	Biomolecules	Application	References
AuNPs	Thiol-terminated CEA aptamer-1	Detection of carcinoembryonic antigen	Shu *et al.*, 2013
RhNPs	Glucose oxidase	Glucose biosensor on platinum electrode	Guo *et al.*, 2014
Graphite nanoparticle	Glucose oxidase	Biosensor to detect glucose in real samples	Piao *et al.*, 2014
Au nanostar @ silica core–shell NPs	Glucose oxidase	Glucose biosensor in saliva	Al-Ogaidi *et al.*, 2014
ZnO nanorods	Choline oxidase and peroxidase	Choline in milk	Pal *et al.*, 2014

PtNPs	Acetyl cholinesterase and choline oxidase	Colorimetric choline and acetylcholine sensor	He *et al.*, 2014
AuNPs	Antibody	Detection of alpha-fetoprotein	Li *et al.*, 2014
AuNPs/ dendrimer	Antibody	Immunosensor for the detection of prostate specific antigen	Kavosi *et al.*, 2014

1.8 State of the art

The monitoring and detection of contaminants in milk/water and clinical samples is the key to identify and prevent problems related to human health and safety. The conventional techniques as well as current wet chemistry and analytical practices are time consuming and may require highly skilled technicians and expensive equipment. There is a need for rapid, reliable, and affordable techniques for food quality control and prognosis as well as diagnosis of clinical analytes. The application of biosensor in environmental analysis and clinical diagnostics is a growing field with increasing demand for reliable biosensors (Bhand *et al.*, 2010).

1.8.1 Aflatoxin M1

Aflatoxins are highly toxic mycotoxins produced by Aspergillus species in a wide range of food and animal feedstuffs stored under temperature and humidity conditions favourable to mold growth. Aflatoxin M1 (AFM1) (Figure 1.6), which is secreted in the milk, is known for its hepatotoxic and carcinogenic effects (Kanungo *et al.*, 2011).

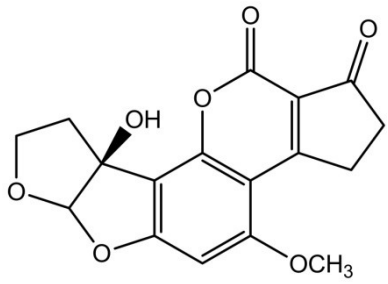

Figure 1.6 Chemical structure of AFM1.

AFM1 is relatively stable during milk pasteurization, storage as well as during the preparation of various dairy products (Badea *et al.*, 2004). Despite MNPs prevalent

applicability in biosensor field, reports on MNPs being deployed for analysis of AFM1 have been scarce. In one such testimony, reported by Radoi *et al.,* 2008, AFM1 detection was done using MNPs coated with protein G by physical adsorption.

1.8.2 Organophosphate pesticide residues

Organophosphate pesticide residues (OPs) acting as anti-cholinesterase substances are widely used throughout the world (Gordon and Rowsey, 1998). Undoubtedly, OPs in crop, livestock, and water pose a severe threat to human life. Various OPs chemical structures are presented as Figure 1.7.

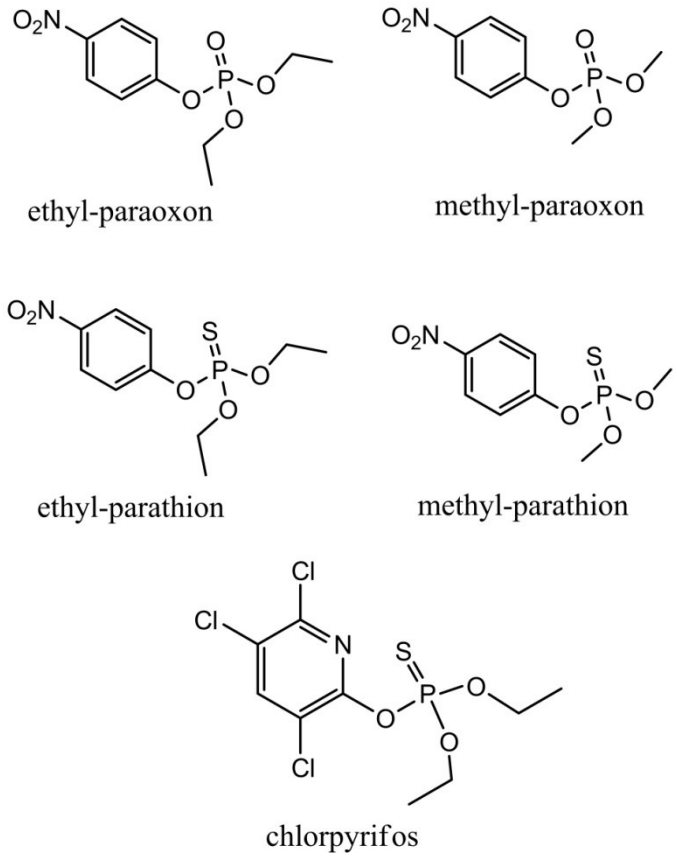

Figure 1.7 Chemical structures of various organophosphate pesticides.

A variety of short-term and chronic effects may be experienced following repeated or prolonged exposure to organophosphate-based pesticides, which include nausea, headache, and confusion (O'Malley, 1997). Little information has been gathered with respect to the long-term effects of sub lethal doses over a period, but reports of depression, memory loss and chronic fatigue syndrome have been documented (Rupa *et al.,* 1989). A carcinogenic

effect of organophosphate-based pesticides has also been postulated (Figa-Talamanca *et al.,* 1993).

1.8.3 Heavy metals

Heavy metal ions constitute a serious environmental problem due to their persistent and non-biodegradable nature. They are toxic to biological systems even at low concentration and there is an obvious need to determine them at trace level (Bontidean *et al.,* 1998). Bioaccumulation of the heavy metals has been reported to be higher in the upper trophic levels at concentrations surpassing those found in water supplies (Krawczyński vel Krawczyk *et al.,* 2000). The conventional methods used for the determination of the heavy metals based on spectrophotometry, chromatography, mass spectrometry and various hyphenated techniques; require sophisticated and expensive equipments, highly trained staff and is usually time-consuming (Dzyadevych *et al.,* 2005). The total amount of heavy metals detected by such means may not always be related to toxicity of such samples because the original biological availability of the metal ions is not taken into account. Thus need arises for the fast and inexpensive methods for the detection of bio-available heavy metals.

1.8.4 Choline

Choline and its derivatives serve as components of structural lipoproteins, blood and membrane lipids, and as a precursor of the neurotransmitter acetylcholine. Choline is oxidized to betaine that serves as an osmoregulator and is a substrate in the betaine–homocysteine methyltransferase reaction, which links choline and betaine to the folate-dependent one-carbon metabolism. The link to one-carbon metabolism and the recent availability of food composition data have motivated studies on choline and betaine as risk factors of chronic diseases in relation to folate and homocysteine status (Ueland, 2011). Abnormal choline metabolism is emerging as a metabolic hallmark that is associated with oncogenesis and tumour progression (Glunde *et al.,* 2011).

1.8.5 Glucose

Real-time monitoring of physiological glucose transport is crucial for gaining new understanding of diabetes. Many techniques and equipment currently exist for measuring glucose, but these techniques are limited by complexity of the measurement, reliability of continuous monitoring and low temporal/spatial resolution (Valgimigli *et al.,* 2014). The development of various types of biosensors (*e.g.*, electrochemical, optical sensors) for

laboratory and/or clinical applications will provide new insights into the cause(s) and possible treatments of diabetes. State-of-the-art is that the biosensors are improved by incorporating catalytic nanomaterials such as CNTs, graphene, electrospun nanofibers, and QDs. These nanomaterials greatly enhance biosensor performance, namely sensitivity, response time, and limit of detection. A wide range of new biosensors that incorporate nanomaterials such as lab-on-chip and nanosensor devices are currently being developed for *in vivo* and *in vitro* glucose sensing. These real-time monitoring tools represent a powerful diagnostic and monitoring tool for measuring glucose in diabetes research and point of care diagnostics.

1.8.6 Carcinoma embryonic antigen

Cancer is one of the most lethal diseases in the world; the estimated mortality is 8.2 million in 2012 (Cho, 2014). The majority of deaths are due to a lack of early diagnosis and timely treatment. The discovery of cancer biomarkers for early detection and theragnosis is a possible solution to tackle this problem (Gupta *et al.,* 2014). Carcinoma embryonic antigen (CEA) in serum is considered as a biomarker related to the presence and progression of a tumor (Barlési *et al.,* 2004). In addition, it is used in clinic as an indicator to a disease recurrence. Therefore, the sensitive determination of CEA is very important in clinical research and early diagnosis. With the development of nanoscience and nanotechnology, various types of nanomaterials have been applied to amplify biosensor response and construct the ultrasensitive biosensors. Most of the signal amplification strategies are performed by conjugating large amounts of signal or signal-related molecules, such as QDs (Tang *et al.,* 2013), metal nanoparticles (Lai *et al.,* 2011), on various nanocarriers, such as CNTs (Wang *et al.,* 2004), magnetic beads (Malhotra *et al.,* 2010), and NPs (Wu *et al.,* 2013). The human health in developing countries like India, suffers greater damage either due to lack of affordable techniques or due to the expensive technology involved.

1.9 Gaps in existing research

Although numbers of article are published in the field of biosensors for environmental and clinical analytes due to its vast potential, there are some areas that still can be explored further. The areas, which need special and immediate attentions, are:

- From literature survey, it is evident that level of toxicity increases with small variation in concentration of toxin. Conventional techniques do not meet higher standards for monitoring their levels in milk, food, water, blood etc. According to European Union

(EU) maximum permissible levels for AFM1 in milk is 50 ng L^{-1}, for the residues of individual pesticides is 10 μg kg^{-1} and for lead in drinking water has been set to be 0.015 mg L^{-1}. CEA and glucose levels tend to increase/or decrease with our daily food habit and as well as age. Thus, broad working range, stable and continues monitoring biosensor for environmental and clinical analytes in milk, water and blood is a current need.

- The conventional methodologies to detect toxins are based on measurements, which are often time consuming and performed with costly and bulky laboratory equipments. Development of sensitive yet affordable detection system for early onset of cancer are needed for ultra sensitive detection at nano and pico levels.

- Biosensor technology has become an important tool for high throughput analysis of biological systems. Currently, these techniques are used independently to detect/or quantify toxin information. In such types of sensors, a single sensing probe cannot detect more than one analyte. If biosensor can detect multiple analyte in a single platform, it can save time, quantity of the sample and the cost of analysis. Thus, development of a single platform for analysis of multiple analytes is of immense interest.

1.10 Objective of present research

The present research work aims at:

(i) Development of nanoparticles/or nanostructure based optical biosensors for environmental contaminants such as aflatoxinM1 (AFM1) in milk, organophosphates (OPs) residues and heavy metal (Pb^{2+}) in water.

(ii) Development of nanoparticles/or nanostructure based biosensing techniques for clinical analytes such as choline in milk, cancer biomarker (carcinoembryonic antigen (CEA)), glucose in blood/serum.

(iii) Development of nanoparticles based biosensor techniques for multiple analyte detection using a single platform.

1.11 Thesis structure

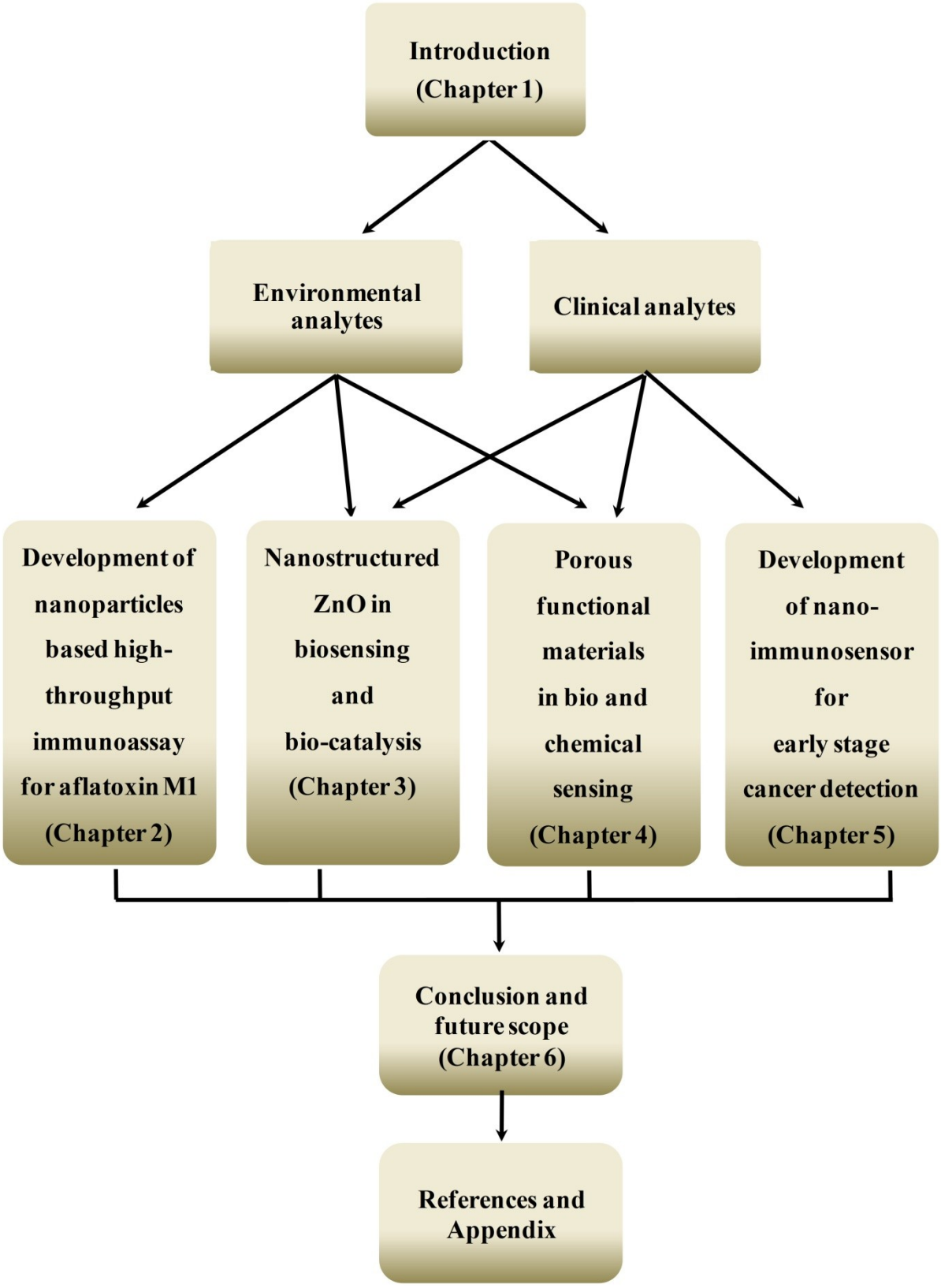

Figure 1.8 Flowchart detailing the different stages of thesis work.

The thesis comprises six chapters and each of these chapters has been described below:

1.11.1 Chapter 1: Introduction

This chapter gives a description about nanotechnology, various NPs; use of NPs in biosensor; surface functionalization of NPs towards biosensor construction; various pathways to attach biomolecules on to NPs; NPs based biosensors for environmental and clinical analysis; state of the art for environmental and clinical samples. In this chapter, the gaps in existing research and objective of the proposed doctoral work have been discussed.

1.11.2 Chapter 2: Development of nanoparticles based high-throughput immunoassay for aflatoxin M1

This chapter gives detailed account for the development of nanoparticles based biosensor technique for analysis of AFM1 in milk. This chapter also describes preparation of nanoparticles and their characterisation techniques. Sample preparation and optimization of parameters like pH, ionic strength of buffer, temperature and other parameters are described in detail. Measurements of real milk samples and recoveries studies are also discussed. The developed technique has potential for detection of AFM1 in milk samples using novel low cost NPs based column.

1.11.3 Chapter 3: Nanostructured ZnO in biosensing and bio-catalysis

This chapter gives a detailed account of various biosensing application based on zinc oxide nanostructures. A novel self assembly technique was developed using phosphonation, which imparted significant stability to ZnO structures resulting in enhanced storage stability and shelf life. The enzyme functionalized via phosphonation on ZnO nanostructures are demonstrated for biosensing of choline in milk, organophosphates pesticide residues in water and bio-catalysis of alkaline phosphatase towards better biomolecule support. The developed user friendly methods provide broad detection range within a short analysis time. In addition, the developed technology facilitates multi-analytes analysis using a single platform.

1.11.4 Chapter 4: Porous functional materials in bio and chemical sensing

Porous functional materials (PFM) as platform for biosensing application have been investigated. Various porous materials possessing nano sized pores used towards the biosensing application has been discussed in this chapter. Use of macroporous silica has also been demonstrated for glucose biosensing using duel read out format. A novel nano sensor

based on fluorescence quenching coupled within the nanosize pores of mesoporous silica has been demonstrated for detection of heavy metals such as Pb^{2+} in water.

1.11.5 Chapter 5: Development of nano-immunosensor for early stage cancer detection

A high throughput novel hybrid miniaturized ELISA assay using antibody immobilized ZnONPs has been developed for the detection of CEA. The immunosensor exhibits an excellent analytical performance in terms of sensitivity, with a much lower detection limit, selectivity, reproducibility of the measurements and thermal stability as compared to microwell plate ELISA.

1.11.6 Chapter 6: Conclusion and future scope of work

This chapter has drawn the conclusion on the basis of review of all the five chapters and proposed the future scope of work followed by references and appendix.

CHAPTER 2: DEVELOPMENT OF NANOPARTICLES BASED HIGH-THROUGHPUT IMMUNOASSAY FOR AFLATOXIN M1

Highlights:

- Sensitive nanoparticles (NPs) based enzyme-linked immunosorbent assay (ELISA) has been developed and coupled with micro plate ELISA for analysis of aflatoxin M1 (AFM1) in milk.
- The hybrid-assay, by coupling the monoclonal antibody immobilized NPs column with microwell plate assay has enabled simultaneous measurement of low and high AFM1 contamination in milk.
- The most promising feature of this NPs-ELISA is the small column size, high capture efficiency and lower cost over other reported materials.

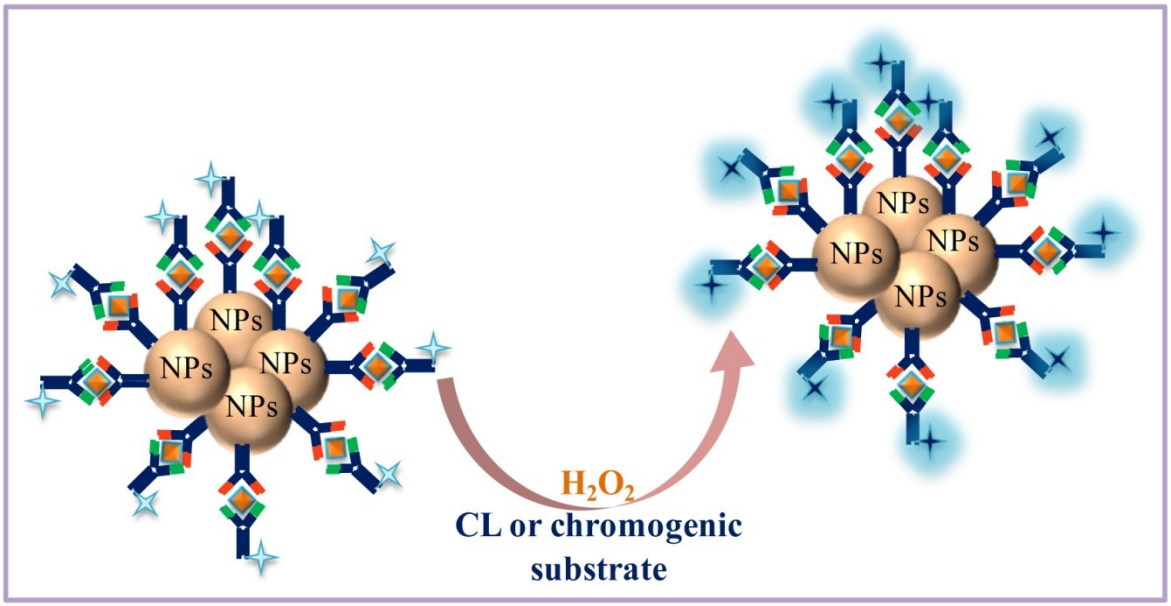

Graphical abstract of sandwich ELISA using nanoparticles

2.1 Introduction

Mycotoxin analysis and detection in food and drinks is vital for ensuring food quality and safety, eliminating and controlling the risk of consuming contaminated foods. Milk is usually contaminated with small amounts of AFM1 as a consequence of the metabolism by the cow of aflatoxin B1 (AFB1), a mycotoxin that is commonly produced by the fungal strains *Aspergillus flavus* and *Aspergillus parasiticus* (López *et al.,* 2001). When AFB1, the most toxic aflatoxin, is ingested by cows through contaminated feed, it is transformed into AFM1 through enzymatic hydroxylation of AFB1 and has an approximate overall conversion rate equal to 0.3 to 6.2% (Creppy, 2002). AFM1 is secreted in milk by the mammary gland of dairy cows (Egmond, 1989). Even though it is less toxic than its parent compound, AFM1 has hepatotoxic and carcinogenic effects (Radoi *et al.,* 2008). This toxin that initially classified as a Group 2B agent, has been reclassified as Group 1 by the International Agency for the Research on Cancer (IARC) (IARC, 2002). Because of its hepatotoxic and carcinogenic activity (Groopman *et al.,* 1988), AFM1 contamination represents a risk for human health, especially for children, who are the major milk consumers. European Community legislation limits the concentration AFM1 in the milk. The maximum allowed content of AFM1 in milk under EU directives is 50 pg mL^{-1} (European Commission (EC), 2006). To date, aflatoxins are regulated in many countries because of the milk intake in infants is high and when they are young the vulnerability to toxins is higher. It is, therefore, necessary to monitor AFM1 in milk at ultra low level, so that, analytical methods with high detectability and analytical throughput are required.

2.1.1 State of the art for analysis of AFM1

Several methods have been developed for AFM1 determination, including chromatography, chromatography–mass spectrometry and immunological methods. The chromatographic methods include thin-layer chromatography (TLC) (Var *et al.,* 2007) and immunoaffinity column purification combined with high-performance liquid chromatography (HPLC) (Shephard, 2009). The chromatographic-mass spectrometry methods include liquid chromatography–tandem mass spectrometry (LC-MS) (Sulyok *et al.,* 2010) and ultra-high-pressure liquid chromatography–tandem mass spectrometry (UHPLC-MS) (Beltrán *et al.,* 2011). Immunochemical analysis includes the ELISA (Anfossi *et al.,* 2008; Guan *et al.,* 2011a; Guan *et al.,* 2011b) and the electro-chemical immunosensor method (Micheli *et al.,* 2005; Neagu *et al.,* 2009). The schematic of conventional ELISA is shown in Figure 2.1.

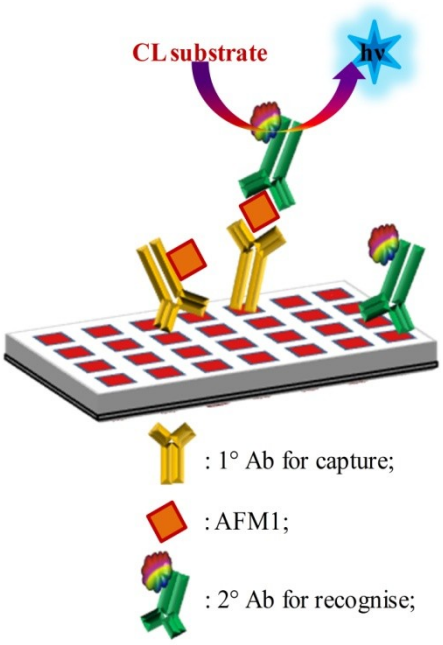

Figure 2.1 Schematic representation of conventional sandwich ELISA for AFM1.

These methods have their specific advantages and disadvantages. The results from conventional methods are accurate, but require expensive equipment, extensive training in operational techniques and extensive sample preparation.

2.1.2 Use of nanoparticles for detection of AFM1

Recent trends in biosensors report extensive use of NPs in combination with the commonly used immunoassay techniques. Owing to their high surface area, nanomaterials can facilitate miniaturization; thereby provide enhanced number of binding sites. Various antibody coupling strategies using NPs have also been reported (Wang et al., 2009; Radoi *et al.,* 2008; Wang and Gan, 2009; Ahirwal and Mitra, 2010). AuNPs have emerged as favourites in biosensing, imaging owing to their biocompatibility, dimensions, ease of characterization and very high chemical reactivity at the nanometer scale, allowing surface modification reactions with a wide variety of chemical and biochemical. One such testimony of using AuNPs has been reported recently (Dinçkaya *et al.,* 2011). MNPs have special relevance in bio-analytical chemistry because of their larger surface to volume ratio, enhanced antibody-antigen kinetics, lower mass transfer resistance and easy separation of immobilized bio-molecules from reaction mixture using magnetic field (Yu, 1998). Recently, widespread use of MNPs in biosensors has been documented through a flurry of literature (Nikitin *et al.,* 2007; Ravindranath *et al.,* 2009). The covalent binding of antibody through self assembled

monolayer is more suitable than the other conventional methods like physical adsorption and polymer entrapment (Liu *et al.,* 2006; Shankaran and Miura, 2007). The advantages of using covalent binding over physical adsorption to anchor antibodies and other proteins to a substrate surface are well documented in the literature (Ivanova *et al.,* 2006). Despite MNPs prevalent applicability in biosensor field, reports on MNPs being deployed for analysis of AFM1 have been scarce. In one such testimony, reported by Radoi *et al.,* 2008, AFM1 detection was done using MNPs coated with protein G by physical adsorption. A schematic of AFM1 detection using NPs is shown in Figure 2.2.

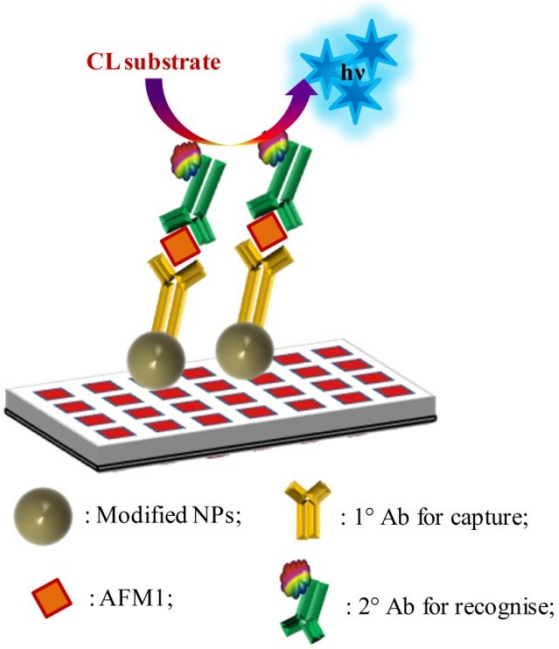

Figure 2.2 Schematic representation of NPs based sandwich ELISA for AFM1.

Apart from MNPs, other NPs are also used for the AFM1 immunosensor. Some recently reported NPs based immunosensors for analysis of AFM1 in milk samples are summarized in Table 2.1.

Table 2.1 Summary of reported nanoparticles based immunosensors for analysis of AFM1.

Nanoparticles used	Detection technique	Dynamic range (ng mL^{-1})	Limit of detection (ng mL^{-1})	Reference
Ab-magnetic NPs	Direct competitive ELISA	0.004 - 0.25	0.015	Radoi *et al.,* 2008
MNPs coated with antibody	Amperometry	0.01 - 0.1	0.01	Paniel *et al.,* 2010

ss-HSDNA modified AuNPs	Impedance spectroscopy	1–14	1	Dinçkaya *et al.*, 2011
Aptamer on MNPs incorporated polyaniline	Label-free electrochemical transduction	0.006 - 0.06	0.00198	Nguyen *et al.*, 2013
3-(trimethoxysilyl)-1-propanethiol grafted MNPs	Spectrofluorimetric	0.04 -8	0.015	Taherimaslak *et al.*, 2014

2.1.3 Advantages of ELISA technique

Immunosensing methods are well suited for detecting aflatoxins because they are simple, fast and specific. The ELISA method has the characteristics of high specificity and sensitivity and low cost. Chemiluminescent enzyme immunoassay (CL-ELISA), a combination of chemiluminescence (CL) and enzyme immunoassay, has the advantages of high CL sensitivity and is also high specificity of immunoassay with characteristics of simplicity, rapidity, and high throughput (Kricka, 2003). Enzyme labels are detected by CL substrates, such as the luminol/peroxide/enhancer system for horseradish peroxidase (HRP) as presented in Figure 2.3. The CL system represents the most sensitive detection systems in immunoassay development (Magliulo *et al.*, 2005).

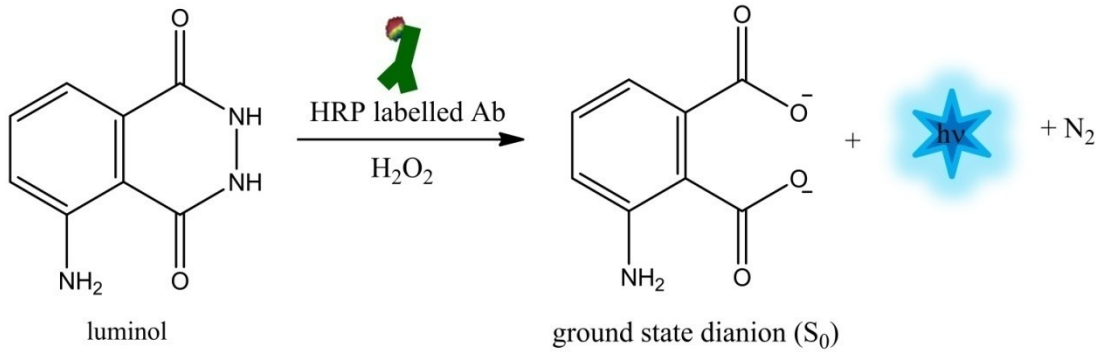

Figure 2.3 Working principle of HRP/luminol/peroxide CL system.

2.1.4 Objectives

The proposed aim of this work is to develop (i) sensitive hybrid immunoassay for detection of AFM1 in milk using various types of particles, namely magnetic (MNPs (Fe_3O_4)) and non-

magnetic (AuNPs, Hafnium dioxide NPs (Hafnia, HfO_2NPs)). The process flow for the development of NPs based AFM1 immunoassay is shown in Figure 2.4.

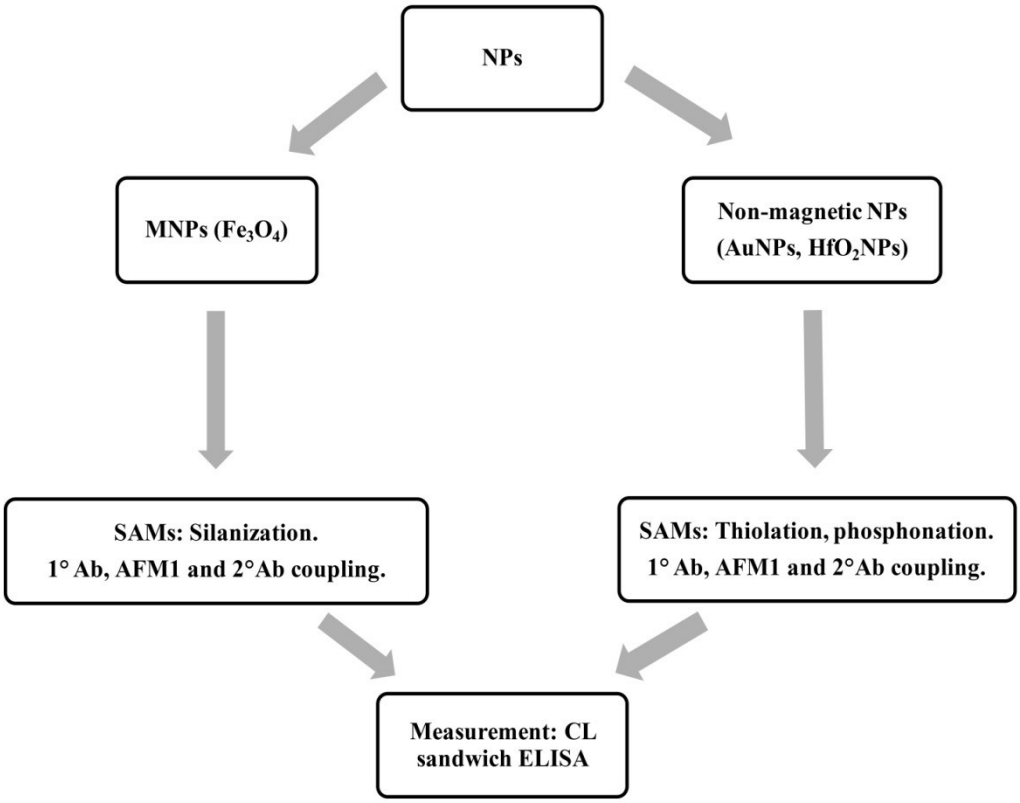

Figure 2.4 Process flow for the development of NPs based immunoassay.

(ii) Another objective of this work is to reduce the cost efficiency of immuno affinity capture column when compared to materials like Protein A and Protein G in affinity column.

2.2 Principle of NPs based hybrid ELISA for AFM1

The immunoassay construction has been based on surface modification of the NPs through the appropriate SAMs molecule. Three different approaches have been chosen for the NPs. MNPs have been modified using 3-aminopropyl-triethoxysilane (APTES). The coupling of 1° Ab has been cross-linked using glutaraldehyde (GA) by activating terminal $–NH_2$ group of APTES. Among the non-magnetic NPs, AuNPs have been modified using 11-mercaptoundecanoic acid (11-MUA) and HfO_2NPs have been modified using 16-Phosphonohexadecanoic acid (16-PHA). Further, 1° Ab has been coupled using EDC/NHS by activating the terminal –COOH group of 11-MUA and 16-PHA. The hybrid immunoassay has been performed in presence of AFM1 and labelled 2° Ab. The CL signal has been generated using HRP/luminol/peroxide system as described earlier. A generalised schematic

procedure for NPs based hybrid AFM1 ELISA is shown in Figure 2.5. In the figure, reference describes the measurement of CL signal in absence of AFM1 and sample describes the measurement of CL signal in presence of AFM1.

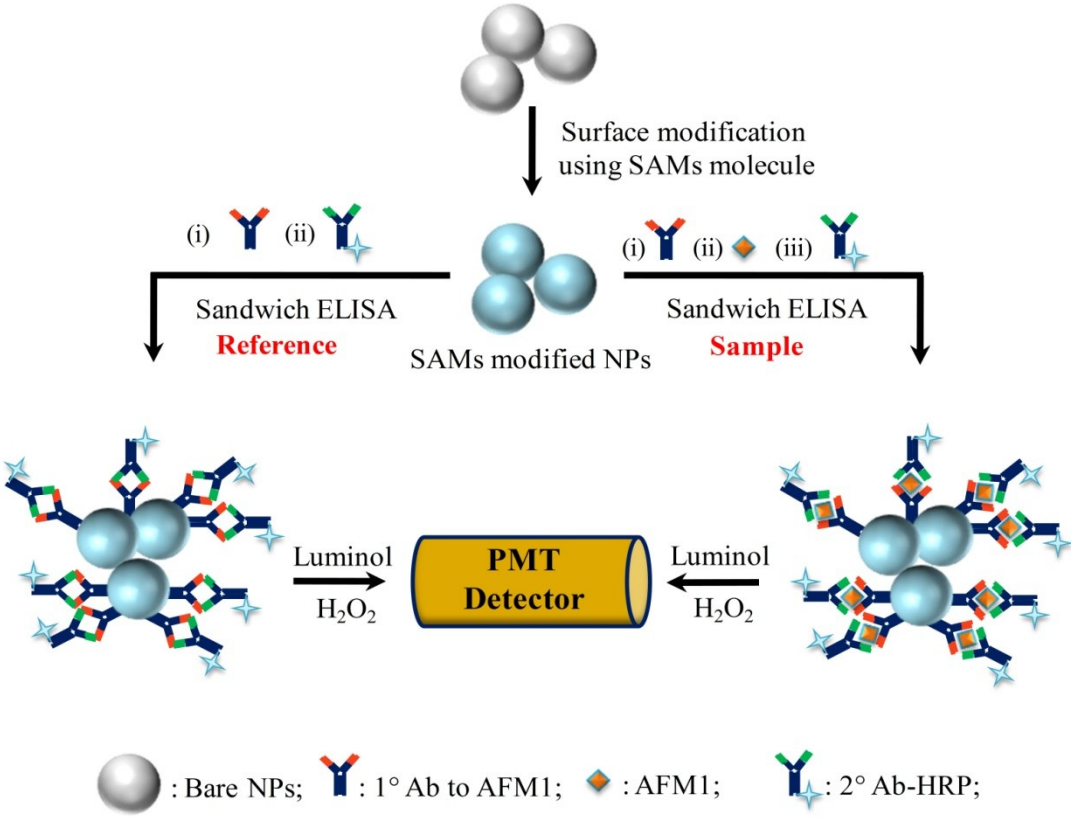

Figure 2.5 Generalised schematic for NPs based hybrid AFM1 ELISA.

2.3 Experimental section

2.3.1 Chemicals and biochemicals

Hydrogen tetrachloroaurate (III) ($HAuCl_4.3H_2O$), Iron (III) chloride anhydrous ($FeCl_3$), Ammonuim ferrous sulphate [$(NH_4)_2Fe(SO_4)_2.6H_2O$], Liquid ammonia and Glutaraldehyde (GA) solution (25%) have been purchased from Merck (India) and used without further purification. Spec-pure powders (99.99%) of hafnium chloride ($HfCl_2$), Nickel (II) nitrate hexahydrate $Ni(NO_3)_2.6H_2O$, 16-Phosphonohexadecanoic acid (16-PHA), 11-mercaptoundecanoic acid (11-MUA), 1-Ethyl-3-[3-dimethylaminopropyl]carbodiimide hydrochloride (EDC), N-Hydroxy succinimide (NHS), O-phenylenediamine dihydrochloride (OPD), AFM1, bovine serum albumin (BSA), tween 20, luminol, protein A agarose fast flow, 50% (v/v), protein G sepharose 4B fast flow(recombinant protein G, in 20% ethanol), Iron oxide (Fe_3O_4, average particle size 15 nm) and certified reference material ERM-BD 282

(AFM1 in whole milk powder, < 0.02 µg/kg) were purchased from Sigma-Aldrich (USA). Hydrogen peroxide (H_2O_2) 30% (w/v), acetonitrile (ACN) HPLC grade, trichloro acetic acid (TCA), sodium chloride (NaCl), methanol (99% pure) were purchased from Merck (Germany). Anti AFM1 fractionated antiserum primary antibody (1° Ab) raised from rat, anti AFM1 HRP conjugated secondary antibody (2° Ab-HRP) raised from rabbit and anti-rabbit (Rat) Fluorescein isothiocyanate (FITC) conjugated secondary antibody (2° Ab-FITC) were purchased from Abcam (UK). 3-aminopropyl-triethoxysilane (APTES) 99% pure and glycerol (99% pure) were purchased from Acros Organics (USA). Sodium hypochlorite (4%) solution was purchased from Fisher Scientific (India).

2.3.2 Materials and instrumentation

Sonication of the sample was done in Toshcon ultrasonic cleaner (Toshniwal process instruments Pvt. Ltd., India). Centrifugation, shaking and filtration of the samples were done by Spinwin mini centrifuge, Spinix shaker and syringe filter, purchased from Tarsons (India). White 384 well polystyrene microtiter plates were purchased from Nunc (Denmark). HybridSPE^{TM} (30 mg/1mL) SPE tubes were purchased from Supelco (USA). For CL measurement, VictorX^4 2030 optiplate reader from Perkin Elmer (USA) was used. Glove box, Cole Parmer (USA) was used for the handling of AFM1 standard solution. Water produced in a Milli-Q system (Millipore, Beford, MA, USA) was used for preparing all the solutions. Certified ultra high pure nitrogen (99.9%), pH meter (Seven Multi Mettler Toledo, 8603, Switzerland) were used. Fourier Transform InfraRed (FT-IR) spectra were recorded using IRAffinity-1 (SHIMADZU, Japan) with attenuated total reflectance (ATR) attachment Specac Diamond ATR AQUA. DELSA Nano DLS Particle size analyzer from Beckmann-Coulter, USA was used for measuring particle size. Room temperature X-ray diffraction spectra of powders were recorded by using a powder X-Ray diffractometer (Mini Flex II, Rigaku, Japan) with Cu Kα (λ = 0.15405 nm) radiation. Room temperature magnetization with respect to external magnetic field was measured for the synthesized powders by using a DC Hysteresis Loop Tracer (Ferrites India, India). High-resolution transmission electron microscopy (HRTEM, FEI, Technai G2 20 S-Twin) operated at 200 keV was employed to study the microstructure. Fluorescence images were acquired on inverted microscope (IX-71 Olympus, Japan) coupled with charged coupled device (CCD), Hamamatsu Orca-ER (Japan).

2.3.3 Solution preparation

2.3.3.1 Preparation of buffers

Buffers were made by the following method. For coating purpose, 0.05 M Carbonate buffer (CB) was prepared. 0.01 M Phosphate buffered saline (PBS) was used for incubation and washing purpose. Another washing buffer (PBST) was made by adding 0.05% Tween 20 (v/v) in PBS. All buffer solutions were stored at 4 °C when not in use.

2.3.3.2 Preparation of AFM1 standard solutions

AFM1 stock solution was prepared by dissolving the AFM1 powder in 5% ACN (v/v) in PBS at a concentration of 5 μg/2mL and stored at - 20 °C. In order to develop the assay, meeting regulatory requirements of European Commission (50 ng L^{-1}), working standard solutions in the range of 250 - 0.5 pg mL^{-1} were prepared by diluting the stock with 5% ACN.

2.3.3.3 Preparation of AFM1 antibody solutions

Working 1° Ab solution was prepared prior to the experiment by serial dilution in CB as 1:1000, 1:2000 etc. The stock solution of 1 mg (2 mg/mL) rabbit polyclonal to rat IgG-H & L (HRP) 2° Ab was diluted and working 2° Ab-HRP solution was prepared prior to the experiment by serial dilution in PBS.

2.3.3.4 Preparation of standard milk based matrix

To assess the performance of the immunosensor, the milk samples were prepared by dissolving 1 g of ERM BD 282 whole milk powder (zero level AFM1) in 10 mL of 0.01M PBS + 0.5% (v/v) Tween20, preheated to 50 °C (as indicated in the protocol). To minimize the matrix effect, the solution was centrifuged for 10 min at 6000 rpm at 4 °C, and the fatty layer was carefully removed and the supernatant was diluted (1/1, v/v) with PBS + 0.5% (v/v) Tween20. For immunosensing studies, centrifuged milk samples were spiked with fixed amount of AFM1.

2.3.4 Nanoparticles based AFM1 capture probe

The glass containers used for monolayer preparation was cleaned with Piranha solution (a mixture of 98% H_2SO_4 and 30% H_2O_2, 7:3, v/v; **caution**: Piranha solution reacts strongly and exothermally reacts with organics) for 1 h and rinsed exhaustively with deionized (DI) water and ethanol.

2.3.4.1 Preparation of MNPs based AFM1 capture probe

2.3.4.1.1 Synthesis of MNPs

For the synthesis of Fe_3O_4 magnetite particles, 1.351 g of $FeCl_3$ and 0.6852 g of $(NH_4)_2Fe(SO_4)_2.6H_2O$ were mixed with 25 mL deionized oxygen free water under N_2 atmosphere. To it, 3 M ammonium hydroxide (NH_4OH) was added drop wise with mechanical agitation using sonicator until a black precipitate was formed. In order to remove the residual ions, the precipitate was washed several times until a pH value of 7 was obtained. The powder was dried at 100 °C for 2 h.

2.3.4.1.2 Surface modification of MNPs

APTES was used for the coating of MNPs as described by Liang *et al.,* 2006. The surface modification step is shown in Figure 2.6.

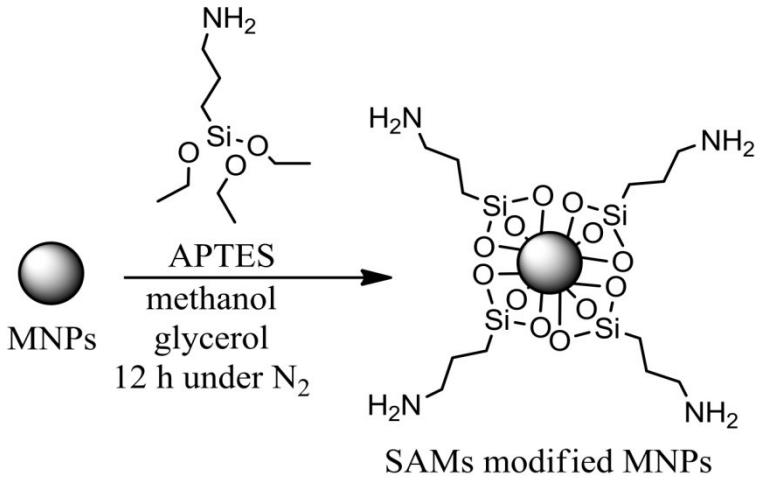

Figure 2.6 Surface modification of MNPs using APTES.

Briefly, 500 mg of MNPs, 0.135 µL water and 0.675 µL APTES were added into 50 mL methanol. After ultrasound treatment for 3 min, the mixture was added with 20 mL glycerol and then transferred to a 100 mL three-necked flask equipped with a mechanical stirrer. The temperature was maintained at 50 °C with rapid stirring for 12 h under N_2 environment. The resulting NPs were washed using a magnet with DI water and methanol for several times. This stock was used for subsequent experiments.

2.3.4.1.3 MNPs-1° Ab conjugation

The -NH_2 group of silane coated MNPs were activated by GA. The antibodies were immobilized via their carboxyl group onto activated MNPs as described by Liu *et al.,* 2006. With some alteration, 0.7 mg of silane coated MNPs (from stock) were first activated by adding 500 µL of 2.5% GA in 0.01 M PBS and the resultant mixture was shaken at room temperature for 2 h. Unbound GA was washed from activated particles with PBS using a magnet. Freshly prepared 1° Ab was diluted 1:1 solution of 1° Ab-PB (1:16000) in CB by giving final concentration of 1° Ab 1:32000. 40 µL of this solution was added to activated MNPs for coating. The resulting mixture was kept for overnight at 4 °C with occasional shaking to avoid aggregation and washed magnetically 3 times with PBS.

2.3.4.2 Preparation of AuNPs based AFM1 capture probe

2.3.4.2.1 Synthesis of AuNPs

AuNPs were synthesized according to the procedure described by Frens, 1973 to obtain AuNPs of 50 nm size. In brief, 100 mL of 0.01% $HAuCl_4 \cdot 3H_2O$ solution was reacted with 2 mL of 1% trisodium citrate solution at 98–100 °C with constant stirring. Development of red colour of the gold colloid solution was monitored. The gold colloidal suspension could be stored at 4 °C for several months.

2.3.4.2.2 Surface modification of AuNPs

AuNPs thus obtained were functionalized with 11-MUA by treating it with 2.5 mM ethanolic solution of 11-MUA as shown in Figure 2.7.

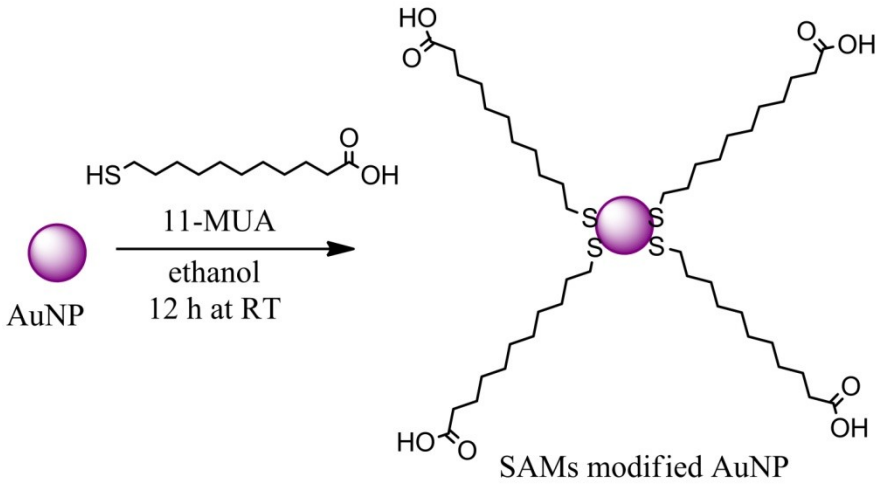

Figure 2.7 Surface modification of AuNPs using 11-MUA.

Aging of 11-MUA and gold hydrosol for 12 h at room temperature yielded capped AuNPs, which were separated and purified by repeated centrifugation at 10,000 rpm for 10 min followed by washing with double distilled water.

2.3.4.2.3 AuNPs-1° Ab conjugation

For antibody immobilization, the carboxylic acid-terminated SAMs were modified using an aqueous equimolar solution of 100 mM EDC /100 mM NHS for 2 h at room temperature. The resultant NHS ester monolayers were reacted for 3 h in 1:32000 solution of 1° Ab and CB. The 1° Ab coated particles (1° Ab-AuNPs) were washed with PB.

2.3.4.3 Preparation of HfO_2NPs based AFM1 capture probe

2.3.4.3.1 Synthesis of HfO_2NPs

The HfO_2NPs were synthesized in collaboration with Department of Physics, IIT-Delhi. The fine-grained nanocrystal ceramic powder samples of HfO_2 were prepared using a solution based chemical method by easily available laboratory reagents as described elsewhere (Sharma *et al.,* 2011). The method involves the complete dehydration of the metal ion ligand complex precursor solution, which is accompanied by the decomposition of the metal complexes.

2.3.4.3.2 Surface modification of HfO_2NPs

The AFM1 capture probe is based on the efficient immobilization of very specific 1° Ab through carboxy terminated SAMs of 16-PHA on HfO_2NPs as presented in Figure 2.8.

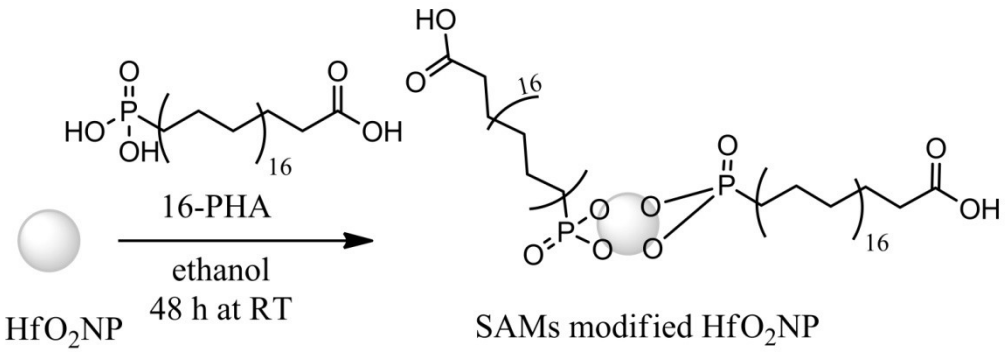

Figure 2.8 Surface modification of HfO_2NPs using 16-PHA.

HfO_2NPs were dispersed in 0.5 mM ethanolic solution of 16-PHA and sonicated for 5 min to obtain well dispersed solution. These samples were stirred on a Spinx shaker for 48 h (self-

assembly time). The SAMs functionalized HfO_2NPs were centrifuged for 15 min at 6000 rpm and rinsed in ethanol followed by DI water and dried with a stream of dry nitrogen.

2.3.4.3.3 HfO_2NPs-1° Ab conjugation

For antibody immobilization, the carboxylic acid-terminated SAMs were modified using an aqueous equimolar solution of 100 mM EDC /100 mM NHS for 2 h at room temperature. The resultant NHS ester monolayers were reacted for 3 h in 1:32000 1° Ab and CB. The 1° Ab coated particles (1° Ab-HfO_2) were washed with PB.

2.3.4.4 Sandwich ELISA process and measurements

AFM1 spiked milk samples were incubated for 2 h at room temperature. The particles were washed again with PBS to remove unbound AFM1. For CL and optical measurements, 2° Ab-HRP (1:32000) was incubated at room temperature for 2 h with the particles. For fluorescence (FL) measurements, the AFM1 bound 1° Ab coated particles were incubated with 2° Ab-FITC (1:64000) at room temperature in dark for 3 h. The excess label was removed by washing with PBS. The schematic measurement using developed capture probe is presented in Figure 2.9.

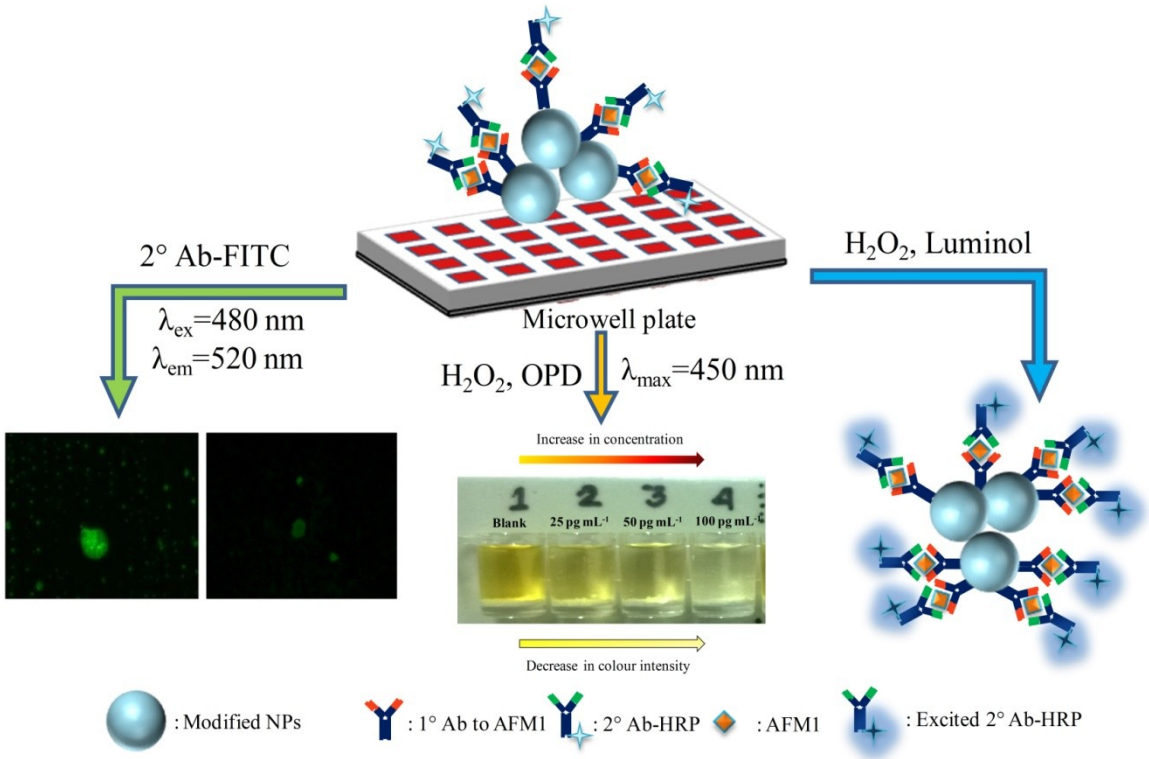

Figure 2.9 Measurement using NPs based AFM1 capture probe.

For CL measurements, VictorX^4 2030 optiplate reader from Perkin Elmer (USA) was used. CL substrate (1.2 µL of 0.5 M H_2O_2 + 8.8 µL luminol) was added to each microwell of the 384 microtiter well plate. The signal intensity was kinetically measured at steady state and stability was found after 35 min.

For colorimetric assay, the washed particles were incubated in presence of 0.5 M H_2O_2 and OPD chromogen for 35 min in dark. After 35 min, stop solution was introduced to stop the reaction. The signal intensity was measured by VictorX^4 2030 optiplate reader.

For FL measurement, 2 µL of the final NPs suspension was placed on a microscopic slide. The optical images were viewed under fluorescence microscope and captured by CCD. The FL intensity was acquired by VictorX^4 2030 optiplate reader.

2.3.5 Preparation of NPs based affinity column

Five HybridSPE^{TM} (30 mg/mL) SPE columns were prepared for capture and detection of AFM1. Among these columns, three were specifically customized for NPs, Protein A and Protein G. The other two were used as control (blank) and PBS. The columns were tested for analysis of 50 pg mL^{-1} [AFM1]. The NPs packed column was prepared by adding 3 mg NPs functionalized with 1° Ab as showed in Figure 2.10.

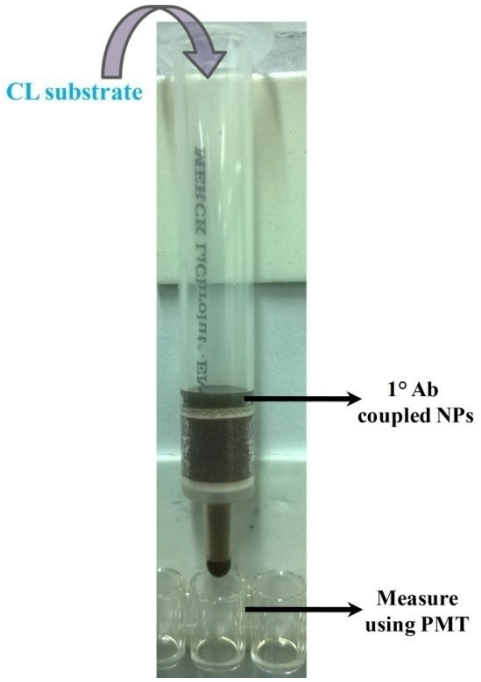

Figure 2.10 1° Ab coupled NPs affinity capture column.

Pre-swollen Protein A and G were washed with distilled water and packed in the SPE columns, as described in data file 18-1012-19 AC, GE Healthcare (Sweden). 20 µL of Protein A was added to 40 µL of 1° Ab (1:16000) and allowed to bind overnight at 4 °C. Similarly, Protein G packed column was prepared. The columns were washed 3 times with 60 µL PBS by applying 10 psi at 9.6 rpm using micro fluidic pump. The remaining protein-binding sites in the columns were blocked by adding 40 µL of blocking solution for about 1h at room temperature. The columns were then washed in running buffer with 60 µL PBST. Subsequently, 40 µL of 2° Ab-HRP (1:32000) and AFM1 (1:1) was added to the columns, kept for 2 h at room temperature. The excess label was removed by washing with PBS in running buffer. 40 µL of the CL substrate was added to the columns. The final eluting solution was collected, added to the microwell plates and it was measured as described earlier.

2.3.6 Safety caution

All necessary precautionary measures should be taken while handling the highly toxic AFM1 to prevent contamination. As the substance is photosensitive (AOAC Official Method, 2008), special care should be taken to ensure that solutions are not exposed to daylight. Safety goggles, respiratory mask and lab coats should be used throughout experiment. All laboratory glassware and consumables, which had been contaminated with AFM1, were soaked in 4% sodium hypochlorite.

2.4 Results and Discussion

2.4.1 Characterisation of MNPs

2.4.1.1 X-Ray diffraction analysis of MNPs

Room temperature powder X-ray diffraction (XRD) of synthesized powder was performed to investigate the phase formation of Fe_3O_4 (Figure 2.11). The crystallite size of Fe_3O_4 has been calculated from X-ray peak-broadening of the diffraction peaks (3 1 1) and (4 4 0) using Scherrer's formula (equation 2.1) and found to be approximately 11 nm.

$$d = \frac{0.9\lambda}{\beta cos\theta} \qquad (2.1)$$

Where, λ is the wavelength, β the full width at half maximum (FWHM) of the peak and θ the Braggs' angle.

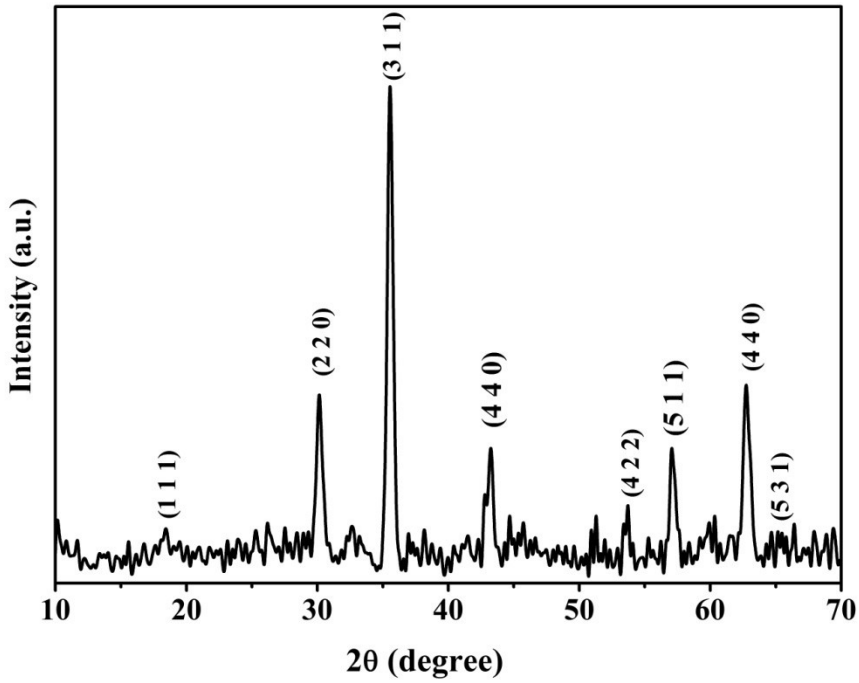

Figure 2.11 X-ray diffraction pattern of MNPs.

It is observed that, XRD spectra of the Fe_3O_4 NPs exhibit diffraction peaks for magnetite [ICDD 75-1610]. Intensity ratio (I/I_0) of the peaks have shown exactly matched with standard values, which indicate that particles are formed with pure crystallinity. The values of lattice parameter (a = b = c) of synthesized Fe_3O_4 NPs (*via* sonication) are found to be 8.37 Å, which agrees well with the standard value of 8.39 Å.

2.4.1.2 Magnetic measurement of MNPs

Room temperature magnetization with respect to external magnetic field was measured for the synthesized MNPs powders by using a DC Hysteresis Loop Tracer (HLT) (Ferrites India, India). For this purpose, powder samples were packed inside a plastic tube of known height, h cm. The weight of the powder was measured. The density of powder (d, gm/cm^3) was determined using Archimedes principle. From the known weight of the sample (in gm), its density (gm/cm^3) and height of the tube (h, cm) its cross sectional area (A, cm^2) were determined. Integrator sensitivity of signal (K = Maxwell Turns/volt) was selected. Magnetization (M) for 'V' volt output signal of the integrator was calculated using equation 2.2.

$$4\pi M = [(V\ K) / A] \times 10^4\ Gs \qquad (2.2)$$

The saturation magnetization (M_s, emu/gm) was calculated using the relationship $M_s = M/ d$. Complete hysteresis curve was obtained applying a maximum magnetic field of 5000 Oe and then M_s and intrinsic coercivity (H_c) were determined.

Room temperature magnetization of the synthesized Fe_3O_4 NPs was measured using HLT with an applied field of 5000 Oe and shown in Figure 2.12.

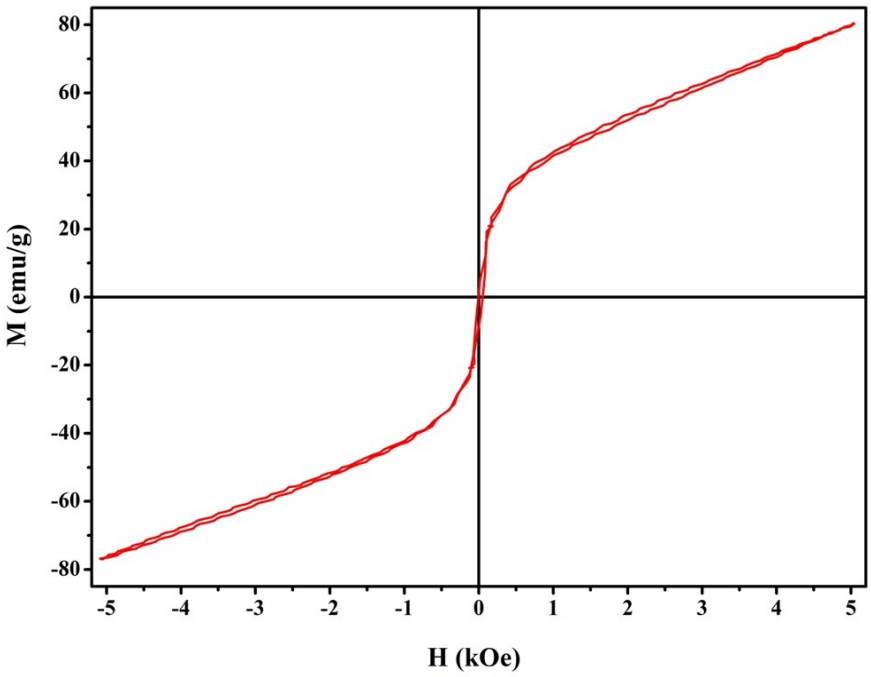

Figure 2.12 Room temperature hysteresis loop for Fe_3O_4 NPs.

The sample prepared by sonication showed superparamagnetic behaviour. The synthesized Fe_3O_4 nano powder possesses a H_c of 29 Oe and M_s of 80.2 emu/g. The values of M_s and H_c are comparable with the values reported by other authors using different preparation technique (Caruntu *et al.,* 2007).

2.4.1.3 Surface characterization of MNPs by SEM

The surface morphology of the MNPs was examined by SEM. Figure 2.13 shows the SEM micrograph of the bare MNPs at magnification 50000 × (15.0 kV). Also, the average particle size was measured as 38.56 nm.

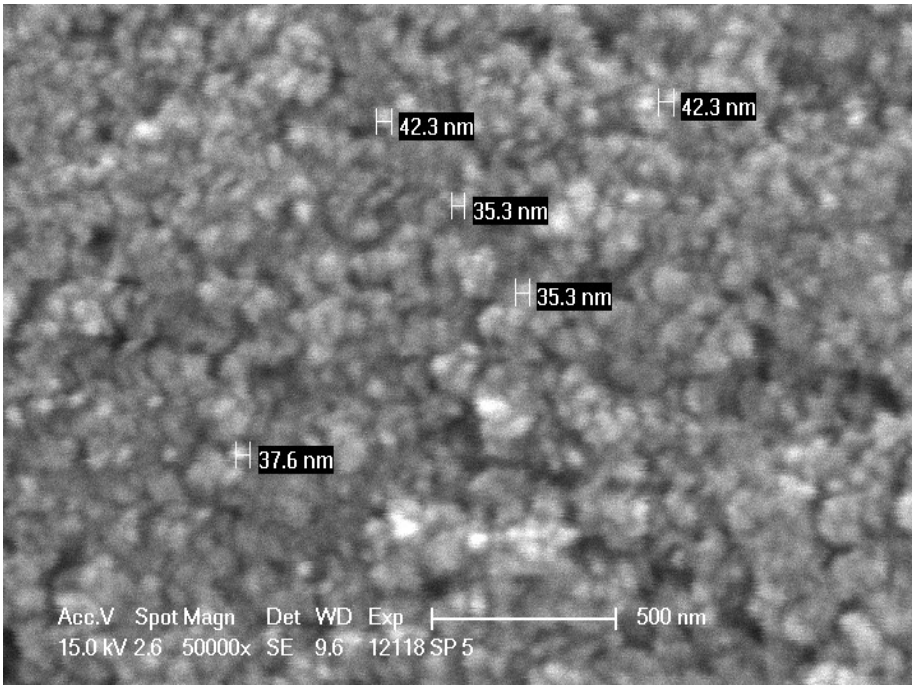

Figure 2.13 SEM image of bare MNPs at 50000 × magnification (15.0 kV).

2.4.1.4 FT-IR analysis of MNPs

The surface chemical structure of MNPs are characterized by FTIR spectroscopy and presented in Figure 2.14. FT-IR ATR spectra are collected at a resolution of 2 cm^{-1} (128 scans).

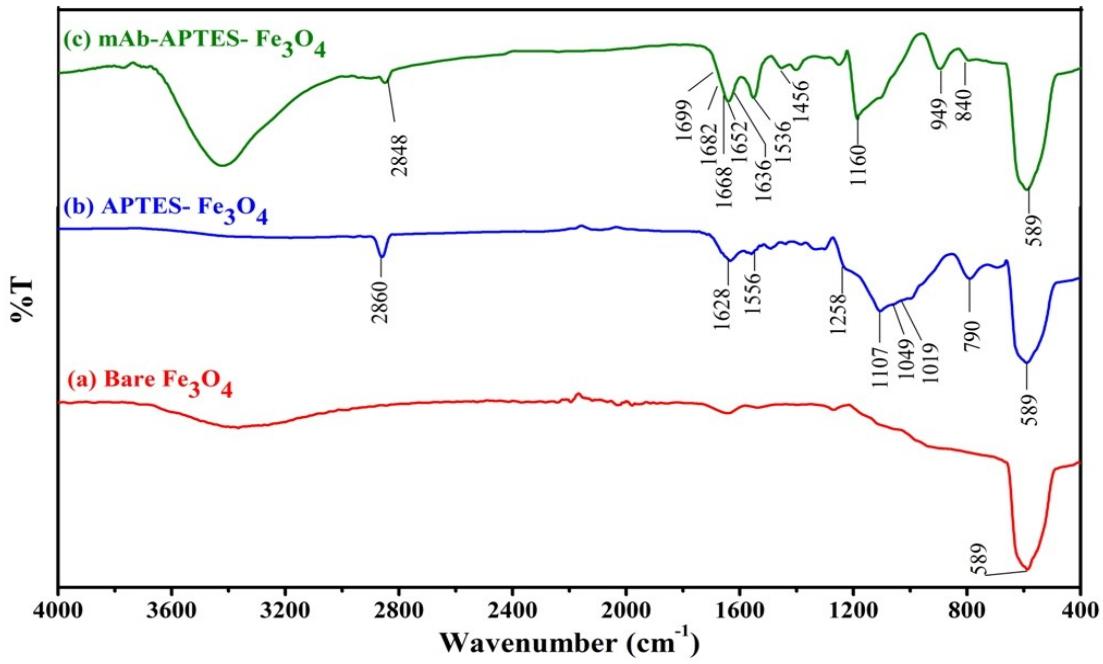

Figure 2.14 FT-IR spectra of Fe_3O_4 NPs (a) bare; (b) APTES modified and (c) 1° Ab coupled via APTES.

Figure 2.14 (a) shows the spectra of bare Fe_3O_4 NPs. The absorption peaks at around 586 cm^{-1} are the characteristic absorption of Fe – O bond that suggests the presence of magnetite NPs.

Figure 2.14 (b) shows the APTES-coated Fe_3O_4 NPs. The covalent anchoring of aminopropylsilane groups is mainly due to their self-polycondensation leading to a highly cross-linked polysiloxane film entrapping each magnetite NP. But the presence of Fe – O – Si bonds are not seen in the FT-IR spectrum because it appears at around 584 cm^{-1} and therefore overlaps with the Fe – O vibration of magnetite NPs (Bruni *et al.,* 1999). So, the adsorption of silane polymer onto the surface of magnetite particles has been confirmed by bands at 1111, 1049 and 1018 cm^{-1} which correspond to the SiO – H and Si – O – Si groups. The absorption bands at 794 cm^{-1} are due to the stretching of Si–O–H on the surface of magnetite. Furthermore, the broad bands at 1628 cm^{-1} are ascribed to the NH_2 stretching (Heiney *et al.,* 2000). All the figures indicate that the coupling agent APTES has been introduced onto the Fe_3O_4 NPs surface.

The 1° Ab coupling through APTES SAMs via the GA cross-linking reaction on Fe_3O_4 surfaces is shown in Figure 2.14 (c). Upon immobilization of 1° Ab new absorption bands have been appeared; three IR bands at 1636 cm^{-1}, 1536 cm^{-1}, and 1456 cm^{-1}, are ascribed to the absorption by the amide group that links 1° Ab to APTES functionalized NPs. In addition, the bands at 1699 cm^{-1}, 1682 cm^{-1}, 1652 cm^{-1} and 1668 cm^{-1} are for the amide I region which is the common structural unit for all bio-molecules (Nakano *et al.,* 2007).

2.4.2 Characterization of non-magnetic NPs

2.4.2.1 UV-Vis spectroscopic analysis of AuNPs

Figure 2.15 shows the UV–Vis spectra of AuNPs before and after surface modification. The characteristic peak observed at 520 nm indicates the formation of stable AuNPs (curve a). However, broadening of the peak, due to coupled plasmon resonance, along with slight shift towards higher wavelength (curve b) indicates attachment of the 11-MUA onto AuNPs surface. In Figure 2.15 inset, the visual images have been taken before and after functionalization of AuNPs with 11-MUA.

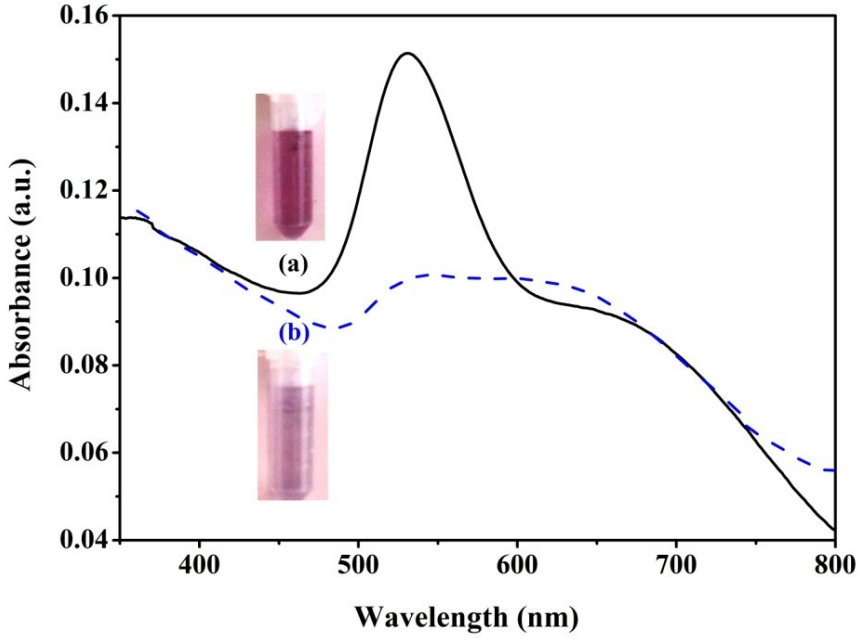

Figure 2.15 UV-Vis spectra of AuNPs (a) synthesized; (b) after surface modification (Inset: image of synthesized and surface modified AuNPs).

2.4.2.2 FT-IR analysis of AuNPs

FT-IR spectroscopy was applied to measure the surface properties of the 1° Ab coupling through 11-MUA SAMs via the carbodiimide cross-linking reaction on AuNPs (Figure 2.16).

FT-IR ATR spectra were collected at a resolution of 2 cm^{-1} (128 scans). The FT-IR spectra are shown Figure 2.16 (a) for bare AuNPs, (b) for 11-MUA modified AuNPs and (c) 1° Ab coupled via 11-MUA on AuNPs.

Figure 2.16 (b) shows the FT-IR spectra of AuNPs treated with 11-MUA. It showed C-H stretches in asymmetric and symmetric modes at 2921 cm^{-1} and 2847 cm^{-1} respectively. The C=O stretch at 1734 cm^{-1}, associated with asymmetric (1647 cm^{-1}) and symmetric (1542 cm^{-1}) COO^{-} stretches, is characteristic of an organic carboxylic acid compound. The additional IR peaks at 1455 cm^{-1}, 1294 cm^{-1} and 1216 cm^{-1} are ascribed to C-H deformation and C-O stretch respectively.

Upon immobilization of 1° Ab coupled in Figure 2.16 (c) new absorption bands have been developed; three IR bands at 1636 cm^{-1}, 1536 cm^{-1}, and 1263 cm^{-1} are ascribed to the absorption by the amide group that links 1° Ab to 11-MUA functionalized AuNPs. Also, the bands at 1699 cm^{-1}, 1682 cm^{-1}, 1668 cm^{-1} and 1652 cm^{-1} are for the amide I region which is the common structural unit for all biomolecules.

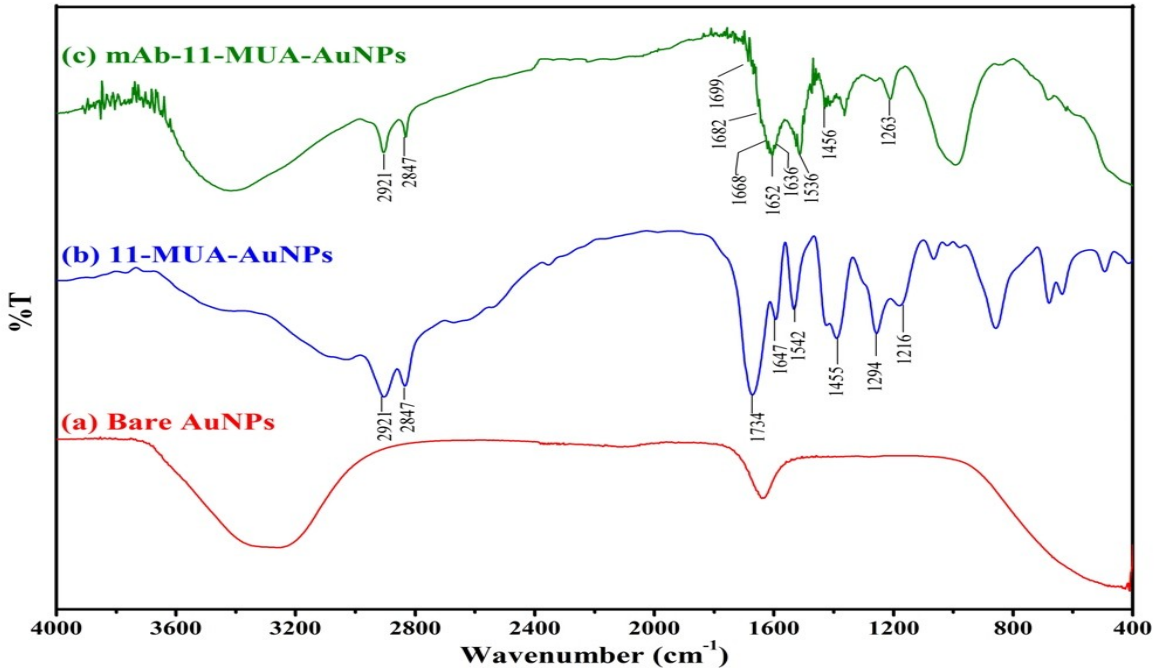

Figure 2.16 FT-IR spectra of AuNPs (a) Bare; (b) 11-MUA modified and (c) 1° Ab coupled via 11-MUA.

2.4.2.3 Transmission Electron Microscopy of HfO_2NPs

Note: The work incorporated in this section of the thesis is a collaborative experimental work with Department of Physics, IIT Delhi.

Figure 2.17 shows the HRTEM images of the HfO_2NPs powder samples. The morphology of all the samples was found to be spherical.

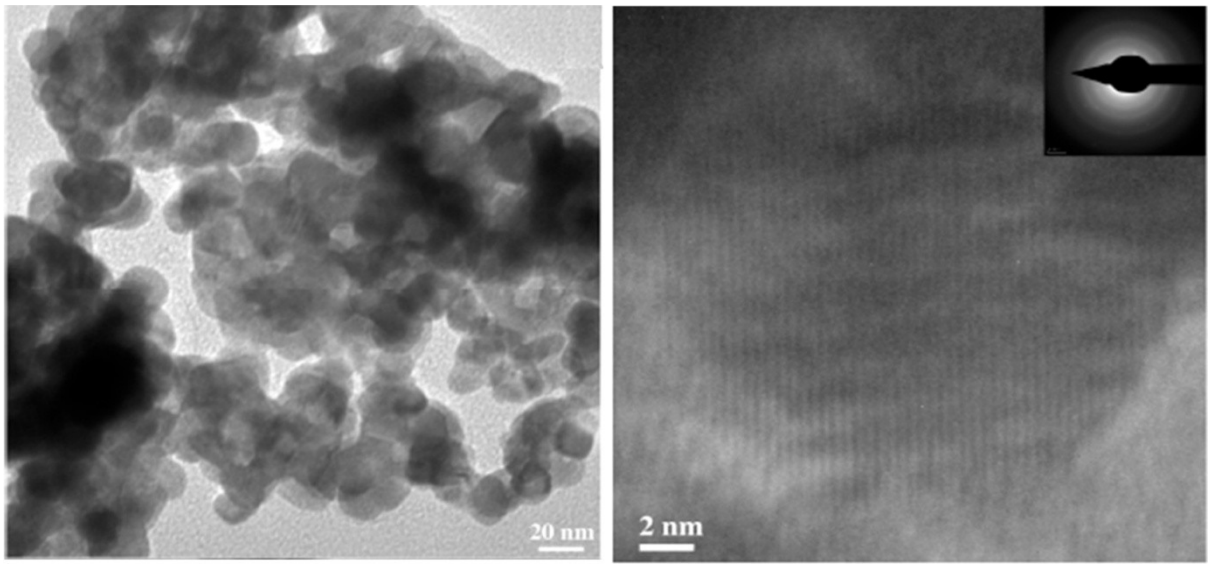

Figure 2.17 HRTEM images and corresponding electron-diffraction patterns of HfO_2NPs. (*Reproduce with permission Sharma et al., 2011*)

The TEM estimates of the average particle size of the crystalline HfO_2NPs is 16.2 nm and agrees well with the particle size measurement estimated values. The selected area of electron diffraction patterns (shown in the inset of Figure 2.17) reveals crystalline nature of the samples. The diffraction pattern also accounts for bulk monoclinic hafnia.

2.4.2.4 FT-IR analysis of HfO_2NPs

FT-IR spectroscopy was applied to measure the surface properties of HfO_2 NPs modified 1° Ab through SAMs via carbodiimide cross-linking reaction. FT-IR ATR spectra were collected at a resolution of 2 cm^{-1} (68 scans). The recorded FT-IR spectra are shown in Figure 2.18.

FT-IR spectrum of the bare HfO_2NPs is presented in Figure 2.18 (a). In the mid-infrared region there is only one strong absorption peak at 510 cm^{-1}. The feature at 660 cm^{-1} is the characteristic of HfO_2 longitudinal-optical (LO) phonon mode. The peak at 753 cm^{-1} is assigned to an A_u mode (atomic displacement parallel to the *c*-axis of the unit-cell). This is also reported by Martínez *et al.,* 2007.

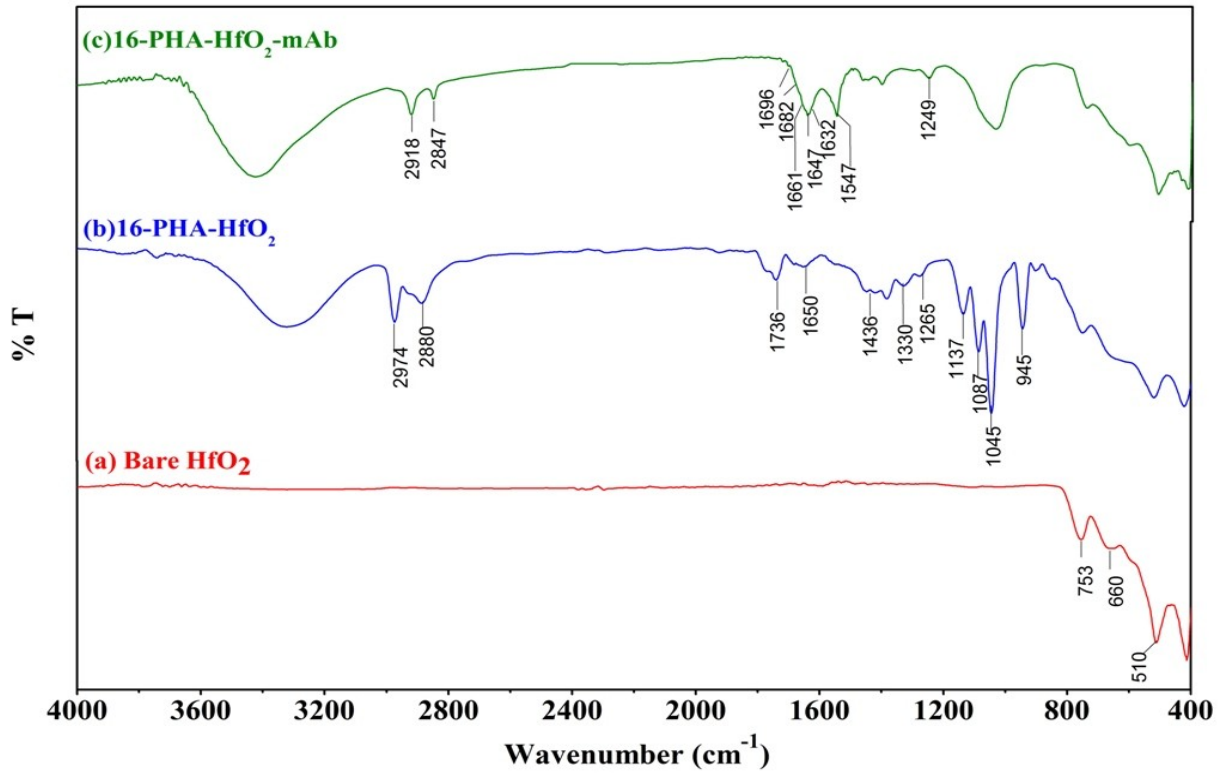

Figure 2.18 FT-IR spectra of HfO_2NPs (a) bare; (b) 16-PHA modified and (c) 1° Ab coupled via 16-PHA.

Figure 2.18 (b) shows FT-IR spectrum of 16-PHA functionalized HfO_2. Asymmetric (ν_{as}) and symmetric methylene stretches (ν_s) of 16-PHA-modified HfO_2 appear at 2974 cm^{-1} and 2880 cm^{-1} respectively. These bands of SAMs modified HfO_2 suggest methylene chains during monolayer growth. The C=O stretch at 1736 cm^{-1} on HfO_2 associated with ν_{as} COO^- stretch at 1650 cm^{-1} is characteristic of an organic carboxylic compound. The additional IR peaks at 1436 cm^{-1}, 1330 cm^{-1} and 1265 cm^{-1} are ascribed to C-H deformation and C-O stretch respectively.

It is very difficult to obtain the P-O stretching region information due to the binding of phosphonic acids onto metal oxides. The presence of several different binding modes for residual P=O and P-O-H sites in phosphonic acid monolayers appear between 1300 cm^{-1} and 800 cm^{-1} in the P-O stretching region. The peak located at 945 cm^{-1} in the spectrum is assigned to a P-OH band that is observed only after binding of 16-PHA on HfO_2. This indicates that the phosphonic acids bind to the surface Hf-OH group via condensation reactions. The linkage between HfO_2 and 16-PHA might be a tridentate chelating binding mode or a bidentate binding moiety rather than the monodentate surface binding mode. The existence of the peak at 1137 cm^{-1}, which is characteristic of the P=O stretching mode, is a possible evidence for bidentate binding modes. The observation of P-OH related modes indicates that the binding of 16-PHA on HfO_2 occurs mainly through the $P(O)(-OH)_2$ groups.

Figure 2.18 (c) is the FT-IR spectrum of covalently coupled 1° Ab on HfO_2. The C=O peak, however, is completely vanished as 1° Ab introduced. The existence of amide region in the samples is confirmed by presence of intense and broad absorption bands at 1647 cm^{-1}, 1547 cm^{-1} and 1249 cm^{-1}. Further new associated absorption bands at 1696, 1682, 1661 and 1632 cm^{-1} suggest the presence of amide group, which is also the evidence for -COOH of 16-PHA and $-NH_2$ of 1° Ab linkage.

2.4.3 Particle size characterization

The operation principle of the instrument is based on dynamic light scattering (DLS) technique. Due to both its applicability to a wide spectrum of particles and dispersion media and its ease of use, DLS technique is a popular for determining particle size. The average hydrodynamic diameter of a particle suspension can be measured by deflection of scattered light produced by particles due to Brownian motion. An intensity autocorrelation function for monodisperse suspension, $G_2(\tau)$, can be described by equation 2.3

$$G_2(\tau) = A\,[1 + B\,e^{-2Dq^2\tau}] \qquad (2.3)$$

where τ is the time delay between intensity measurements, A and B are the baseline and intercept of the correlation function, D is the diffusion coefficient and q = (4πn/λ)sin(θ/2), where n is the refractive index of the solvent, λ is the wavelength of the laser and θ is the scattering angle.

During the particle movement in Brownian motion, short time delays in τ the intensities will be highly correlated, while there is decay for long delays. The measured diffusion coefficient for a monodisperse system can then be related to the hydrodynamic diameter using the Stokes–Einstein equation (equation 2.4).

$$D = \frac{K_B T}{3\pi\eta_0 d} \qquad (2.4)$$

where, d is the particle's hydrodynamic diameter, D is diffusion coefficient, K_B is the Boltzmann constant, T is the absolute temperature and η_0 is the viscosity of the medium. The correlation function of a polydisperse system can be described by the sum of the exponential decays of different populations of particles present in the sample. A more detailed analysis of DLS has been reported elsewhere (Finsy, 1994; Brown, 1993).

The differential intensity related to particle size distributions is obtained from DLS study at 30 °C. A normalized particle size distribution is presented in Figure 2.19. Instrument performance was first evaluated using particle standards (20 and 100 nm) supplied in solution by the manufacturer. For each particle standard, the diameter, polydispersity index (PDI) and quality report were generated by the instrument. Samples were prepared by dispersing 1 mg of sample into 100 mL of PB. The intensity particle size distributions of the MNPs (Fe_3O_4) via sonication obtained from DLS study (Figure 2.19 (a)). The graph shows a single modal distribution with the main peak average around 60.3 nm. The cumulant mean diameter of the particles is 64.6 nm with a PDI of 0.282. The intensity particle size distributions of the AuNPs are obtained from DLS study (Figure 2.19 (b)). The particle size results of the AuNPs are plotted as cumulative percentage frequency curves. The average particle size of the bare AuNPs is 59 ± 4.04 nm with PDI 0.337. Figure 2.19 (c) depicts the particle size distribution of bare HfO_2NPs. The cumulant mean diameter of the particles is found to be 12.91 nm with PDI 0.221.

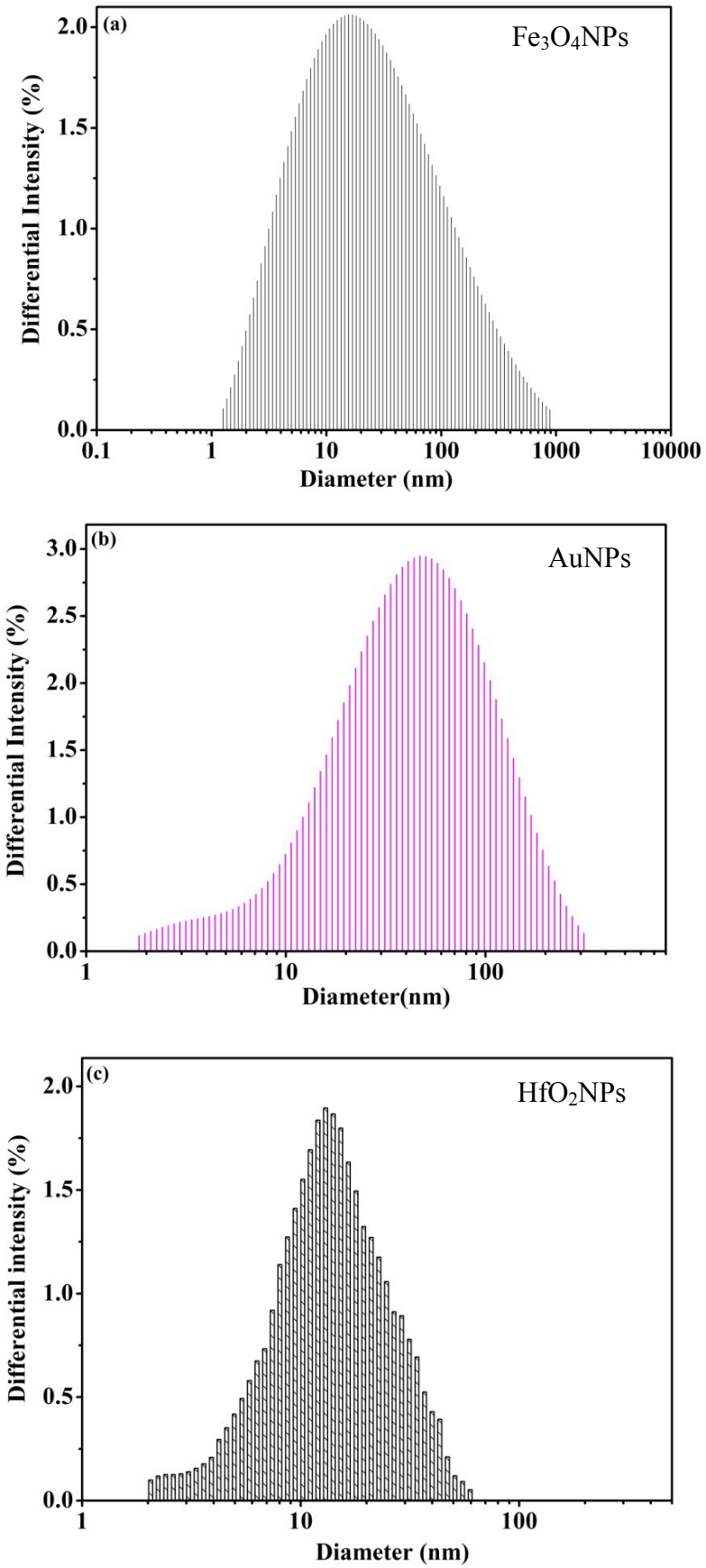

Figure 2.19 Particle size distribution of prepared (a) MNPs; (b) AuNPs and (c) HfO_2NPs.

Further, the particle size is increased upon the treatment with SAMs and 1° Ab. The Table 2.2 summarizes all particle size analysis data. It has been observed that the cumulant diameter of the modified particles increases as the carbon chain of the SAMs increased. Subsequently, an increment is observed for the particles modified with 1° Ab. The increment in particle size is about 10 nm after surface modification and about 26-30 nm after 1° Ab attachment that suggests the successful fabrication of AFM1 capture probe.

Table 2.2 Cumulative particle size data of the various NPs before and after attachment of 1° Ab.

NPs	Bare NPs		SAMs modified NPs		1° Ab attached NPs	
	average particle size (nm)	PDI	average particle size (nm)	PDI	average particle size (nm)	PDI
MNPs	60.3	0.282	69.41	0.301	97.90	0.410
AuNPs	59.0	0.337	70.12	0.370	100.70	0.447
HfO_2NPs	12.91	0.221	22.60	0.397	48.62	0.567

2.4.4 Fluorescence microscopy study

The binding of 1° Ab to functionalized NPs was also confirmed by fluorescence microscopy. Two microscopy slides were prepared as reference 1° Ab-NPs without 2° Ab-FITC and sample 1° Ab-NPs coupled with 2° Ab-FITC NPs (Figure 2.20).

The sample 1° Ab-NPs was incubated with 2° Ab-FITC (1:64000) for 2 h at room temperature in dark. Before excitation, the sample was rinsed with 0.01 M PBS to remove unbound 2° Ab-FITC. The reference 1° Ab-NPs without 2° Ab-FITC showed negligible fluorescence signal (Figure 2.20 (a)). The binding between 1° Ab on NPs and 2° Ab-FITC was demonstrated by a bright fluorescence signal (Figure 2.20 (b)). These observations suggest that the 1° Ab on NPs preserves excellent biological recognition of antibody to their targets.

Further, the samples were prepared to study the inhibition caused by AFM1. Two microscopic slides were prepared by the method as described earlier. The reference slide was incubated with 2° Ab-FITC in absence of AFM1 as described in earlier conditions. In another slide, sample, was prepared by incubating 1° Ab-NPs with AFM1 (50 pg mL^{-1}).

The sample slide was washed and incubation process was performed using 2° Ab-FITC as described earlier. Before excitation both reference and sample were rinsed with 0.01 M PBS to remove unbound 2° Ab-FITC. The intense signal from the reference again suggests the attachment of 2° Ab-FITC on 1° Ab-NPs (Figure 2.20 (c)). The signal intensity of sample slide was drastically quenched in presence of AFM1 (Figure 2.20 (d)). The observations suggest that the signal intensity is decreased due to binding of AFM1 to 1° Ab. Thus, the sensor exhibits as an excellent bio-recognition towards AFM1.

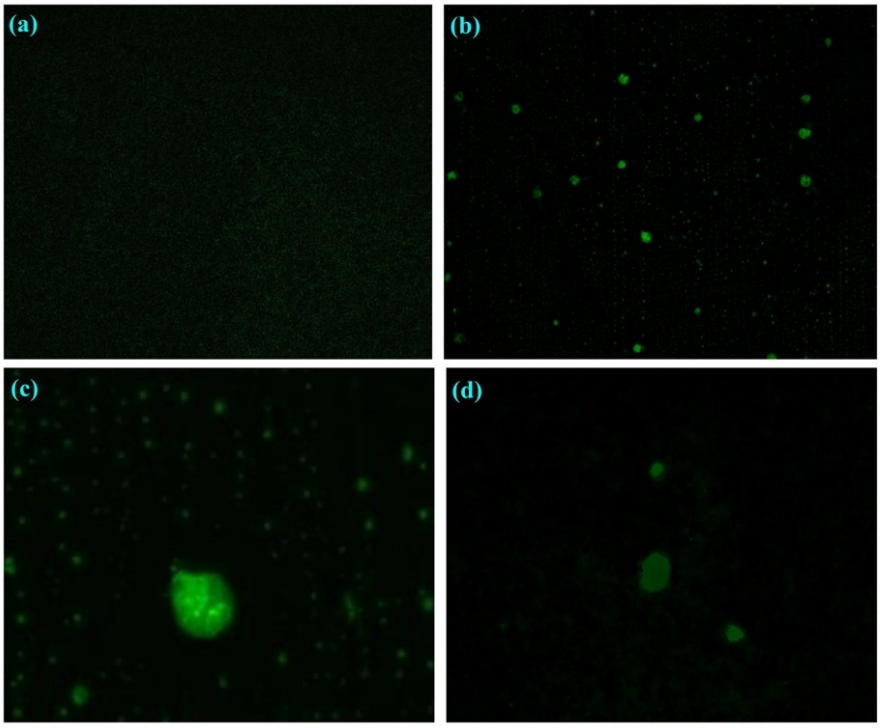

Figure 2.20 Fluorescence image of (a) reference 1° Ab-NPs without 2° Ab-FITC; (b) sample 1° Ab-NPs coupled with 2° Ab-FITC at 10× magnification; (c) reference 1° Ab-NPs coupled with 2° Ab-FITC at 40× magnification in absence of AFM1; (d) sample 1° Ab-NPs coupled with 2° Ab-FITC at 40× magnification in presence of AFM1; 1° Ab (1:32000) incubated with 2° Ab-FITC (1:64000); captured using 2° Ab-FITC (λ_{ex} 480 nm / λ_{em} 520 nm).

2.4.5 Optimization of influential parameters

2.4.5.1 Optimization of antibody dilution

The principle of the NPs based immunosensor is based on a sandwich immunoreaction. Capturing antibodies were immobilized on the NPs to capture antigen complex. Effective

antibody immobilization is very important to produce reproducible results and reduce non-specific bindings, which produce false signals. Figure 2.21 presents the CL signal intensity of different dilutions of 1° Ab against different 2° Ab dilutions. It is observed that signal response of the 1:32000 1° Ab dilution against 1:32000 2° Ab dilution is higher than that of the other dilutions.

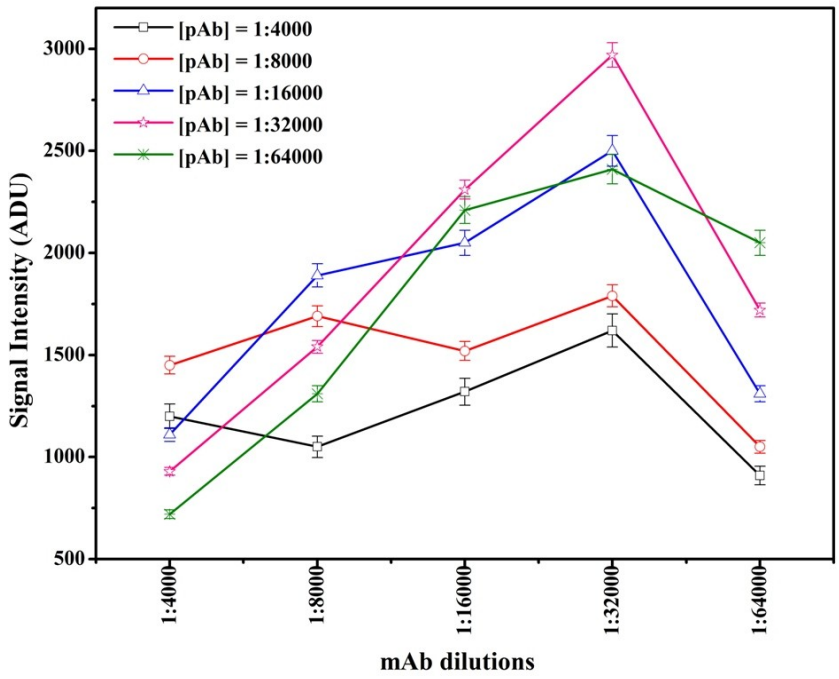

Figure 2.21 The CL signal intensity of different dilutions of 1° Ab against different 2° Ab dilutions.

2.4.5.2 Optimization of assay parameters

The ionic strength and pH of assay buffer and the temperature during measurement play key role towards the development of immunosensor. These parameters were optimized for the developed immunosensor and presented in Figure 2.22.

The influence of the ionic strength and pH on the activity of the 1° Ab was studied. Measurements were carried out on NPs system with various pH (6.4–8.0), ionic strength (1, 10, 50, 100, 150 and 200 mM) of PB and temperature (20 – 50 °C).

The results are presented in Figure 2.22 (a) and (b) respectively. It is evident from Figure 2.22 (a) that 1° Ab exhibits maximum activity at pH 7.4 which is ideal pH balance for a healthy body. Therefore, the pH of 7.4 was selected as a good compromise for our experiment.

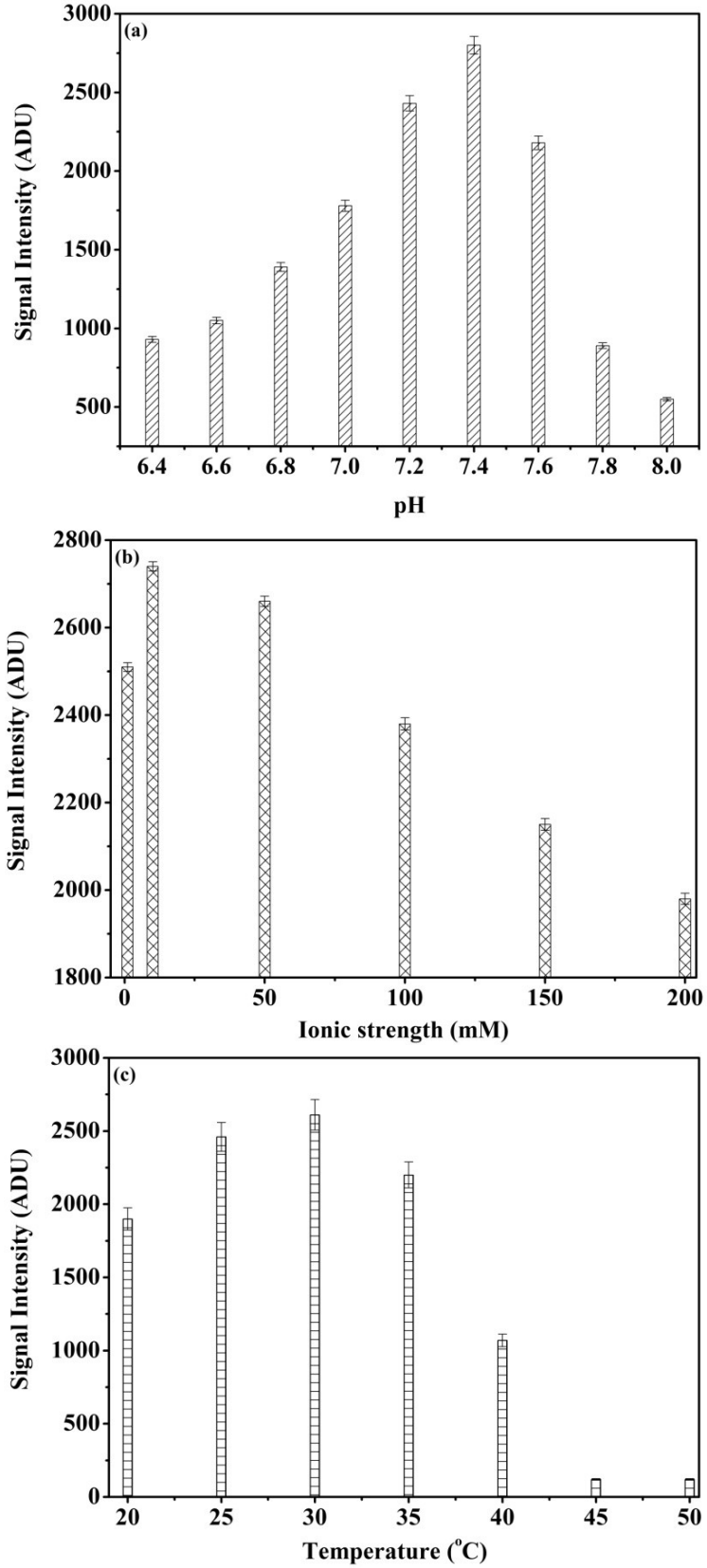

Figure 2.22 Influence of PBS (a) pH (6.4–8.0); (b) ionic strength (1, 10, 50, 100, 150 and 200 mM); (c) temperature in the range of 20-50 °C on the response of NPs immunoassay.

It is clear from Figure 2.22 (b) that with increase in the ionic strength of PB, response signal increases up to 10 mM, and then the signal starts decreasing. Thus, further experiments were carried out with 10 mM PB. Also thermal stability of the 1° Ab-NPs was evaluated by performing experiments in temperature ranging from 20 °C to 50 °C (Figure 2.22 (c)). Immobilized 1° Ab through SAMs exhibits the highest signal intensity in the range 25-30 °C. But the signal intensity was almost stable up to 35 °C. The immobilized 1° Ab looses activities in the temperature range 40 - 50 °C. The residual activity was 2.9% for immobilized 1° Ab at temperature 50 °C. Above 35 °C, the 1° Ab activity is dropped significantly due to the thermal inactivation. This indicates that the elevated temperature leads to denaturation of immobilized biomolecules.

2.4.5.3 Optimization of amount of NPs

The used amount of NPs is a key factor in NP-based immunosensor. The effect of the different amounts of NPs on the CL intensity was investigated and plotted in Figure 2.23.

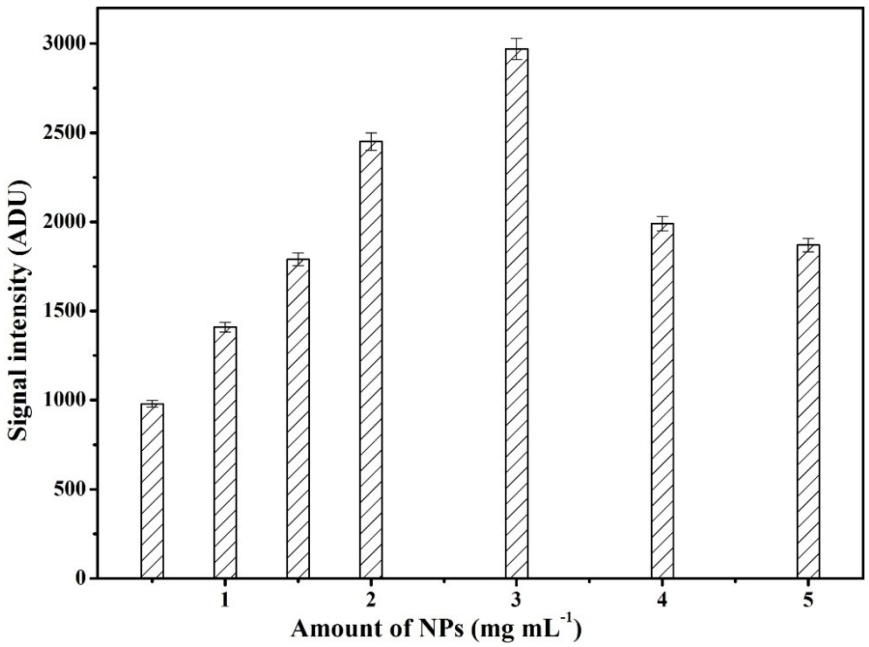

Figure 2.23 Optimization of amount of NPs under optimized assay condition.

The experimental results show that the CL intensity firstly increases with increasing amount of NPs, probably because of increase of the amount of the absorbed 1° Ab. However, above the amount of 3 mg mL^{-1}, the CL intensity declines probably because of discontinuous assembly of 1° Ab on too many NPs or mass-transfer processes of substrate and product. The

introduction of more particles could afford lower intensity due to self aggregation of 1° Ab at nano-platform.

2.4.6 Assay kinetics

The NPs based immunosensor was monitored in the kinetic mode using luminometry protocol with exposure time of 0.1 sec (Figure 2.24).

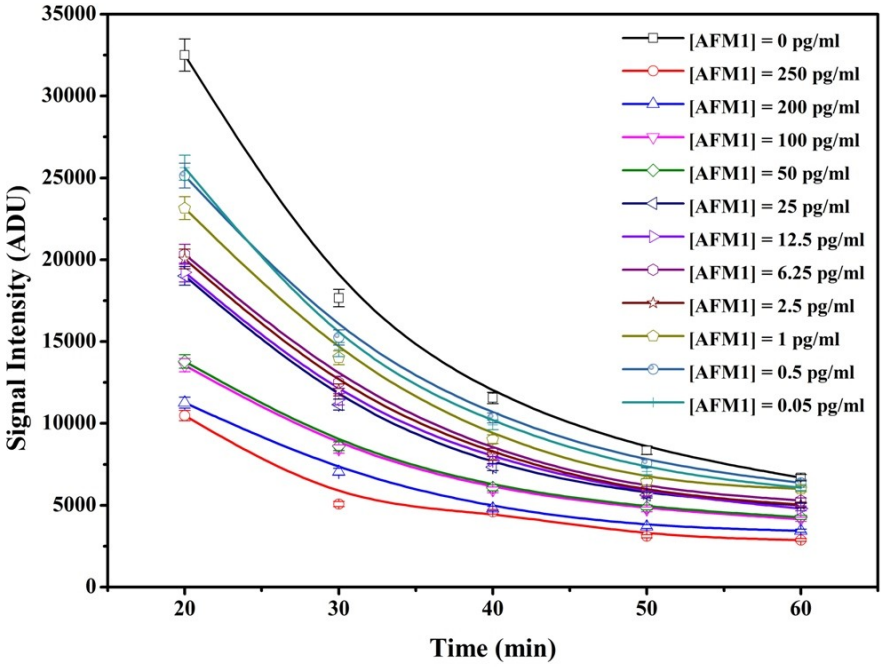

Figure 2.24 Kinetic measurements for different AFM1 concentrations (1° Ab diluted to 1:32000 in CB; 2° Ab diluted to 1:32000 in 0.01 M PBS at pH 7.4).

NPs coupled with 1° Ab were used for real time monitoring of the interactions with AFM1 in milk. The signal intensity of different concentrations of AFM1 spiked milk ranging from 0.05 pg mL^{-1} to 250 pg mL^{-1} was measured kinetically. As seen in figure, all steps including interaction between 1° Ab and AFM1 were almost completed in 40 min. Increase in concentration decreases the immunosensor response. The interaction time (40 min) is not long enough to reach steady state. Therefore, data might be obtained from steady state analysis. The kinetic analysis suggests that this is due to a rather low value of the association rate constant.

2.4.7 Calibration curve of NPs-ELISA for AFM1

To evaluate the analytical performance of sensor, calibration for milk samples was done with respect to the NPs based ELISA. The inhibition curve for AFM1 spiked milk samples in NPs

was obtained for different concentrations of AFM1 *i.e.* 0.5 – 200 pg mL^{-1} by CL detection. The calibration curves were fitted by using Origin Pro 8 SR0 software. Percentage inhibition (I %) was calculated using equation 2.5 as described by Arduini *et al.,* 2009 in presence and absence of analyte

$$I\,\% = \left[\frac{I_0 - I_A}{I_0}\right] \times 100 \qquad (2.5)$$

Where, I_0 = Signal Intensity of blank; I_A= Signal Intensity of spiked sample

The percentage of inhibited activity (I %) that obtained after exposure to the AFM1 is quantitatively related to the inhibitor concentration according to the above equation.

2.4.7.1 Calibration using MNPs

The calibration curve has been plotted for the MNPs based AFM1 immunosensor as presented in Figure 2.25.

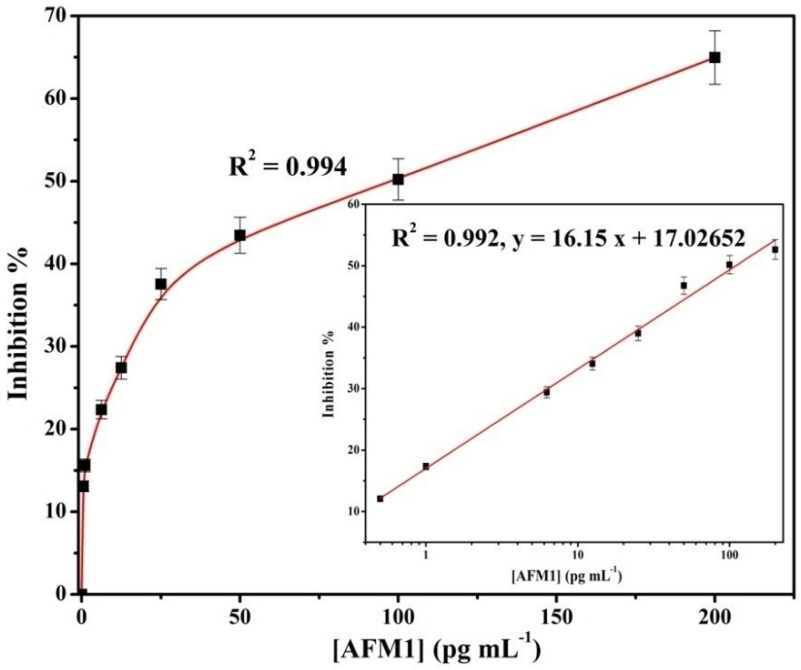

Figure 2.25 Inhibition curve for MNPs based sandwich ELISA under optimized assay condition (Inset: linear fit of inhibition curve).

The data points were fitted and unknown [AFM1] could be detected from mean standard deviation curve in NPs based ELISA. A good assay sensitivity of about 6% with standard deviation (S.D.) = 1.23 and coefficient of determination (R^2) = 0.994 is obtained. The limit of detection (LOD), which is defined as the lowest concentration of analyte that exhibits a signal

of 15% inhibition (Jiang *et al.,* 2011), is found to be 0.5 pg mL^{-1}. The half maximal inhibitory concentration (IC_{50}) value for MNPs based ELISA was found at 95.73 pg mL^{-1}. The plot shows a good linear relationship with regression equation; y = 16.15 x (pg mL^{-1}) + 17.02652 with R^2 = 0.992.

2.4.7.2 Calibration using AuNPs

The calibration curve using the CL intensity has been plotted for various AFM1 concentrations ranging from 0.5 – 200 pg mL^{-1} in milk using AuNPs immunosensor. The fitted data is presented in Figure 2.26. The precision of the measurement is satisfactory in the linear range of 20 – 80% inhibition, while the results become much less reproducible below 20% inhibition. Thus, under the experimental conditions mentioned here AFM1 might be determined in the 2.5 – 100 pg mL^{-1} range (corresponding to 20 – 80 % inhibition) with a S.D. equal to 2.8 (n = 5).

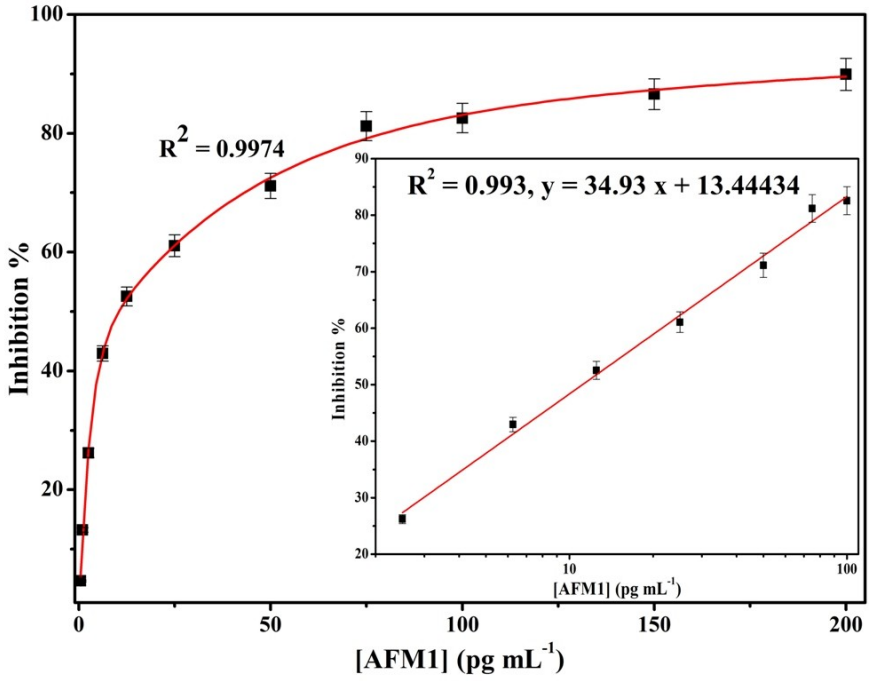

Figure 2.26 Inhibition curve for AuNPs based sandwich ELISA under optimized assay condition (Inset: linear fit of inhibition curve).

A good assay sensitivity, about 7.8% with S.D. = 2.8; R^2 = 0.9974 is achieved. The LOD is found to be 2.5 pg mL^{-1}. The IC_{50} value for AuNPs based ELISA is found at 10.35 pg mL^{-1}. The plot shows a good linear relationship with regression equation; y = 34.93 x (pg mL^{-1}) + 13.44434 with R^2 = 0.993. The limit of quantification (LOQ) is found to be 2.5 pg mL^{-1}.

2.4.7.3 Calibration using HfO_2NPs

Using the optimized parameters, the calibration curves were performed with 1° Ab immobilized on HfO_2NPs. The data points were fitted and unknown [AFM1] could be detected from mean standard deviation curve in HfO_2NPs based ELISA. The inhibition curve obtained using CL technique is shown in Figure 2.27. A good assay sensitivity, about 2.068% with S.D. = 0.85 and R^2 = 0.996 is achieved. The LOD is found to be 0.5 pg mL^{-1}. The IC_{50} value for developed immunosensor based on sandwich ELISA is at 61.48 pg mL^{-1}.

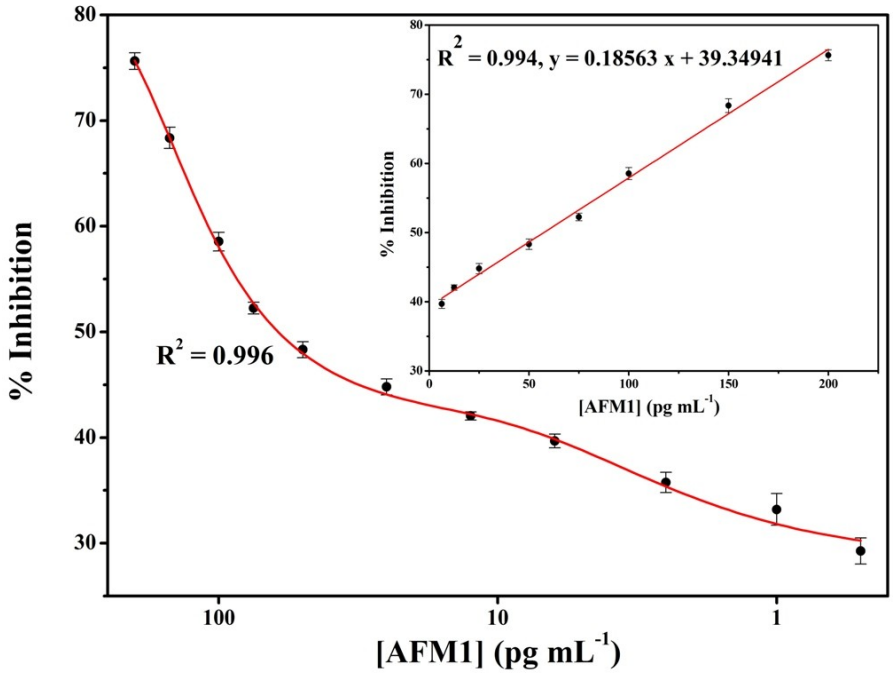

Figure 2.27 Inhibition curve for HfO_2NPs based sandwich ELISA under optimized assay condition (Inset: linear fit of inhibition curve).

The signal inhibited due to presence of AFM1 in milk was calculated and a significantly low detection limit 0.5 pg mL^{-1} could be achieved in case of HfO_2NPs based sandwich ELISA. The curve was also fitted linear and presented as Figure 2.27 (Inset). The plot shows a good linear relationship with regression equation; y = 0.18563 x (pg mL^{-1}) + 39.34941 and R^2 = 0.994. LOQ is found to be 6.25 pg mL^{-1}.

Thus the NPs based ELISA presented here is one of the sensitive methods for AFM1 analysis, comparable with other established methods (Table 2.1). The signal inhibition as calculated due to presence of AFM1 in milk shows a significantly low detection limit 0.5 pg mL^{-1} with analysis time of 40 min. The reported LOD using NPs based immunosensor are the

lowest ever LOD, achieved in ELISA for detection of AFM1. The significant findings using various NPs based immunosensor are summarized in the Table 2.3.

Table 2.3 Significant analytical findings of NPs based immunoassay.

Analytical parameter	MNPs (Fe_3O_4) ELISA	Non-magnetic NPs ELISA	
		AuNPs ELISA	HfO_2NPs ELISA
Linear range (pg mL^{-1})	0.5 – 200	2.5 – 100	6.25 – 200
LOD (pg mL^{-1})	0.5	2.5	0.5
LOQ (pg mL^{-1})	0.5	2.5	6.25
Sensitivity	6.0%	7.8%	2.068%
IC_{50} (pg mL^{-1})	95.73	10.35	61.48

2.4.8 Performance of affinity capture column

Various approaches have been reported on affinity capture columns for pre-separation or enrichment of the analytes. Herein we have studied 1° Ab immobilized NPs as affinity capture column and compared it with other reported columns such as Protein A & Protein G for AFM1 (Badea *et al.,* 2004; Radoi *et al.,* 2008). For evaluation of the capacity of these three materials, affinity columns were prepared as described in section 2.3.5. Here, these columns were deployed in an integrated fashion wherein after trapping the AFM1, the trace AFM1 were measured by deploying the ELISA in microplate. A stock solution of 50 pg mL^{-1} and 100 pg mL^{-1} AFM1 was eluted and the efficiency of the columns to capture AFM1 was determined. A significant binding is observed in functionalized NPs as compared to protein A & G column. The signal intensity of ELISA by using these materials is plotted and shown in Figure 2.28.

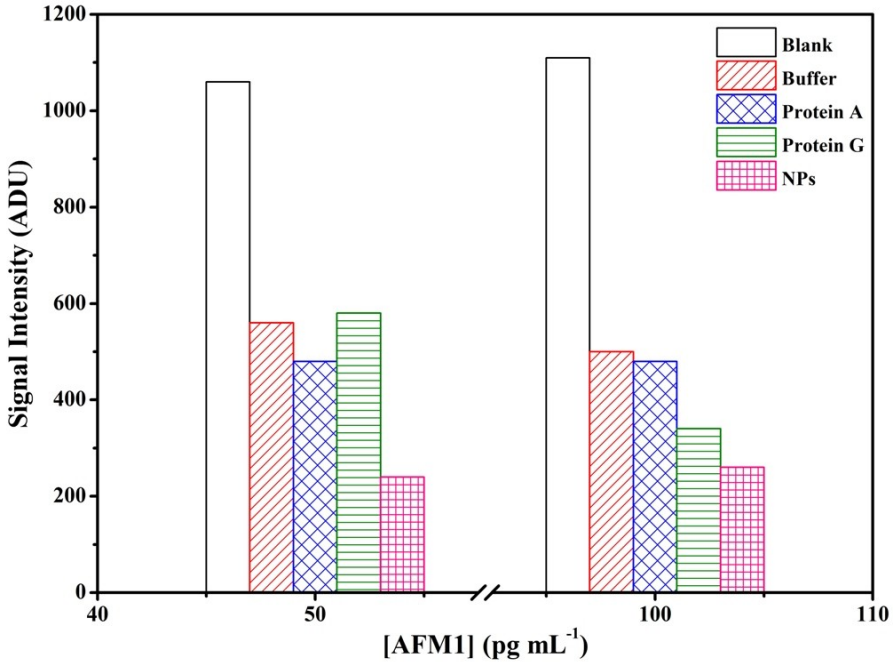

Figure 2.28 Comparison of Protein A, G and NPs as affinity entrapment materials for AFM1 (1˚Ab = 1:16000; 2˚Ab = 1:32000).

Quantitative efficiencies for the three affinity capture columns were calculated by performing the inhibition measurements. Inhibition for both concentrations of AFM1 as high as 73.58% and 75.57% respectively were measured using NPs packed columns against protein A (54.71% and 56.75%) and protein G (45.28% and 69.36%) (Table 2.4).

The results show that the NPs affinity column is more efficient in trapping of AFM1 from milk samples than existing others.

Table 2.4 Comparison of signal suppression (I %) of different affinity entrapment materials in SPE columns measured in 384 well plate.

Matrix	**I %** **[AFM1] = 50 pg mL^{-1}**	**I %** **[AFM1] = 100 pg mL^{-1}**
Buffer	47.16	54.95
Ab-Protein A	54.71	56.75
Ab-Protein G	45.28	69.36
Ab-NPs	73.58	75.57

2.4.9 Recovery of AFM1 from spiked and CRM milk samples

The developed microplate ELISA was further validated with certified reference material (CRM) (ERM-BD 282, zero level of AFM1) for milk powder. The milk powder was reconstituted as indicated in the certification report supplied by the IRMM, Belgium. To test the accuracy of developed assay, AFM1 concentrations ranging from 1 to 100 pg mL^{-1} were added to the milk samples and assayed by ELISA. Known CRM milk samples not containing AFM1 were compared with samples deliberately contaminated with known amounts of AFM1. Recovery was assessed by spiking AFM1 with the BD 282 reconstituted material and presented in Table 2.5.

Table 2.5 Recovery of AFM1 from certified reference material milk sample as determined by ELISA: BD 282, zero level of AFM1 certified reference material employed to assess the recovery efficiency using developed assay.

AFM1 added (pg mL^{-1})	AFM1 found (pg mL^{-1})	R.S.D %	R.E.%	Recovery %
1.00	0.96	1.56	-4.00	96.00
2.50	2.41	0.77	-3.40	96.40
6.25	6.02	1.12	-3.68	96.32
12.50	12.14	7.92	-2.88	97.10
25.00	24.72	5.77	-1.12	98.88
50.00	47.47	4.42	-5.06	94.94
100.00	89.46	2.04	-1.54	98.46

The fortified (1, 2.5, 6.25, 12.5, 25, 50, 100 pg mL^{-1} of AFM1) milk samples (0.5% fat) were interpolated from the calibration curve performed using reconstituted CRM. The precision and reliability of the developed assay is notable from the data presented in Table 2.5. The result show an excellent percentage of recovery, close to 100% for CRM. The precision is determined by calculating the relative standard deviation (R.S.D.%) for the replicate measurements and the accuracy (R.E.%) is calculated by assessing the agreement between measured and nominal concentration of the fortified samples.

R.E. (relative error) % = [(measured value − true value) / true value] × 100

R.S.D. (relative standard deviation) % = standard deviation/mean × 100; $n = 3$

2.4.10 Photometry study and comparison with commercial NPs

Simultaneously, the immunosensor was examined colorimetrically using OPD chromogen suitable for use in ELISA procedures which utilize horseradish peroxidase conjugates. This substrate produced a soluble end product that was orange-brown in colour and could be read spectrophotometrically at 450 nm. The OPD reaction could be stopped with 3N HCl and read at 490 nm. Also, the immunosensor based on synthesized NPs was compared visually as well as photometrically with commercially available NPs (Figure 2.29).

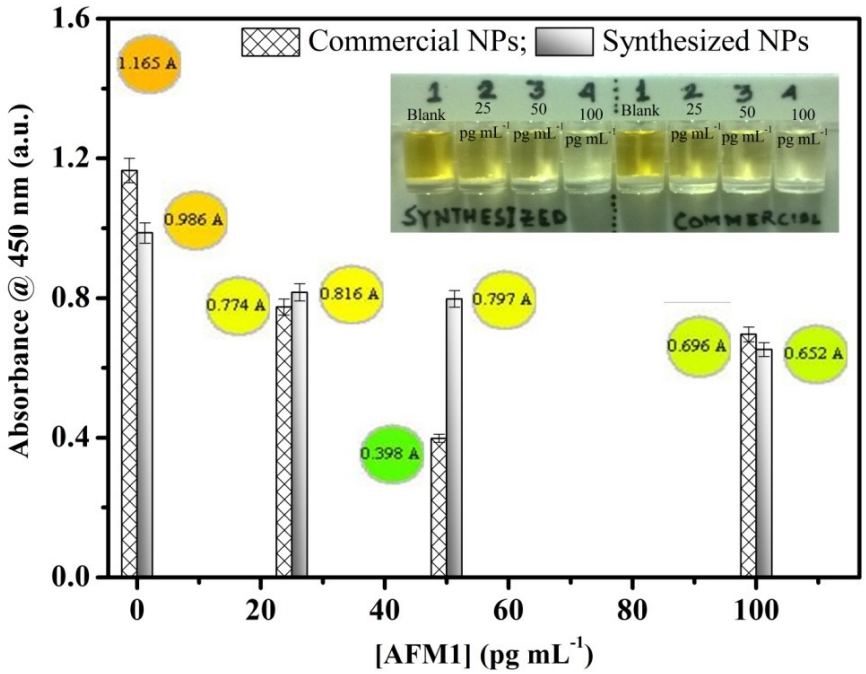

Figure 2.29 Comparison of signal intensity associated with real time images obtained using 1° Ab coupled on synthesized and commercial NPs for various [AFM1].

The I% for the both cases was calculated and plotted for the AFM1 concentration above, near and below IC_{50} values (100 pg mL^{-1}, 50 pg mL^{-1} and 25 pg mL^{-1}) obtained from the CL data (Figure 2.30).

At lower concentration of AFM1 *i.e.*, 25 pg mL^{-1}, the I% values are almost equal for both synthesized and commercial particles. But the results at the AFM1 concentrations near and above IC_{50} have shown almost 46.67% and 23.01% higher I% values respectively using the immunosensor based on synthesized NPs. The large binding surface area of the synthesized

NPs may allow the proper orientation of the antibody binding sites, improving the sensitivity of immunoassays.

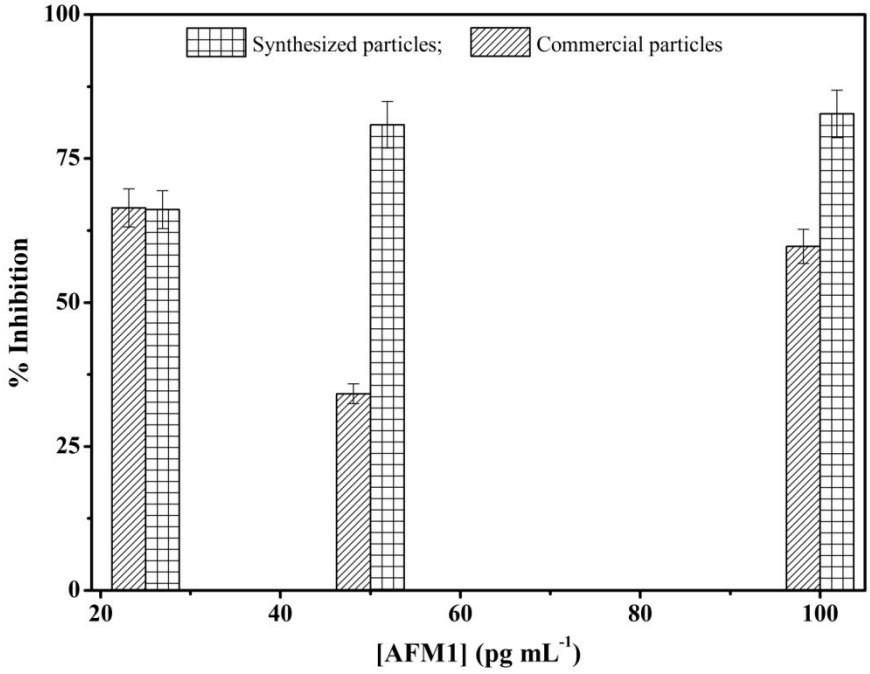

Figure 2.30 Comparison of I % calculated for 1° Ab coupled on synthesized and commercial NPs for various [AFM1].

2.4.11 Specificity of sensing probe

The specificity of 1° Ab, which was used during construction of sensing probe, is one of the most important factors and is usually represented by cross-reactivity (CR). The reliability and specificity of 1° Ab may be determined by lowering of CR value. AFM1, aflatoxin M2 (AFM2), AFB1 and aflatoxin G1 (AFG1) have similar structures. Thus the capture antibody recognizes not only its specific analyte but also partly the other structural analogues. The results has shown high specificity of AFM1 towards 1° Ab and partial recognition towards AFM2 and AFB1 but negligible towards AFG1.

2.4.12 Storage stability

Along with other features, the storage stability of immunosensor was investigated with a series of repeated experiments over 30 days (Figure 2.31). The storage stability of developed immunosensor was examined at two different temperatures (i) at 4 °C and (ii) at room temperature (28 °C). The response was found excellent even after 30 measurements (Intraday RSD% = 3.13 and Interday RSD% = 2.19). Under both conditions, the immunosensor

showed good stability. The environmental condition at 4 °C produced better response. The response of 1° Ab modified NPs at 4 °C remains constant for the first 15 days and after 30 days the response is decreased to 89% of its original response. The 1° Ab modified NPs at room temperature retains 82% of its original response after 30 days. The decrease in response may be due to the reduction of antibody activity. It is found that 16-PHA modified HfO_2NPs based immunosensor holds good storage stability, sensitivity and reusability for longer duration.

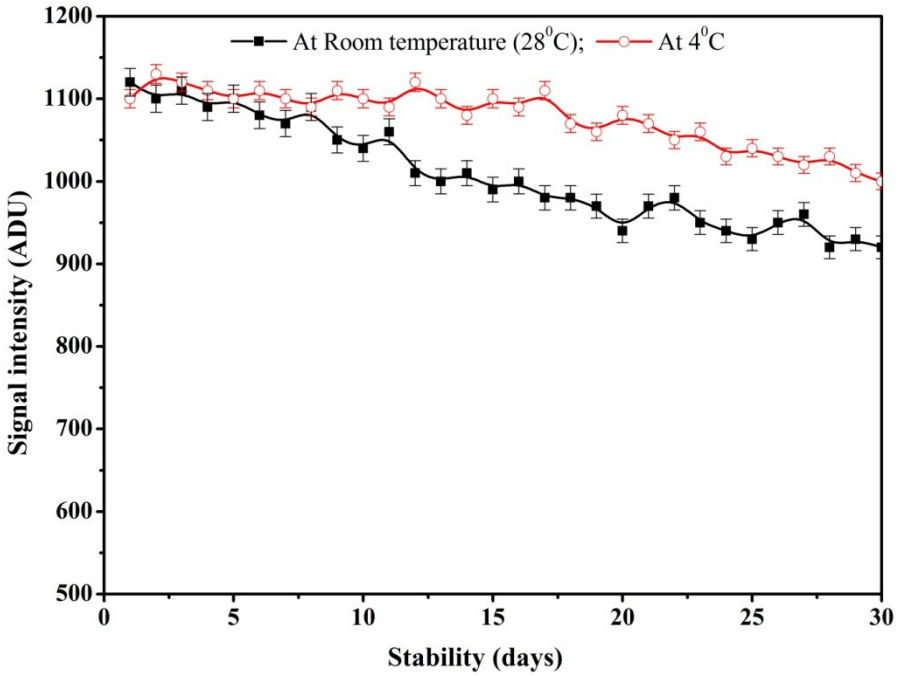

Figure 2.31 Comparison of storage stability for NPs based nano-immunosensor at 4 °C and room temperature (28 °C).

2.5 Conclusion

In this chapter, fast, reliable and ultra sensitive NPs based sandwich ELISA has been developed for detection of AFM1 in milk. Various NPs *e.g.* AuNPs, MNPs and HfO_2NPs have been exploited towards immunosensor development. Using SAMs, the NPs have been modified towards suitable bio-immobilization. Surface modification techniques like thiolation, silanization and phosphonation have been deployed. The miniaturised assay has enabled ultra trace analysis of AFM1 in milk with much improved lower limit of detection at 0.5 pg mL^{-1} as compared to other various reported methods. The total assay time to detect AFM1 is approximately 3 h. The hybrid system by coupling the 1° Ab immobilized NPs column with microwell plate assay has enabled simultaneous measurement of low (0.5 pg

mL^{-1}) and high AFM1 contamination (200 pg mL^{-1}). The most promising feature of this NPs-ELISA is the small size, high capture efficiency and lower cost over other reported materials. It may be extended further for separation of AFM1 from the contaminated milk.

CHAPTER 3: NANOSTRUCTURED ZnO IN BIOSENSING AND BIO-CATALYSIS

Highlights:

- Nanostructured ZnO (NPs, nanorod, whiskers) has been investigated for biosensing application.
- Phosphonation as a cross-linker has been tested successfully to provide highly stabilized enzyme coupled nanostructures.
- The enzyme functionalized ZnO nanostructures has been demonstrated for biosensing of choline, acetylcholine, organophosphate pesticide residues and bio-catalysis of 4-nitrophenyl phosphate (*p*NPP).

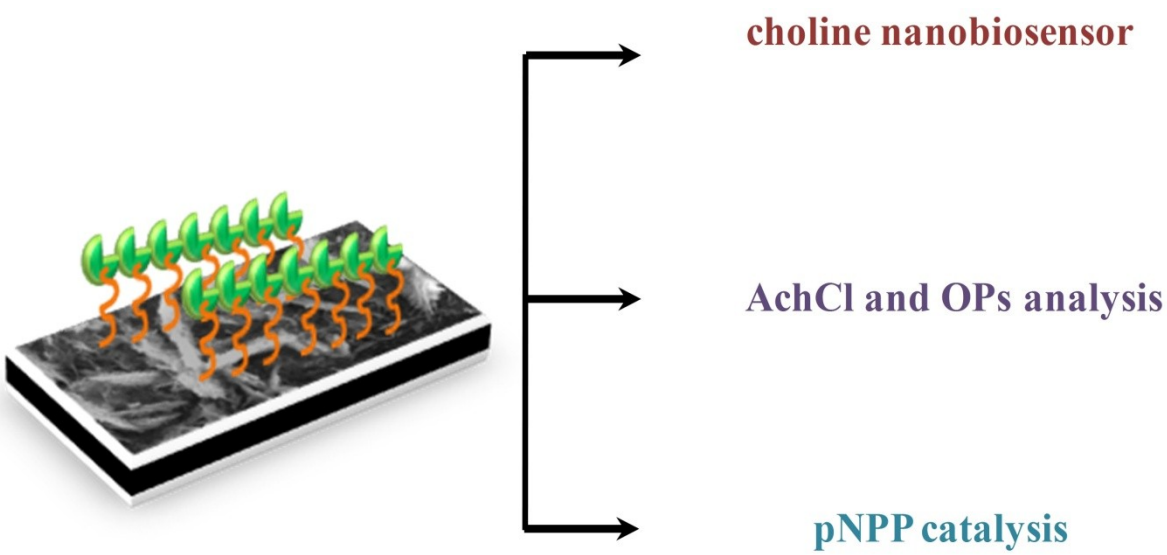

Graphical abstract of ZnO based biosensing and bio-catalysis

3.1 Introduction

Nanomaterials have been extensively studied in various applications and used widely in chemical industry, medical diagnostics, food technology, ultraviolet testing and our daily life (Willander *et al.,* 2014; Comini *et al.,* 2009; Barth *et al.,* 2010; Fang *et al.,* 2011; Pal *et al.,* 2014). Among these nanomaterials, ZnO nanostructures are good candidates because of their low toxicity, good thermal stability, good oxidation resistibility, good biocompatibility, large specific surface area and high electron mobility (Asif *et al.,* 2010). Notably, IEP of ZnO is as high as about 9.5, *i.e.* suitable for immobilization of the enzymes and proteins (Topoglidis *et al.,* 2001). Also, ZnO is a optically transparent semiconductor with a direct band gap (E_g = 3.37 eV) and a large exciton binding energy (60 meV), exhibiting near UV emission (Wang, 2008). The morphology-controlled synthesis of ZnO nanostructures have been extensively studied. The morphology of ZnO can vary from nanorods, nanotubes, nanoneedles, nanocomb to nanoinjector, nanohelixes and nanodisks simply by adjusting preparation method and preparation conditions (Willander *et al.,* 2014). The various morphologies and mature growth methods lead to easy preparation of ZnO-based devices. ZnO nanostructures have been gained much attention for sensing applications (Arya *et al.,* 2012). Several properties of ZnO that have been utilized for gas sensors, are based on the fact that conductance changes with the reversible chemisorption process of reactive gases on the surface of ZnO (Kim and Yong, 2011). Pressure sensors based on the piezoelectric property of ZnO was observed first time by Wang (Wang, 2008). So far, various ZnO nanostructures such as NPs, porous films, nanocombs and nanorods have been deployed for development of biosensors (Ahmad and Zhu, 2011; Solanki *et al.,* 2011). ZnO nanostructures based biosensor are presented in Table 3.1 to detect various analytes.

Table 3.1 Various reported ZnO nanostructures based biosensor

ZnO nanostructures	Biomolecule immobilization	Detection technique	Analyte	Reference
Nanoporous films	Physisorption	Electro-chemistry	Cytochrome *c*	Topoglidis *et al.,* 2001
Nanorods	Physisorption	Amperometry	Uric acid	Zhang *et al.,* 2004
Nanoporous thin film	Physisorption	Cyclic voltammetric	Cholesterol	Singh *et al.,* 2007

$Si/SiO_2/Si_3N_4/Cr/Au/ZnO$ thin plate	Cystamine activated by GA	Colorimetric ELISA	Immuno-globulin E	Huang and Lee, 2008
Nanorods on Au wire	Electrostatic	Amperometry	Phenol	Gu *et al.*, 2008
ZnO-chitosan nanobiocomposite	Physisorption	Cyclic voltammetry and impedance	Urea	Solanki *et al.*, 2008
Nanoflake	Physisorption	Potentiometric	Glucose	Fulati *et al.*, 2010
Hexagonal nanorod	Physisorption	Potentiometric	Glucose	Asif *et al.*, 2010
Nanowalls	Physisorption	Potentiometric	Cholesterol	Israr *et al.*, 2011
Nanowires	Electrostatically immobilized	Potentiometric	Uric acid	Usman Ali *et al.*, 2011

3.2 Objectives

The aim of this work is to explore use of ZnO based nanostructures for (i) development of choline nanobiosensor; (ii) development of biosensors for organophosphate pesticide residues (OPs) and (iii) bio-catalysis using novel whiskers.

3.3 Development of nanobiosensor for choline analysis

3.3.1 State of the art for analysis of choline

Milk, containing high level of choline, is an essential nutritional food for all age group (Phillips, 2012). Choline, as "vitamin-like", is synthesized in the human body, but dietary supplementation is necessary to maintain proper function (Blusztajn, 1998; Zeisel, 2000). Choline has essential roles in brain development and memory function for infants as well as adults. It also has an important role to maintain the central nervous system and numerous metabolic functions in the body such as: (a) methyl donor (b) as a precursor of the signalling lipids, platelet-activating factor and sphingosylphosphoryl choline and (c) as a precursor for

acetylcholine, phosphatidyl choline and sphingomyelin biosynthesis (Dietary Reference Intakes, 1998). The adequate intake for choline ranges from 125 mg/day in infants to 550 mg/day in males over age 14 years and in breast-feeding women (Michel *et al.,* 2006). Neurodegenerative disorders such as Alzheimer's, Parkinson's diseases and an increased risk of lethal prostate cancer have been implicated owing to abnormal metabolism of choline (Zeisel and Blusztajn, 1994; Richman *et al.,* 2012). Since infant's nutritional intake is limited to a single source in general milk, choline supplementation is critically important. Therefore, the need for the development of a sensitive and efficient method for the estimation of the choline level in milk is extremely important.

Enzymatic choline biosensors based on thermal (Deshpande *et al.,* 2011a), colorimetric (Takayama *et al.,* 1977), fluorimetric (Chen *et al.,* 2011; Li *et al.,* 2013) and electrochemical detection (Qin *et al.,* 2010; Shimomura *et al.,* 2009) have been reported for choline analysis. The reported choline biosensors use the enzyme choline oxidase (COD) that catalyses choline in the presence of oxygen and produces betaine aldehyde and H_2O_2 as product of this reaction. The produced H_2O_2 in the reaction is highly susceptible to undergo spontaneous reaction with second enzyme *i.e.* co-immobilized HRP. H_2O_2 thus produced was quantified using CL technique wherein, the numbers of photons emitted in presence of luminol can be counted using a sensitive photomultiplier system as presented in Figure 3.1. Owing to low background, high sensitivity, low cost of instrumentation and suitability for miniaturization in analytical chemistry, CL has been recognized as one of the most useful analytical techniques (Dodeigne *et al.,* 2000).

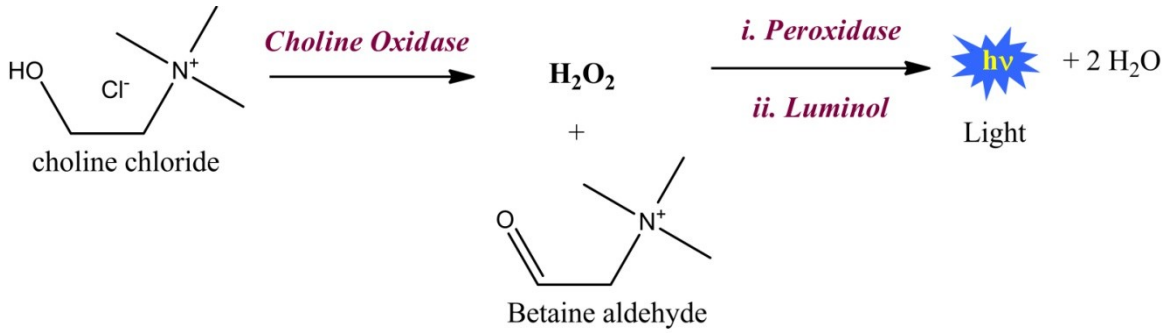

Figure 3.1 Working mechanism for the choline biosensor.

3.3.2 Enzyme immobilization on transducer surface

Enzyme immobilization on the transducer surface is a critical step in the design of biosensors as enzyme molecules might retain their activity after the immobilization in order to achieve

enhanced stability and shelf life. Self-assembled monolayers (SAMs) provide versatility and novel properties to surfaces and interfaces by conjugating biomolecules to facilitate a low-cost method of fabricating miniaturized biosensor devices with improved enzyme activity, stability and selectivity (Samanta and Sarkar, 2011). A unique approach to utilizing CL technique for the detection of acetylcholine has been reported using enzyme coupled multiple-branched nanostructures (Risveden *et al.,* 2010). Moreover, carboxylic acid, phosphonic acids, alkyl phosphonic acids and phosphoric acids (Laibinis *et al.,* 1989; Textor *et al.,* 2000; Pawsey *et al.,* 2002) have been reported to form favourable functionalized surfaces of metal oxides. Alkyl phosphonates and phosphonic acid can form well-packed SAMs with excellent thermal and hydrolytic stability. Moreover, these SAMs are reported to exhibit much improved binding over carboxylic acids to a wide range of metal oxides (Zhang *et al.,* 2010a).

3.3.3 Experimental section

3.3.3.1 Chemicals and biochemicals

Choline oxidase (EC 1.1.3.17) from Alkaligenes sp. (COD), peroxidase (EC 1.11.1.7) from Horseradish (HRP), choline chloride (ChCl), Zinc nitrate hydrate ($Zn(NO_3)_2$, xH_2O), Sodium hydroxide (NaOH) 99.99% trace metals basis, 16-phosphonohexadecanoic acid (16-PHA), 1-Ethyl-3-[3-dimethylaminopropyl]carbodiimide hydrochloride (EDC), N-hydroxy succinimide (NHS), Tween-20 and luminol (5-amino-2,3-dihydro-1,4-phthalazinedione) were purchased from Sigma Chemical Co. (USA). Sodium phosphate dibasic, sodium phosphate monobasic and other chemicals were of GR grade, Merck (Germany). Commercial milk samples of different fat content were purchased from the local supermarket of Goa, India.

3.3.3.2 Materials and instrumentation

Centrifugation, shaking and filtration of the samples were done by Spinwin mini centrifuge, Spinix shaker purchased from Tarsons (India). White 384 well polystyrene microtiter plates were purchased from Nunc (Denmark). A Rigaku MiniFlex X-ray diffraction (XRD) using Cu K_α radiation was used to obtain the structural information. Raman spectra were recorded using Renishaw inVia micro-Raman spectrometer with 514 nm Argon laser. Fourier Transform Infrared (FT-IR) spectra were recorded using IRAffinity-1 (SHIMADZU, Japan) with attenuated total reflectance (ATR) attachment Specac Diamond ATR AQUA. For chemiluminescence measurement, Victor™ X4 2030 Opti-plate reader Perkin-

Elmer (USA) was used. Water produced in a reverse osmosis system (arium61316, Sartorius, Germany) was used for preparing all the solutions. Certified ultra-high pure nitrogen (99.9%), pH meter (Seven Multi Mettler Toledo, 8603, Switzerland) were used.

3.3.3.3 Preparation of ZnONR film

Vertically aligned ZnONR films were deposited by hybrid wet chemical route at room temperature onto glass substrate by high pressure sputtering at ~30 Pa argon pressure with pre-deposited ZnO seed particles. The detailed method of preparation has been described elsewhere (Dalui *et al.,* 2008). The ZnONR films thus produced were used in the construction of biosensor as presented in Figure 3.2.

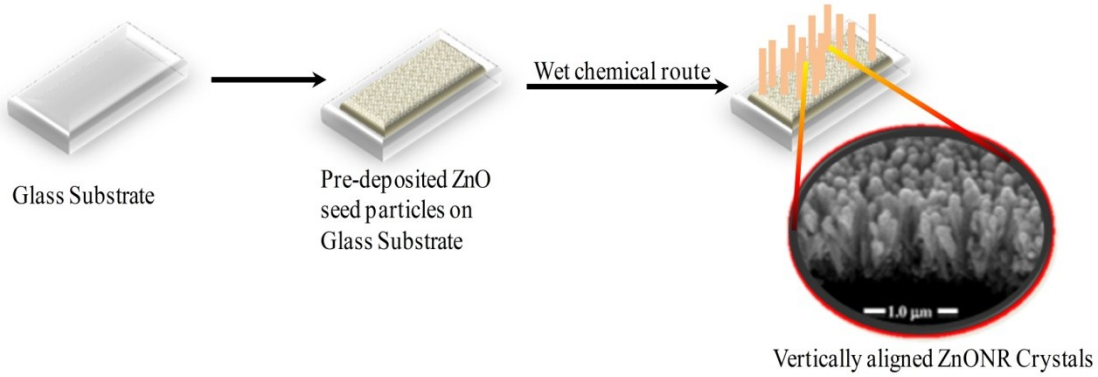

Figure 3.2 Schematic representation for construction of ZnONR films.

3.3.3.4 Buffers and standard solution preparation

Phosphate buffer (PB) 100 mM, pH 7.4 was prepared by mixing 100 mM of sodium di-hydrogen phosphate monohydrate and 100 mM of disodium hydrogen phosphate monohydrate in DI water. A stock solution of ChCl (100 mM) was prepared by dissolving 0.139 g in 10 mL of PB (100 mM, pH 7.4). Working solution of ChCl was prepared freshly before daily use. All enzyme stock solutions were prepared in PB (100 mM, pH 7.4).

For the determination of free choline a 5 mL aliquot of raw milk was added with 15 µL of Tween-20 (to give a final concentration of 0.3% v/v). To minimize the matrix effect, the solution was centrifuged for 10 min at 12000 rpm at room temperature. A 1:4 (v/v) final dilution with PB was made prior to analysis so that the amount of choline lies in the calibration range. With the given protocol for dilution/centrifugation/filtration with 0.22 µM filter (Whatman, USA) the maximum of milk fat was successfully separated.

3.3.3.5 Construction of choline biosensor

Construction of choline biosensor is based on the efficient immobilization of bi-enzyme through SAMs. The glass containers used for monolayer preparation were cleaned with Piranha solution as described in section 2.3.4 (**caution**: Piranha solution reacts strongly and exothermally with organics). ZnONR thin film was washed with ethanol, and dried under a stream of high purity nitrogen before use. These samples were immersed into 0.5 mM ethanolic solution of 16-PHA for 72 h to achieve self-assembly. The SAMs functionalized ZnONR were again rinsed in ethanol followed by DI water and dried under a stream of nitrogen. For enzyme immobilization, the carboxylic acid-terminated SAMs were modified using an aqueous equimolar solution of 100 mM EDC /100 mM NHS for 2 h at room temperature. The resultant NHS ester monolayers were reacted for 3 h in a solution of COD (1 IU/µL) and HRP (0.1 IU/µL) in PB (100 mM, pH ~ 7.4). The covalently coupled bi-enzyme (COD/HRP) ZnONR thin film was taken out from solution and washed as described earlier. The reaction pathway for enzyme attachment on the ZnONR is shown in Figure 3.3. Similarly, same amount of the enzyme was also incubated on the ZnONR for 12 h to prepare physisorbed COD/HRP ZnONR films.

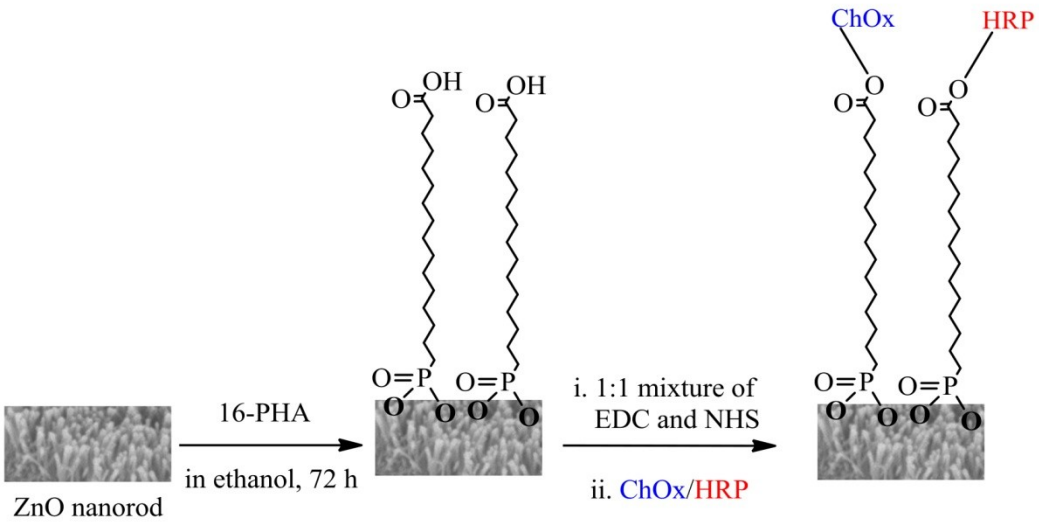

Figure 3.3 Reaction pathway of covalently coupled bi-enzyme on ZnONR.

3.3.3.6 Measurement of choline

In the biosensor presented here, COD provides the specificity and acts as a catalyst to initiate the bi-enzyme reaction. The schematic of choline measurement using physically adsorbed

(path A) and covalent coupled (path B) enzyme on ZnONR nanobiosensor are presented in Figure 3.4.

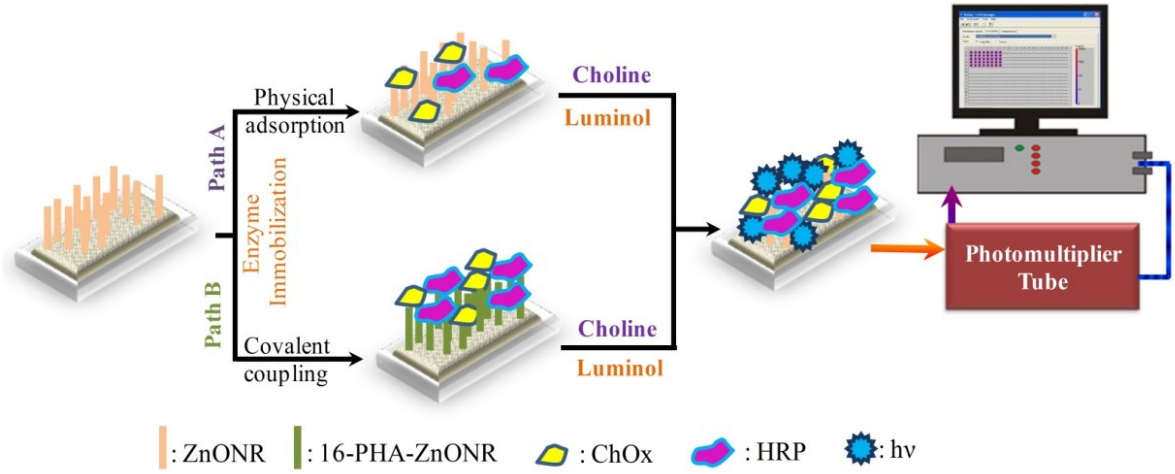

Figure 3.4 Schematic representation for constructing ZnONR nanobiosensor.

3.3.4 Results and Discussion

3.3.4.1 Surface morphology of ZnONR thin films

Figure 3.5 shows the field emission scanning electron micrograph (FESEM) of ZnO nanorod-film on glass substrate. It is observed that ZnO nanorods deposited on glass substrate are mostly vertically aligned.

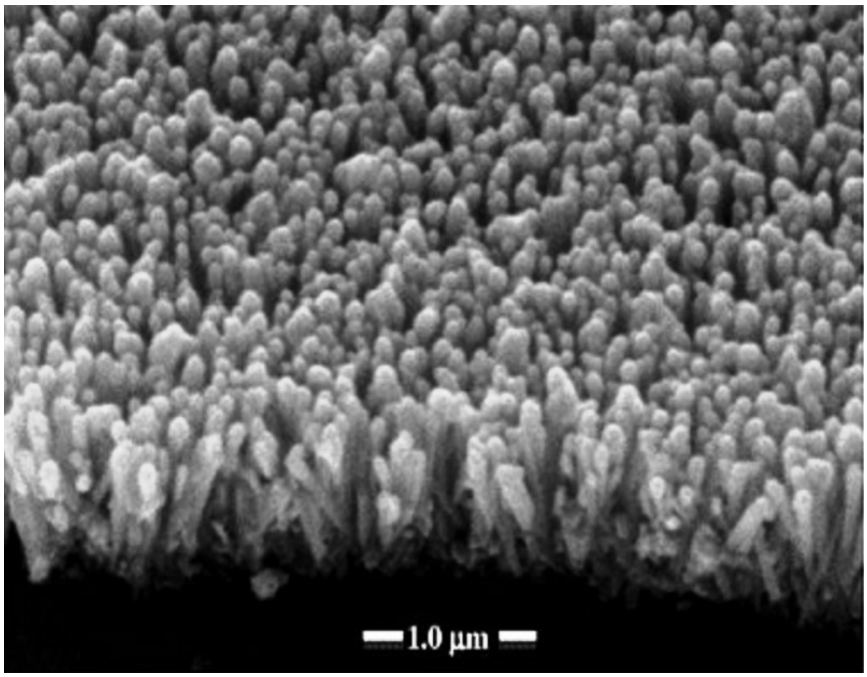

Figure 3.5 FESEM of ZnONR film on glass substrate.

3.3.4.2 X-ray diffraction analysis and Raman studies of ZnONR thin films

The XRD measurements (Figure 3.6) suggest the polycrystalline nature of ZnONR with preferential [0 0 2] direction orientation [JCPDS No. 80-0075]. Raman spectroscopy offers a non-destructive tool for obtaining information about both the local and the non-local vibrational states related to the structure of ZnO. The reported Raman spectra of ZnONR film is shown in the inset of Figure 3.6. The spectrum is dominated by the presence of a strong sharp peak located at ~438 cm^{-1} identifying the good crystalline quality of ZnONR films. The peak at ~438 cm^{-1} may be identified as high frequency branch of E_2 mode of ZnO. The broad and asymmetric nature of this peak is typical of the Raman active mode specially observed in wurtzite structure. The peak is preceded by peaks at ~332 cm^{-1} and ~378 cm^{-1} as reported for ZnO films (Dalui *et al.,* 2008). There is only one peak at ~577 cm^{-1} in the higher wave number region. The peak at ~577 cm^{-1} might be attributed to the A_1 longitudinal optical (LO) mode of ZnO. Origin of the above mode may be due to Zn interstitials present in the films. Raman spectroscopy results of ZnONR thus leads to the conclusion that these nanorod-films are of good crystalline quality with some Zn interstitials present in the film.

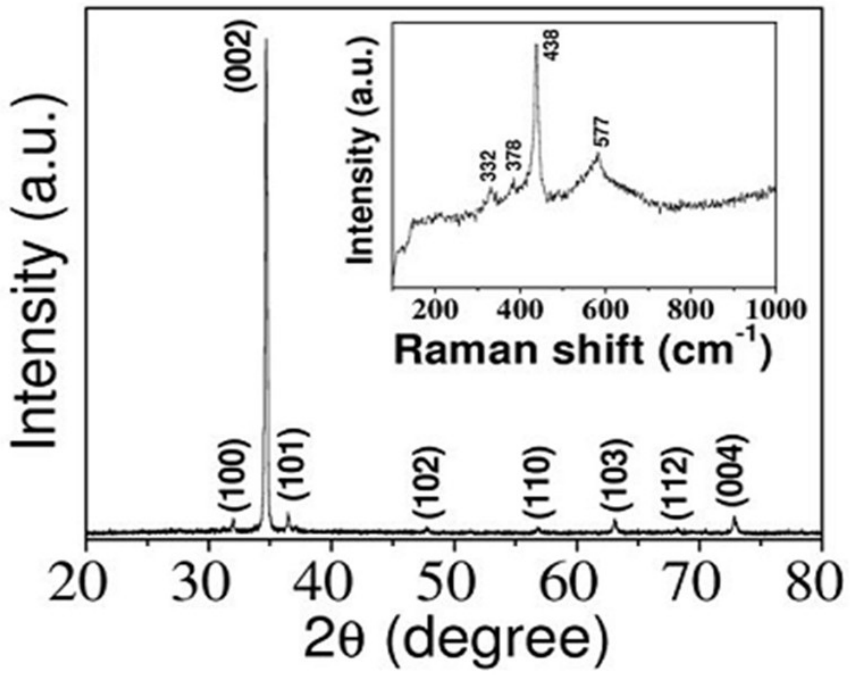

Figure 3.6 XRD pattern of ZnONR (Inset: Raman spectrum of ZnONR).

This is essentially a hybrid technique where the size and distribution of the ZnO seed crystallites may easily be manipulated to modulate the growth of ZnONRs. Thus, the ZnONR

used in this work are [0 0 2] aligned polycrystalline as is evident from XRD and Raman measurements.

3.3.4.3 Spectroscopic characterization by FT-IR

FT-IR spectroscopy was applied to measure the surface properties of the bienzyme COD/HRP coupling through SAMs via the carbodiimide cross-linking reaction on ZnONR surfaces. For the ZnONR samples, FT-IR ATR spectra were collected at a resolution of 2 cm^{-1} (128 scans). The FT-IR spectra recorded for ZnONR coupled enzyme (COD/HRP) via 16-PHA crosslinker are shown in Figure 3.7.

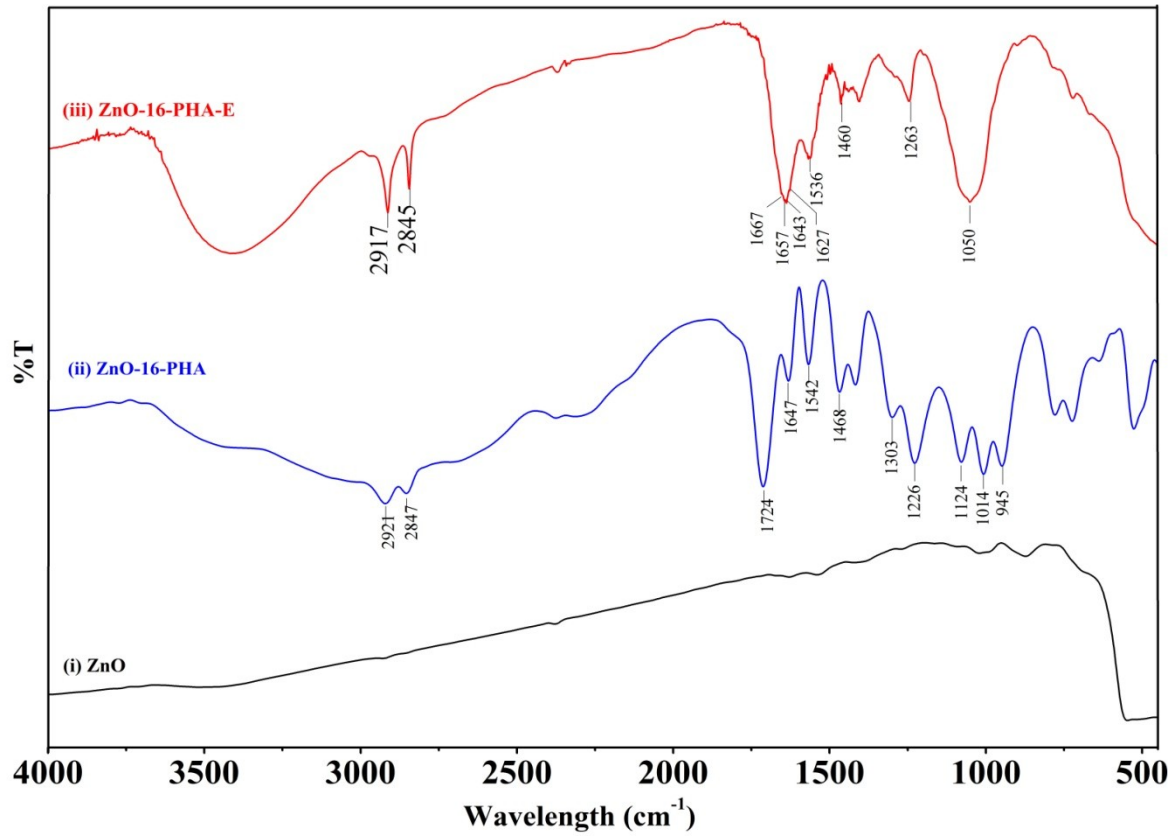

Figure 3.7 FT-IR spectrum of ZnONR (i) bare; (ii) 16-PHA functionalized ZnONR and (iii) covalently coupled enzyme.

Figure 3.7 (i) shows FT-IR spectrum of the bare ZnONR. Figure 3.7 (ii) shows the asymmetric (ν_{as} (C-H)) and symmetric methylene stretches (ν_s (C-H)) of 16-PHA-modified ZnONR that appear at 2925 cm^{-1} and 2853 cm^{-1} respectively. These bands of 16-PHA modified ZnO suggest methylene chains during monolayer growth. The C=O stretch at 1724 cm^{-1} on ZnONR associated with asymmetric and symmetric COO^-stretches at 1647 cm^{-1} and 1542 cm^{-1} respectively are characteristics of an organic carboxylic compound. The additional

IR peaks at 1455 cm^{-1}, 1294 cm^{-1} and 1216 cm^{-1} are ascribed to C-H deformation and C-O stretch respectively. In the P-O stretching region [Figure 3.7 (ii)], the binding mode information of phosphonic acids onto metal oxides is not easy to obtain. The peaks in the P-O stretching region appear between 1300 cm^{-1} and 800 cm^{-1} and the presence of several different binding modes in phosphonic acid monolayers is indicated by the presence of residual P=O and P-O-H sites. The peak located at 945 cm^{-1} in the spectrum of 16-PHA is assigned to a P-OH band that is observed only after binding to the ZnO surface. This indicates that the phosphonic acids bind to the surface Zn-OH group via condensation reactions. The linkage to the ZnO surface mode might be a tridentate chelating binding mode or a bidentate binding moiety rather than the monodentate surface binding mode. The existence of the peak at 1124 cm^{-1}, which is characteristic of the P=O stretching mode, is a possible evidence for bidentate binding modes. The observation of P-OH related modes indicates that the binding of 16-PHA on ZnONR occurs mainly through the P(O) $(-OH)_2$ groups. Similar coordination of binding modes of organic phosphonic acids on ZnO was also confirmed by Zhang *et al.* (Zhang et al., 2010a).

The enzyme COD/HRP coupling through 16-PHA SAMs via the carbodiimide cross-linking reaction on ZnONR surfaces is presented in Figure 3.7 (iii). Upon immobilization of COD/HRP in Figure 3.7 (iii) new absorption bands have been appeared; three IR bands at 1643 cm^{-1}, 1536 cm^{-1}, and 1263 cm^{-1} are ascribed to the absorption by the amide group that links COD/HRP to 16-PHA functionalized ZnONR. Also the bands at 1667 cm^{-1}, 1657 cm^{-1} and 1627 cm^{-1} are for the amide I region which is common structural unit for all biomolecules (Nakano *et al.*, 2007).

3.3.4.4 Optimization of assay parameters for choline analysis

CL biosensors based on luminol involve appropriate enzymatic reaction between substrate and enzyme and the subsequent reaction between luminol and enzymatically produced H_2O_2. A minor change in enzyme concentration, pH, ionic strength and temperature may sometimes be responsible to lose the biological activity, as immobilized enzymes are very much sensitive towards environmental changes.

3.3.4.4.1 Optimization of HRP units

Since HRP catalyses the reaction of H_2O_2 with luminol, the ratio of COD and HRP enzymes on biosensor surface might influence the overall performance of the bienzyme biosensors.

The effect of enzyme COD/HRP ratio (ranging from 0.5 to 20) on response for choline biosensor was examined (Figure 3.8).

The largest CL intensity response is observed for COD/HRP ratio of 1IU : 0.1IU (*i.e.*, when COD unit is 10 times higher than HRP). Thus, it suggests that the HRP molecules at this ratio are sufficient in the sequential reactions by comparison with COD in COD/HRP system.

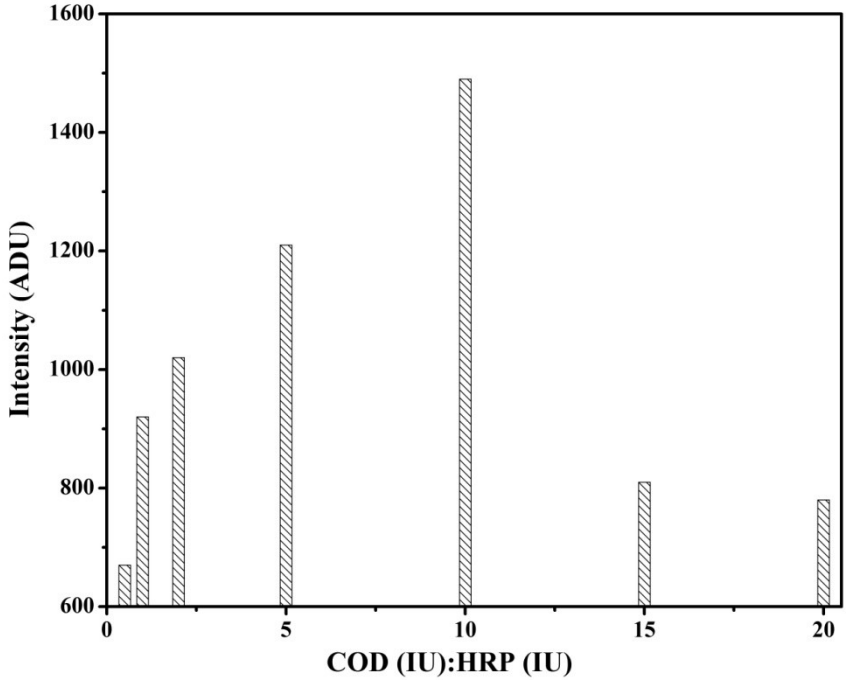

Figure 3.8 Optimization of HRP: COD units (all solutions are in 100 mM PB at pH~ 7.4; 1 mM ChCl).

3.3.4.4.2 Optimization of the COD units

As COD is the main enzyme that imparts selectivity for choline, thus its optimization in concentration is needed in the construction of ZnONR biosensor keeping other parameters like temperature, pH, ionic strength and amount of HRP constant.

The optimal concentration of COD used in the CL ZnONR biosensor system was investigated by measuring the CL intensities in the presence of different concentration of COD and same quantity of the other reagents. Immobilized COD amount on the biosensor response was studied by varying the concentration of COD from 0.4 to 2 IU/µL keeping the HRP units constant (0.1 IU/µL). From Figure 3.9, it is found that the effect has been enhanced with the increasing quantity of COD up to 1 IU/µL.

The figure clearly shows that the stable CL intensity that has been measured after 15 min is for the 0.8 IU/µL and 1 IU/µL COD using 1 mM ChCl. However, the stability of signal intensity extends to varying concentrations of ChCl only when 1 IU/µL COD is used. Thus, in order to realize the system effectively, 1 IU/µL COD has been used for subsequent experiment.

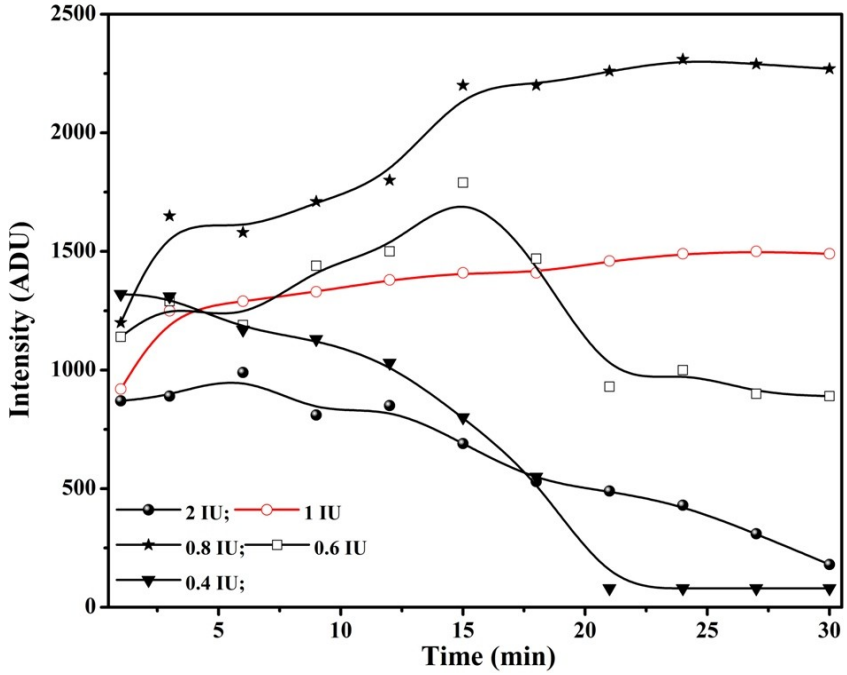

Figure 3.9 Influence of COD concentration; 0.4, 0.6, 0.8, 1.0 and 2 IU/µL (all solutions are in 100 mM PB pH~ 7.4; 1 mM ChCl).

Further, the reaction time of COD on ZnONR choline biosensor was optimized (Figure 3.7). The CL intensity of the mixture is gradually increased to a maximum value within 15 min. The result suggests that the catalysed oxidation process of choline is finished in 15 min. Thus, the time of 15 min has been adopted as the incubation time for subsequent experiments.

3.3.4.4.3 Optimization of ionic strength and pH

The influence of the ionic strength and pH of PB on the activity of the enzyme was studied. Measurements were carried out on ZnONR system with various ionic strengths (10, 50, 100, 150 and 200 mM PB) and pH (6.4–7.8) for 1 mM ChCl. The results are presented in Figure 3.10.

It is evident from Figure 3.10 (i) that COD/HRP exhibits maximum activity at pH 7.4 which is ideal pH balance for a healthy body. It is also clear from Figure 3.10 (ii) that with increase

in the ionic strength of PB, response signal increases up to 100 mM, and then decreases. This suggests to carry out the future experiments at the pH of 7.4 with 100 mM PB. For this, milk and PB were mixed in different ratios (1:1-1:12) for the analysis of pH and ionic strength. Milk : PB at 1:4 dilutions has been stabilized at the pH and ionic strength.

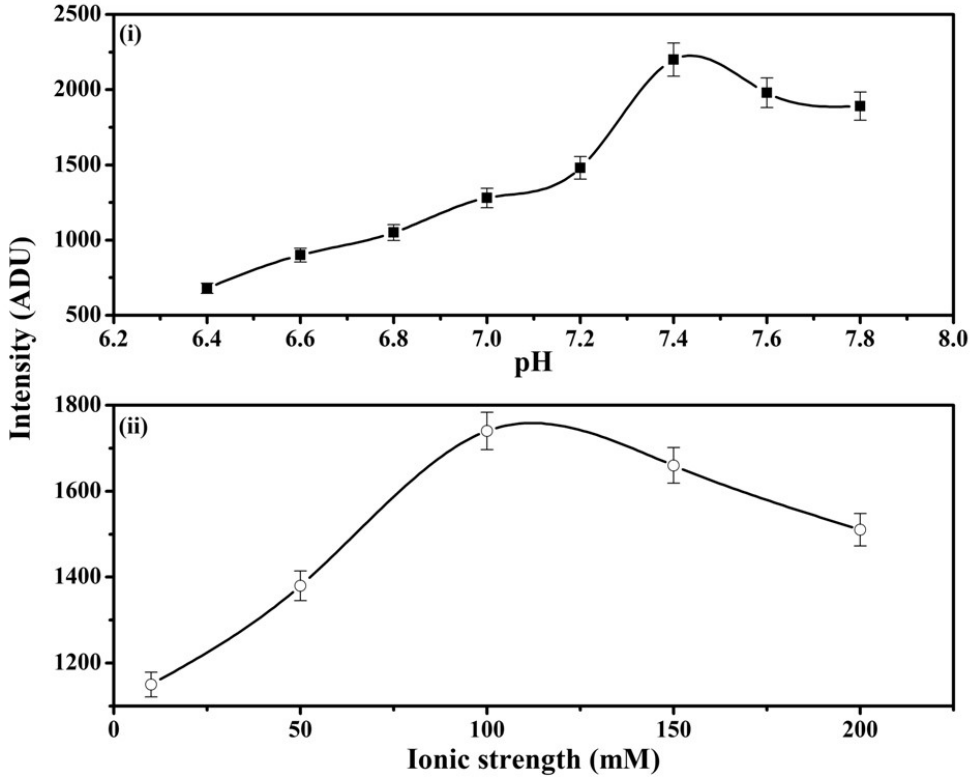

Figure 3.10 Effect of PB (i) pH (6.4–7.8); (ii) ionic strength (10, 50, 100, 150 and 200 mM) on the response of ZnONR choline biosensor for 1 mM ChCl.

3.3.4.4.4 Optimization of temperature

The activities of free and immobilized enzyme were measured at different temperatures in the range 25 to 50 °C to determine optimal temperature for enzyme activity. The optimum temperature was determined for free and immobilized enzymes as shown in Figure 3.11.

While the physisorbed enzymes show low signal response in the studied temperature range (25 – 50 °C), the co-immobilized enzymes exhibit significantly higher activity in the same temperature range. Enzymes immobilized through 16-PHA exhibit the highest change over the free enzyme activity. Both physisorbed and immobilized enzymes loose activities in the temperature range 40 - 50 °C. The residual activity is 3.7% for the physisorbed enzymes and

5.5% for enzymes immobilized at the same temperature (50 °C). Above 35 °C, the enzyme activity is dropped significantly due to the thermal inactivation.

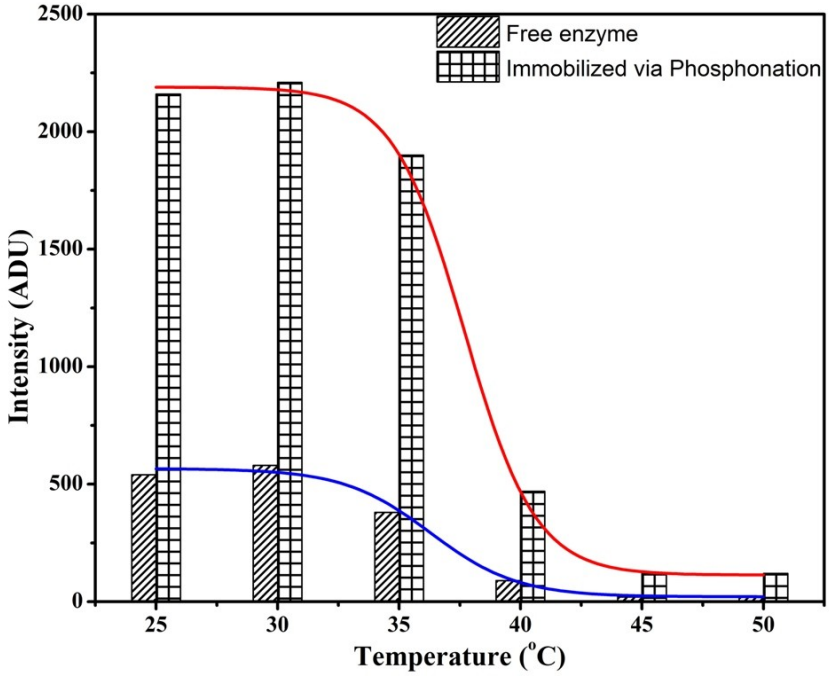

Figure 3.11 Influence of temperature on activity of enzyme over physisorbed ZnONR and 16-PHA-ZnONR in the range of 25 – 50 °C; 100 mM PB at pH ~ 7.4; 1 mM ChCl.

3.3.4.4.5 Enzyme kinetics

The enzyme activities were determined at different substrate concentrations under the optimum conditions. Michaelis–Menten constant (K_m) (equation 3.1) values of the immobilized enzymes were determined using LineWeaver-Burk plot.

$$1/V = K_m/ V_{max} \times 1/[S] + 1/V_{max} \quad (3.1)$$

Where V, V_{max}, [S] and K_m are initial velocity, maximum velocity and initial substrate concentration, respectively.

3.3.4.5 Effect of surface modification

The stability of the bienzymes (COD/HRP) coupled to the ZnONR was evaluated when enzymes were attached on the surface via covalent coupling as against the physically adsorbed COD/HRP. The kinetic intensity profile of the resulting signal was recorded as Figure 3.12.

The signal attends a stable value (95% of the steady state) after 15 min (as is evident from Figure 3.12). The covalently attached enzyme shows significantly higher signal intensity over the physically adsorbed enzymes.

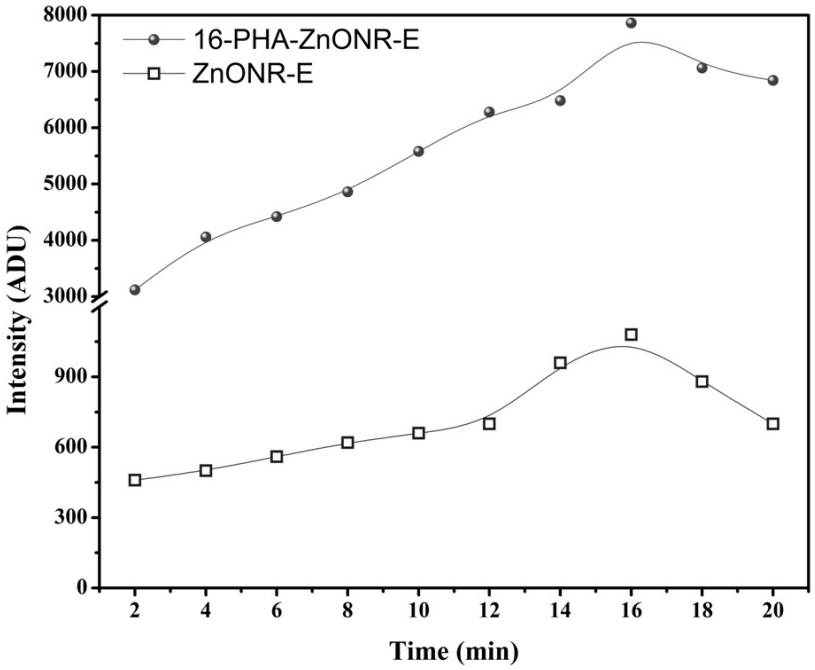

Figure 3.12 Comparison of the kinetic response of COD/HRP activity (covalently coupled against physically adsorbed) on ZnONR film.

The order of the stable signal intensity recorded for COD/HRP functionalized ZnONR is found to be 7880 ADU (via phosphonation) and 1070 ADU (physisorbed *i.e.* non-specifically adsorbed COD/HRP) respectively. The signal intensities are found to be almost 7 times higher for phosphonated ZnONR as against physisorbed COD/HRP nanorods. These important features of the presented biosensor play an important role to enhance efficacy and specificity towards the rapid signal transfer rate and bio-recognition properties.

3.3.4.6 Calibration of choline nanobiosensor

A calibration curve for choline (0.0005–2 mM), measured in triplicate, using ChCl as substrate is presented in Figure 3.13. The calibration is found to be linear in the range 0.006 mM to 2 mM ($R^2 = 0.99$, n = 5) with R.S.D of 4.1% ± 0.5 for the 16-PHA modified ZnONR (Figure 3.13). The linear equation is; y = 7100.77 + 2519.38x (mM). LOD and LOQ are found to be 0.0005 mM and 0.006 mM respectively by analysing replicate sets of 16-PHA modified ZnONR with good sensitivity about 193 ADU change per decade. Whereas for physisorbed enzyme ZnONR, the linearity is found in the range 0.0125 mM to 0.5 mM (R^2 =

0.98, n = 5) with R.S.D of 6.9% ± 0.8 (Figure 3.13 Inset). The linear equation is; y = 1318.99 + 424.7x (mM). LOD and LOQ are determined as 0.0125 mM by analysing replicate sets with very low sensitivity about 19 ADU change per decade. Lower LOD, LOQ value, R^2 and sensitivity indicate that 16-PHA-ZnONR is much superior over physisorbed enzyme ZnONR. The reported linear range for the developed biosensor covers the free choline concentration (125 mg/day) found in infant formula, and thus the method may be adopted for routine measurements. Moreover, the method may also be easily applied to analyse the normal concentrations of dietary choline intake in milk by mere centrifugation and dilution of samples.

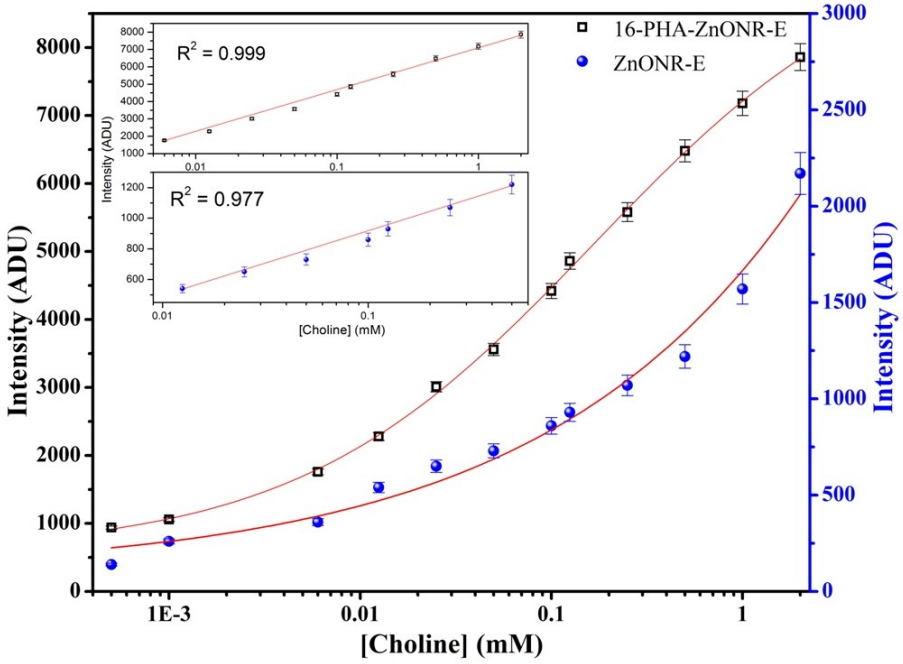

Figure 3.13 Calibration curve for different choline concentration obtained using 16-PHA-ZnONR coupled enzyme and physisorbed enzyme on ZnONR (Inset: linear calibration graph).

3.3.4.7 Operational stability

The stability and reusability of 16-PHA-ZnONR choline biosensor was evaluated against physically adsorbed choline biosensor by performing a series of repeated experiments over 30 days by using a single biosensor as represented in Figure 3.14. The choline biosensor was stored under appropriate environmental conditions *e.g.* at 4 °C before and after the measurements. The response of the biosensor was found consistent for the first 10 days and after 30 days the biosensor response decreased to 78%. The decrease in response may be due

to the reduction of enzyme activity and denaturation of the peroxidase. It is also clear that 16-PHA modified choline biosensor holds good storage stability, sensitivity and reusability for longer duration than physisorbed enzyme on ZnONR surface.

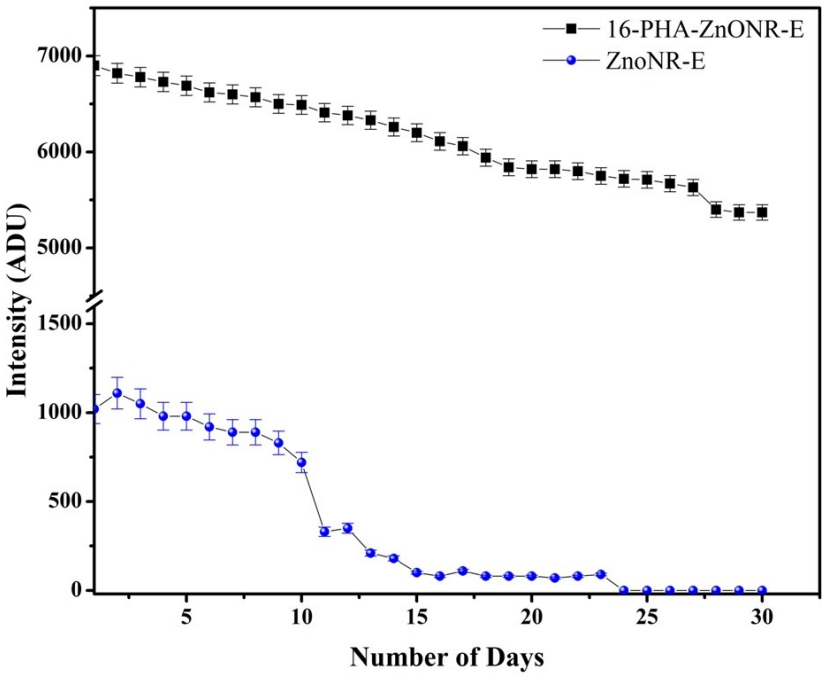

Figure 3.14 The storage stability over 30 days of ZnONR modified with COD/HRP via16-PHA and physisorbed enzyme on ZnONR in 100 mM PB at pH ~ 7.4 at 4 °C.

The enhanced stability of the developed biosensor may be explained in terms of the stability imparted by SAM of 16-PHA crosslinker. The results of the experiment revealed good consistency in the calibration traces even as the surfactant residuals of the solution from 16-PHA-ZnONR choline biosensor was detached by washing in PB solution before each measurement. Repeated measurements on physically adsorbed choline biosensor revealed an unstable and non-reproducible response. The ZnONR is coupled with the phosphate group of the 16-PHA chain on one side. The other end of 16-PHA is covalently coupled to the enzyme COD/HRP via activation of the -COOH group. Thus, the 16-PHA SAMs provide strong binding to the either side of the chain. The improved stability is also established by FT-IR after washing the surface for both physisorbed and chemisorbed ZnONR sensor using PB (Figure 3.15 & Figure 3.16). It is observed that the chemisorbed enzyme is held strongly even after 15 repeated wash as evident from the FT-IR spectra. Due to the fact that enzyme coupled SAMs are retained even after the multiple washing steps. In contrast, for the physisorbed enzyme, these peaks are found absent after the washing step in the FT-IR.

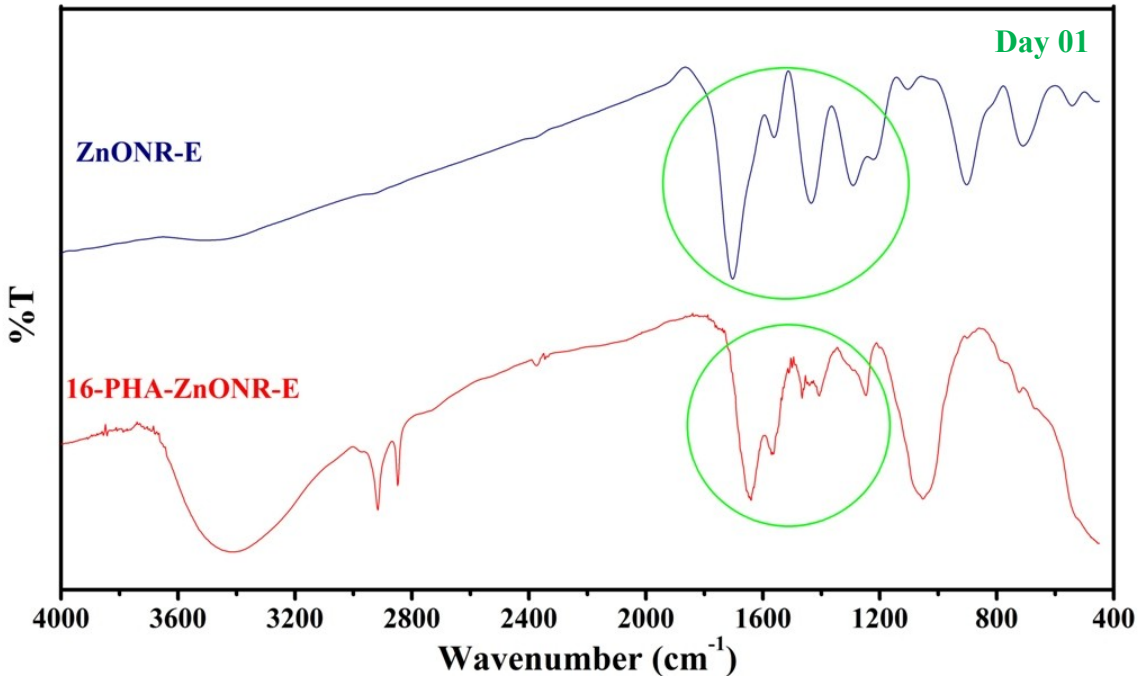

Figure 3.15 FT-IR spectra of physisorbed and chemisorbed enzymes on ZnONR (Day 01) showing all characteristic peaks attributed to the enzyme coupling.

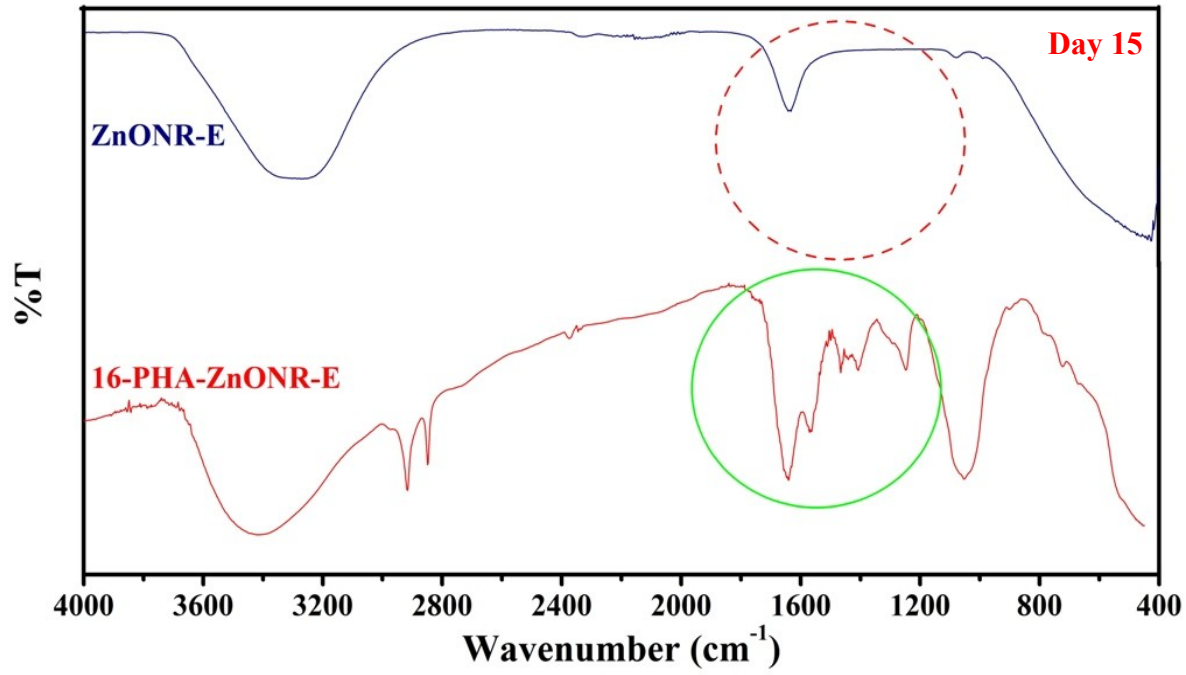

Figure 3.16 FT-IR spectra of physisorbed and chemisorbed enzymes on ZnONR (Day 15) where chemisorbed enzymes on ZnONR showing all characteristic peaks attributed to the enzyme coupling and the characteristic peaks attributed to the enzyme coupling is absent for physisorbed enzymes on ZnONR.

3.3.4.8 Kinetic parameters

The immobilization of enzyme is a well-accepted approach towards stabilization of enzyme (Mateo *et al.,* 2007). An important feature that accounts for enzyme stability is the improvement obtained in the value of K_m. The K_m value obtained using LineWeaver-Burk plot is estimated as 0.062 mM ± 0.06 for COD/HRP coupled via phosphonated ZnONR and 0.2 mM ± 0.09 for COD/HRP coupled via physisorbed enzyme ZnONR. The lower K_m value (almost 0.32 time) reflects higher enzymatic affinity of COD/HRP-coupled via phosphonated ZnONR towards choline as the affinity of phosphate group of 16-PHA is high with ZnO. The figures of merit of choline biosensor has been compared with other recent reported methods and presented in Table 3.2.

Table 3.2 Comparison of various established biosensing techniques for analysis of choline.

Biosensor configuration	**Transducer**	**Linearity (mM)**	**Detection limit (mM)**	**K_m (mM)**	**Stability (response retained)**	**Reference**
CL 16-PHA-ZnONR	Optical	0.006 - 2	0.0005	0.062 ± 0.06	78% after 1 month	This work
Amperometric ChOx /HRP immobilized on carbon paste electrode	Electro-chemical	0.00005-0.007	0.00001	n.r[#]	1 month	Razola *et al.*, 2003
ChOx in CdTe quantum dots	Optical	0.005 - 0.15	0.0001	0.20	n.r.[#]	Chen *et al.*, 2011
Flow Injection Analysis-Enzyme immobilized on CPG support	Thermal	0.03 - 0.5	0.03	0.45	more than 85% after 15 months	Deshpande *et al.*, 2011a
Fluorescent conjugated polymer	Optical	0.0001-0.02	0.00005	n.r[#]	n.r[#]	Li *et al.*, 2013

[#]Not reported

3.3.4.9 Recovery studies and real sample analysis

Recovery studies were performed on 16-PHA modified ZnONR for three different fat% milk samples (0.5, 1.8 and 3.5). The study was repeated with milk samples spiked with standard choline solution (1, 0.1 and 0.01 mM) to evaluate sensor performance for inter-batch and intra-batch reproducibility. The summaries of findings are tabulated in Table 3.3 with mean recovery intra-day R.S.D% 0.53 ± 0.17 and mean inter-day R.S.D% was calculated as 0.93 ± 0.16.

Table 3.3 Recovery of choline from different fat % milk sample as determined by ZnONR choline biosensor to assess the recovery efficiency using developed assay.

Milk samples with different fat %	Choline spiked (mM)	Intraday		Interday	
		Recovery %	R.S.D. %	Recovery %	R.S.D. %
Milk-1 (0.5%)	1	98.1 ± 0.30	0.33	97.3 ± 0.21	0.64
	0.1	97.4 ± 0.65	0.49	94.0 ± 0.57	0.75
	0.01	101.0 ± 0.23	0.57	96.1 ± 0.60	1.04
Milk-2 (1.5%)	1	97.1 ± 0.60	0.70	93.3 ± 0.37	0.84
	0.1	103.1 ± 0.78	0.67	97.5 ± 0.41	0.93
	0.01	98.3 ± 0.43	0.42	96.0 ± 0.69	1.10
Milk-3 (3.5%)	1	95.2 ± 0.29	0.28	94.7 ± 0.47	0.92
	0.1	97.9 ± 0.71	0.78	91.3 ± 1.01	1.05
	0.01	98.6 ± 0.56	0.53	97.0 ± 1.09	1.07

3.4. Development of ZnONPs based bioassay for OPs

Note: The work incorporated in this section of the thesis had resulted in Intellectual Property, Indian Patent application No. 3456/MUM/2013. Thus, due to non disclosure commitment to the funding agency, some of the details are not disclosed.

3.4.1 State of the art for analysis of OPs

OPs are the most widely used pesticides of both agricultural and residential settings in the world. Owing to the high toxicity, extensive use of OPs for pest control results in excessive pesticide residues in food, water as well as environment, posing a highly severe threat on human life (Pocai *et al.,* 2006). Organophosphate-based chemicals, acting as anti-cholinesterase substances, are widely used throughout the world (Gordon and Rowsey, 1998). Undoubtedly, OP residues in crop, livestock, and water pose a severe threat to human life. A variety of acute and chronic effects may be experienced following repeated or prolonged exposure to organophosphate-based pesticides, which include nausea, headache, and confusion (O'Malley, 1997). Little information has been gathered with respect to the long-term effects of sub lethal doses over a period of time, but reports of depression, memory loss and chronic fatigue syndrome have been documented (Rupa *et al.,* 1989). The carcinogenic effect of organophosphate-based pesticides has also been postulated (Hayden *et al.,* 2010). EU has set a limit for pesticides in baby foods. According to this regulation, infant foods must not contain residues of individual pesticides at levels exceeding 0.1μg L^{-1} (ppb) per pesticide and 0.5 μg L^{-1} (ppb) for the total amount of pesticides, which is in practice, the minimum detectable level using the officially accepted detection methods (European Commission (EC), 1999). FSSAI has set the limits for pesticides in different matrices. For milk and milk products, the tolerance level is 0.01 ppm for chlorpyrifos and 0.001 ppm for Malathion (FSSAI, 2006). Therefore, rapid determination and reliable quantification of trace level of OPs have become increasingly important. Well established methods over the past decades for OPs monitoring include various chromatographic techniques coupled with various detectors (Albanis *et al.,* 2004; Rotiroti *et al.,* 2005; Leandro *et al.,* 2006). These methods, however, require complicated pre-treatment steps, extensive labour resources, and are not applicable for on-site determination.

For food safety, quick and accurate tests are essential to allow the detection of contamination in foods before they are distributed to consumers. Therefore, portable biosensors that might be applied for on-site rapid detection are of great practical interest. Various biosensors with

different signal transduction mechanisms, including enzymatic bio-assay (Mishra *et al.,* 2010b; Deshpande *et al.,* 2011b), ELISA (Kim *et al.,* 2003; Liu *et al.,* 2009b), electrochemistry (Mulchandani *et al.,* 2001b; Mishra *et al.,* 2012), microcantilevers (Yang *et al.,* 2003; Karnati *et al.,* 2007) and quartz crystal microbalances (QCM) (Kim *et al.,* 2007) have been reported to detect OP compounds. Most of these methods involve the inhibitory effect of OP compounds on the enzymatic activity of acetylcholinesterase (AChE) (Van Dyk and Pletschke, 2011).

3.4.2 Nanomaterials for detection of OPs

The obstacles to exploitation have been fundamentally related to the presence of biomaterial in the biosensor, the development of the sensor device and the integration of biosensors into complete systems. Major fundamental and technological advances need to be made towards enhancing sensitivity, selectivity and reliability of OPs residues biosensors, and the emergence of nanotechnology may open new horizons and satisfy the above targets. Nanomaterials are attractive because of their unique electrical, chemical and physical properties (*i.e.* size, composition, conductivity, magnetism, mechanical strength, and light-absorbing and emitting). The most studied nanomaterials, CNTs, graphene, NPs and QDs have been especially targeted for developing novel biosensors (Liang *et al.,* 2014; Walcarius *et al.,* 2013) (Table 3.4).

Table 3.4 Nanomaterials based biosensors for detection of OPs residues.

Nanomaterials used	Transduction principle	Limit of detection (LOD)	Reference
CNT-modified glassy carbon electrode	Electrochemical	0.0004 mM	Liu and Lin, 2006
ZrO_2 NPs	Electrochemical Immunosensor	0.02 nM	Du *et al.,* 2011
AuNPs	Colorimetric assay	1.40 ng mL^{-1}	Li *et al.,* 2011
Rhodamine B covered AuNPs	Dual readouts (colorimetric and fluorometric)	Diazinon 0.1 µg L^{-1}, malathion 0.3 µg L^{-1}, phorate 1 µg L^{-1}.	Liu *et al.,* 2012a
Fe_3O_4NPs	Electrochemical	0.1 nmol L^{-1}	Chauhan and Pundir, 2012

Aggregation of AuNPs	Photometric	36.3 µg L^{-1}	Kim *et al.*, 2014

By utilizing nanomaterials, the biosensors have shown great promising feature for the detection of chemical markers and biomarkers of exposure, primarily because the nanomaterials are used as signal transducers to mediate current flow or as recognition agents and electroactive tags to indicate the detection of analyte. Nanotechnology may be expected to be an effective approach to develop more sophisticated multi-analyte detection systems with low costs.

3.4.3 Experimental section

3.4.3.1 Chemicals and biochemicals

Reference material for organophosphate residue analysis pesticide mixture-174 PESTANAL grade purity 99.8% was purchased from Dr. Ehrenstorfer GmbH (Germany). Zinc oxide nanopowder (<100 nm particle size) (ZnONPs), Acetylcholinesterase (EC 3.1.1.7) from Electrophorus electricus (electric eel) (AChE), acetyl choline chloride (AchCl) were purchased from Sigma-Aldrich (USA). Other chemicals and biochemicals are used as described earlier section 3.3.3.1.

3.4.3.2 Solutions and sample preparation

Stock solutions (1 µg mL^{-1}) of OPs were prepared in 5% ACN (v/v) in water. Further dilution of pesticide was made in PB (0.1 M, pH 7.4). Other stock solutions of AChCl (0.01 M), AChE, COD and HRP were prepared in PB and stored at 4 °C. Working solutions were prepared every day by appropriate serial dilutions in 0.1 M PB. EDC (100 mM), NHS (100 mM) solution was prepared freshly in 0.1M PB, pH 7.4.

3.4.3.3 Construction of ZnONPs sensing probe

Conjugation of AChE on ZnONPs is based on the efficient immobilization enzyme through SAMs. The glass containers used for monolayer preparation were cleaned using Piranha solution as described in section 2.3.4 (**caution**: Piranha solution reacts strongly and exothermally with organics). 16-PHA was used for surface modification of ZnONPs as described elsewhere (Section 3.3.3.5). Briefly, 3 mg of ZnONPs was dispersed into 0.5 mM ethanolic solution of 16-PHA under continuous agitation for 72 h. The SAMs functionalized

ZnONPs were rinsed in ethanol followed by DI water. For enzyme immobilization, the carboxylic acid-terminated SAMs were activated using an aqueous equimolar solution of 100 mM EDC /100 mM NHS for 2 h at room temperature. The resultant NHS ester monolayers were reacted for 3 h in a solution of AChE (1 IU/µL). The covalently coupled enzyme (AChE) on ZnONPs was washed using PB.

The enzymatic reaction was carried further by adding reaction mixture containing AChCl, COD, HRP and luminol. H_2O_2 thus produced using ZnONPs-AChE in presence and absence of pesticide residues, were counted and quantified using CL technique (Figure 3.17).

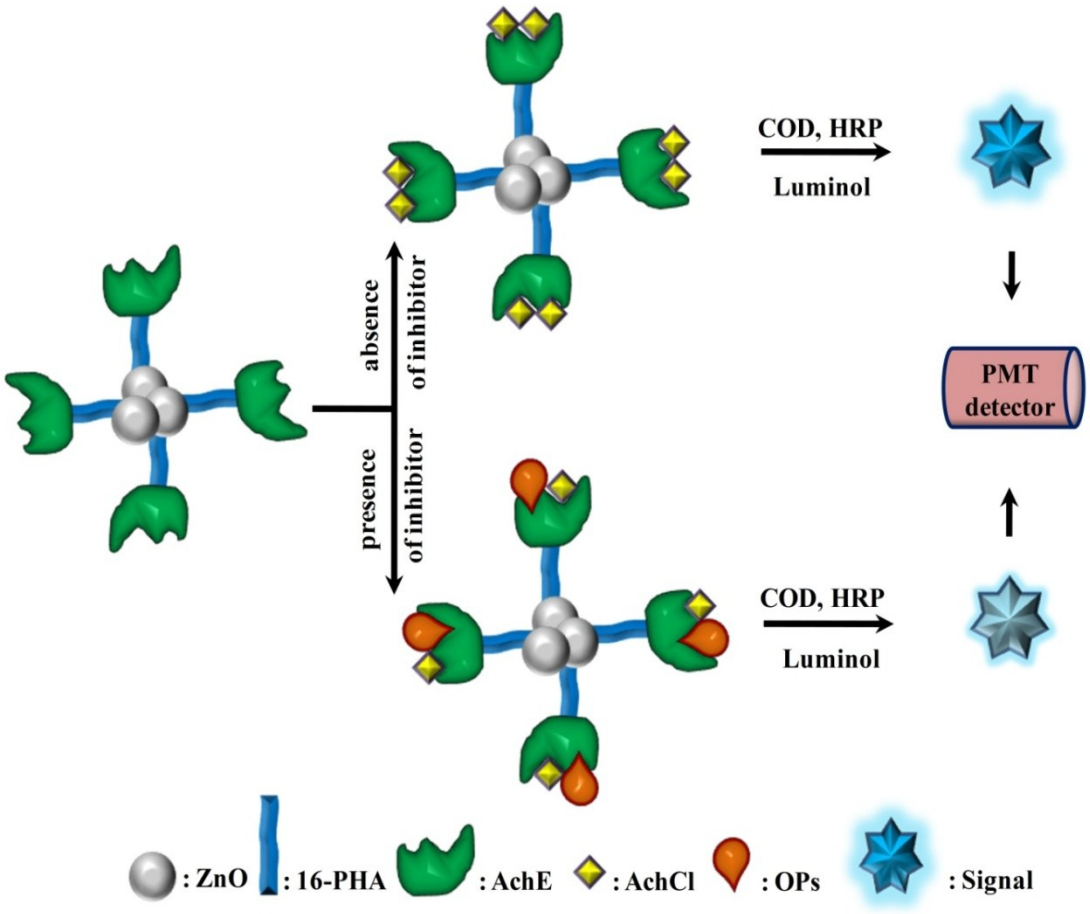

Figure 3.17 Schematic pathway for the detection of OPs using ZnONPs particles.

3.4.4 Results and Discussion

3.4.4.1 Optimization of assay parameters

The CL method described earlier relies of trienzyme reaction resulting in light emission that involves the enzyme AChE, COD and HRP. The optimized experimental parameters such as

pH, ionic strength of PB, temperature, COD and HRP units were used as described in earlier section 3.3.4.4. It is observed that AChE in trienzyme reaction gives optimum performance with 0.1 M PB, pH 7.4 at 30 °C with COD/HRP ratio of 1IU : 0.1IU in presence of 0.5 mM luminol.

The amount of AchE to be immobilized was also optimized keeping the other parameters constant. The plot of the graph is presented in Figure 3.18. Varying amount of AchE immobilized particles were tested to obtain a stable result for a fixed time interval. The AchE amount of 0.045 IU μL^{-1} has been shown promising result as it gives a stable signal intensity almost through out the measurement.

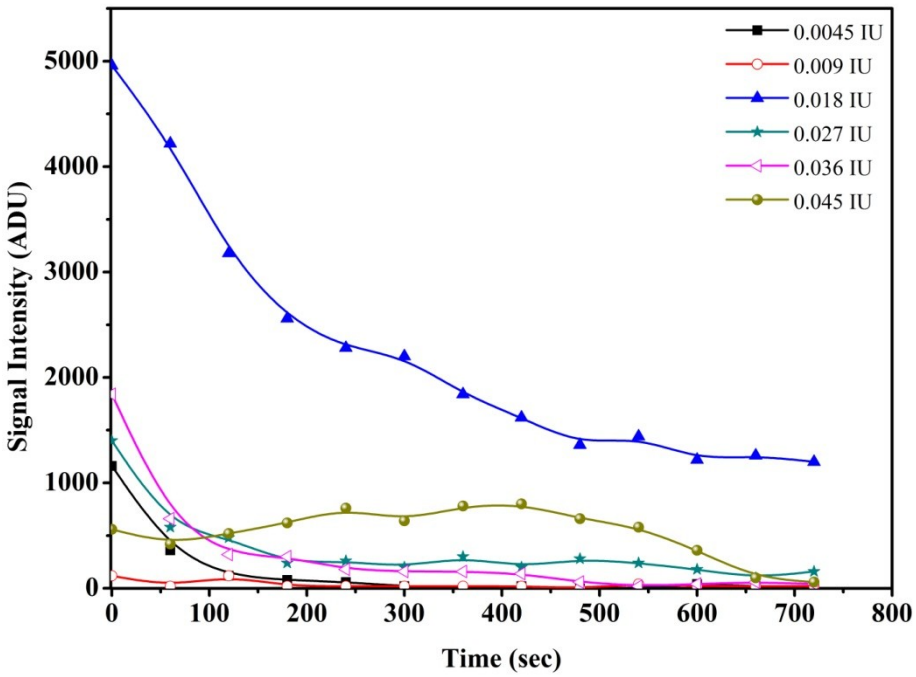

Figure 3.18 Optimization of AchE amount on the ZnONPs.

Also the amount of particles is an influential factor for the system. The high amount of particles as well as low could cause lowering of the intensity. The graph has been plotted as shown in Figure 3.19. The varying amounts of particles (0.5, 1.0, 1.5, 2 and 3 mg mL^{-1}) were taken for the kinetic measurement. The 2 mg mL^{-1} of particle has shown the highest signal intensity with respect to the other. So, subsequent experiments have been carried out using 2 mg mL^{-1} particles.

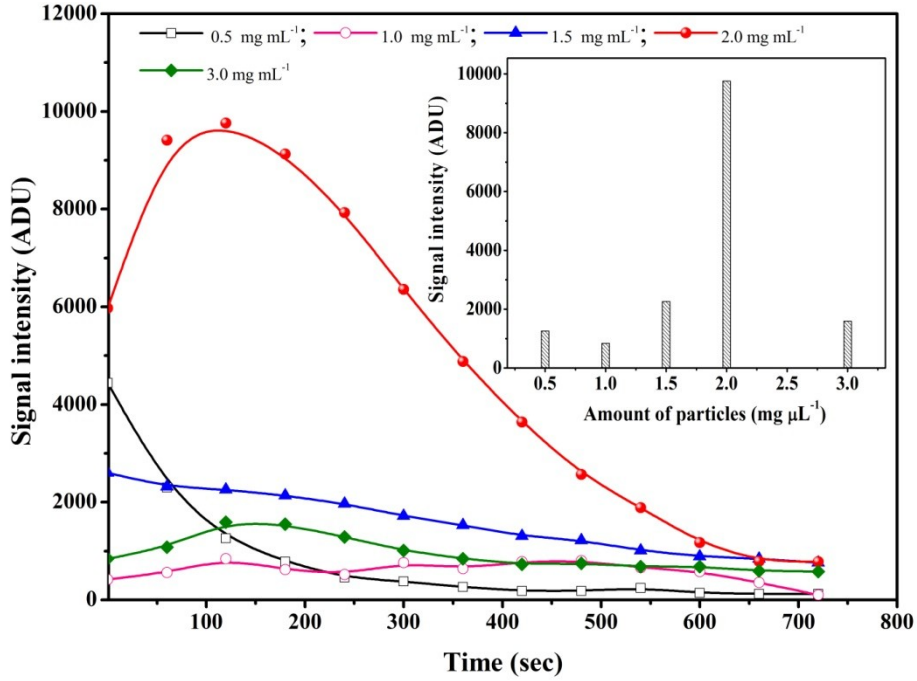

Figure 3.19 Optimization of ZnONPs amount.

3.4.4.2 Calibration curve for AchCl

The initial activity of the immobilized enzyme was first determined by recording the change in CL intensity. The enzyme kinetics was monitored using various concentrations of AchCl ranging from 0.01 mM to 10 mM. The kinetics data was recorded for 900 sec and presented in Figure 3.20 (a). It is clear from the figure that the kinetic response reaches its maximum at 120 sec. Also higher signal intensity is observed by increasing substrate concentration. The highest signal intensity is observed at 120 sec for all the AchCl concentrations. After 120 sec the signal intensity tends to decrease to attend almost no change in signal. Using the stable maximum response, a calibration curve has been plotted and presented in Figure 3.20 (b). The data fitting curve shows a linear plot in the range 0.01 mM to 10 mM. R^2 is found to be 0.994. The linear equation of the fitted curve is; y = 565.01609 x (mM) + 955.22035. Among the several tested AchCl concentrations, 1 mM AchCl is found optimal one for the enzyme inhibition experiment. Further, the K_m that obtained using LineWeaver-Burk plot (equation 3.1), is found at 0.591 ± 0.013 mM.

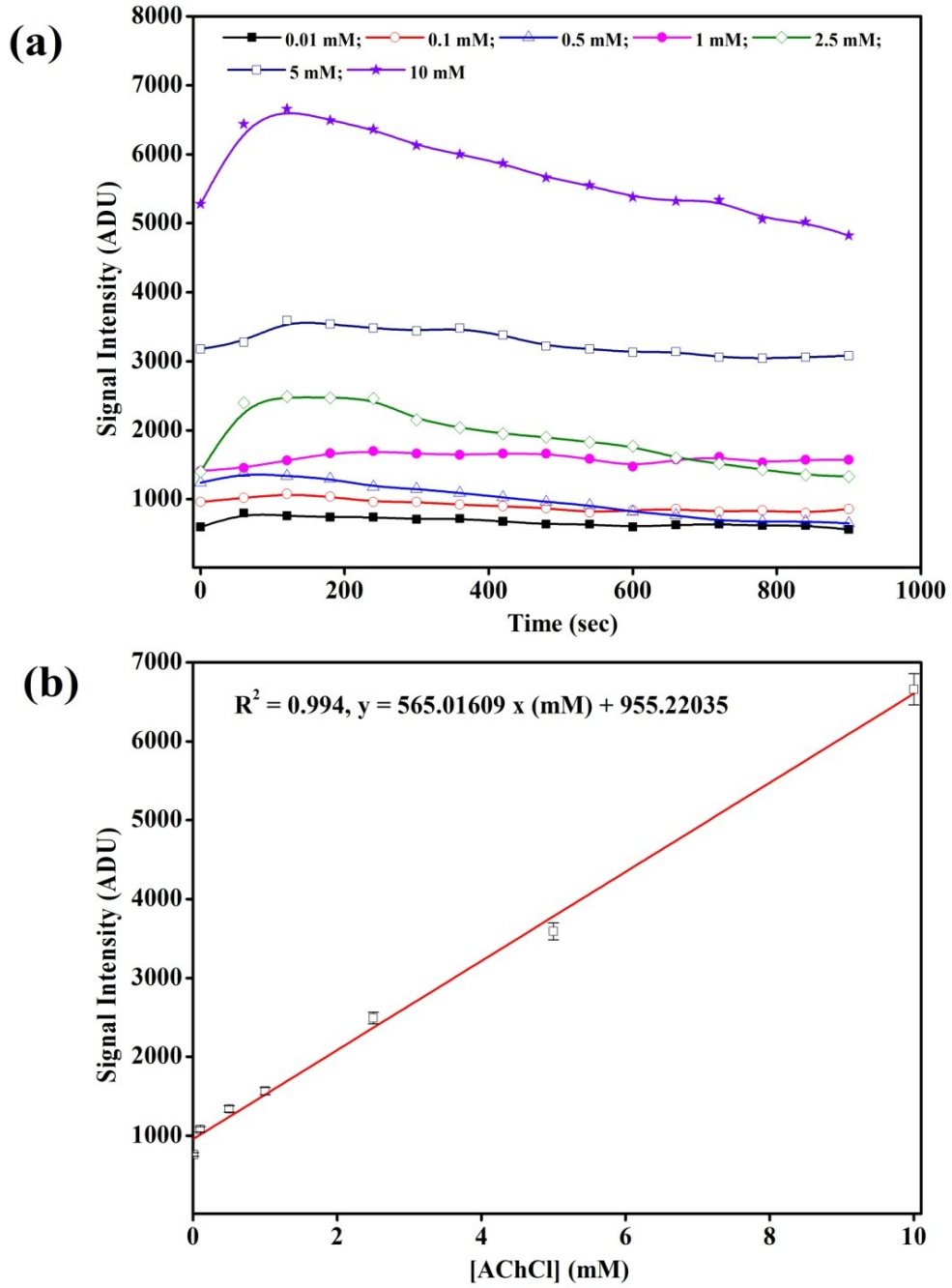

Figure 3.20 (a) Enzyme – substrate (AchE - AchCl) kinetics using optimized parameters; (b) calibration curve for different AchCl concentrations.

3.4.4.3 Optimization of incubation time

In order to optimize incubation time, most influential parameter for OPs and enzyme reaction, inhibition assay has been performed using 1 ppb OPs mixture at different incubation time (5 min, 10 min and 15 min). The plotted data has been presented in Figure 3.21. The signal intensity is found to decrease gradually with increasing incubation time. The signal

intensity during inhibition was saturated slowly and reached its maximum at 180 sec. The I % has been calculated using the signal intensity at 180 sec (equation 2.5). The highest I % value (78.56%) is observed for the sample incubated for 15 min. For the time longer than 15 min, the curve tends to a stable value, indicating that the binding interaction with active target groups in enzyme reaches saturation.

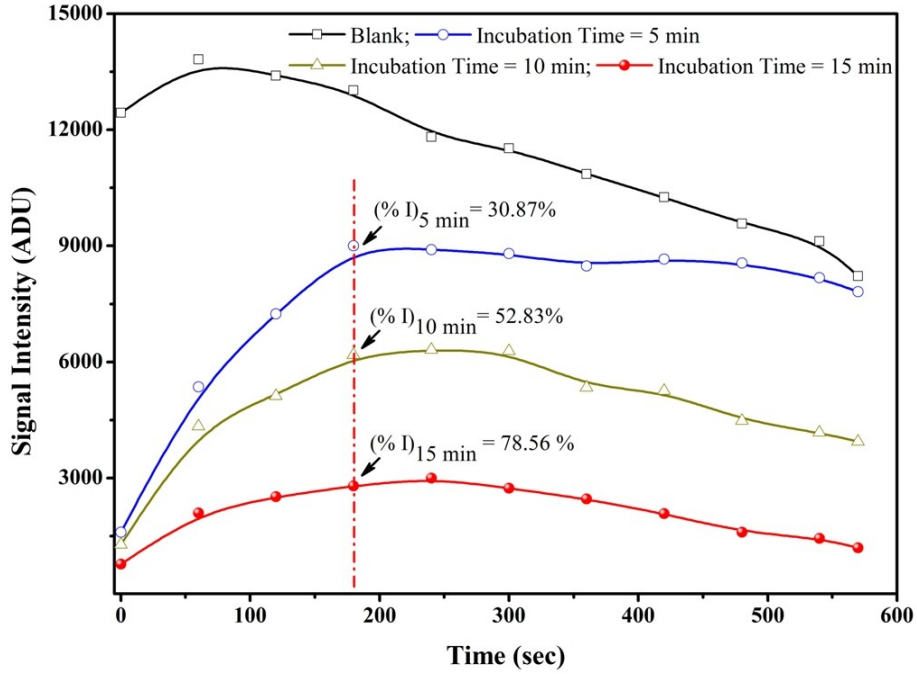

Figure 3.21 Optimization of incubation time for inhibition using optimized assay parameters.

However, the maximum value of inhibition is not 100%, which is likely attributed to the binding equilibrium between pesticide and binding sites in enzyme. Thus, time of 15 min incubation is used in subsequent experiment.

3.4.4.4 Inhibition studies and calibration curve

Based on the results obtained above, this work further explored pesticide sensitivity to AChE. Organophosphate pesticide mixture was used for this purpose. Figure 3.22 illustrates the inhibition curves for various concentrations of OPs ranging from 0.01 ng mL^{-1} to 5 ng mL^{-1}. With an increase in concentration of different pesticide solutions, the signal intensity decreases greatly *i.e.*, increasing inhibition on AChE. The maximum signal intensity for inhibition is not more than 3 min after which the signal intensity tends to attain a stable value, indicating the binding interaction with active target groups in enzyme attains saturation. The

maximum values of inhibitions for OPs were not 100%, likely due to the binding equilibrium between pesticide and binding sites in enzyme.

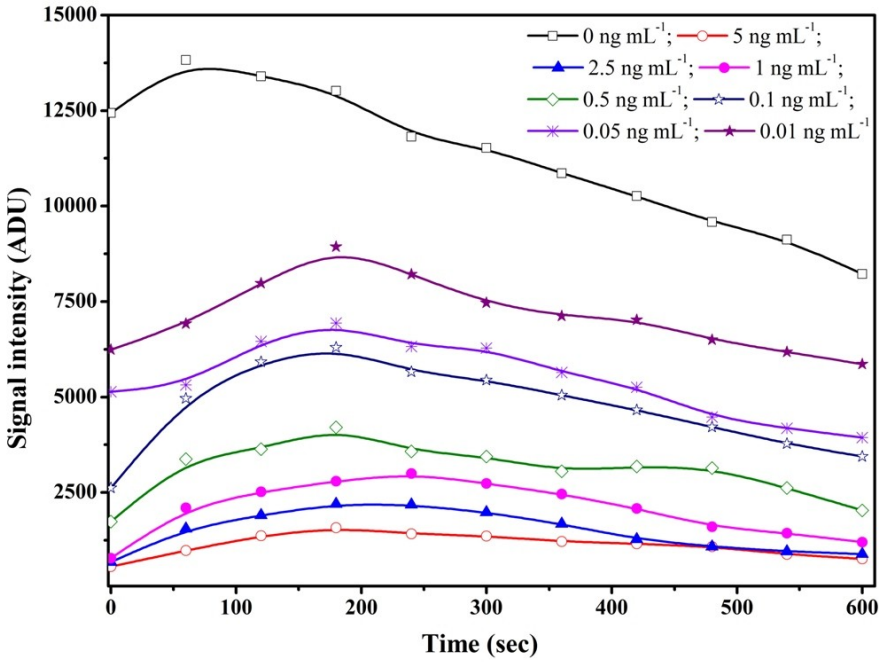

Figure 3.22 Inhibition curves for various concentrations of OPs mixture ranging from 0.01 – 5 ng mL^{-1}.

The two way inhibition curve in the range 0.01 ng mL^{-1} to 5 ng mL^{-1} using signal intensity and I % against the various concentrations of OPs has been plotted in Figure 3.23.

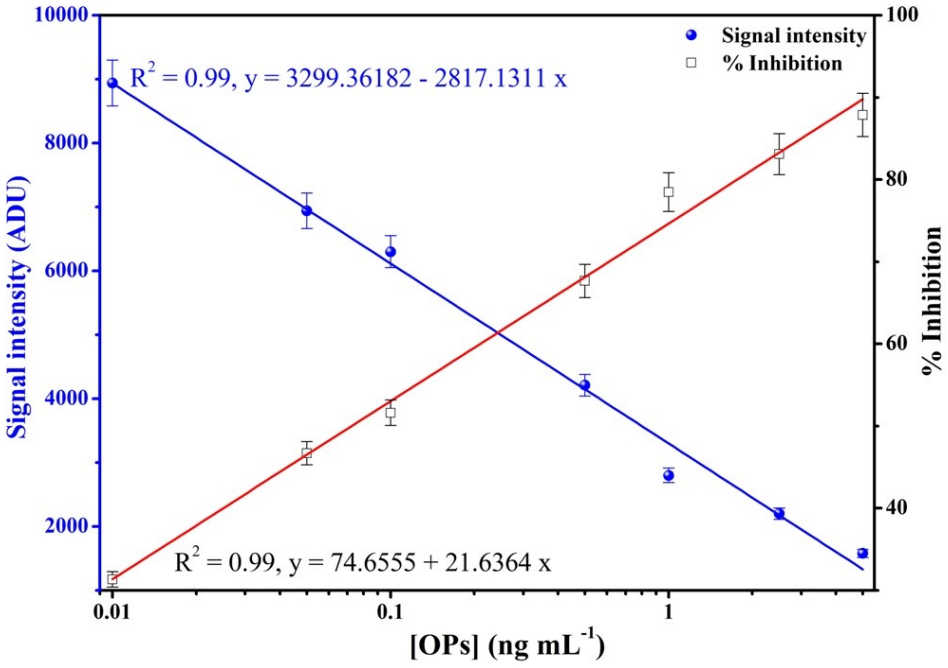

Figure 3.23 Calibration curve for OPs under optimized condition.

The I % was calculated using the equation 2.5. The signal intensity is found to decrease with increasing OPs concentration. The linear equation is; y = 3299.36182 - 2817.1311 x (ng mL^{-1}) (R^2 = 0.99, n = 5). The calculated I % is plotted against various OPs concentration and also fitted linear in the range 0.01 – 5 ng mL^{-1} (R^2 = 0.99, n = 5). The linear equation is; y = 74.6555 + 21.6364 x (ng mL^{-1}). The LOD and LOQ of the developed sensor are found to be 0.01 ng mL^{-1}. The K_m for the inhibition as calculated using previous equation 3.1 is found to be 0.853 ± 0.011 ng ml^{-1}.

3.5 Bio-catalysis using novel ZnO-$ZnAl_2O_4$ whiskers

3.5.1 Introduction

Recently, it has been reported that the performances in applications can be improved by alloying ZnO (Chen *et al.,* 2010). The sensing properties can be improved by alloying with other metals such as titanium and antimony (Shokry Hassan *et al.,* 2013). Doping of vanadium in ZnO has improved piezoelectric properties (Yang *et al.,* 2008). ZnO doped with Al_2O_3 is known as Zinc aluminate ($ZnAl_2O_4$). It has been used as a catalytic and optical material (Farhadi and Panahandehjoo, 2010). Although $ZnAl_2O_4$ has been synthesized in the form of nanotubes, nanoparticles and hierarchical form but the reports on composite of ZnO/$ZnAl_2O_4$ NPs are scarce. From biological application point of view, both ZnO and $ZnAl_2O_4$ are biocompatible (Suárez-Franco *et al.,* 2013; Zhao *et al.,* 2012; Rico *et al.,* 2011; Alvarez-Pérez *et al.,* 2009; Zhao *et al.,* 2009). One such testimony for biological application using enzyme coupled ZnO nanostructure biosensor technique has been reported recently (Pal *et al.,* 2014).

3.5.2 Importance of Alkaline phosphatase

Alkaline phosphatase (ALP), a nonspecific phosphomonoesterase found widely in many mammalian tissues (Lallès, 2010), involves in various metabolic functions such as fat absorption, mucosal defense and skeletal mineralization. ALP catalyzes the hydrolysis of phosphomonoesters, releasing free inorganic phosphate and alcohol (Chung *et al.,* 2010; García Sánchez *et al.,* 2003). In analytical chemistry, ALP is often used as a major target to probe causative disease mechanisms. In the milk industry, determination of ALP activity is a significant matter, since it is used as a parameter for pasteurization control and for disease diagnostic purposes (Claeys *et al.,* 2002). Studies of ALP activity and screening of its

inhibitors are required to develop potential drug therapies for osteoarthritis, idiopathic infantile arterial calcification and end-stage renal diseases (Iqbal, 2011). Many ALP assays use free enzyme in a homogeneous solution, which may be susceptible to denaturation. It is difficult to reuse or recover enzyme in solution forms. Immobilized enzymes are reported to retain enzymatic activity and also contribute to improve its stability (Wang *et al.,* 2012). Effectively, immobilized ALP has potential applications in the fields of biochemistry, food industry, clinical diagnosis and environmental engineering (Goriushkina *et al.,* 2009; Liu *et al.,* 2012b). Thus, the need for the development of a novel yet simple, efficient and economic immobilized biochip is extremely important.

ALP catalyses the hydrolysis of phosphate esters in alkaline buffer and produces a yellow colour compound *para*-nitro phenol and inorganic phosphate which can be measured at 405 nm. The principle of *p*NPP bio-catalysis is presented in Figure 3.24.

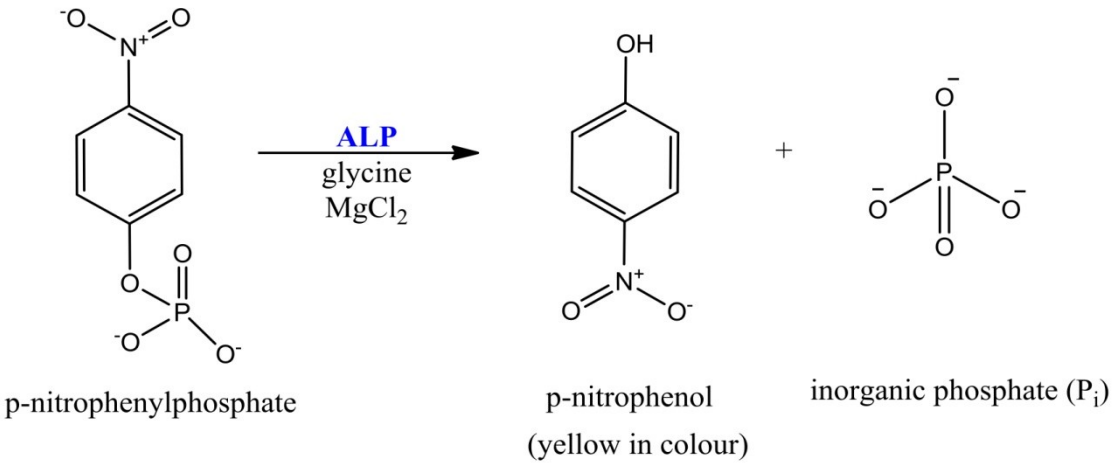

Figure 3.24 Reaction pathway for bio-catalysis of *p*NPP using ALP.

3.5.3 Experimental section

3.5.3.1 Chemicals and biochemicals

Phosphatase, alkaline from calf intestine, grade 1 was purchased from Roche Diagnostics (Germany) and 4-Nitrophenyl phosphate disodium salt hexahydrate (*p*NPP) was purchased from Fluka (UK). Magnesium chloride, Glycine, Sodium hydroxide and other chemicals were of GR grade Merck (Germany). Micro pipettes (Eppendorf, Germany) were used to carry out enzyme assay. Corning, Costar 96 strip-well plates were obtained from Sigma (USA).

3.5.3.2 Device fabrication

The novel device was designed and fabricated at Centre for Applied Research in Electronics CARE, IIT Delhi. The fabrication and characterisation of ZnO-$ZnAl_2O_4$ composite were reported elsewhere (Behera *et al.*, 2015). The formation of ZnO-$ZnAl_2O_4$ composite nanostructures is shown schematically in Figure 3.25.

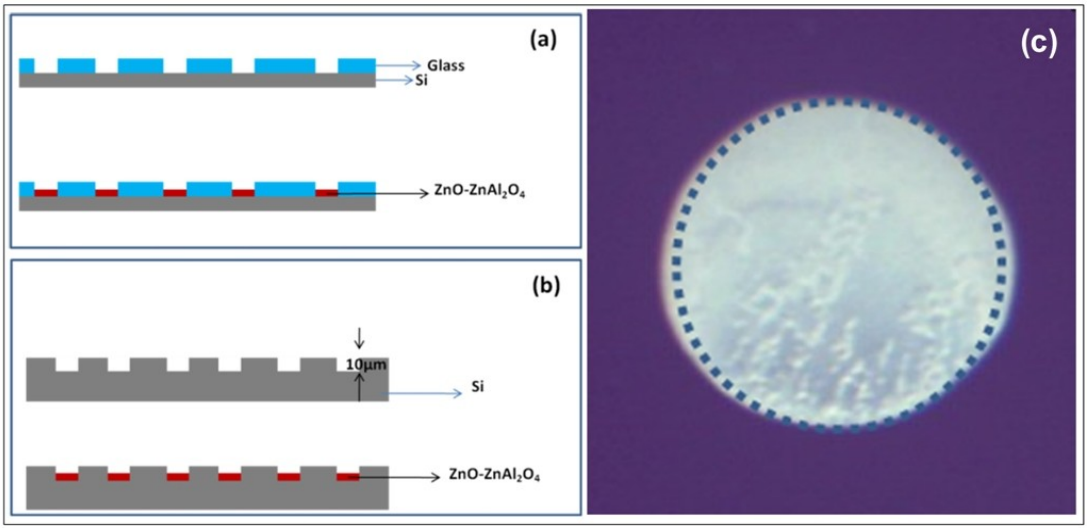

Figure 3.25 Schematic of microwells fabricated using (a) Si-Glass anodic bonding and (b) Si bulk micromachining. (c) Image showing 10 µm depth Si containing ZnO-$ZnAl_2O_4$.

3.5.3.3 Solutions and sample preparation

Glycine (0.1 M) was prepared by dissolving 1.875 g in 250 mL double distilled water. 25 mL of this solution was pipetted out and made to 250 mL. The pH was adjusted to 10.6 using NaOH solution at 27 ^oC. 30 mg *p*NPP was dissolved in 10 mL GB to prepare the strength of 0.01 M substrate. $MgCl_2$, $6H_2O$ (0.01M) was prepared using 20 mg solids in 100 mL double distilled water. The *p*NPP working solutions were prepared in GB ranging from 0.001 mM to 10 mM.

3.5.3.4 Construction of the biochip

Realization of ALP biochip is based on the efficient immobilization of enzyme through SAMs. The glass containers used for monolayer preparation were cleaned with Piranha solution as described in section 2.3.4 (**caution**: Piranha solution reacts strongly and exothermally with organics). ZnO-$ZnAl_2O_4$ microwells were washed with ethanol, and dried under a stream of high purity nitrogen before use. These samples were immersed into 0.5 mM

ethanolic solution of 16-PHA for 72 h to achieve self-assembly. The SAMs functionalized ZnO-$ZnAl_2O_4$ microwells were again rinsed in ethanol followed by double distilled H_2O and dried under a stream of nitrogen. For enzyme immobilization, the carboxylic acid-terminated SAMs were modified using an aqueous equimolar solution of 100 mM EDC /100 mM NHS for 2 h at room temperature. The resultant NHS ester monolayers were reacted for 3 h in a solution of ALP (0.045 IU/µL) in PB (100 mM, pH ~ 7.4). The covalently coupled enzyme microwells (ALP/16-PHA/ZnO-$ZnAl_2O_4$) was taken out from solution and washed as described earlier. To prepare physisorped microwells (ALP/ZnO-$ZnAl_2O_4$), 0.44 IU/µL of the enzyme was also incubated on the microwells for 48 h. The schematic diagram of the enzyme immobilization process is presented in Figure 3.26.

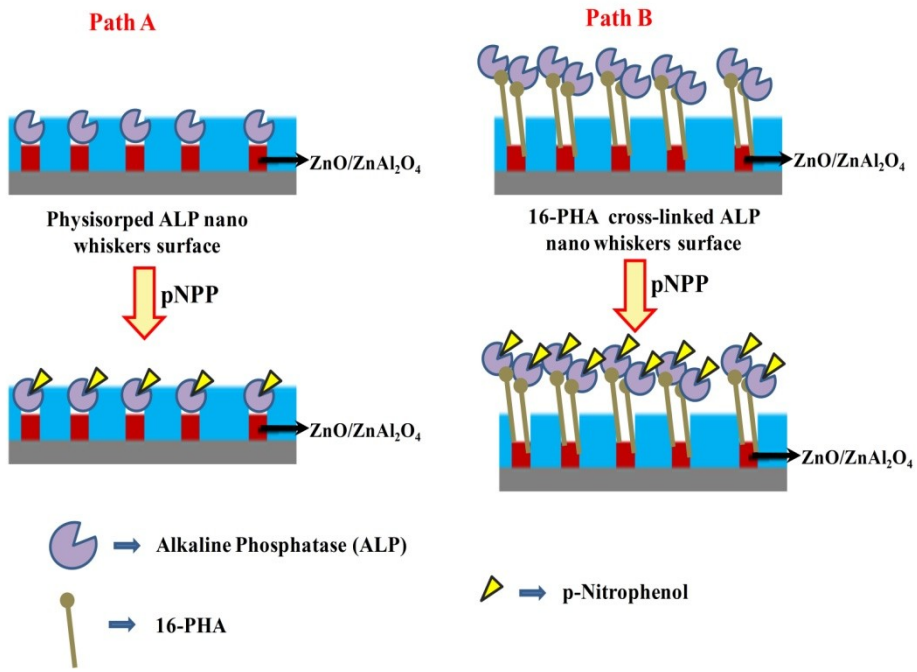

Figure 3.26 Schematic pathway for working mechanism of the ZnO-$ZnAl_2O_4$; Path A: using physisorped ALP and Path B: chemisorped ALP.

In the developed biochip, ALP provides the specificity and acts as a catalyst to initiate the bio-catalysis reaction. The enzyme catalysed reaction between ALP and substrate *p*NPP solution produces yellow coloured water soluble *p*-NP as product of this reaction. The substrate (*p*NPP) is colourless but yellow coloured *p*-NP has a strong absorbance at 405 nm. The rate of increased absorbance at 405 nm is proportional to the enzyme activity. Thus produced colour was quantified using a sensitive photomultiplier system Victor™ X4 2030 Opti-plate reader Perkin Elmer (USA). Fourier Transform Infrared (FT-IR) spectra were

recorded using IRAffinity-1 (SHIMADZU, Japan) with attenuated total reflectance (ATR) attachment Specac Diamond ATR AQUA.

3.5.4 Results and Discussion

3.5.4.1 Surface morphology of ZnO-$ZnAl_2O_4$ whiskers

Figure 3.27 shows the SEM of synthesized ZnO-$ZnAl_2O_4$ whiskers. It is observed that the nanostructures are randomly oriented.

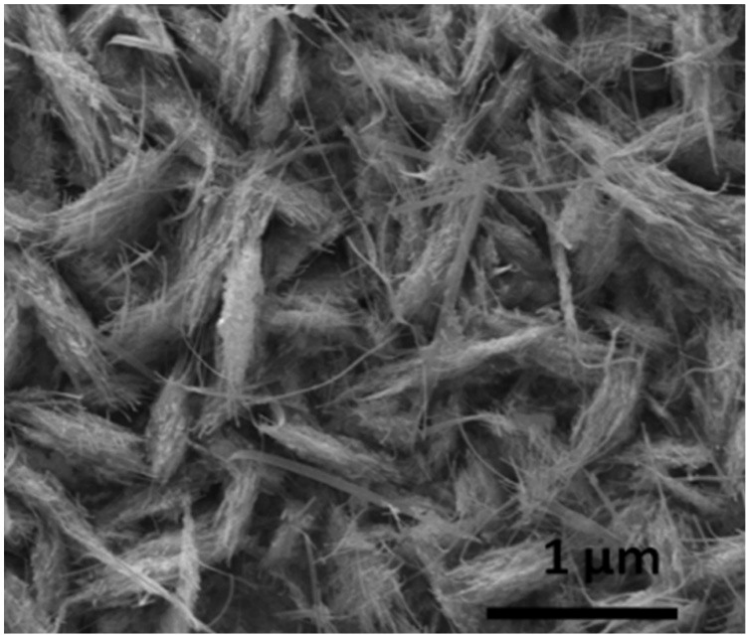

Figure 3.27 SEM of synthesized ZnO-$ZnAl_2O_4$ whiskers.

3.5.4.2 Spectroscopic characterization of biochip

FT-IR spectroscopy was applied to measure the surface properties of the enzyme ALP coupling through SAMs via the carbodiimide crosslinking reaction on ZnO-$ZnAl_2O_4$ surfaces. FT-IR ATR spectra were collected at a resolution of 4 cm^{-1} (128 scans). The FT-IR spectra recorded for ZnO-$ZnAl_2O_4$ coupled enzyme (ALP) via 16-PHA crosslinker are shown in Figure 3.28.

In Figure 3.28 (a), the peaks appearing in the range of 440 – 510 cm^{-1} may be assigned to the stretching vibrations of Zn–O. Figure 3.28 (b) shows the asymmetric (ν_{as}(C-H)) and symmetric methylene stretches (ν_s(C-H)) of 16-PHA-modified ZnO-$ZnAl_2O_4$ that appear at 2920 cm^{-1} and 2849 cm^{-1} respectively. These bands of 16-PHA modified ZnO whiskers

suggest methylene chains during monolayer growth. The C=O stretch at 1740 cm^{-1} on ZnO-$ZnAl_2O_4$ associated with asymmetric and symmetric COO^- stretch at 1640 cm^{-1} is characteristics of an organic carboxylic compound. The additional IR peak at 1452 cm^{-1} is ascribed to C-H deformation. The existence of the peak at 1095 cm^{-1}, which is characteristic of the P=O stretching mode, is a possible evidence for bidentate binding modes. The observation of P-OH related modes due to binding of 16-PHA has been reported elsewhere (Pal *et al.,* 2014).

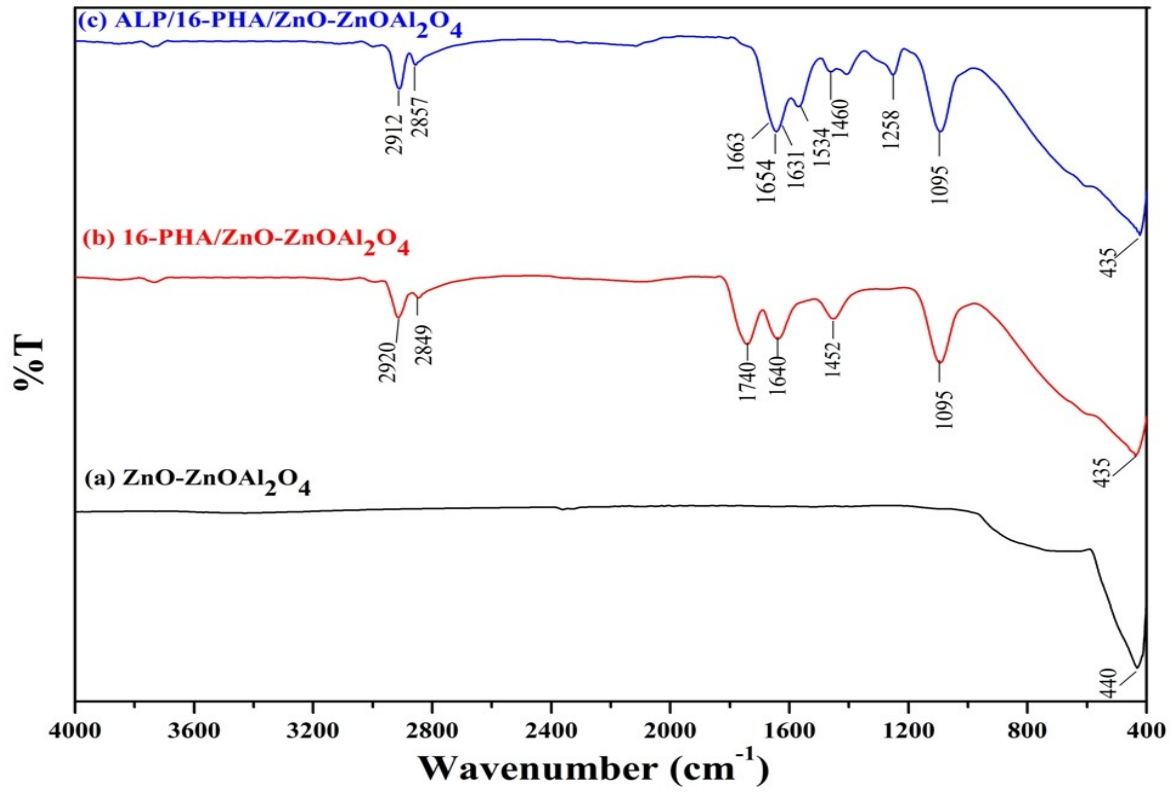

Figure 3.28 The ATR FT-IR spectrum of ZnO-$ZnOAl_2O_4$ (a) bare; (b) treated with 16-PHA and (c) coupled with enzyme (ALP) through 16-PHA.

ALP coupling through 16-PHA SAMs via the carbodiimide cross-linking reaction on ZnO-$ZnAl_2O_4$ surfaces is presented in Figure 3.28 (c). Upon immobilization of enzyme three new absorption bands have appeared; IR bands at 1654 cm^{-1}, 1534 cm^{-1}, and 1258 cm^{-1} are ascribed to the absorption by the amide group that links enzyme to 16-PHA functionalized ZnO-$ZnAl_2O_4$. Also the bands at 1663 cm^{-1}, 1631 cm^{-1} and 1460 cm^{-1} are for all biomolecules' common structural unit *i.e.*, the amide I region.

3.5.4.3 Biochip based bio-catalysis of *p*NPP

Bio-catalysis reaction on biochip involves appropriate enzymatic reaction between substrate and catalyst enzyme. A minor change in pH, ionic strength and temperature can sometimes be responsible to lose the biological activity, as immobilized enzymes are very much sensitive towards environmental changes. Herein the optimized parameters have been reported elsewhere (Mishra *et al.,* 2013).

The enzyme activity was tested on the novel biochip by addition of different concentrations of *p*NPP. 6 µL of *p*NPP and $MgCl_2$ (2:1 ratio) was added to the wells of biochip. It was incubated for 1h at room temperature. Then the yellow coloured products were transferred to a 96 well optiplate and further diluted in 100 µL GB. The absorbance was measured at 405 nm for 0.1 s. The absorbance plot of different *p*NPP concentrations ranging from 0.001 mM to 10 mM is presented in Figure 3.29.

It is observed that, the absorbance values tend to increase as the concentration of substrate is increased resulting in production of more coloured product by the catalyst (ALP). The calibration is found to be linear in the range 0.001 mM to 10 mM (R^2 = 0.99, n = 5) with R.S.D of 3.21% ± 0.27 for the ALP/16-PHA/ZnO-$ZnAl_2O_4$ (Figure 3.29 (a) Inset). The linear equation is; y = 0.4057 + 0.10673x (mM). LOD and LOQ are found to be 0.001 mM by analyzing replicate sets of ALP/16-PHA/ZnO-$ZnAl_2O_4$ with good sensitivity about 1.25 unit change per decade. Whereas for physisorbed enzyme ALP/ZnO-$ZnAl_2O_4$, the linearity is found in the range 0.01 mM to 10 mM (R^2 = 0.98, n = 5) with R.S.D of 5.49% ± 0.61 (Figure 3.29 (b) Inset). The linear equation is; y = 0.11509 + 0.23882x (mM). LOD and LOQ are determined as 0.01 mM and 0.1 mM respectively by analyzing replicate sets with very low sensitivity about 0.29 unit change per decade. Lower LOD, LOQ value, R^2 and sensitivity indicate that ALP/16-PHA/ZnO-$ZnAl_2O_4$ is much superior over physisorbed enzyme ZnO-$ZnAl_2O_4$.

In developing an enzyme based process, kinetic constants are the most important informations. Simple enzyme kinetics is generally described by the Michaelis–Menten kinetics (equation 3.1). The determination of numerical values of K_m is obtained by plotting 1/V versus 1/S (known as a Lineweaver–Burk plot). An important feature that accounts for enzyme stability is the improvement obtained in the value of K_m. The K_m value is found to be 0.63 mM for ALP/16-PHA/ZnO-$ZnAl_2O_4$ whereas 1.04 mM for physisorped enzyme on ZnO-$ZnAl_2O_4$.

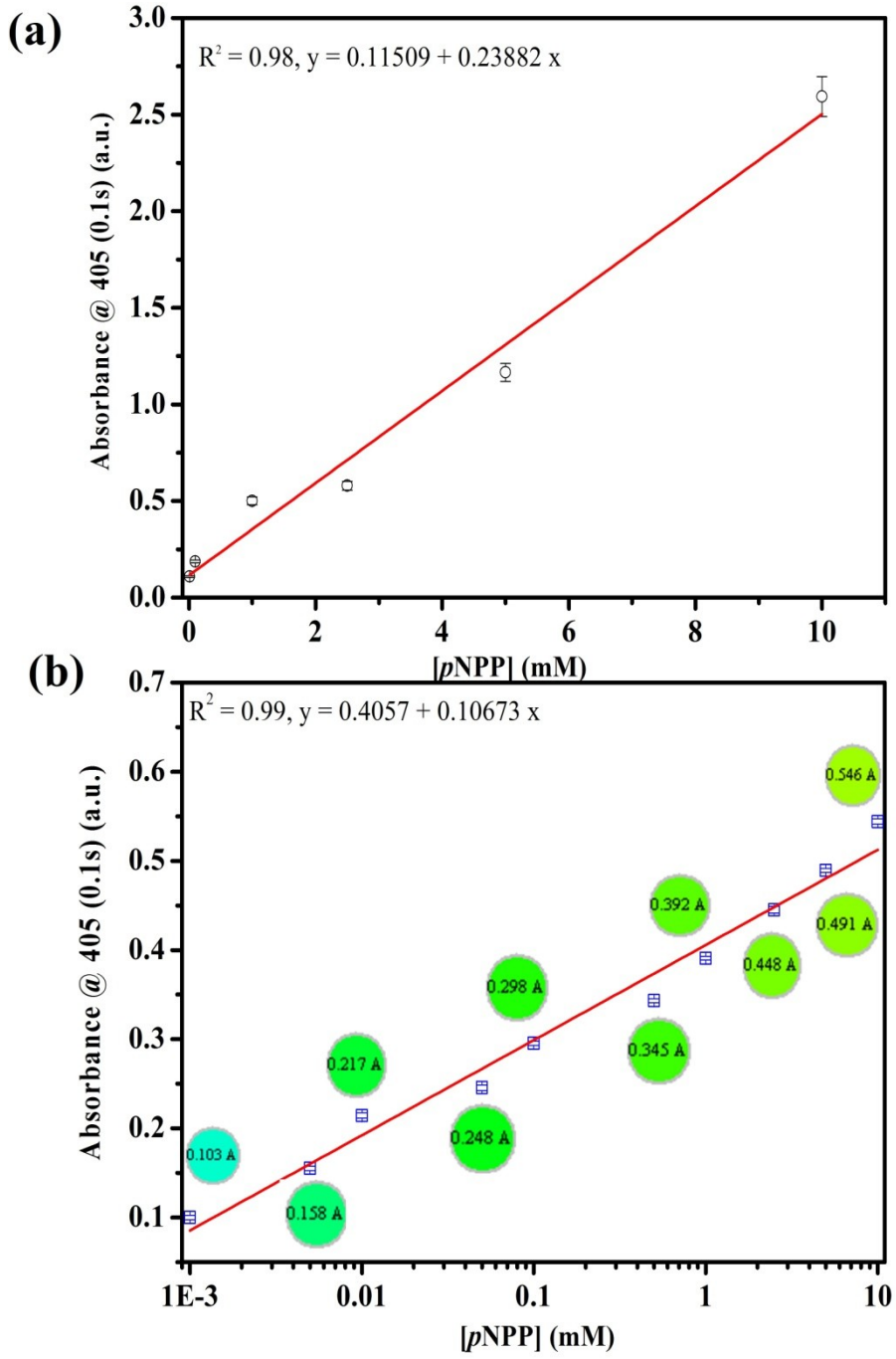

Figure 3.29 Calibration curve for different *p*NPP concentration obtained using ZnO-$ZnAl_2O_4$ biochip (a) physisorped ALP (b) chemisorped ALP.

The lower K_m value (almost 0.61 time of K_m for physisorped enzyme) reflects the covalently coupled enzyme over the physisorped enzymes facilitated enhanced stability of ZnO-$ZnAl_2O_4$ biochip. This has established that the catalyst (ALP) has been successfully bound to the novel nanomaterials proving its efficiency in product formation. Thus the presented material provides a suitable substrate for development of high catalytic efficiency, miniaturized devices.

3.6 Summary of ZnO nanostructures in biosensing

The significant findings using various ZnO nanostructures based biosensor have been summarized in the Table 3.5.

Table 3.5 Significant findings using ZnO nanostructures based biosensor

Analytical parameters	**ZnO Nanostructures used in biosensor fabrication**				
	Nanorods		**Nanoparticles**	**Whiskers**	
Biomolecules immobilized	COD/HRP		AchE	ALP	
Application tested	Choline biosensing		AchCl and OPs biosensing	Bio-catalysis of pNPP	
Immobilization technique	Physisorption	Covalent	Covalent	Physisorption	Covalent
Linear range (mM)	0.0125-0.5	0.006-2	0.01-10	0.01-10	0.001-10
LOD (mM)	0.0125	0.0005	0.01	0.01	0.001
K_m (mM)	0.2 ± 0.09	0.062 ± 0.06	0.591 ± 0.013	1.04	0.63

The measured lower LOD, higher sensitivity and improved K_m of various enzyme activity has suggested enhanced biosensor and bio-catalytic efficiency of ZnO nanostructures. The developed biochips thus have satisfactory repeatability with cross-linked immobilized enzyme over physically adsorbed for analysis.

3.7 Conclusion

In this chapter, various ZnO nanostructures have been studied towards biosensing application. Vertically aligned ZnONR-films with an average diameter of ~80 nm and length ~780 nm (film thickness) have been successfully demonstrated for the construction of a stable and reproducible choline nanobiosensor. The covalent immobilization of the enzymes

on the ZnONR was achieved using 16-PHA as a cross-linker. The novel self assembly technique *i.e.*, phosphonation on ZnO nanostructure imparted significant stability to the immobilized enzyme as against physisorbed enzyme. The phosphonation of the ZnONR imparted significant stability to the immobilized enzyme as against physisorbed enzyme. A lower value of K_m, of 0.062 mM for the covalently coupled enzyme over the physisorbed enzymes has enhanced stability of ZnONR nanobiosensor. The ZnONR-choline biosensor has been investigated over a wide range of choline from 0.0005 mM to 2 mM. Importantly, the recovery of choline in milk samples is closed to 99%. Using the developed biosensor, choline was measurable even after 30 days with 60 repeated measurements proving the stability of the sensor (Intraday R.S.D%=2.83 and Interday R.S.D%=3.51).

Further, using the novel technique of forming SAMs on ZnO, OPs sensor in water has been developed using ZnO particles. Using the methodology for detecting of OPs, a field portable and user friendly kit has been developed. Developed biosensor can detect multiple analyte, a neurotransmitter (acetylcholine) and environmental contaminant (OPs) in a single platform; it can save time, quantity of the sample and the cost of analysis. The linear range for acetylcholine has been found in the range 0.01 mM to 10 mM (R^2 = 0.994) and for OPs, it is in the range 0.01 ng mL^{-1} to 5 ng mL^{-1} (R^2 = 0.99, n = 5).

Furthermore, biochip based on ZnO-$ZnAl_2O_4$ composite nanostructures have been successfully demonstrated for bio-catalysis. The developed biosensors may easily be extended for routine environmental analysis. The formation of ZnO-$ZnAl_2O_4$ whiskers were performed on oxidized Si using a simple route at low temperature. The measured lower LOD and LOQ for *p*-NPP, higher sensitivity and improved K_m of ALP have established enhanced bio-catalytic efficiency. The developed biochip is also suitable for satisfactory reproducibility with whisker having cross-linked immobilized enzyme over physically adsorbed for analysis of *p*-NP.

CHAPTER 4: POROUS FUNCTIONAL MATERIALS IN BIO AND CHEMICAL SENSING

Highlights:

- Porous functional materials (PFM) as platform for biosensing application have been investigated. Use of macroporous silica is demonstrated for glucose biosensing using duel read out format.
- A novel nano sensor based on fluorescence quenching coupled within the nanosize pores of mesoporous silica have been demonstrated for detection of heavy metals such as Pb^{2+} in water.

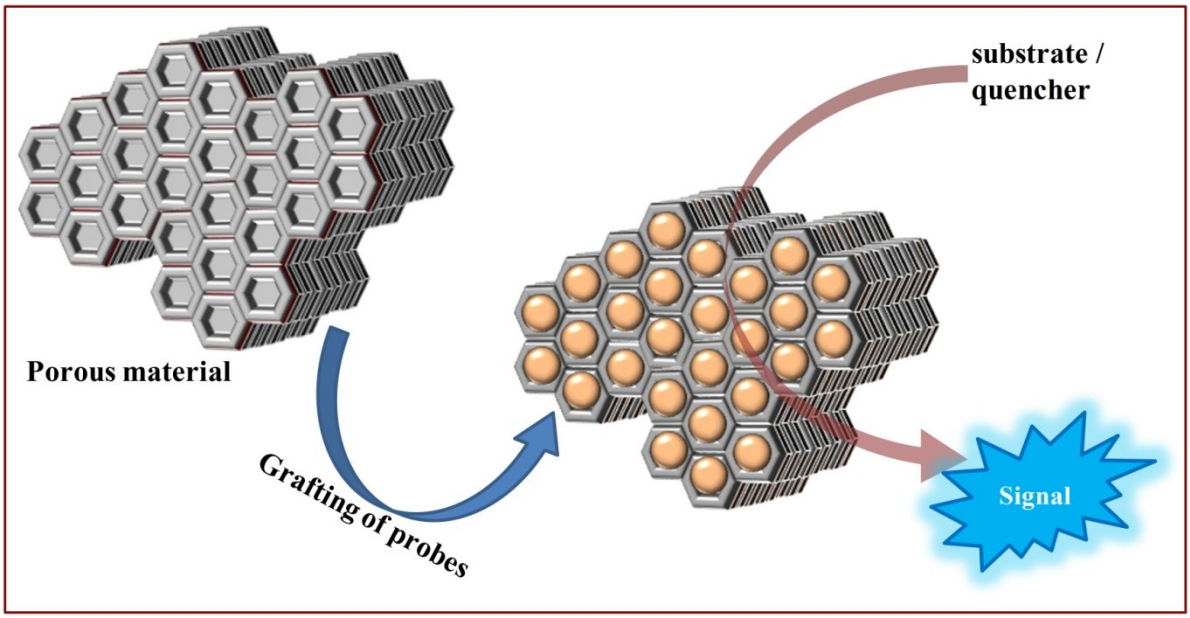

Graphical abstract of sensing using porous material

4.1 Introduction

A pore, which can be widely defined as a limited space or spatial confinement, is one of the most ancient concepts. The understanding, design, and manipulation of pores have significantly advanced science and technology, and are playing increasingly important role in new technologies (Zhao, 2006). Porous materials have attracted considerable attention since the 1960s because of their wide variety of scientific and technological applications (Hasanzadeh *et al.,* 2012a). In its most generalized definition, the term ‘‘pore’’ means a limited space or cavity in a continuous material. According to the International Union of Pure and Applied Chemistry (IUPAC), pores are classified into three categories micropores, mesopores, and macropores (IUPAC, 1997) and listed in Table 4.1.

Table 4.1 Pore-size regimes and representative porous inorganic materials.

Pore-size regimes	Definition	Examples
Macroporous	> 50 nm	Glasses, Controlled pore glass
Mesoporous	2–50 nm	Aerogels, MCM-41, SBA-15, pillared layer clays
Microporous	< 2 nm	zeolites, zeotypes, activated carbon

Several other classifications can also be proposed because of the considerable variety of porous materials. Thus, according to the distribution of pores within the material, it can be distinguished between regular and irregular porous materials, whereas, according to the size distribution of pores, it can be distinguished between uniformly-sized and non-uniformly sized porous materials (Hasanzadeh *et al.,* 2012b). Porous materials can range from highly-ordered crystalline materials (*e.g.*, aluminosilicates or MOFs) to amorphous sol-gel compounds, polymers and fibers. In addition, since 1990, there has been growing interest in the preparation of nanostructures of metal and metal oxides with controlled interior nanospace, they are currently subject to intensive research (Zhao, 2006). The most relevant characteristic of porous materials is the highly effective surface:volume relationship, usually expressed in terms of specific surface area (area per mass unit), which can be determined from nitrogen adsorption/ desorption data (Lu and Zhao, 2004). In recent years, more attractive possibilities have arisen by the development of various new silica materials with ordered structures (Ariga *et al.,* 2014). Compared to polymers, inorganic mesoporous

material is an excellent support for molecular catalysts due to its excellent thermal and chemical stability. However, highly hydro-thermally stable mesoporous material has not only all the virtues of inorganic material but also a large specific surface area, well-defined tunable pore sizes and an adjustable hydrophobic or hydrophilic character, which provide great opportunities for immobilization of large catalytic species and catalytic conversion of bulky organic substrates (Sayari and Hamoudi, 2001).

4.2 Porous materials for biosensing application

4.2.1 Macroporous materials in biosensing

One of the macroporous materials, Controlled Pore Glass (CPG), is a promising candidate for enzyme immobilisation. CPG exhibits a broad pore size ranging between 3 and 1000 nm, high thermal, mechanical and chemical stability and high resistance towards aggressive chemicals *e.g.* acids. Thus, CPG can be regenerated several times by heating or boiling in acid to remove all organic residues adsorbed and to create more silanol groups on the support surface for further functionalization (Weetall, 1993; Inayat *et al.,* 2013). The surface properties of CPG is mainly determined by the silanol groups. Thus, porous glasses can be easily modified by a variety of functional groups in a similar manner than mesoporous silica molecular sieves. These properties render them attractive supports for enzyme immobilization (Inayat *et al.,* 2013; Enke *et al.,* 2003). CPG has been widely exploited to construct various biosensors for analysis of different analytes (Table 4.2).

Table 4.2 Use of CPG towards the construction of biosensors

Construction of Biosensor	Biomolecule	Analyte	Transduction principle	References
Enzyme immobilization via GA activated APTES modified CPG	Urease	Urea	Flow injection conductimetric system	Limbut *et al.,* 2004
GA-activated silanized CPG	Acetyl-cholinesterase	Malaoxon and isomalathion pesticide	Uv-vis detection on basis of colour change	Krstić *et al.,* 2008

Immobilized enzymes on GA-activated silanized CPG	Glucose oxidase	Glucose	Amperometric	Martín-Fernández et al., 2008
Enzyme immobilization via GA activated silanized CPG	Urease	Urea	Flow injection analysis-enzyme thermistor	Mishra *et al.*, 2010a
GA-activated silanized CPG	Hexokinase	Fructose	Flow injection analysis-enzyme thermistor	Bhand *et al.*, 2010
Antibody immobilized GA-activated silanized CPG	Antibody	Ochratoxin A	Displacement immunoassay technique	Lates *et al.*, 2012
GA-activated silanized CPG	Cellobiose dehydrogenase	lactose	Combination of thermometric and amperometric technique	Yakovleva *et al.*, 2012
Direct ELISA using GA-activated silanized CPG	Antibody	Atrazine pesticide	Thermometric technique	Qie *et al.*, 2013
Biomolecule immobilized via APTES modified CPG	Bovine trypsin	Caroteno-proteins	pH change	Li *et al.*, 2014a

4.2.2 Mesoporous materials in biosensing

Biosensor research is driven by the increasing need for specific sensors to enable fast, routine measurements in many fields of analysis. Since the discovery of ordered mesoporous silica molecular sieves (Beck *et al.*, 1992), interest in this research field has been expanded. With

distinctive properties, mesoporous silica has attracted much attention and broad applications in biosensor (Hasanzadeh, M, 2012b). One of the well known mesoporous silica (MPS) is the Santa Barbara Amorphous material (SBA-15) which is a structurally well ordered mesoporous material with a narrow pore-size distribution of 1.5–300 Å. It has regular, cylindrical, ordered hexagonal pores, with a large surface area (Yang *et al.,* 2005). SBA-15 with uniform tubular channels has been widely used for the construction of sensors (Table 4.3).

Table 4.3 Use of SBA-15 towards the construction of biosensors

Construction of Biosensor	Biomolecule	Analyte	Transduction principle	References
Encapsulation of hemoglobin on SBA-15 and Au-SBA-15	Hemoglobin	H_2O_2	Direct electrochemistry	Xian *et al.,* 2007
Enzyme immobilized on APTES modified AuNPs-SBA-15	IO_4^--oxidized-glucose oxidase	Glucose	Cyclic voltammetry and amperometry technique	Bai *et al.,* 2007
Entrapment of enzymes in SBA-15	Glucose oxidase and horseradish peroxidase	Glucose	Amperometry technique	Dai *et al.,* 2008
Adsorption of Cytochrome *C* on SBA-15	Cytochrome *C*	H_2O_2	Amperometry technique	Zhu *et al.,* 2008
Adsorption of antibody on chitosan-SBA-15	ALP labelled antibody	α-fetoprotein	Immunoassay	Lin *et al.,* 2009
Enzyme immobilized on APTES modified SBA-15	Glucose oxidase	Glucose	Amperometry technique	Khan *et al.,* 2014

Recently, ionic liquids have been used as modifiers of mesoporous materials for fabrication of biosensors due to their high ionic conductivity and good biocompatibility for enhanced response (Haghighi *et al.,* 2014; Zou *et al.,* 2014).

4.3 Objectives

The proposed aim of this work is to develop and demonstrate novel bio and chemical sensing using porous materials. The work in this chapter has been divided into two parts: (i) glucose oxidase immobilized macroporous silica (CPG) for glucose biosensing; and (ii) functionalized mesoporous silica (SBA-15) for heavy metal sensing.

4.4 Functionalized CPG for glucose biosensing

4.4.1 Introduction

Diabetes mellitus is a growing epidemic with a prevalence rate of 346 million people worldwide. In 2004, an estimated 3.4 million people died from the consequences of high blood sugar, and it has been projected that diabetes deaths will be double between 2015 and 2030 (WHO, 2011). Diabetes control involves glucose management, including self-monitoring and maintenance of glucose levels within normal ranges 110 mg dL^{-1} ± 25 mg dL^{-1} (6.1 mM ± 1.4 mM) (Wilkins and Atanasov, 1996). Since Clark and Lyons proposed the first initial concept of glucose enzyme electrodes in 1962 (Clark Jr *et al.,* 1958), tremendous efforts have been made to develop reliable devices for diabetes control. Many approaches including surface plasmon resonance (SPR) (Singh and Gupta, 2013), electrochemiluminescence (Kremeskotter *et al.,* 1995), fluorescence (Moschou *et al.,* 2004), colorimetric (Jiang *et al.,* 2010), flow injection with spectrophotometry (de Oliveira *et al.,* 2005) and electrochemical (Liu *et al.,* 2013) have been reported for the development of glucose biosensor. They are mostly based on the analysis of hydrogen peroxide generated by reaction between glucose and glucose oxidase (GOD). However, for the development of an ultrasensitive glucose biosensor, an efficient immobilization of enzyme (*e.g.* GOD) is desired. Moreover, interference free sensing another desired property which usually results in low signal to noise ratio (Liu *et al.,* 2013). Lack of continuous monitoring of glucose concentrations can be avoided by immobilizing GOD on proper surface.

Herein the proposed aim is to develop a novel CPG support for immobilising GOD. Further, this GOD immobilized CPG has been exploited as duel read out system and to develop a reusable glucose sensing device.

4.4.2 Principle of colorimetric glucose sensing

Glucose biosensing is based on the principle that GOD oxidizes β-D-glucose to gluconic acid and H_2O_2 in the presence of oxygen. The H_2O_2 is then utilized to oxidize a chromogenic substrate (OPD) in a secondary reaction with second enzyme, HRP, with a resultant colour change that is monitored spectrophotometrically. The schematic pathway of colorimetric glucose sensing is shown in Figure 4.1.

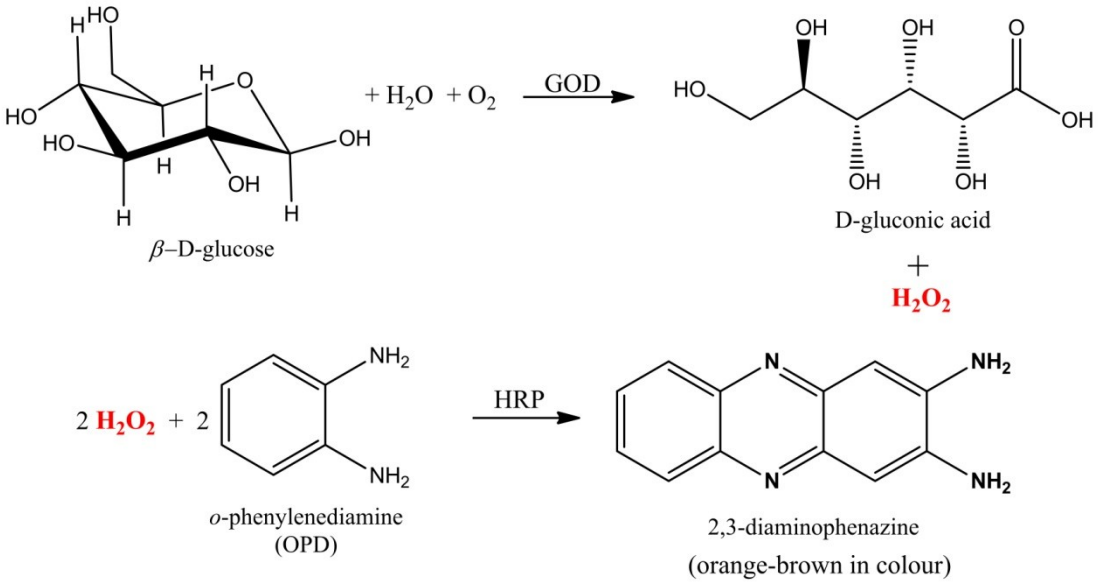

Figure 4.1 Reaction pathway of colorimetric glucose sensing.

4.4.3 Experimental Section

4.4.3.1 Materials and instrumentation

Amino silanized CPG spherical beads (Trisoperl, size 125–140 μm, pore size 50 nm) were purchased from VitraBio (Germany). Glucose oxidase Type II-S (EC 1.1.3.4) from Aspergillus niger (GOD), peroxidase (EC 1.11.1.7) from Horseradish (HRP) and luminol (5-amino-2,3-dihydro-1,4-phthalazinedione) were purchased from Sigma Chemical Co. (USA). Potassium Chloride (KCl), sodium phosphate dibasic (Na_2HPO_4), sodium phosphate monobasic (NaH_2PO_4), sodium chloride (NaCl), potassium chloride (KCl), glutaraldehyde solution 25% (GA), tri-ethanol amine, Hydrogen peroxide (H_2O_2), β-D-glucose, O-phenylenediamine dihydrochloride (OPD), luminol and other chemicals were of GR grade, Merck (Germany). HybridSPETM (30 mg mL^{-1}) SPE tubes were purchased from Supelco (USA). Centrifugation, shaking and filtration of the samples were done by Spinwin mini

centrifuge, Spinix shaker Tarsons (India). For chemiluminescence (CL) and colorimetric measurement, Victor™ X4 2030 optiplate reader from Perkin Elmer (USA) was used. Chemiluminescence images were acquired on inverted microscope (IX-71 Olympus, Japan) coupled with charged coupled device (CCD), Hamamatsu Orca-ER (Japan).

4.4.3.2 Solution preparation

PB 10 mM, pH 7.4 was prepared by mixing appropriate amount of Na_2HPO_4 and NaH_2PO_4 in double distilled water. 10 mM PBS was prepared by dissolving appropriate amount of Na_2HPO_4, NaH_2PO_4 and NaCl for washing purpose. A stock solution of glucose (100 mM) was prepared by dissolving 0.180 g in 10 mL of PBS (10 mM, pH 7.4) containing 0.027 M KCl and 0.137 M NaCl. Working solution of glucose was prepared freshly before daily use. Enzyme stock solutions were prepared in PB.

4.4.3.3 Enzyme immobilization on CPG

Enzyme immobilization was achieved by GA cross-linking on amine functionalized CPG beads (Weetall, 1976) as shown in Figure 4.2.

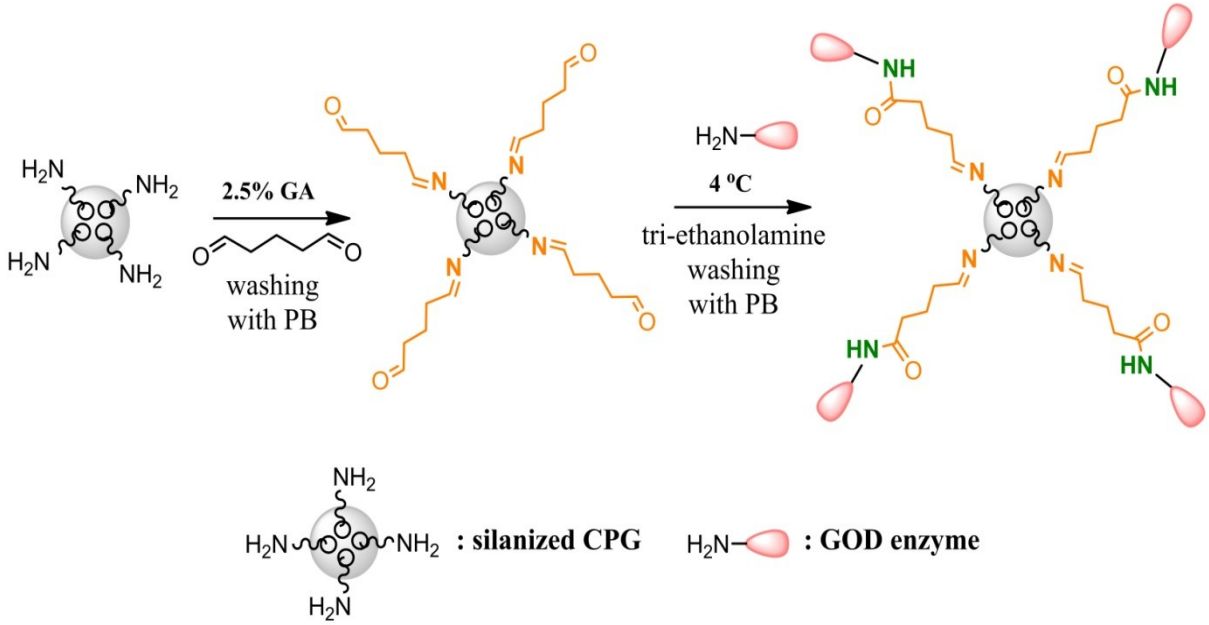

Figure 4.2 Reaction pathway of enzyme immobilization procedure on CPG beads.

In brief, an optimized amount of GOD was covalently immobilized on amine functionalized CPG beads by activating with 2.5% GA in 10 mM PB, pH 7.4. GOD (1 IU μL^{-1}) dissolved in PB was added to the GA activated CPG. The coupling was allowed to proceed for overnight

at 4 °C under gentle shaking. The GOD coupled CPG beads were washed with buffer. Tri-ethanolamine (15 mg) was added to terminate all unreacted groups on the matrix and then washed with PB.

4.4.3.4 Column preparation

Initially, batch kinetic experiments were carried out to evaluate the suitability of GOD coupled CPG for glucose determination. Parameters such as amount of GOD coupled CPG, ionic strength, pH and temperature were evaluated. Based on the batch kinetic experiments, column studies were carried out to achieve the detection of glucose. GOD-CPG beads were packed in HybridSPE™ columns for detection of glucose using slurry pack method. Packed column was conditioned using sufficient 10 mM PB (pH 7.4). The schematic setup with a real time image is presented in Figure 4.3.

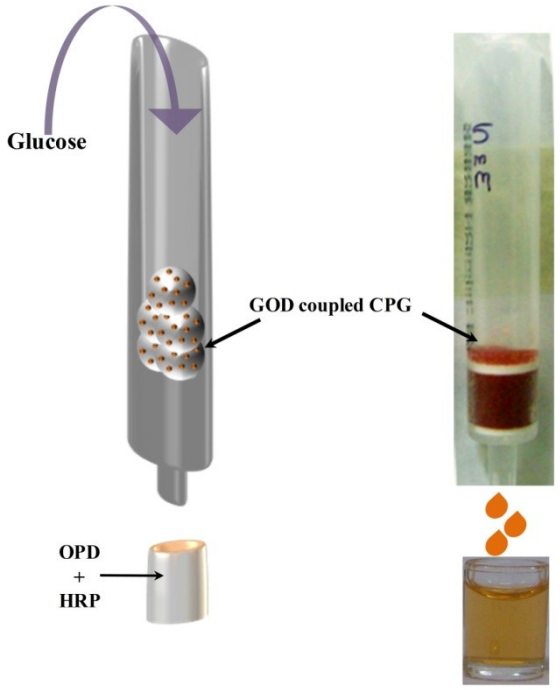

Figure 4.3 Schematic setup for colorimetric glucose biosensing using functionalized GOD-CPG loaded column.

4.4.4 Results and Discussion

4.4.4.1 Spectroscopic characterisation by FT-IR

FT-IR spectroscopy was applied to confirm the coupling of GOD *via* GA cross-linking reaction on silanized CPG beads. The FT-IR spectra were recorded ATR mode at a resolution

of 4 cm^{-1} (60 scans) and presented in Figure 4.4. The spectrum in Figure 4.4 (a) shows typical IR vibration bands for silanized CPG and interpreted as 3458 and 1543 cm^{-1} for N-H stretching and N-H bending vibrations respectively. The bands appeared at 2920 cm^{-1} and 2850 cm^{-1} are described as the C – H stretching vibrations in asymmetric and symmetric mode. The asymmetric stretch at 1070 cm^{-1} associated with symmetric stretch 795 cm^{-1} is characteristic for stretching vibrations of Si–O–Si. Further, the band at 960 cm^{-1} for bending mode of Si–OH and 448 cm^{-1} for bending vibration of Si–O–Si suggest the APTES functionalization on the CPG.

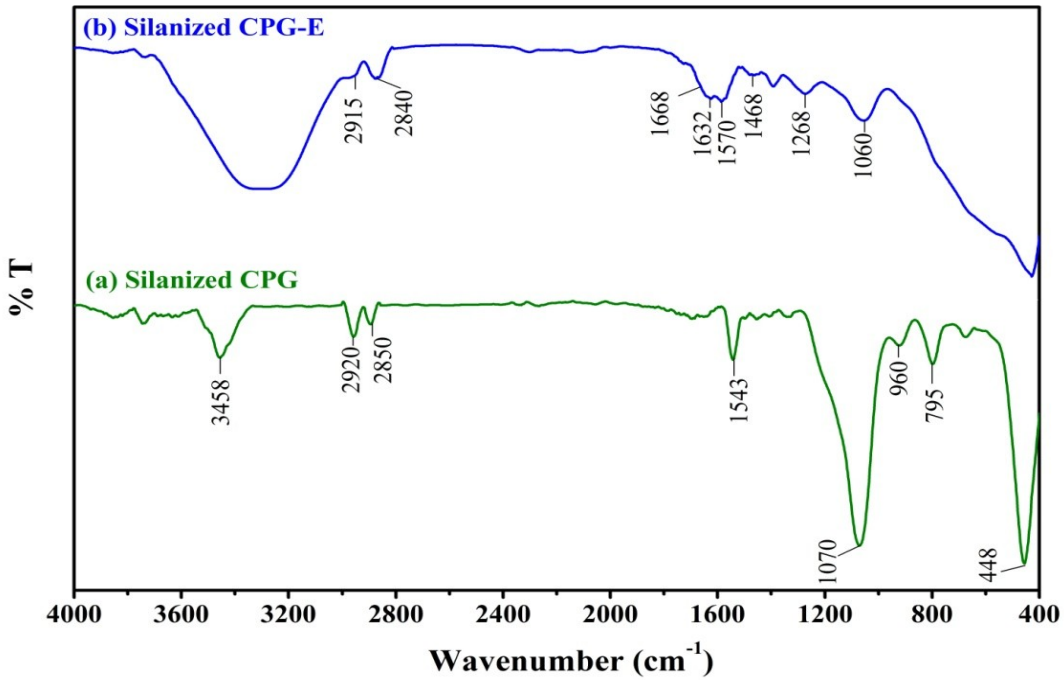

Figure 4.4 ATR FT-IR spectra for CPG beads (a) bare silanized and (b) GOD coupled.

Further, the presence of new band is observed due to the cross link of enzyme (GOD) *via* GA on the CPG beads (Figure 4.4 (b)). The new three absorption bands appeared at 1632 cm^{-1}, 1570 cm^{-1}, and 1268 cm^{-1} may be ascribed to the absorption by the amide group, which is the structural unit common to all bio-molecules. These results suggest that enzyme (GOD) is successfully coupled on the CPG beads via GA crosslinker.

4.4.4.2 Surface characterization by SEM

The surface modification of the silanized CPG and the attachment of GOD enzyme on CPG were examined by SEM to confirm the changes in surface morphology. Figure 4.5 (a) shows the SEM micrograph of the bare silanized CPG bead at magnification 650 ×. Figure 4.5 (b)

shows the bare pores on CPG surface at magnification 2500 ×. Further one of the pore surface has been magnified at 15000 × (Figure 4.5 (c)). The GOD coupled on silanized CPG pore was also imaged at magnification 10000 × (Figure 4.5 (d)). Subsequently, the pore surface has been magnified at 20000 × (Figure 4.5 (e)). The change in the CPG pores surface after GOD immobilization is clearly distinct as shown in Figure 4.5 (c) and (e). It is clear from figure that GOD has been successfully coupled to the pores of CPG. Moreover, it is also clear that the pores surface are completely covered by GOD.

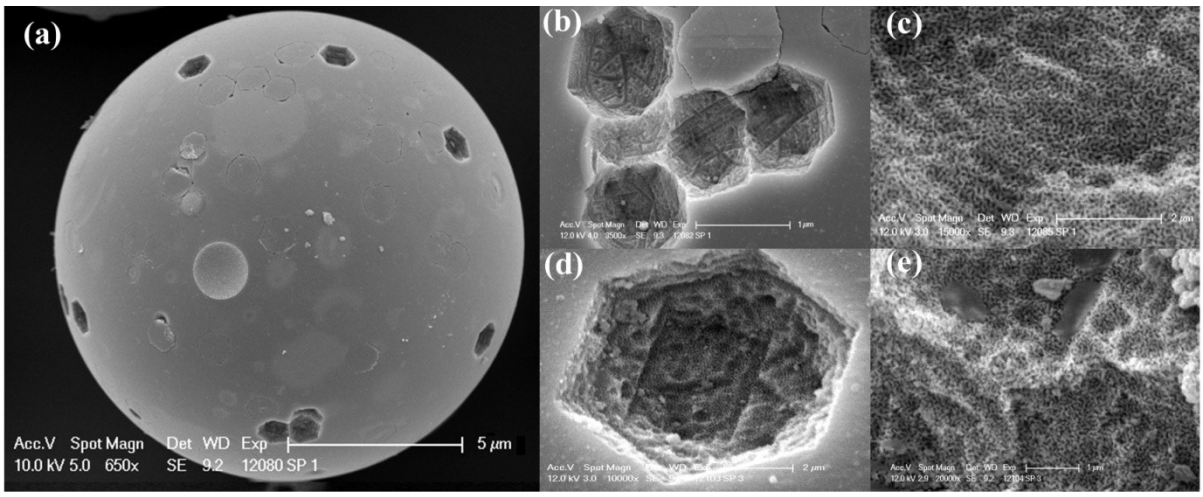

Figure 4.5 SEM images of bare silanized CPG and GOD coupled CPG (a - e); (a) bare silanized CPG bead image at 650 × magnification; (b) bare pores of silanized CPG image at 2500 × magnification; (c) bare pore surface of silanized CPG image at 15000 × magnification; (d) pores of GOD coupled silanized CPG image at 10000 × magnification and (e) pore surface of GOD coupled silanized CPG image at 20000 × magnification.

4.4.4.3 Chemiluminescence imaging of GOD-CPG

In order to confirm the activity of GOD coupled CPG pores, CL imaging assay was performed. GOD – CPG beads were placed on microscopic glass slide. In one slide, GOD – CPG beads with HRP and luminol were placed in absence of glucose. The image of reference slide without adding glucose is presented in Figure 4.6 (a). On the other slide, which acts as sample, HRP and luminol were placed in presence of Glucose. The image of the sample slide is presented in Figure 4.6 (b). The binding of the GOD to the CPG bead is clearly distinguished from the CL images. Also, presence of small bright spots on the particles due to the CL reaction of GOD/HRP/luminol system (Figure 4.6 (b)) has established the enzyme loading into the pores of CPG.

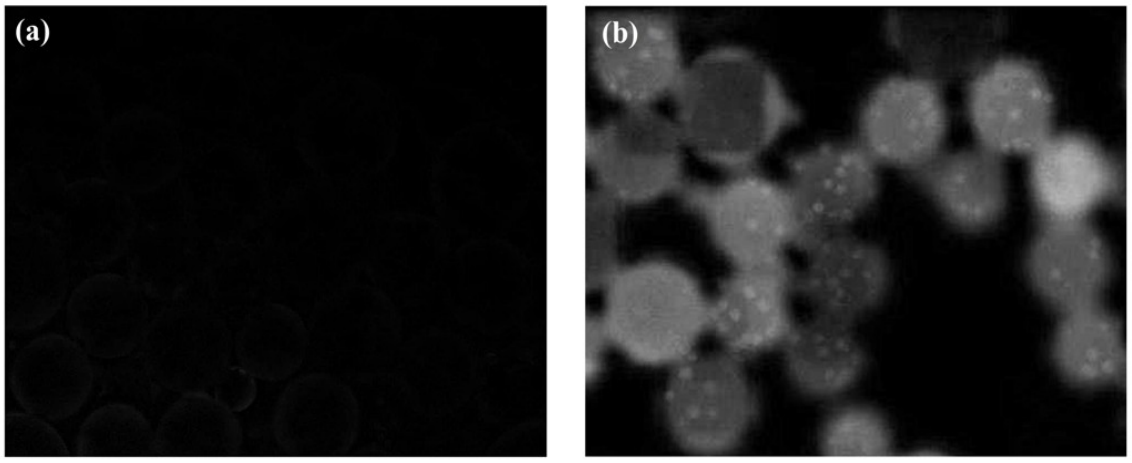

Figure 4.6 Chemiluminescence image of (a) reference GOD-CPG without glucose (b) sample GOD-CPG with glucose.

4.4.4.4 Optimization of experimental conditions

4.4.4.4.1 Optimization of pH, ionic strength and temperature

Various experimental parameters, such as pH, ionic strength and temperature, may affect the performance of a biosensor. In this work, these parameters were first studied to ascertain the optimal working conditions and presented in Figure 4.7.

The effect of pH and ionic strength of buffer on the biosensor performance was investigated by measuring the CL signal intensity to 1 mM glucose. The pH value ranging from 6.4 to 7.8 was adopted in this study. The ionic strength of the buffer was studied in the range 10 mM to 200 mM. As seen in Figure 4.7 (a) and (b), the biosensor shows an maximum signal intensity at pH 7.4. The ionic strength of buffer also affects the system. Maximum signal intensity was observed for the buffer of 10 mM. Although, the signal intensity corresponds to the ionic strength 50 mM exhibits almost similar with 10 mM. But ionic strength of 10 mM PBS was chosen for the further experiments as the higher ionic strength may interfere in the reaction. In this case, the PBS solution is adjusted to pH 7.4 and ionic strength 10 mM to perform all subsequent experiments.

The effect of varying temperature on the biosensor response has been also examined between 25 °C and 50 °C as illustrated in Figure 4.7 (c).

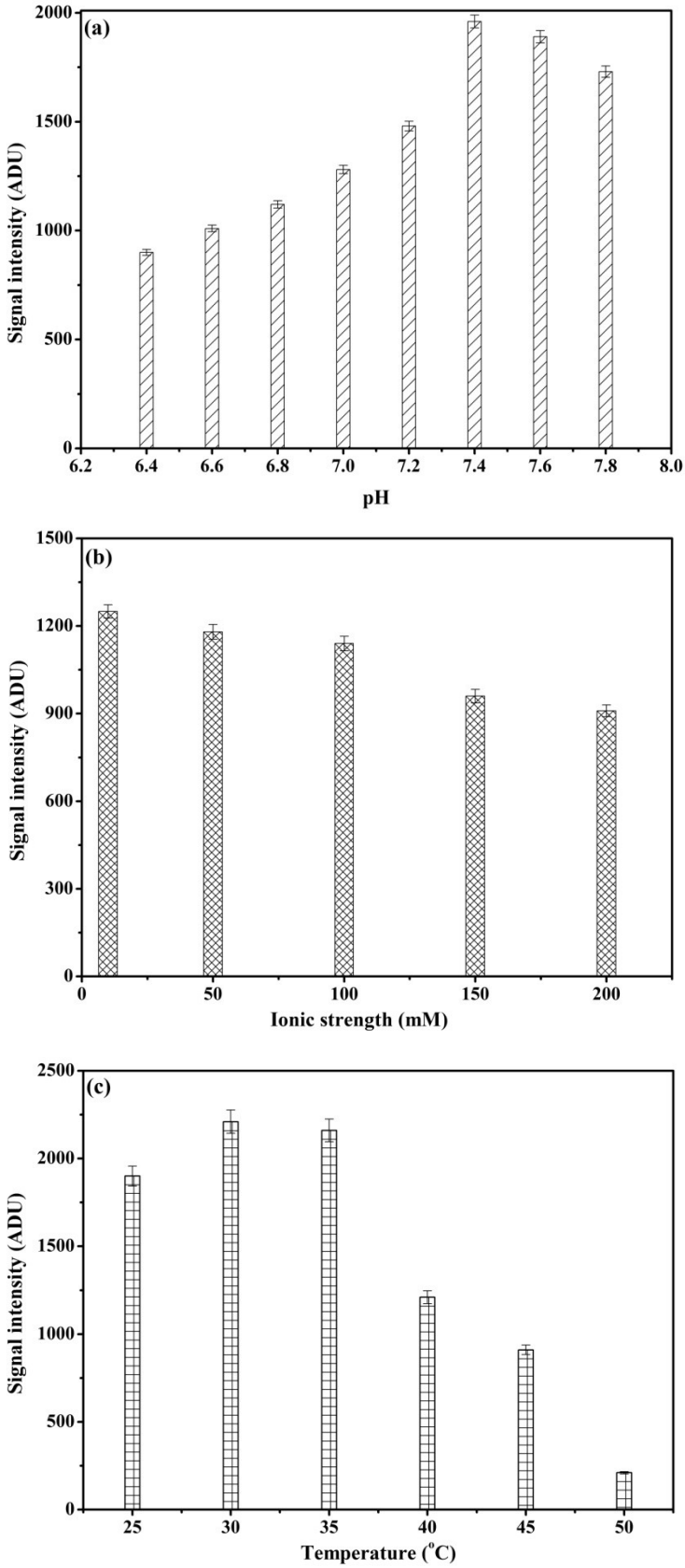

Figure 4.7 Optimization of parameters (a) pH of buffer; (b) ionic strength of buffer; (c) temperature of the system using 1 mM glucose.

The signal intensity gradually increases with the increasing temperature and reaches to its maximum value at 30 °C and stable up to 35 °C. The enzyme retains its activity at higher temperature. This may be due to the highly aminated CPG pores that may accommodated enzyme inside the pores. After 35 °C, the response decreases which is due to the natural thermal degradation of the enzymes. In order to retain the enzyme activity and for long-term usage 30 °C is chosen for this work. But the biosensor shows a stable response at 35 °C and that is a useful information if it is applied in the field.

4.4.4.4.2 Optimization of amount of enzyme and CPG

Optimization of amount of enzyme (GOD:HRP) and the amount of particles used to prepare the column are the crucial factor. The ratio of these two enzymes on biosensor surface might influence the overall performance of the bienzyme biosensors. Also on other hand the amount of particles is crucial with respect to its substrate consumption. Figure 4.8 (a) and (b) represent the signal intensity for the various enzyme ratios and particle amount respectively.

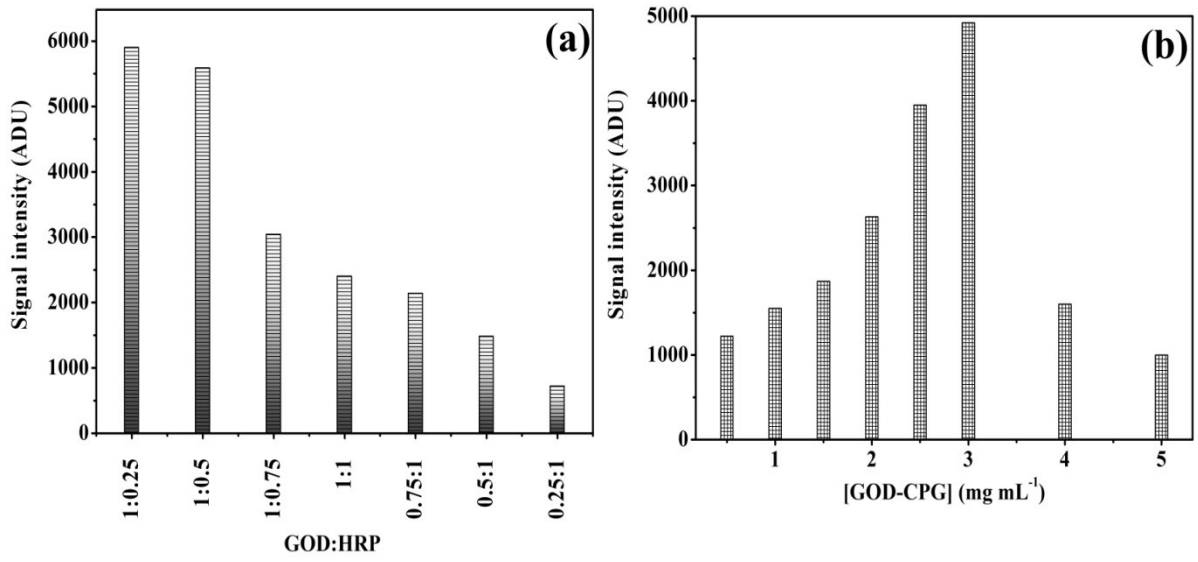

Figure 4.8 Optimization of (a) bi-enzyme (GOD:HRP) ratio; (b) amount of particles using 1mM glucose.

The maximum sensor response was found when GOD:HRP was 1:0.25. Also GOD:HRP ratio found stable at 1:0.5. After 1:0.5, signal intensity was decreased. For the increasing amount of particle, signal response was increased up to 3 mg mL^{-1}. After the highest signal intensity at 3 mg mL^{-1}, signal response was very low which could be due to insufficient substrate concentration. So subsequent experiments are carried out using enzyme ratio (GOD:HRP) 1:0.25 and amount of particles at 3 mg mL^{-1}.

4.4.4.5 Kinetic response and calibration curve

The glucose solutions of varying concentrations ranging from 0.001 to 10 mM were passed through the column. The product of the reaction between GOD and glucose was collected in a well of 96 opti-well plate containing optimized amount of HRP and OPD. A residing time of 2 min was found optimal for colorimetric glucose sensing. The formation of yellow colour establishes the presence of glucose (Figure 4.9).

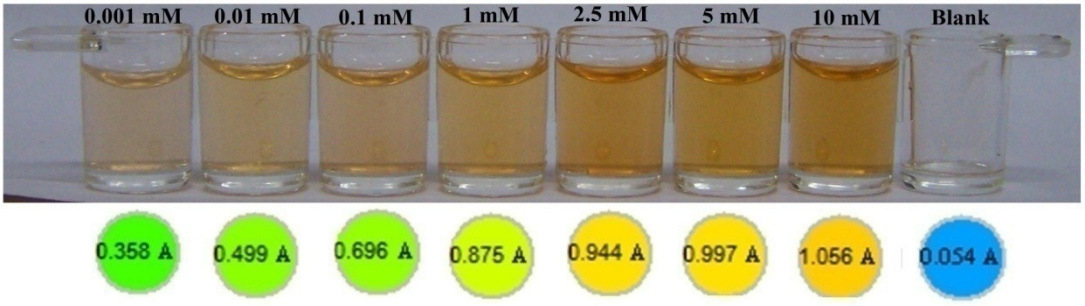

Figure 4.9 Developed colour with the maximum absorbance readings for various glucose concentrations under optimized conditions.

The kinetic response was measured up to 600 sec. The kinetic response was found stable at 120 sec and after 120 sec, no change in absorbance was observed (Figure 4.10).

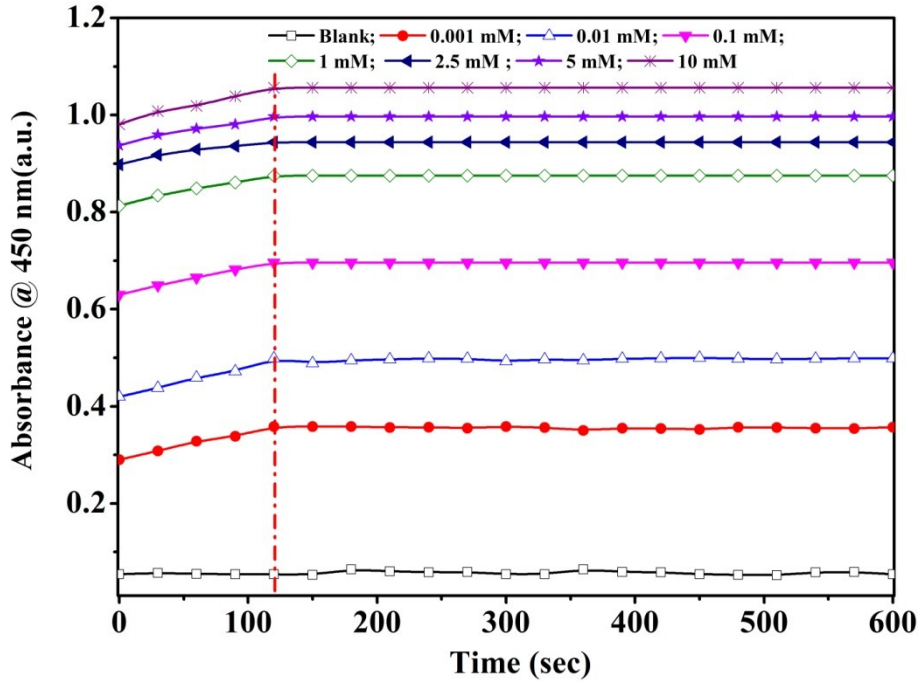

Figure 4.10 Kinetic response for various concentrations of glucose at optimized conditions.

From the kinetic data, K_m (equation 3.1) values of the immobilized enzymes were determined. K_m was found to be 0.013 mM. The stable response at 120 sec was described as maximum absorbance at 450 nm for the respective concentrations.

The maximum absorbance at 120 sec is plotted against various glucose concentrations and presented in Figure 4.11. It is found that absorbance increases with increasing concentration of glucose. The linear range is found to be 0.001 mM to 10 mM. The data points are fitted using linear equation; y = 0.87374 x (mM) + 0.17708, R^2 = 0.998 (n = 5). LOD and LOQ are found to be 0.001 mM.

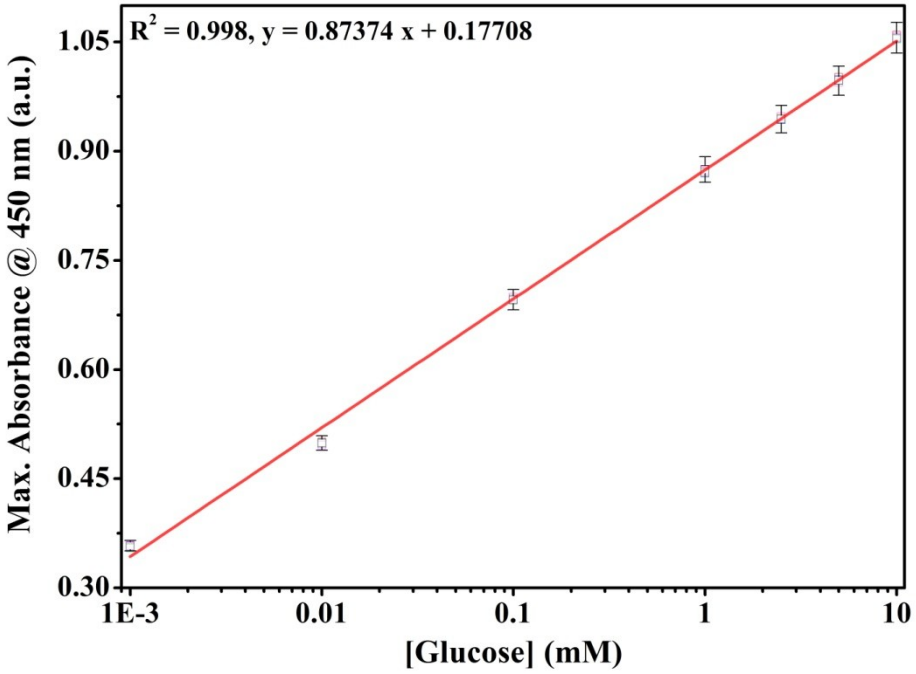

Figure 4.11 Calibration plot for various concentration of Glucose.

4.4.4.6 Column stability and reproducibility

The column was stored dry at 4 °C for a successive stability test over a period of 30 days as presented in Figure 4.12. The data was recorded at 450 nm using 1 mM glucose followed by a washing step. The data is plotted against the number of days. It is found that the enzyme has retained almost 100 % of its activity up to 16 days. The column is usable up to 21 days with 79.88% retaining of enzyme response.

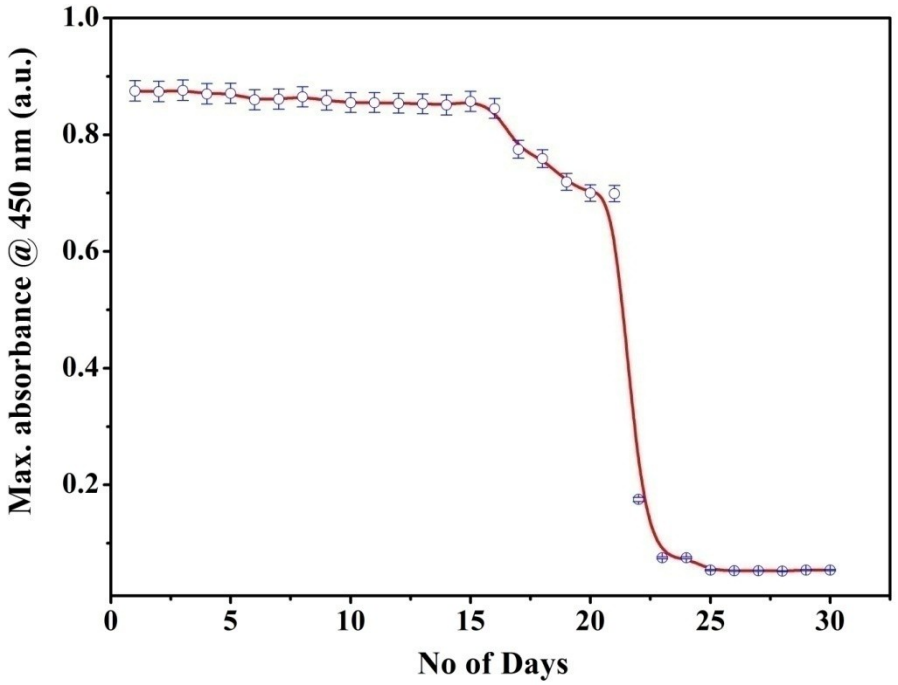

Figure 4.12 Stability performance of the column using 1 mM glucose; washing with 10 mM PBS at pH 7.4.

Reproducibility of a biosensor is an important consideration towards its practical use. Thus, the reproducibility of the developed biosensor has also been evaluated through batch studies. The developed colorimetric glucose biosensor shows good reproducibility (Table 4.4).

Table 4.4 Signal response of five diverse set of GOD-CPG column

[Glucose] mM	Maximum absorbance at 450 nm					Mean ± S.D.
	Set-1	Set-2	Set-3	Set-4	Set-5	
0	0.054	0.053	0.055	0.054	0.053	0.0538 ± 0.00084
0.001	0.358	0.356	0.357	0.358	0.355	0.3568 ± 0.0013
0.01	0.499	0.5	0.498	0.496	0.499	0.4984 ± 0.00152
0.1	0.696	0.697	0.696	0.699	0.695	0.6966 ± 0.00152
1	0.875	0.872	0.87	0.874	0.871	0.8724 ± 0.00207
2.5	0.944	0.945	0.943	0.947	0.944	0.9446 ± 0.00152
5	0.997	1.001	0.998	0.995	0.997	0.9976 ± 0.00219
10	1.056	1.059	1.055	1.057	1.054	1.0562 ± 0.00192

The stability and reproducibility of the column demonstrate that porous functional material (PFM) may provide a favourable microenvironment for the GOD immobilization and towards

the stabilization of its biological activity to a large extent due to high surface area.

4.4.4.7 Selectivity studies

Interference of other substances in human's blood can degrade the efficacy of glucose sensing. To verify the selectivity, the response of GOD-CPG column was recorded in presence and absence of glucose, uric acid (UA), ascorbic acid (AA), and dopamine (DA) under optimized conditions. AA, DA and UA normally co-exist with glucose in natural samples. As the normal physiological level of glucose in the human blood is about 30 times of AA, DA and UA (Chen *et al.,* 2008). Thus, the interference of AA, DA and UA was measured using 5 mM glucose and 5 mM glucose mixed with 0.5 mM AA, DA and UA through the column respectively. The results show that UA, AA and DA do not obviously perturb the detection of the glucose in its normal physiological level (Figure 4.13).

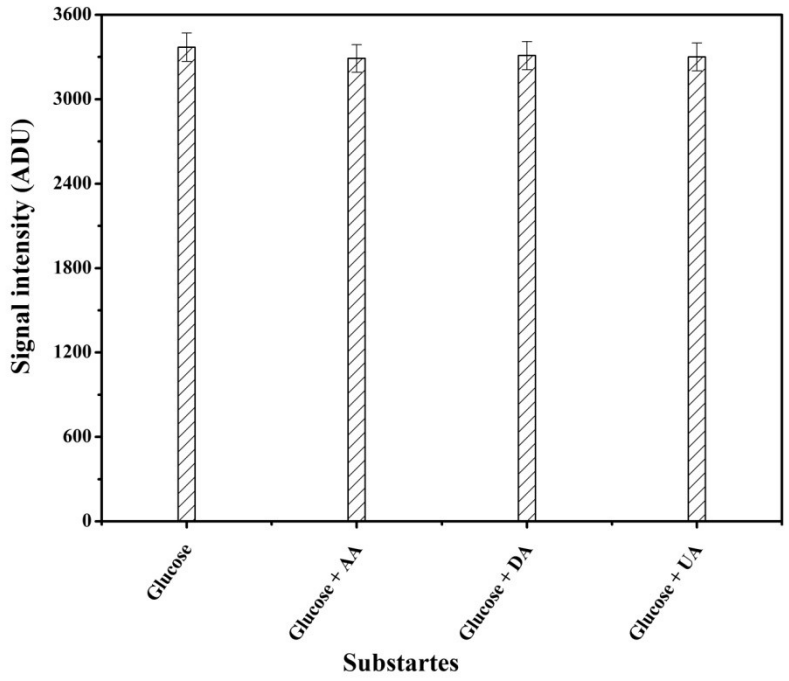

Figure 4.13 Interference study of the GOD-CPG column against 5 mM glucose and 5 mM glucose mixed individually with 0.5 mM AA, DA and UA.

Also, individually 0.5 mM AA, DA and UA were passed through the column to evaluate the selectivity of the GOD-CPG. The signal response was compared with the response against 5 mM glucose (Figure 4.14). It is found that the column is very much selective towards the glucose with respect to other interfering analytes present in the blood.

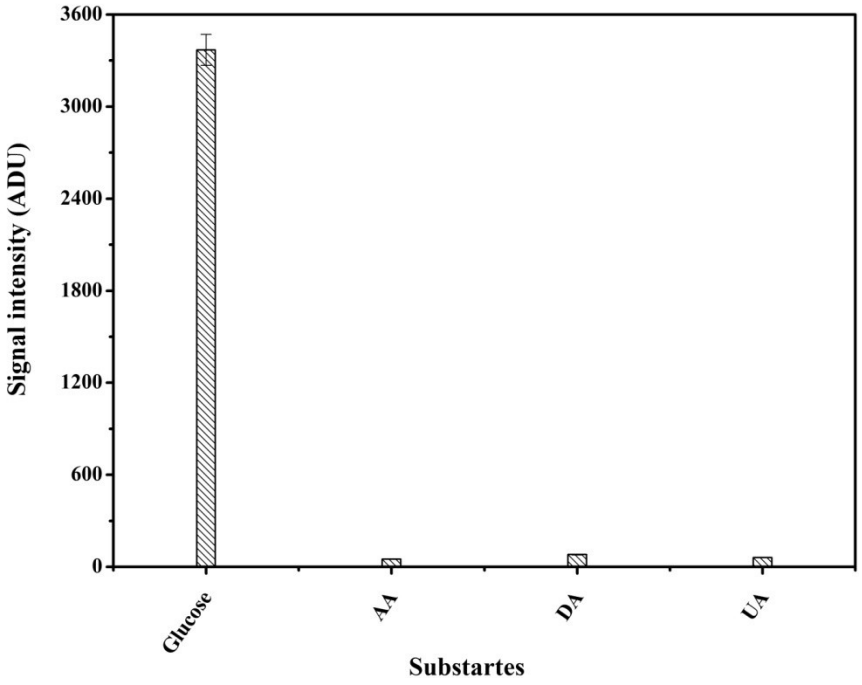

Figure 4.14 Selectivity study of the GOD-CPG column against 5 mM glucose and individual 0.5 mM AA, DA and UA.

4.5 A novel PFM entrapment sensing device

As a part of collaborative project between Biosensor Lab., BITS, Pilani-KK Birla Goa Campus and Raja Ramanna Centre for Advanced Technology (RRCAT), Indore, a novel device was designed and fabricated using copper (Cu) PCB as substrate material. The device was fabricated using synchrotron X-ray lithography beamline (BL-07) facility at Indus-2, (RRCAT, Indore). While the application of coli micro electrode array (CMEA) device for glucose sensing as a biochip device has been reported elsewhere, herein the use of CMEA as a novel entrapment device incorporating PFM has been reported.

4.5.1 Device fabrication

The device comprises of coil micro electrode with a spacing about 225 μM and width of 35 μM (Figure 4.15 (a)). 5 μL suspension containing 3 mg μL^{-1} of GOD-CPG bead suspension was dispensed onto the CMEA (Figure 4.15 (b)). The device retained GOD-CPG beads as entrapped materials. Glucose has been measured based on the electrochemical impedance spectroscopy (EIS) technique using the CMEA-PFM device as shown in Figure 4.15.

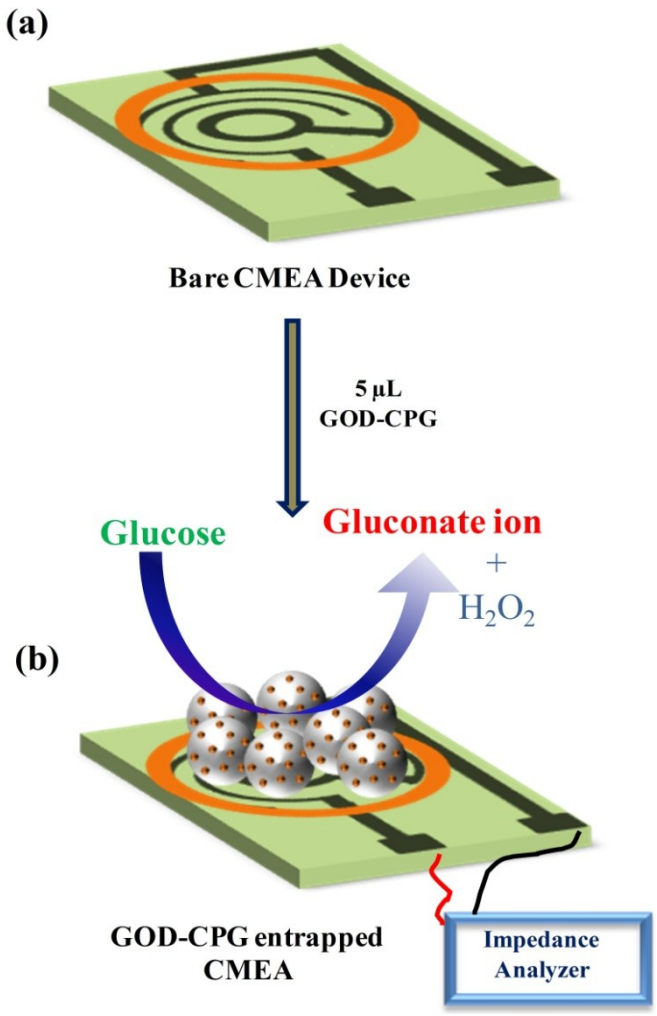

Figure 4.15 Schematic of (a) bare coil micro electrode device; (b) GOD-CPG entrapped CMEA device.

4.5.2 Principle of EIS glucose sensing

The sensing mechanism of electrochemical glucose sensor is based on the enzymatic reaction catalysed by GOD upon addition of glucose. The generation of gluconate ion can be explained according to the following reaction:

$$H_2O + O_2 + \beta\text{-D-Glucose} \xrightarrow{GOD} \delta\text{-D-gluconolactone} + H_2O_2 \qquad (4.1)$$

As a result of this reaction, δ-D-gluconolactone and H_2O_2 are produced. The concentration of these two products and the oxygen consumption can be used for the glucose detection. With H_2O available in the reaction, gluconolactone is spontaneously converted to gluconic acid, which at neutral pH forms the charged products of gluconate$^-$ and H^+, according to the equation below:

$$\delta\text{-D-gluconolactone} \xrightarrow{\text{Spontaneous}} \text{Gluconic acid} \xrightarrow{H_2O} \text{D-gluconate}^- + H^+ \qquad (4.2)$$

The gluconate ions thus produced have been monitored by change in double layer capacitance using EIS technique.

4.5.3 EIS measurements and calibration curve using PFM entrapment device

The adsorption of biomolecules typically causes the electrode capacitance and overall cell resistance to decrease and increase, respectively. However, the maximum sensitivity will be triggered by binding events that occur within the diffuse double layer whose thickness can be controlled by changing the ionic strength of the buffer electrolyte. Thus, if the electrolyte concentration is high, the double layer is compressed and the capacitance is dominated by changes occurring close to the electrode surface. However, if the electrolyte concentration is reduced, the sensitivity for the detection of larger entities, such as cells, is increased. Thus, the experiments on the device are carried out under the optimized PBS (10 mM, pH 7.4).

When the deposition time is fixed, the surface coverage of GOD is expected to be dependent on its bulk concentration. The surface coverage can change both the overall cell resistance and the capacitance, since adsorption may involve at least some displacement of water and ions from the interface. The GOD surface coverage was systematically varied by changing its concentration in the deposition solution, and the associated impedance changes were then measured as a function of the glucose concentration. The results indicate that an amount of 1.5 mg of GOD-CPG beads leads to suitable optimization for subsequent experiments.

Various glucose concentrations were spiked by standard addition method to the standard serum solution. The impedance was measured by adopting two electrode system (Bacher *et al.,* 2012) and the dynamic range and limit of detection were determined using the low electrolyte concentration.

Figure 4.16 shows a plot of the dependence of the impedance against various glucose concentrations in the frequency range of 1 Hz to 10 KHz at the applied potential of 5 mV. The total impedance is contributed for interfacial electrode impedance and dominated by capacitance, which is the imaginary part of the measured impedance, as the measurement is non-faradic. In this case the change in capacitance is due to the reaction of glucose and GOD; resulting ions were observed at low frequency of 1 Hz. For all interactions, an increase in concentration causes the overall magnitude of the impedance to decrease. The decreasing impedance suggests the higher current which is due to decomposition of β-D-Glucose to

gluconate$^-$, generated due to glucose and GOD reaction. This suggests that the generation of more gluconate$^-$ affects the double layer capacitance.

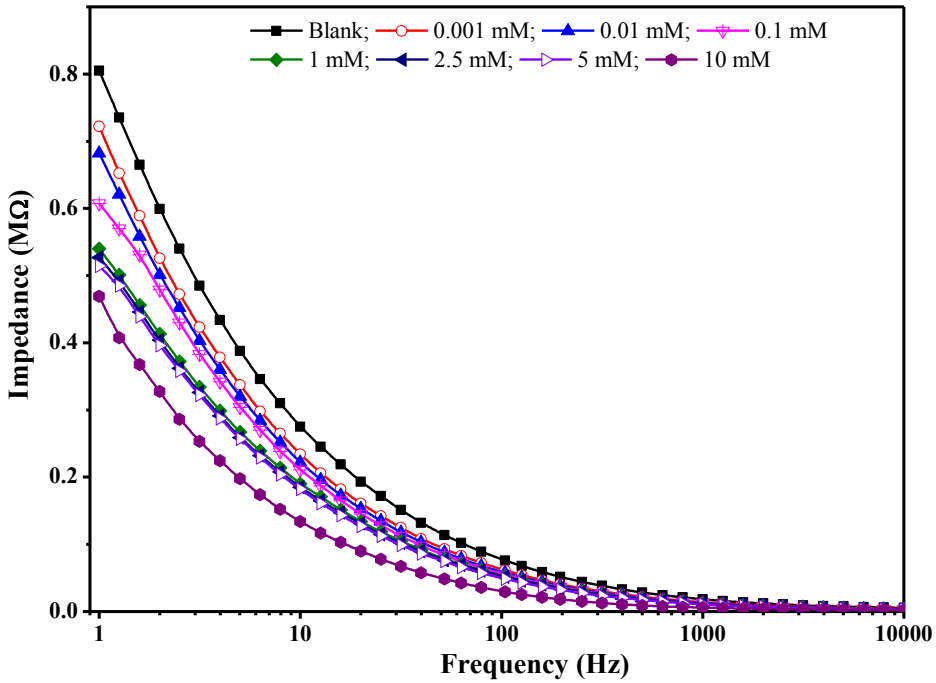

Figure 4.16 Impedance spectra for various concentrations of glucose. Frequency range: 1 Hz to 10 KHz, 5 mV ac applied potential.

Impedance data were recorded for the functionalized GOD-CPG beads after exposing it to increasing glucose concentration (0.001 mM – 10 mM). A frequency of 1 Hz at applied ac potential 5 mV was selected for analysis since at this frequency significant change in impedance was observed. The percentage impedance change has been calculated for each concentrations of glucose. The resulting data has been plotted against various glucose concentrations and presented in Figure 4.17.

The calibration is found to be linear in the range of 0.001 mM – 10 mM (R^2 = 0.9905, n = 5) with R.S.D. of 1.28 ± 0.023. The linear equation is; y = 7.49751 x (mM) + 31.866642. LOD is found to be 0.001 mM. The K_m is found at 0.0159 mM using GOD-GPG EIS system, almost near to the colorimetric assay.

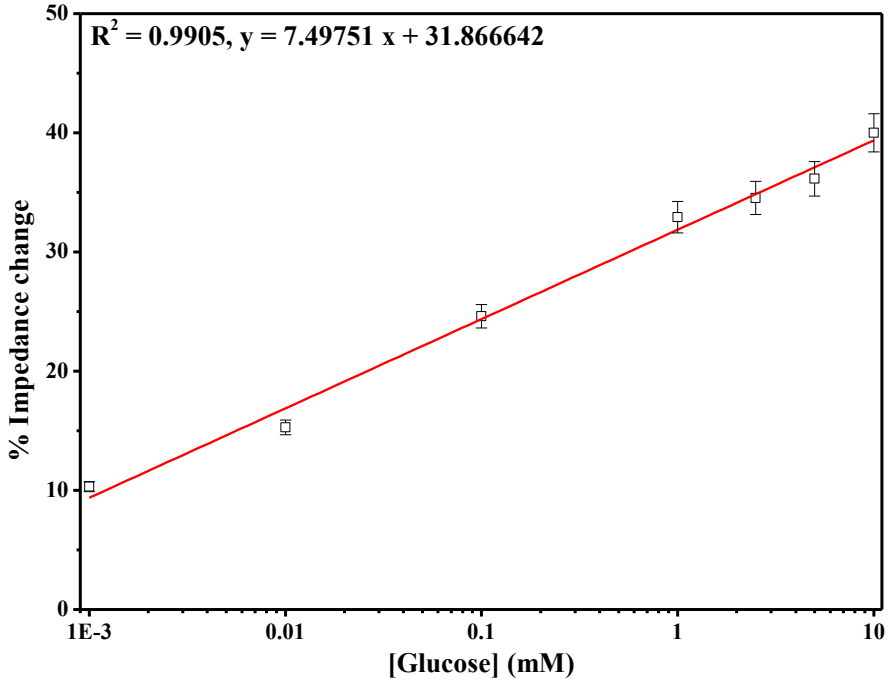

Figure 4.17 Calibration curve for glucose biosensing using GOD-CPG in device.

Finally the three diverse set of devices were tested for a continuous monitoring of glucose. For this purpose, one device was monitored continuously 15 days with 3 measurements per day using 5 mM glucose. The results have been plotted in Figure 4.18.

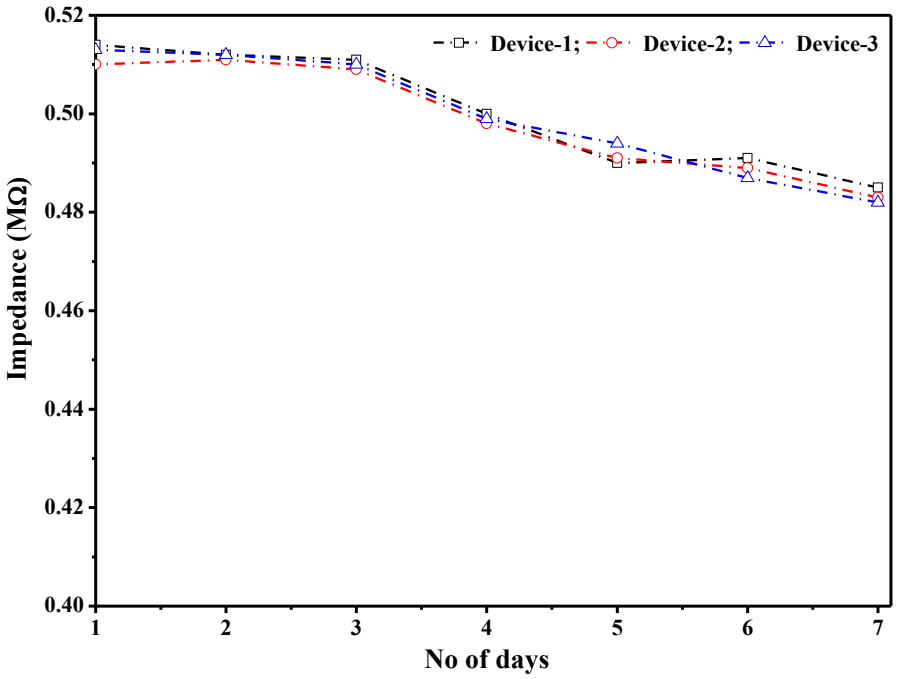

Figure 4.18 Impedance response for three different GOD-CPG devices for continuous glucose measurement using 5 mM glucose.

Using GOD-CPG device, glucose can be monitored continuously up to 7 days with 3 repeated times per day. The enzyme retains 94.28% of its original activity. But, after 7th day, no significant impedance value was measured using the same device.

Thus, GOD-CPG PFM CMEA device has been successfully demonstrated and found to be suitable for glucose sensing using EIS. This novel feature provides enhanced capability infield detection and storage. The measured K_m value using colorimetric and EIS technique are almost similar. So, in entrapment of GOD-CPG approach, enzyme activity has not been affected.

4.6 Functionalized mesoporous silica for heavy metal detection

4.6.1 Introduction

Heavy metals are commonly defined as those having a specific density of more than 5 g cm^{-3}. The main threats to human health from heavy metals are associated with exposure to lead, cadmium, mercury and arsenic (arsenic is a metalloid, but is usually classified as a heavy metal). Heavy metal contamination is potentially a significant problem in several community and agricultural areas because agrochemicals, including plant nutrients and fertilizers, are the primary source of toxic heavy metals (Godwin, 2001). These heavy metals that contaminate groundwater via percolation or run-off through soils and landfills are a major concern for human health and environment. Among them, lead (Pb^{2+}), a major environmental pollutant, can cause serious damage to brain and central nervous system of human health, especially to children in low-level exposure (Needleman, 2004; Bellinger, 2004). Pb^{2+} is widely distributed in water due to its use in batteries and pigments (ATSDR, 2005). Therefore, Pb^{2+} can be accumulated in human body through water intake or food chains. Accumulation of Pb^{2+} may cause adverse effects on human health including hypertension, nervous system effects, kidney damage, and reproductive problem (Apostoli *et al.,* 1998; Navas-Acien *et al.,* 2007). The maximum contaminant level (MCL) for lead in drinking water has been set to be 0.015 mg L^{-1} and 0.5 mg L^{-1} by the USEPA and FSSAI respectively. However, recent studies have shown that levels <10 µg dl^{-1} in children may lead to substantial neuro-behavioural problems (Bernard, 2003; Canfield *et al.,* 2003; Bellinger, 2008). It is of great importance to monitor the trace amounts of Pb^{2+} in environmental samples. Therefore, highly sensitive monitoring of lead in water is essential for environmental risk assessment.

The development of sensors to detect Pb^{2+} in environmental and biological samples is of considerable significance in current research. Many sensitive analytical methods including atomic absorption spectrometry (AAS), inductively coupled plasma-mass spectrometry (ICP-MS), inductively coupled plasma-atomic emission spectrometry (ICP-AES), UV-vis spectrometry have been reported for detection of Pb^{2+} etc. (Ma *et al.,* 1994; Liu *et al.,* 2000; Hu *et al.,* 2003). Owing to costly apparatus and requirement of complicated pre-treatment procedures, these techniques are inappropriate for on-site and real-time detection. Due to high sensitivity, facile operation, non-sample-destructing and ability to provide *in situ* and real-time information for variety of applications, fluorescence Pb^{2+} sensors have attracted great attention (Telting-Diaz and Bakker, 2002). As a result, various sensitive Pb^{2+} fluorescence sensors employing peptides, proteins and DNAenzymes as recognition modules have been developed in the last decades (Table 4.5).

Table 4.5 Various reported fluorescence detection probe for detection of Pb^{2+}

Sensor configuration	Transduction principle	Detection range (nM)	References
Pb^{2+} -regulatory protein *Ralstonia metallidurans* CH34 as probe	Fluorescence reporter	500 – 10000	Chen *et al.,* 2005
Thrombin-binding aptamer (TBA) labelled DNA probe	Fluorescence resonance energy transfer (FRET)	0.5−30	Liu *et al.,* 2009a
DNAzyme catalytic beacon sensor	Temperature independent fluorescence	25 – 50000	Nagraj *et al.,* 2009
DNA logic gate utilizing a K^{+}–Pb^{2+}-switched G-quadruplex DNAzyme	Zinc protoporphyrin IX fluorescence	5 – 100	Li *et al.,* 2009
Graphene–DNAzyme Based Biosensor	Amplified fluorescence "Turn-On"	1 – 1000	Zhao *et al.,* 2011

Among the reported sensors, DNA-based biosensors have received an increasing attention for the detection ultra traces of Pb^{2+}. However, these high sensitive DNA based biosensors suffer from some major drawbacks including high enzyme cost, complicated processing steps and instability of bio-molecules such as RNA (Bahrami *et al.,* 2014). Therefore, there is need for the development of inexpensive, sensitive and selective sensors for detecting Pb^{2+} ions in water.

Herein, the aim is to develop a nano sensing probe using fluorescein isothiocyanate (FITC) modified SBA-15. Further, FITC has been grafted into SBA-15 pores via covalent coupling and deployed for the fabrication of a low cost miniaturized selective and sensitive Pb^{2+} sensor.

4.6.2 Experimental Section

4.6.2.1 Materials and instrumentation

Pluronic P123 (poly(ethylene glycol)–poly(propylene glycol)–poly(ethylene glycol)) (PEG–PPG–PEG) was procured from Aldrich (USA). 3-aminopropyltriethoxysilane 99% (APTES) was purchased from Acros Organics (USA). Fluorescein isothiocyanate (FITC) Isomer-I was procured from Calbiochem (U.S.A.). AAS grade, lead (Pb^{2+}) and cadmium (Cd^{2+}) standard solutions were purchased from Sigma Chemical Co. (USA). Sodium phosphate dibasic (Na_2HPO_4), sodium phosphate monobasic (NaH_2PO_4, H_2O), tetraethyl orthosilicate (TEOS) and other chemicals were of GR grade, Merck (Germany. Fourier Transform InfraRed (FT-IR) spectra were recorded using IRAffinity-1 (SHIMADZU, Japan) with attenuated total reflectance (ATR) attachment Specac Diamond ATR AQUA. Nitrogen adsorption–desorption isotherms were obtained using a Micromeritics Tristar 3000 (N_2-BET) surface area and porosity analyzer (USA). Transmission electron microscope (TEM) images were recorded using Jeol JEM 1400Plus (Japan) at University of Leeds, UK. Fluorescence images were recorded using an upright confocal microscope (Zeiss LSM510 META, Bio-imaging facilities at University of Leeds UK).

4.6.2.2 Synthesis of SBA-15

The synthesis of mesoporous silicate SBA-15 was a part of a collaborative UKIERI-DST project between BITS, Pilani-KK Birla Goa Campus and University of Leeds, UK. The detail synthesis of material was reported elsewhere (Naik *et al.,* 2010) and the product was received from Prof. N. N. Ghosh, Department of Chemistry, BITS, Pilani-KK Birla Goa Campus.

4.6.2.3 Solution preparation

All buffer solutions were prepared as discussed earlier. A 100 mg L^{-1} stock solution of Pb^{2+} was prepared by diluting in PB (100 mM, pH 7.4). Working solutions of Pb^{2+} (100 ng mL^{-1} to 0.01 ng mL^{-1}) were prepared freshly in PB.

4.6.2.4 Construction of sensing probe

Fabrication of sensing probe was based on the efficient immobilization of FITC through SAMs of APTES. The glass containers used for preparation of SAMs were cleaned with Piranha solution as described in section 2.3.4 (**caution**: Piranha solution reacts exothermally and strongly reacts with organics). APTES was used for functionalizing of SBA-15 as described by Zhang *et al.* (Zhang *et al.,* 2012), with some alteration. Before surface modification, SBA-15 was activated by refluxing in 0.1 M HCl for 12 h to increase the hydroxyl group content on the surface. Activated SBA-15 (500 mg) was dispersed into 17.5 mL toluene. After gradually adding APTES (0.5 mL), resulting mixture was refluxed under stirring for 12 h. The APTES functionalized material (NH_2-SBA-15) was filtered, washed and dried under vacuum. Subsequently, FITC probe molecules were attached on the modified NH_2-SBA-15 particles. The NH_2-SBA-15 particles (4 mg) and FITC (20 mg) were dispersed in ethanol (2 mL) and the resulting solution was allowed to shake at room temperature. After 24 h, FITC grafted mesoporous particles (FITC–NH–SBA-15) were obtained and thoroughly washed with ethanol and then were re-dispersed into water. The grafting of FITC onto the pores of SBA-15 is shown in Figure 4.19.

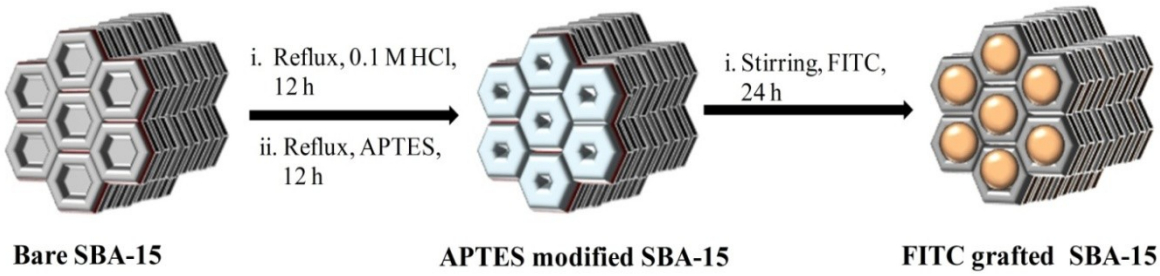

Figure 4.19 Schematic for construction of detection probe.

Finally, a drop of water dispersion of FITC–NH–SBA-15 particles was placed on a glass slide to take fluorescence microscopy images using a laser scanning confocal microscope (LSCM).

During measurement, suspended FITC–NH–SBA-15 particles (3 μL) were spotted onto a glass slide that were dried by keeping in dark for 30 min. 1 μL of varying concentrations of Pb^{2+} in the range from 0.01 ng mL^{-1} to 100 ng mL^{-1} were incubated for 15 min and the images were taken using LSCM. The schematic of experimental steps is presented in Figure 4.20.

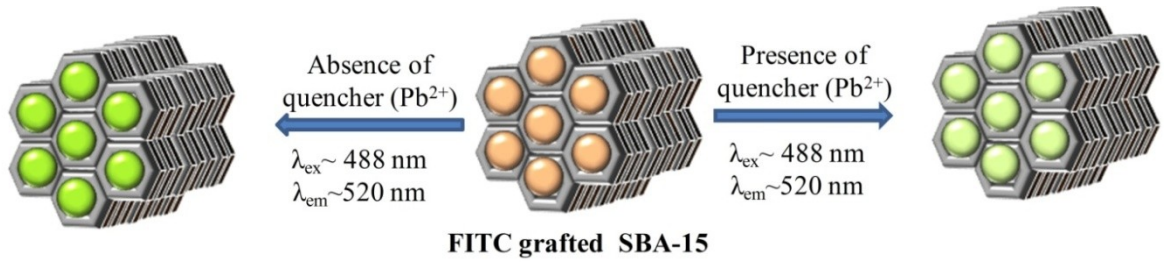

Figure 4.20 Schematic representation of experimental steps of developed sensor.

4.6.3 Results and Discussion

4.6.3.1 TEM analysis of SBA-15

The pore size and periodicity in the mesostructure of SBA-15 materials were confirmed directly by transmission electron microscopy (TEM) (Figure 4.21). TEM image for a representative material (SBA-15), exhibits a highly ordered hexagonal arrangement of mesopores.

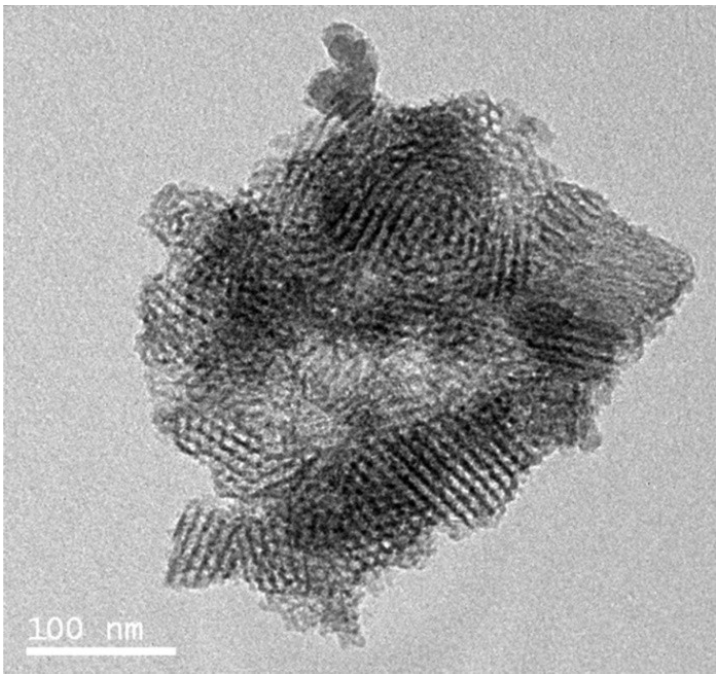

Figure 4.21 TEM micrograph of SBA-15

4.6.3.2 Spectroscopic characterization by FT-IR

FT-IR spectroscopy was applied to measure the surface properties of FITC coupling through APTES on SBA-15 surface. FT-IR ATR spectra were collected at a resolution of 4 cm^{-1} (68 scans). Figure 4.22 shows the FT-IR spectra of SBA-15, NH_2-SBA-15 and FITC–NH–SBA-15.

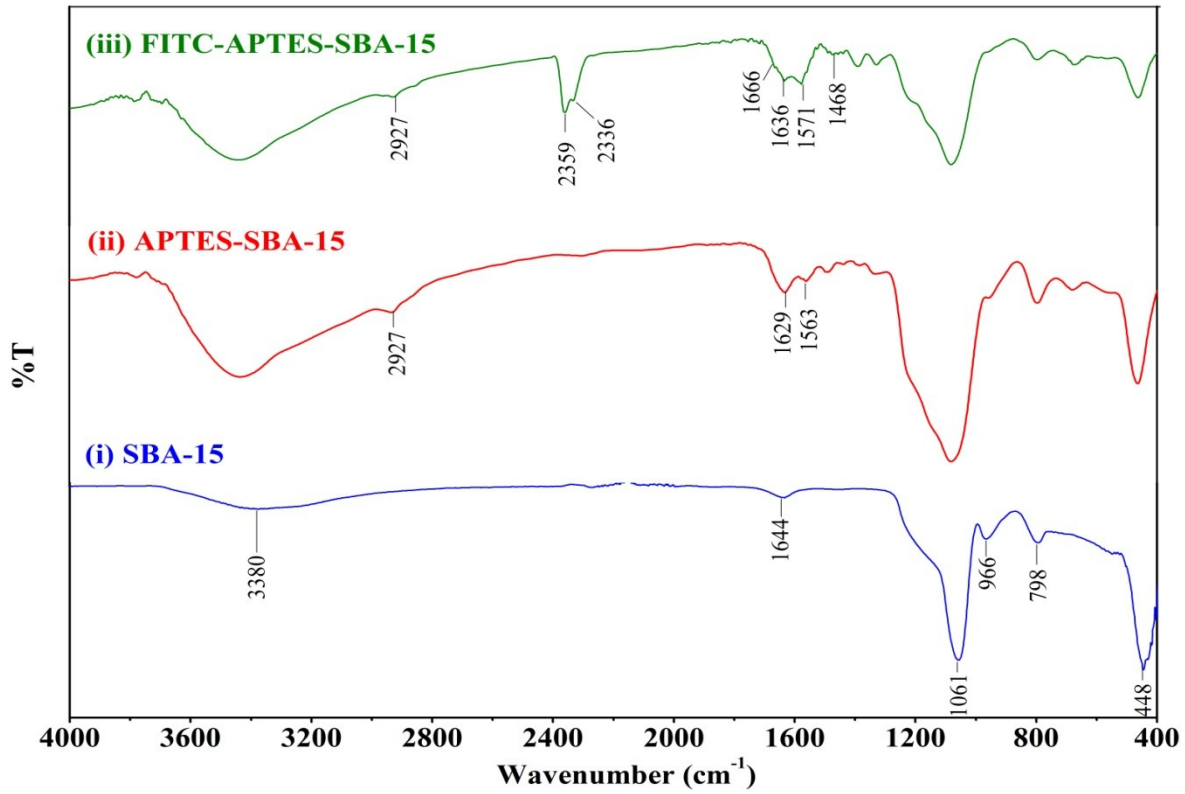

Figure 4.22 ATR FT-IR spectrum of SBA-15: (i) bare; (ii) functionalized with APTES and (iii) coupled with FITC *via* APTES.

The spectrum in Figure 4.22 (i) shows typical IR vibration bands for SBA-15 and interpreted as 3380 and 1644 cm^{-1} for H-bonded hydroxyls -O-H stretching and adsorbed water bending vibrations, 1061 cm^{-1} for asymmetric stretching vibrations of Si–O–Si, 798 cm^{-1} for symmetric stretching vibrations of Si–O–Si, 966 cm^{-1} for bending mode of Si–OH and 448 cm^{-1} for bending vibration of Si–O–Si. After functionalizing by APTES, the band at 966 cm^{-1} completely disappeared and several new vibration bands appeared at 2927 cm^{-1} for C–H group and 1629 cm^{-1}, 1563 cm^{-1} for two N–H bending vibrations showing that the APTES has successfully reacted with surface silanol groups and covalently attached to the SBA-15 (Figure 4.22 (ii)).

These peaks, however, have completely vanished upon the FITC treatment (Figure 4.22 (iii)). The existence of isothiocyanate (-N=C=S) in the samples is shown by presence of an absorption band at 2359-2336 cm^{-1}, corresponding to the characteristic –N=C=S stretching vibration. Further new three absorption bands at 1666, 1636 and 1571 cm^{-1} are ascribed to the absorption by the amide group, which links NH_2-SBA-15 and FITC to produce FITC-NH-SBA-15. The additional IR peak at 1468 cm^{-1} may be due to C-H deformation.

4.6.3.3 LSCM fluorescence microscopy study

To confirm the FITC grafting on the surface of SBA-15, a drop of water dispersion of FITC–NH–SBA-15 particles was placed on a glass slide to acquire fluorescence microscopy images using a laser scanning confocal microscope (LSCM) and presented in Figure 4.23. During measurement, suspended FITC–NH–SBA-15 particles (3 μL) were spotted onto a glass slide that was dried by keeping in dark for 30 min and the images were taken using LSCM. Further, 1 ng mL^{-1} of Pb^{2+} (1 μL) were incubated for 15 min with FITC–NH–SBA-15 particles and the images were acquired.

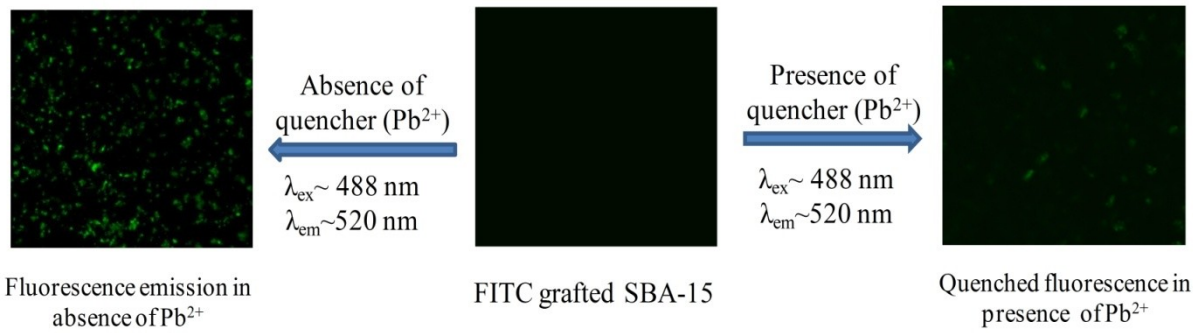

Figure 4.23 LSCM Fluorescence images in presence and absence of quencher.

4.6.3.4 Surface area and porosity analysis

The nitrogen (N_2) adsorption - desorption isotherms as well as pore size distributions of functionalized SBA-15 samples were recorded and presented in Figure 4.24. Samples were prepared for surface area and porosity analysis by drying at 180 ºC for 12 h with a constant flow of dry N_2 gas. For all the samples, type IV isotherm with H1 hysteresis loop was observed, which is the characteristic of mesoporous material. Pore volume and BET surface area are found to decrease significantly with increasing functional content.

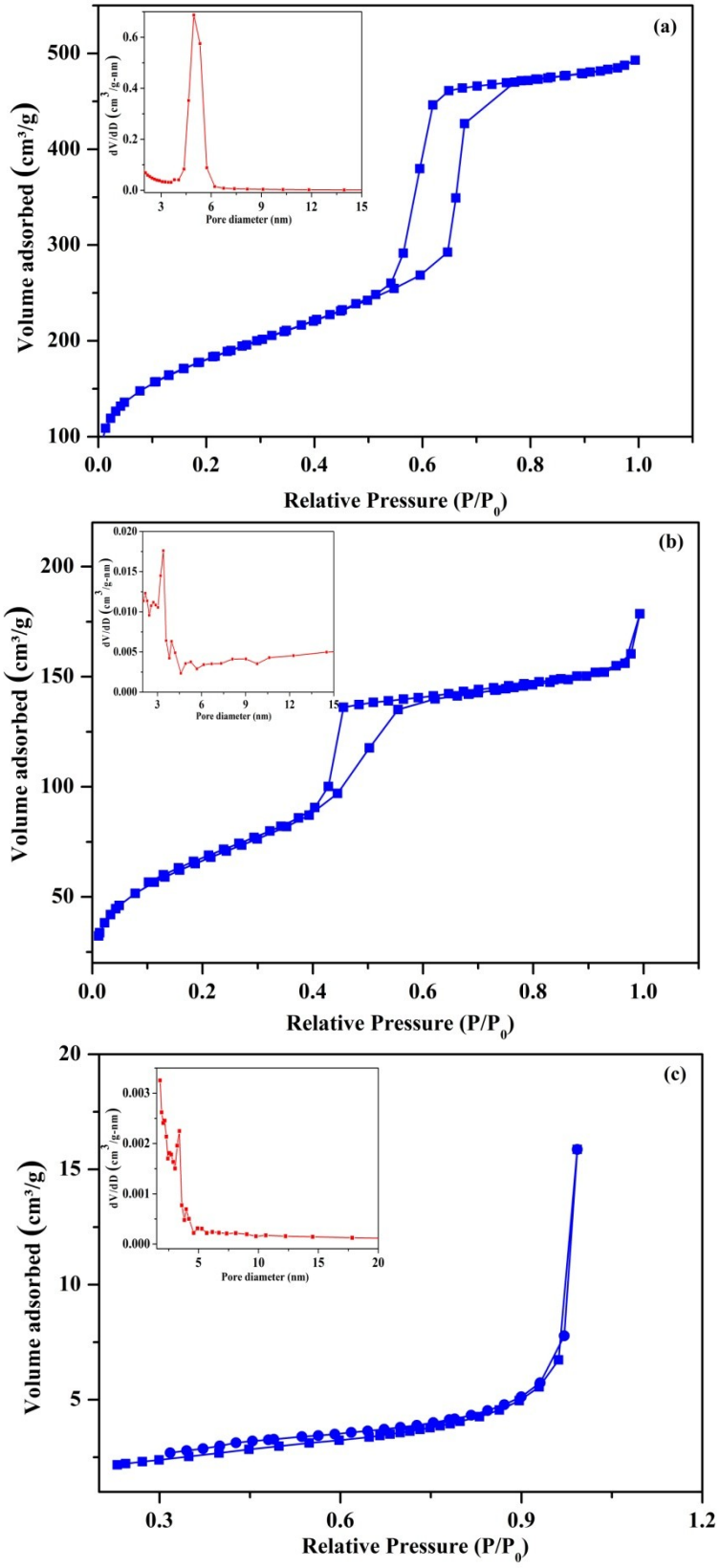

Figure 4.24 N_2 adsorption–desorption isotherms and pore size distribution (Inset) curves of (a) SBA-15; (b) APTES modified SBA-15; (c) FITC grafted SBA-15.

Due to APTES functionalization on SBA-15, pore volume was decreased from 0.798 cm^3 g^{-1} to 0.280 cm^3 g^{-1}; whereas the BET surface area was lowered from 624 m^2 g^{-1} to 241 m^2 g^{-1}. Upon further modification with FITC, the pore volume and BET surface area were decreased dramatically from 0.280 cm^3 g^{-1} to 0.025 cm^3 g^{-1} and 241 m^2 g^{-1} to 7.14 m^2 g^{-1} respectively. These results can be attributed to the occupancy of FITC into the pores of mesostructure. A comparison between pore volume and BET surface area is plotted and presented in Figure 4.25.

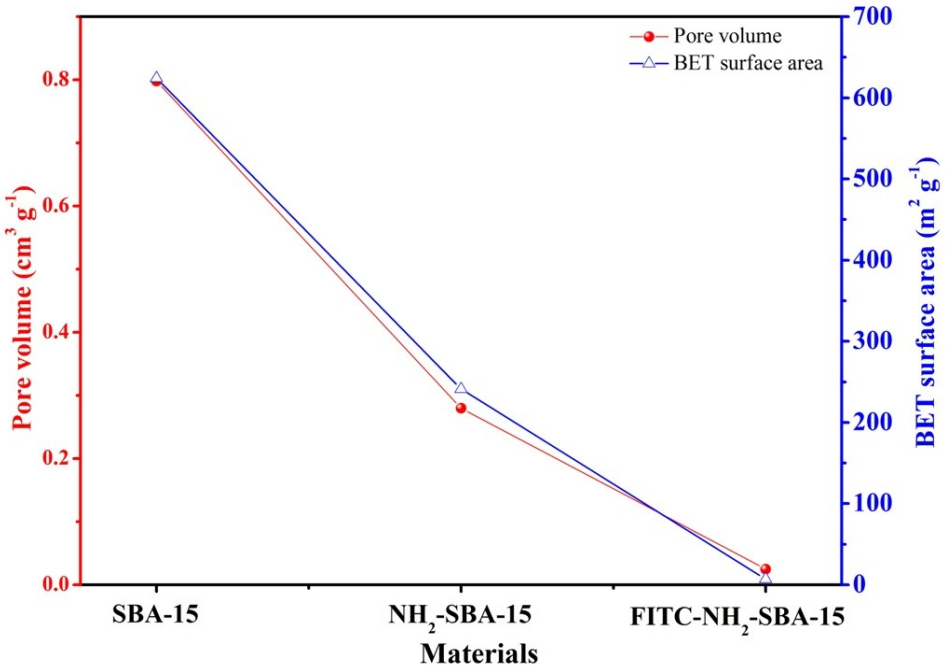

Figure 4.25 Comparison of pore volume and BET surface area of SBA-15, APTES modified SBA-15 and FITC grafted SBA-15.

4.6.3.5 Optimization of sensing probe

In order to achieve the best performance of fluorescence sensing probe (FITC-NH-SBA-15), the reaction was optimized under pH~7.4. Optimizing concentration of the sensing probe in the system is very critical, because presence of its higher as well as at lower concentration may cause lowering of fluorescence. So the optimum concentration of the particles *i.e.* 0.65 mg μL^{-1} has been used in the reaction. Fluorescence quenching property of the synthesized probe has been evaluated with Pb^{2+} solutions having concentration range of 0.01 ng mL^{-1} to 100 ng mL^{-1}.

The optimized amount of probe particles was spotted on a glass slide to produce an array and was incubated for 15 min in dark. Subsequently, the fluorescence of incubated samples was measured under the LSCM. Figure 4.26 (i) shows the inhibition kinetics with respect to 1 ng mL^{-1} of Pb^{2+}. For the inhibition studies, the signal intensity is saturated within 120 sec (Figure 4.26 (ii)). So, the analysis time of 120 sec was found to be optimal for inhibition studies throughout the experiment.

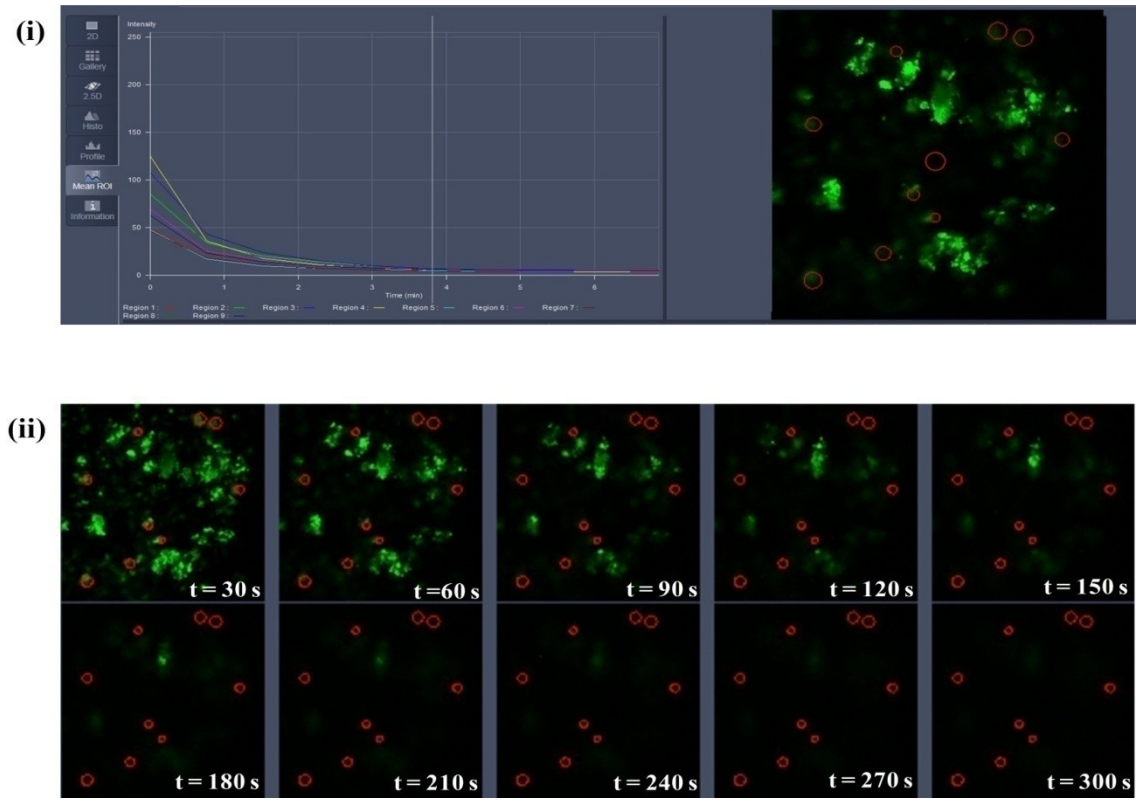

Figure 4.26 (i) LSCM real time fluorescence intensity profile (ii) kinetic image profile; for Pb^{2+} inhibition using [Pb^{2+}] = 1 ng mL^{-1}; in PB at pH ~ 7.4.

4.6.3.6 Sensor performance and calibration curve

The image analysis and the intensity calculation were done with the help of software Zen 2009 and ImageJ. It is observed that, with increasing Pb^{2+} concentration, the intensity of the fluorescence signal is decreased. It is also observed that the particles are agglomerated with increasing concentration of Pb^{2+} ions. This property of sensor has been utilized to detect the Pb^{2+} in water.

The inhibited signal intensity against varying concentrations of Pb^{2+} is presented in Figure 4.27. The I % was calculated using the equation 2.5. Calibration was performed for Pb^{2+}

samples in water. The inhibition curve for Pb^{2+} spiked water samples was obtained for five different concentrations of Pb^{2+} *i.e.* 0.01, 0.1, 1, 10 and 100 ng mL^{-1} by LSCM in quantitative mode. The data points are fitted to detect an unknown [Pb^{2+}] from mean standard deviation curve. The linearity is found in the range 0.01 to 100 ng mL^{-1} (n = 3) with an R.S.D of 4.77% ± 0.8. A good sensitivity of about 80 ADU change per decade with S.D. = 0.57 and R^2 = 0.9984 has been observed. The linear equation is; y = 12.522 x (ng ml^{-1}) + 50.0524. The LOD is found to be 0.01 ng mL^{-1}. The IC_{50} value of developed sensor is found at 0.94 ng mL^{-1}.

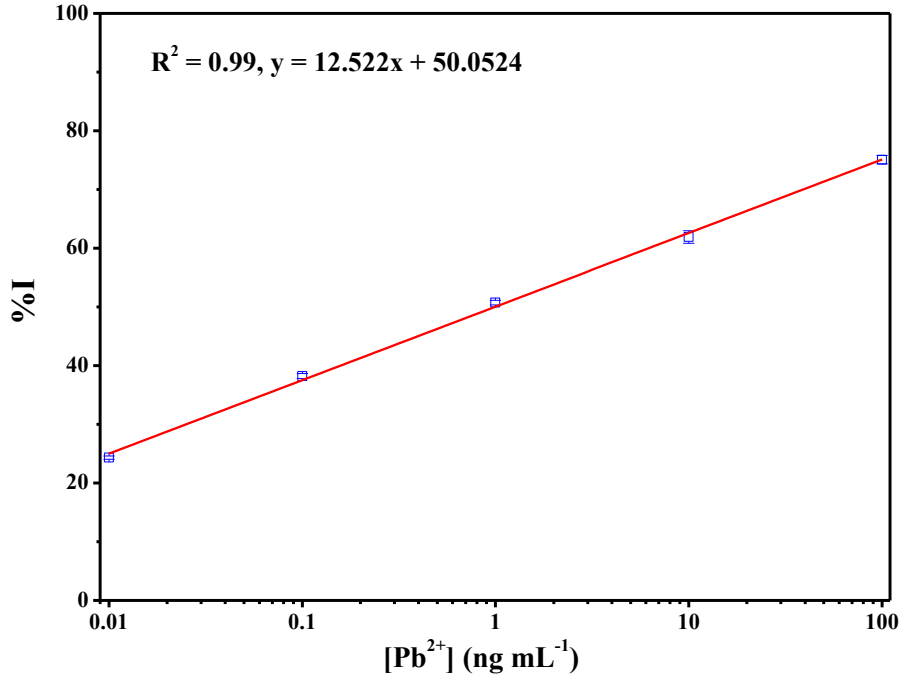

Figure 4.27 Inhibition curve for different Pb^{2+} concentrations.

4.6.3.7 Selectivity of sensing probe

To establish whether the sensing probe is Pb^{2+}-specific, control experiments were performed using another divalent metal ion, Cd^{2+}. Figure 4.28 (a) shows a comparative sensing of modified SBA-15 towards Pb^{2+} and Cd^{2+} (0.01 – 100 ng mL^{-1} concentration range) at t = 60 sec. It is very much evident from the figure that with increasing Pb^{2+} concentration, there is a pronounced effect on the sensing probe whereas no such effect of increasing Cd^{2+} concentration on the sensing probe has been revealed. Agglomeration of sensing probes is increased with increasing Pb^{2+} concentration in the range 0.01 to 100 ng mL^{-1}. Larger atomic weight and lower electronegativity of the heavy Group 14 post-transition element coupled with relative standard reduction potential of Pb^{2+} over Cd^{2+} might play major roles in the preference of sensing probe for Pb^{2+} (Pearson, 1963; Klopman, 1968). The mixture of two

metal ions was used to corroborate the selectivity towards Pb^{2+}. Three micro-spots were respectively incubated in presence of Pb^{2+}, Cd^{2+} and Pb^{2+}- Cd^{2+} mixture each with 10 ng mL^{-1} concentration. The fluorescence response behaviour is presented in Figure 4.28 (b).

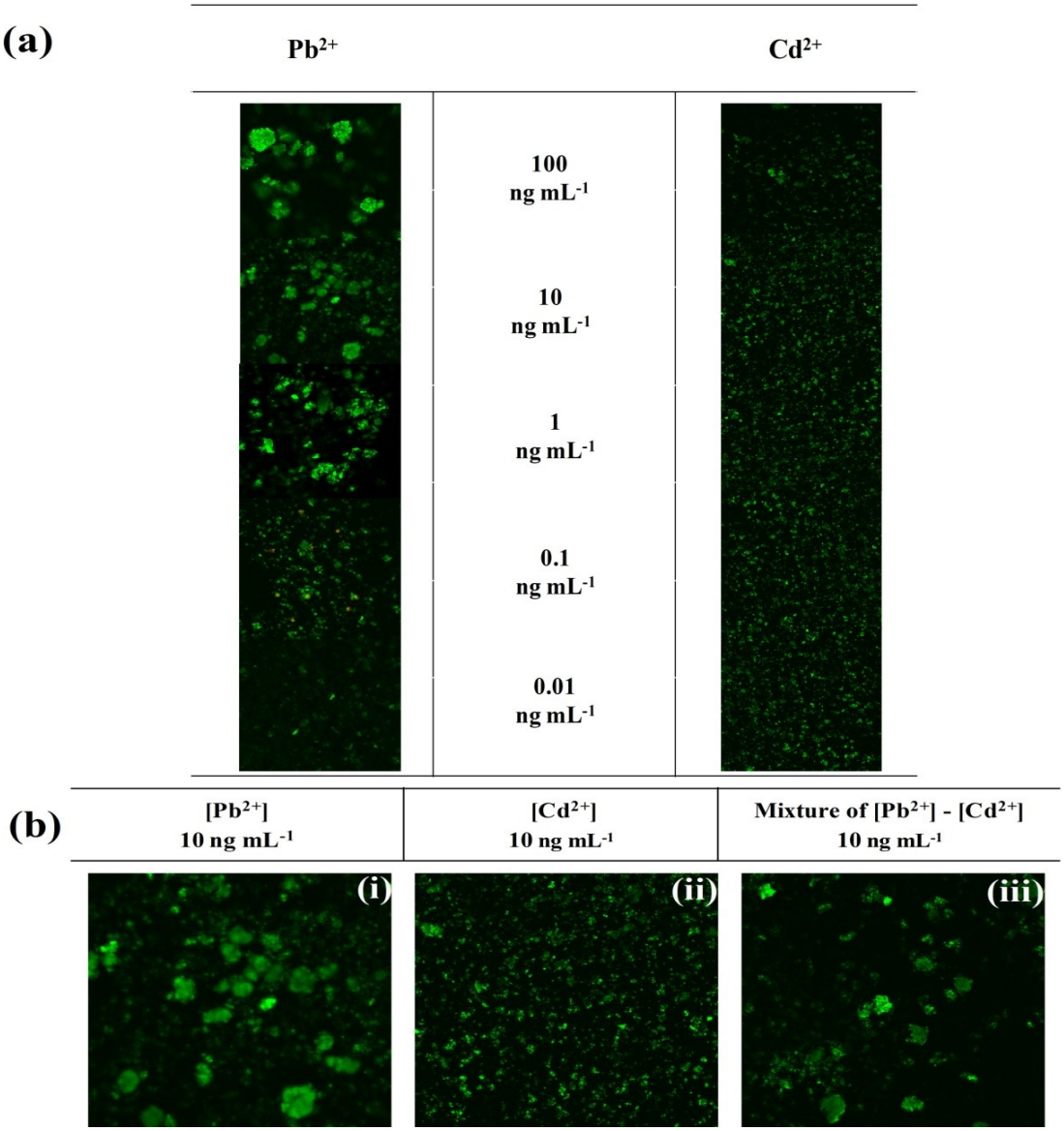

Figure 4.28 (a) Comparison of rate of agglomeration for different concentrations of Pb^{2+} and Cd^{2+}; (b) Comparison of spot fluorescence image incubated with (i) 10 ng mL^{-1} of Pb^{2+}, (ii) 10 ng mL^{-1} of Cd^{2+}, (iii) 10 ng mL^{-1} of Pb^{2+}- Cd^{2+} mixture.

The spot incubated with Pb^{2+} (Figure 4.28 (b) (i)) shows usual agglomeration whereas Figure 4.28 (b) (ii) exhibits no such behaviour for addition of Cd^{2+}. On the other hand, Figure 4.28 (b) (iii) shows agglomeration for Pb^{2+}- Cd^{2+} mixture. The appearance of such agglomeration behaviour in the spot test with the mixture is strongly suggestive of the presence of Pb^{2+} in the sample. This observed difference in agglomeration of Pb^{2+} might be a cause of enhanced

selectivity and specificity. The fluorescence intensity was also recorded and plotted for various concentrations of Pb^{2+} and Cd^{2+} (Figure 4.29). The significant decrease in fluorescence intensity (On to OFF transition) in the graph indicates that the Pb^{2+} complexes with immobilized FITC. Interestingly, significant change in fluorescence intensity was not observed with other metal ions.

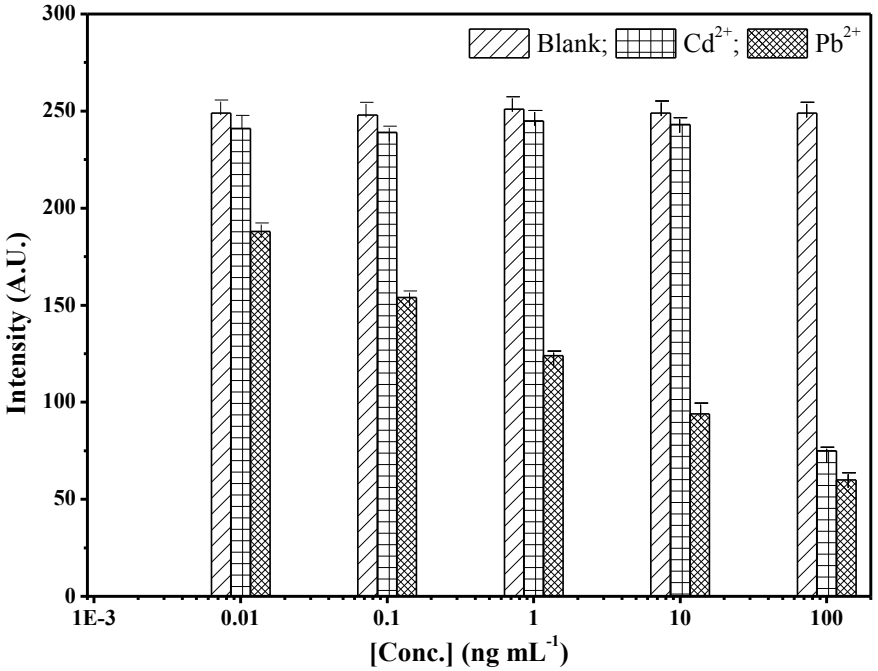

Figure 4.29 Comparison of signal intensity for the various concentration of Pb^{2+} and Cd^{2+} against blank response.

4.7 Significant findings on PFM as sensors

The porous materials have been exploited as sensor applications. A glucose biosensor based on GPG and also a heavy metal sensor using SBA-15 have been demonstrated. Significant findings using the PFM based bio and chemical sensors are summarized in Table 4.6.

Table 4.6 Significant findings using the porous materials based bio and chemical sensors

Sensor configuration	Analyte	Transduction principle	Detection range	Detection limit
GOD immobilized GA activated silanized CPG	Glucose	Colorimetric	10 – 0.001 mM	0.001 mM
		Impedimetric	10 – 0.001 mM	0.001 mM
FITC grafted GA activated silanized SBA-15	Pb^{2+}	Fluorescence quenching	100 - 0.01 ng mL^{-1}	0.01 ng mL^{-1}

4.8 Conclusion

In summary, biocompatible macroporous material (CPG) has been successfully constructed as an efficient capture probe and applied for glucose sensing as a model analyte. The sensing probe has been applied simultaneously as duel read out system *i.e.* colorimetric and impedimetric. In both cases, glucose is measurable in the range from 0.001 mM to 10 mM. It is also found that the enzyme retains its activity for a longer time even after multiple measurements. The K_m using colorimetric and EIS technique is found to be 0.013 mM and 0.0159 mM, respectively. Thus, almost similar K_m indicates that enzyme retained its activity during entrapment of the materials. The developed sensor may be applied for regular and continuous monitoring system for glucose. The high sensitivity and good stability of a modified GPG have led to construct a practical glucose biosensor successfully, which might also be extended further to the immobilization of some other biomolecules.

Furthermore, another application has been developed using FITC functionalized mesoporous silica (SBA-15) and demonstrated for the application of Pb^{2+} sensing. So far as knowledge is concerned, this is the first report of a FITC coupled SBA-15 nano sensor for amplified fluorescence detection of Pb^{2+}. The nano sized pores of SBA-15 were exploited as host for anchoring FITC molecule. The developed sensor for Pb^{2+} is found linear in the range 0.01 – 100 ng mL^{-1} with LOD 0.01 ng mL^{-1} and IC_{50} 0.94 ng mL^{-1}. An important feature of developed sensor is low sample volume (1 µL) with short analysis time 2 min. Further, the developed sensor has exhibited good sensitivity and selectivity in presence of another divalent ion Cd^{2+}. Therefore, this sensing strategy provides a simple, quick, and sensitive method for the detection of heavy metal ions in water samples.

CHAPTER 5: DEVELOPMENT OF NANO-IMMUNOSENSOR FOR EARLY STAGE CANCER DETECTION

Highlights:

- A high throughput novel hybrid miniaturized ELISA assay using antibody immobilized ZnONPs has been developed for the detection of CEA.
- The immunosensor has exhibited an excellent analytical performance in terms of sensitivity, with a much lower detection limit, selectivity, reproducibility of the measurements and thermal stability as compare to microwell plate ELISA.
- The most promising feature of this ZnONPs – ELISA is the high capture efficiency and lower cost over other reported materials.

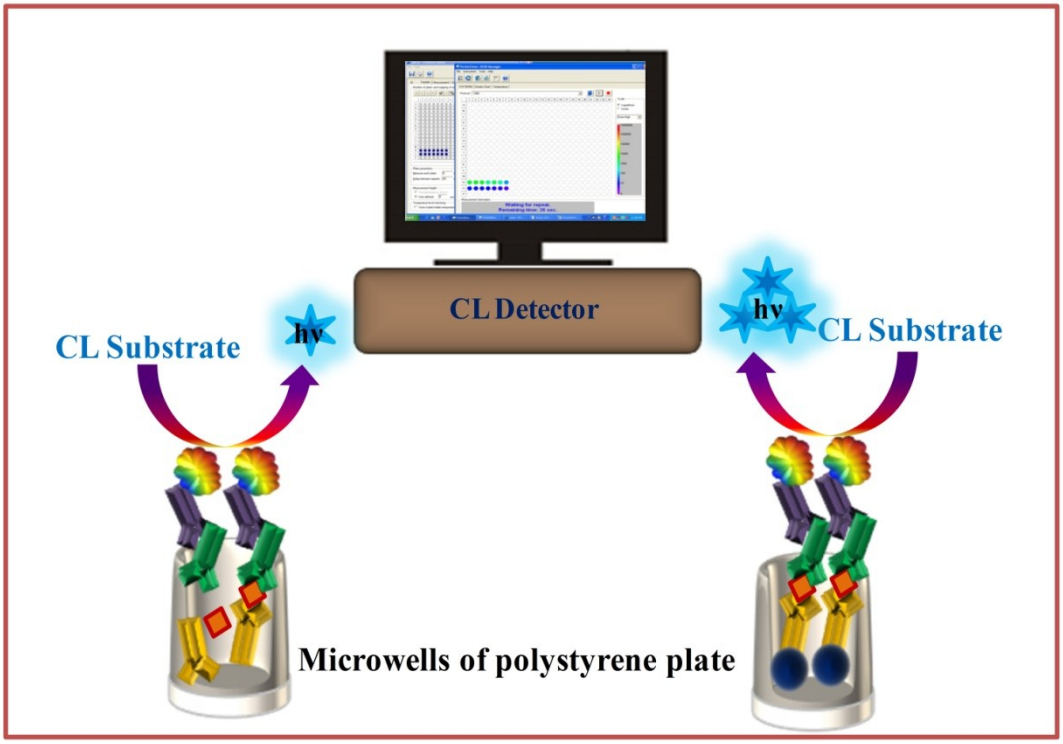

Graphical abstract of nano-immunosensor for cancer marker detection

5.1 Introduction

Cancer is one of the major diseases threatening people's health and its incidence is increasing in the world. There will be a predicted global burden of 20.3 million new cancer cases by 2030 compared with an estimated 12.7 million cases in 2008, and a predicted 13.2 million cancer-related deaths worldwide by 2030, up from 7.6 million in 2008 (Bray *et al.,* 2012).The determination of tumour makers is one of the important prognosis factors in clinical research and diagnosis. The levels of tumour markers in blood or tissue provide essential information for clinical cancer screening and disease diagnosis. Due to the association with liver cancer, colon cancer, colorectal cancer, breast cancer and existence in endoblast origin digestive system cancer, CEA, a polysaccharide–protein complex, is one of the most studied tumour markers (Borras *et al.,* 1995). Higher levels of CEA in serum were observed for individuals with colorectal, gastric, pancreatic, lung, and breast carcinomas, as well as from individuals with medullary thyroid carcinoma than healthy individual (Grunnet and Sorensen, 2012). The reported concentrations of CEA are 2.5 ng mL^{-1} for non-smokers and 5.0 ng mL^{-1} for smokers, respectively (Chon *et al.,* 2009). Also, with respect to a healthy adult, CEA level is raised for heavy smokers in the blood. Thus, accurate determination of CEA is of significance for monitoring and screening disease recurrence. The long term survival of cancer patients can be improved by considering the levels of CEA in human organism which reflects the disease progression or regression status (Kulasingam and Diamandis, 2008). Thus, the need for a sensitive immunoassay technique to detect a sub-nanogram per millilitre level is extremely important.

5.1.1 State of the art for immunoassay of CEA

Many alternative analytical methods with high sensitivity have been developed for early stage detection of cancer. However, drawbacks such as high cost method, the need for sophisticated equipment restrict the application in routine diagnosis. Immunoassay is an easy and low-cost method for the detection of antigen or its specific antibody in clinical diagnostics (Qu *et al.,* 2013). Up to date, various immunoassay methods have been proposed to meet the clinical analysis for CEA. Some of them are listed in the Table 5.1.

Table 5.1 Various reported immunoassay for analysis of CEA

Types of immunoassay	Detection range (ng mL^{-1})	Limit of detection (ng mL^{-1})	Reference
Radioimmunoassay (RIA)	0.7 – 74	0.7	Peters *et al.,* 1989
Enzyme linked immunosorbent assay (ELISA)	1.0 – 25	0.5	Lin *et al.,* 2004
Surface-enhanced Raman scattering (SERS)-based immunoassay	0.001 – 10	0.001	Chon *et al.,* 2009
Chemiluminescence enzyme immunoassay (CLEIA)	0.5 – 50	0.05	Yang *et al.,* 2010
Chemiluminescence enzyme immunoassay (CLEIA)	0.004 – 8	0.001	Wang *et al.,* 2011
Time-resolved fluoro-immunoassay (TRFIA)	1.0 – 1000	0.5	Hou *et al.,* 2012

Among the reported immunoassay techniques, ELISA is one of the most widely used analytical techniques in clinical research because of its adaptability, simplicity and sensitivity (Zhou *et al.,* 2011; Ambrosi *et al.,* 2009). As the concentrations of cancer biomarkers are extremely low *i.e.* nanogram per mL or lower *in vivo* (Wang *et al.,* 2007; Cassiday, 2010), conventional polystyrene plate ELISA fails in terms of sensitivity due to low surface-to-volume ratio of the plate and the random orientation of the adsorbed antibody or antigen which is not optimum for subsequent antibody – antigen recognition and binding (Park *et al.,* 2009). Therefore, developing new techniques with improved selectivity, sensitivity and a LOD are a current need in routine diagnosis. Sensitive detection of biomarkers is vitally important for timely diagnosis and treatment of early stage cancers (Cheow *et al.,* 2010), which largely determines the survival rate of cancer patients (Choi *et al.,* 2010).

5.1.2 Advantages of using ZnO

Methods based on sandwich-type immunosensors and immunoassays have been developed for detection of antigens with more than one eptiope due to the use of matched antibodies. High-affinity antibodies and appropriate labels are usually employed for the amplification of detectable signal. Recently, attempts have taken for the development of innovative and powerful novel nanoparticle labels, controlling and tailoring their properties in a very predictable manner to meet the requirements of specific applications by exploiting nanoparticle labels, in the sandwich-type immunosensors and immunoassays (Zhou *et al.,* 2011). Routine approaches involve noble metal nanoparticles, carbon nanomaterials, semiconductor nanoparticles, metal oxide nanostructures, and hybrid nanostructures. The enormous signal enhancement associated with the use of nanoparticle labels and with the formation of nanoparticle-antibody-antigen assemblies provides the basis for sensitive detection of disease-related proteins or biomolecules (Vashist *et al.,* 2014). Biosensing techniques commonly rely on the use of bio-functionalized nanoparticles, inorganic-biological hybrid nanoparticles, and signal tag-doped nanoparticles (Solanki *et al.,* 2011).

In recent years, owing to its nontoxicity, good bio-compatibility and high chemical stability, ZnO nanoparticles (ZnONPs) have been used widely in construction of biosensors (Arya *et al.,* 2012). The high IEP of ZnO, which is about 9.5, plays an important role in biological pH (Norouzi *et al.,* 2011). Due to lowering of IEP in biological pH, the surface of ZnO has a positive charge, for which protein with low IEP (in case of CEA is 4.7) can be immobilized on it by an electrostatic force (Casey and Kofinas 2008).

5.1.3 Objectives

A novel support for biomolecules immobilization on ZnO surface using 16-PHA was demonstrated in Chapter 3. Herein, the application for the detection of CEA labels in human serum based on ZnONPs has been developed and compared with conventional microplate ELISA.

5.2 Experimental section

5.2.1 Chemicals and biochemicals

Mouse monoclonal anti-carcino embryonic antigen CEA antibody (1° Ab), rabbit polyclonal anti-carcino embryonic antigen CEA antibody (2° Ab), goat polyclonal secondary antibody to

rabbit IgG – H&L (HRP) (3° Ab – HRP) , carcino embryonic antigen CEA protein (CEA) and goat F(ab) polyclonal secondary antibody to rabbit IgG – H&L (FITC) (3° Ab – FITC) were procured from Abcam (UK). 30% aqueous solution of human Serum was purchased from Calbiochem (USA). Zinc oxide nanopowder (<100 nm particle size), 16-phosphonohexadecanoic acid (16-PHA), 1-Ethyl-3-[3-dimethylaminopropyl]carbodiimide hydrochloride (EDC), N-hydroxy succinimide (NHS), bovine serum albumin (BSA), tween 20, luminol were purchased from Sigma-Aldrich (USA).

5.2.2 Materials and instrumentation

384 well polystyrene microtiter plates were purchased from Nunc (Denmark). For CL measurements, Victor™ X4 2030 multiplate reader from Perkin Elmer (USA) was used. For the handling of CEA standard solution, biological safety cabinet (Labgard ES, Class II, Type B2) from Nuaire (USA) was used. Quartz crystal microbalance (QCM) study was performed using EQCN-700 system integrated with flow cell model FC-6 (M/s Elchema, Potsdam, New York, USA). Water produced in a Milli-Q system (Millipore, Beford, MA, USA) was used for preparing all the solutions. Fluorescence images were acquired on inverted microscope (IX-71 Olympus, Japan) coupled with charged coupled device (CCD), Hamamatsu Orca-ER (Japan).

5.2.3 Preparation of buffers and samples

Buffers were made by the following method. For coating purpose, a 50 mM CB was prepared. The pH was adjusted to 9.6. As CB changes composition over time, it was made fresh each time. 10 mM PBS was used for incubation and washing purpose. The pH was adjusted to 7.4. Another washing buffer (PBST) was made by adding 0.05% Tween 20 (v/v) in PBS. All buffer solutions were stored at 4 °C when not in use. The blocking solution was prepared by adding 2.5% (w/v) BSA to PBS.

The stock 1° Ab (2 mg mL^{-1}) was diluted in 10 mM PBS to the final concentration (0.2 µg mL^{-1}). The stock 2° Ab (2 mg mL^{-1}) specifically to 1° Ab was diluted to 0.5 µg mL^{-1} as indicated by manufacturer's protocol. 1 µL of the stock solution of 3° Ab-HRP (2 mg mL^{-1}) was diluted with 50 µL of de-ionized water. From the 1:50 dilution, working 3° Ab-HRP solution was prepared prior to the experiment by diluting 1:100, 1:500 and so on in PBS. The standard serum was used without any further dilution. CEA spiked serum solution was prepared by standard addition method in the range 0.001 – 20 ng mL^{-1}.

5.2.4 Immunoassay procedure

5.2.4.1 CEA analysis using conventional ELISA

Conventional sandwich ELISA was performed in 384 microwell plate. An optimized 1° Ab was diluted to 0.2 µg mL^{-1} in CB and coated in microwell. The plate was covered and kept at room temperature for 3 h. The microwells were washed with PBS. The remaining protein binding sites in the coated wells were blocked by adding 20 µL of 2.5% BSA blocking solution for 1 h at room temperature. The plate was washed with PBST. Following this step, CEA spiked serum samples in the range 0.001 – 20 ng mL^{-1} were added. The plate was incubated for about 2 h at room temperature. Then 1:1 mixture of optimized 2° Ab and 3° Ab-HRP was prepared. The final solution of 30 µL was added in each well. The plate was kept for 2 h at room temperature. The excess label was removed by washing with PBS. The CL substrate (1 µL of 0.05 M H_2O_2 + 4 µL of 0.5 mM luminol) was added. The signal intensity was kinetically measured at steady state.

5.2.4.2 CEA analysis using CEA-ZnONPs probe

Surface modification: The CEA capture probe is based on the efficient immobilization of capture efficient very specific 1° Ab through carboxy terminated SAMs on ZnONPs. The glass containers used for monolayer preparation was cleaned using Piranha solution as described in section 2.3.4 (**caution**: Piranha solution reacts exothermally and strongly reacts with organics). 16-PHA modified ZnONPs were prepared as described in section 3.3.4.5.

Coupling of 1° Ab onto ZnONPs: For antibody immobilization, the carboxylic acid-terminated SAMs were modified using an aqueous equimolar solution of 100 mM EDC /100 mM NHS for 2 h at room temperature. The resulting NHS ester monolayers were used for reaction in 1:1 solution of 1° Ab (0.2 µg mL^{-1}) and CB for 3 h in room temperature. The 1° Ab coated ZnONPs (1° Ab-ZnONPs) were washed with PBS. The schematic diagram of 1° Ab immobilization *via* SAMs is shown in Figure 5.1.

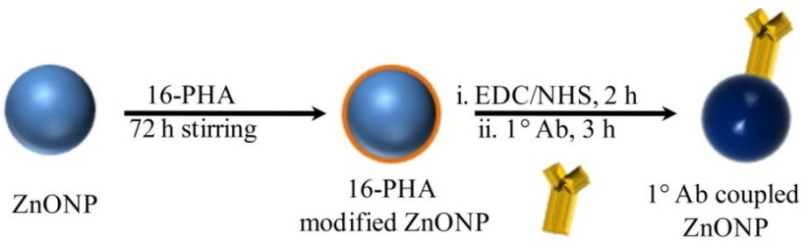

Figure 5.1 Schematic of monoclonal antibody immobilization steps *via* SAMs.

CEA-ZnONPs based ELISA: The CEA-ZnONPs capture probe was coated in the bottom of the 384 well plates for enhanced capture of CEA antigen. The remaining protein binding sites in the ZnONPs were blocked by adding 2.5% BSA blocking solution for about 1h at room temperature. After washing step by PBST, CEA spiked serum samples were incubated for 2 h at room temperature. The particles were washed again with PBS to remove unbound CEA. The 2° Ab (0.5 µg mL^{-1}) was incubated at room temperature for 2 h with the particles. Finally, for CL measurements, 3° Ab-HRP (1:2000) was incubated at room temperature for 1 h with the particles. The excess label was removed by washing with PBS. The CL substrate was added. The signal intensity was kinetically measured at steady state and stability was found after 25 min. The schematic pathway of CEA detection is shown in Figure 5.2.

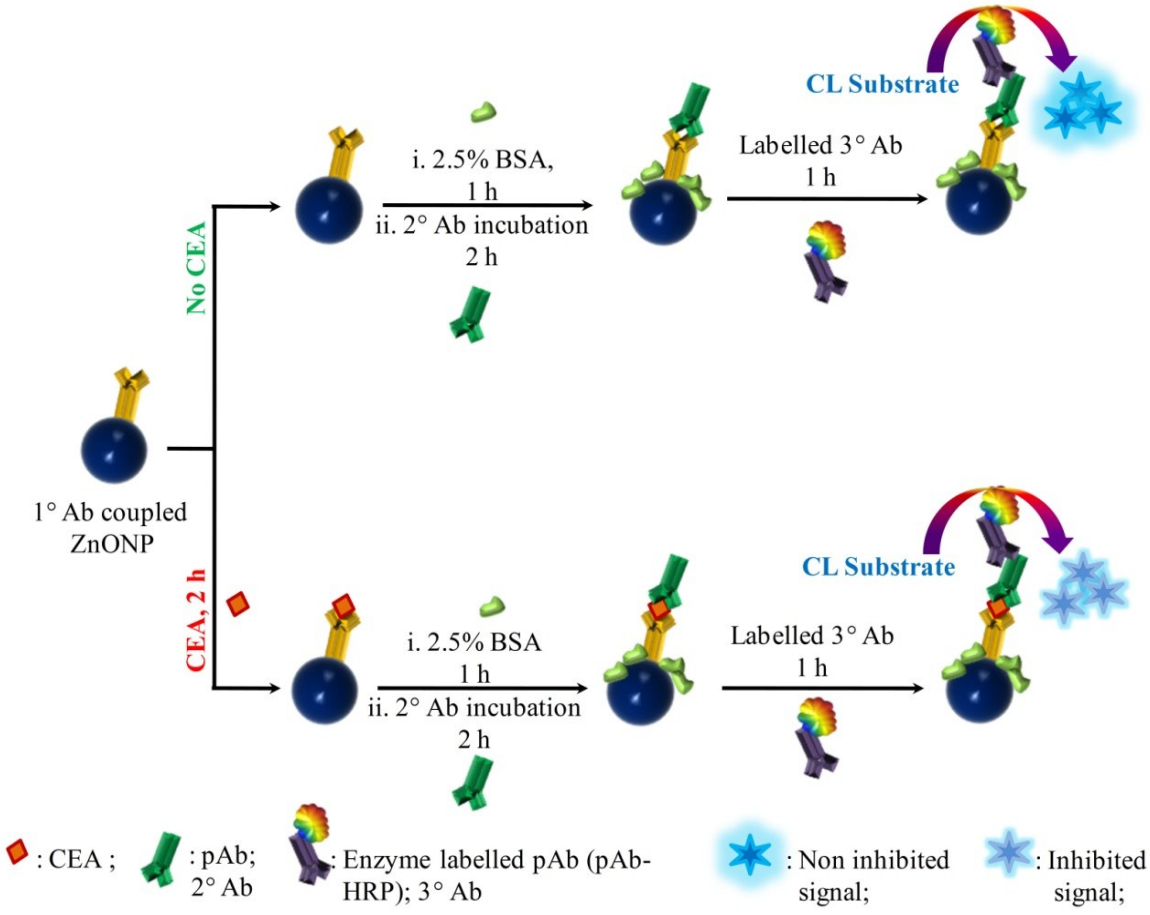

Figure 5.2 Schematic representation of the CEA recognition process.

The hybrid- immuno assay was realised in 384 micro well plates using anti CEA- monoclonal antibody (1° Ab) immobilized on ZnONPs via SAMs as capture probes. The captured antigen was quantified using sandwich ELISA wherein a polyclonal anti CEA 2° Ab was used for detection and quantified using an enzyme labelled secondary antibody 3° Ab.

5.3. Results and Discussion

5.3.1 Binding study of Ab onto ZnONPs

5.3.1.1 Affinity analysis of CEA-ZnONPs probe

Real time binding analysis using QCM was performed to confirm the CEA binding on the 16-PHA modified ZnO surface. The functionalized quartz crystal ZnO-16PHA (10 MHz, non-bonded) was placed in a plexiglass flow cell in static mode, sandwiched between two O-rings and connected to the frequency-measuring unit. The 16-PHA modified ZnO quartz crystal was placed in the flow cell. 1° Ab was incubated on the EDC/NHS activated crystal for 3 h in room temperature. After the incubation step the crystal was washed using PBS. The CEA spiked sample (2.5 ng mL^{-1}) was injected and incubated for 2 h at room temperature. Followed by a washing step with PBS, the 2° Ab was incubated for 2 h at room temperature. Finally, after washing, the 3° Ab-labelled was injected and incubated for 1 h. The excess label was washed using PBS. The direct mass change was recorded using Voltascan 5 software after each washing step. Figure 5.3 represents the step wise binding protocol.

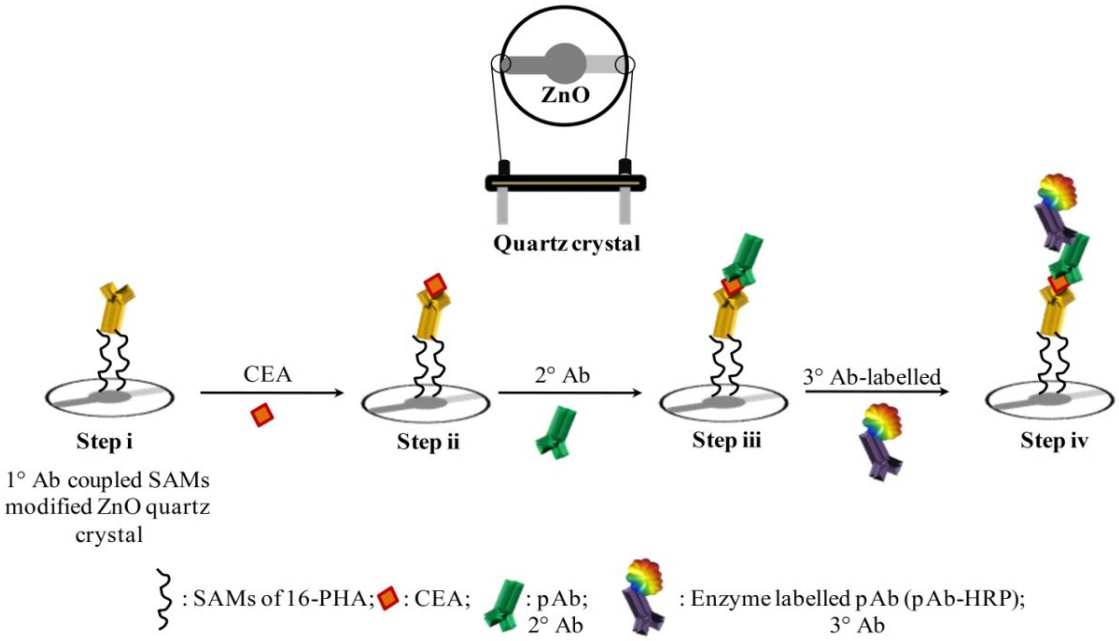

Figure 5.3 The schematic representation of step wise binding process on ZnO quartz crystal.

The recorded data was plotted and presented in Figure 5.4. The binding of 1° Ab, CEA, 2° Ab and 3° Ab-HRP were performed in static mode using the optimized condition as earlier.

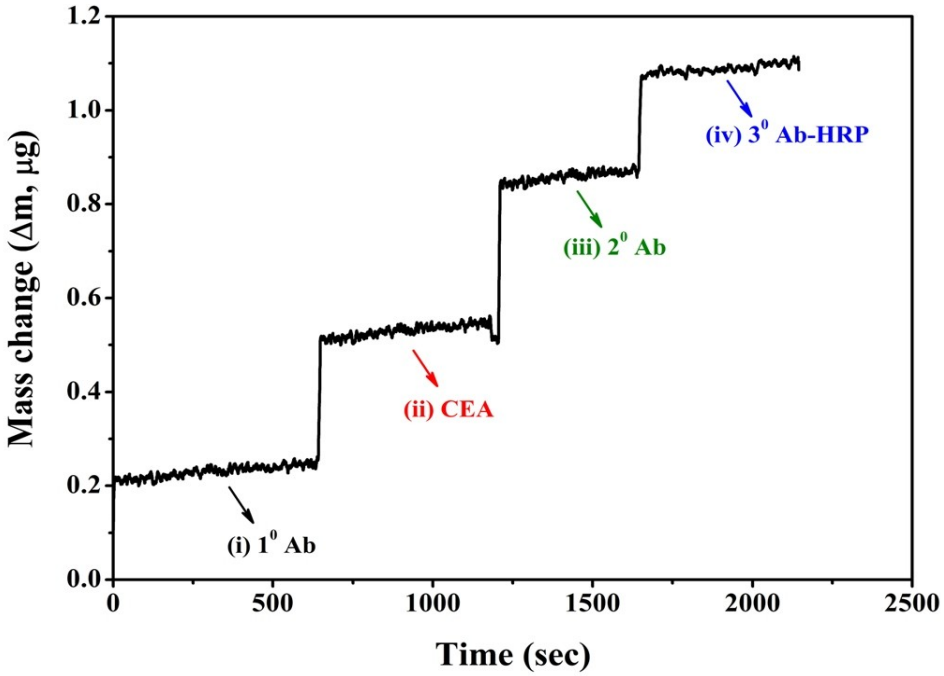

Figure 5.4 Stepwise mass change responses on SAMs modified ZnO crystal after attachment of (i) 1° Ab (anti-CEA); (ii) CEA; (iii) 2° Ab, and (iv) 3° Ab-HRP.

The mass change was recorded after each step. The increasing change in mass suggests the stepwise binding of (i) 1° Ab, (ii) CEA, (iii) 2° Ab and (iv) 3° Ab-HRP. The 1° Ab attached on SAMs modified ZnO crystal showed the initial mass of 121 ng. Subsequent mass changes of 91, 303, 331 and 223 ng were observed for the attachment of 1° Ab, CEA, 2° Ab and 3° Ab-HRP respectively as shown in Figure 5.4. The significant mass change observed for CEA capture using the ZnO-16-PHA-anti CEA is a strong evidence of the enhanced surface to volume ratio available for successful construction of a ZnONPs based immunosensor.

5.3.1.2 Fluorescence binding studies

The specificity of the 3° Ab was further established by fluorescence microscopy (Figure 5.5). Microscopy slides were prepared as (i) reference 1° Ab-ZnONPs without 3° Ab-FITC, (ii) sample 1° Ab-ZnONPs directly coupled with labelled 3° Ab (3° Ab-FITC) and (iii) sample 1° Ab-ZnONPs coupled with unlabelled 2° Ab and 3° Ab-FITC. The sample 1° Ab-ZnONPs was incubated with 3° Ab-FITC (1:8000) for 2 h at room temperature in dark. Before excitation, the sample was rinsed with 10 mM PBS to remove unbound 3° Ab-FITC. The reference 1° Ab-ZnONPs without 3° Ab-FITC and sample 1° Ab-ZnONPs directly coupled with labelled 3° Ab (3° Ab-FITC) showed negligible fluorescence signal (Figure 5.5 (a) and (b)). The binding between 1° Ab on ZnONPs and 1° Ab specific unlabelled 2° Ab, 3° Ab-

FITC has been demonstrated by a bright fluorescence signal spots (Figure 5.5 (c)). These observations suggests that the 1° Ab on ZnONPs preserved the excellent biological recognition of antibody to their targets.

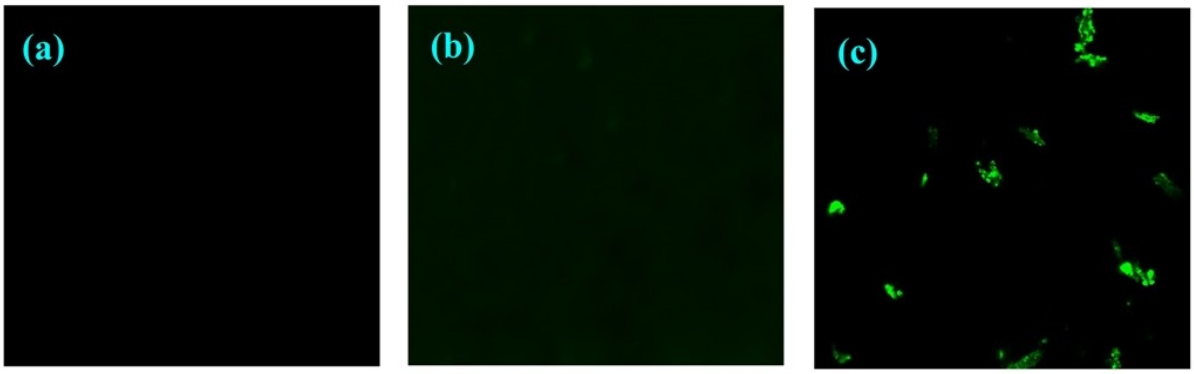

Figure 5.5 Fluorescence image of (a) reference 1° Ab-ZnONPs without 3° Ab-FITC, (b) sample 1° Ab-ZnONPs directly coupled with labelled 3° Ab (3° Ab-FITC), (c) sample 1° Ab-ZnONPs coupled with unlabelled 2° Ab and 3° Ab-FITC at 20× magnification; incubated with 3° Ab-FITC (1:8000) (λ_{ex} 480 nm / λ_{em} 520 nm).

5.3.2 Development of immunoassay

5.3.2.1 Optimization of ionic strength and pH of buffer

Several physicochemical factors that influence the CL- ELISA performance have been studied. To evaluate the influence of buffer ionic strength and buffer pH, standard curves were prepared. A constant concentration of 3° Ab-HRP was added to serial dilutions (from 100 to 1 mM PBS) of a concentrated buffer. Increment in signal intensity was found up to 10 mM. A slight decrease in signal intensity was observed for 50 mM and 100 mM. Influence of pH on the 1° Ab and 2° Ab was studied in the range 5.0 to 9.0. The optimum results for the ionic strength and pH of PBS are found at 10 mM and pH 7.4 respectively (Figure 5.6 (a) and (b)).

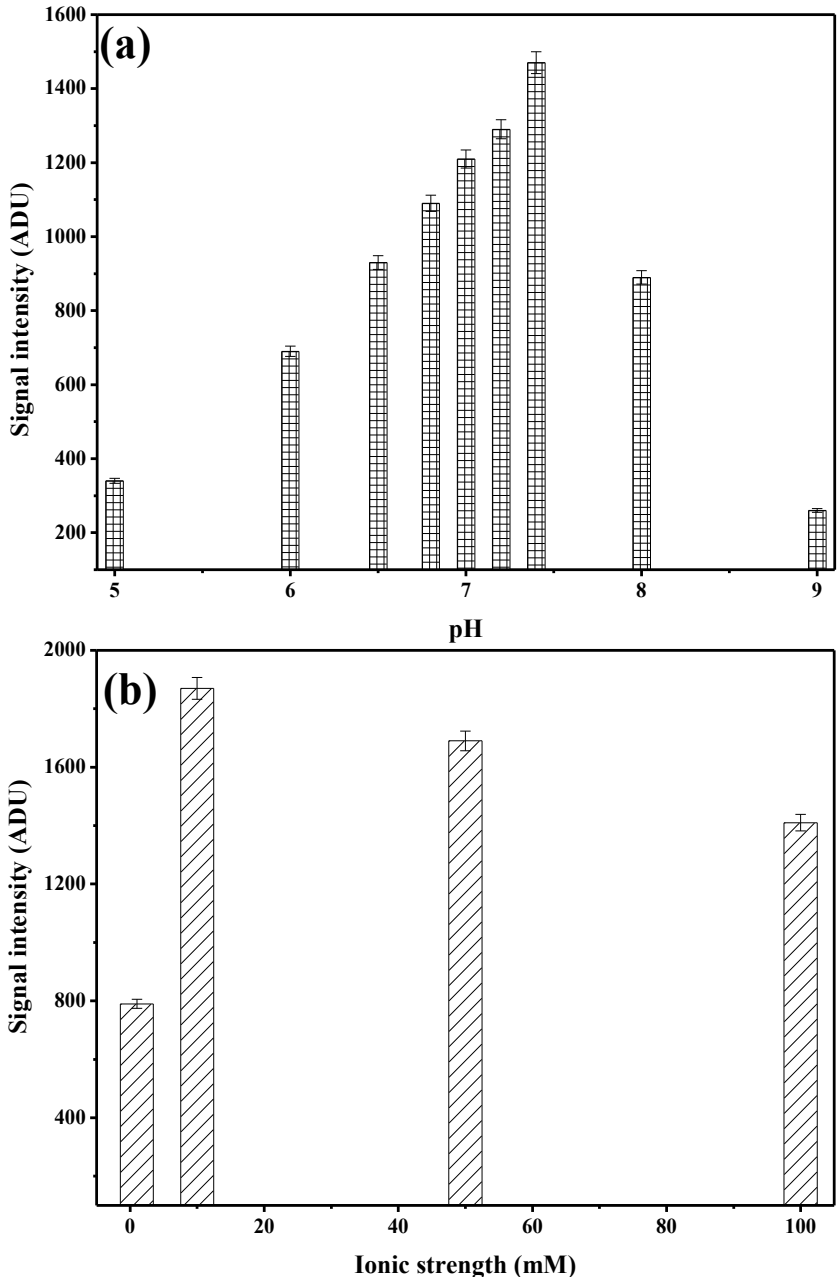

Figure 5.6 (a) Optimization of pH of buffer (5.0 – 9.0) for ZnONPs based CEA immunoassay; in triplicate; (b) Optimization of ionic strength of buffer (1 – 100 mM) for CEA-ZnONPs immunoassay; in triplicate.

5.3.2.2 Thermal stability of CEA-ZnONPs probe

The thermal stability was compared for the 1° Ab coupled of ZnONPs and 1° Ab immobilized on the microwell plate (Figure 5.7). The effect of temperature on the immunoassay was evaluated in the range 20 °C to 50 °C and presented in Figure 5.7. Both 1° Ab immobilized on plate and 1° Ab immobilized on ZnONPs showed similar behaviour. However, enhance signal intensity was found in the range 26 °C to 35 °C for the 1° Ab-

ZnONPs over the 1° Ab immobilized on plate. Above 40 °C, the signal intensity was decreased and reached to the blank value *i.e.* signal intensity without any 3 °Ab-HRP. Thus, all experiments were carried out at 30 °C. The above results suggest that the 1° Ab on modified ZnONPs exhibits good thermal stability as compared to the 1° Ab immobilized on polystyrene plate.

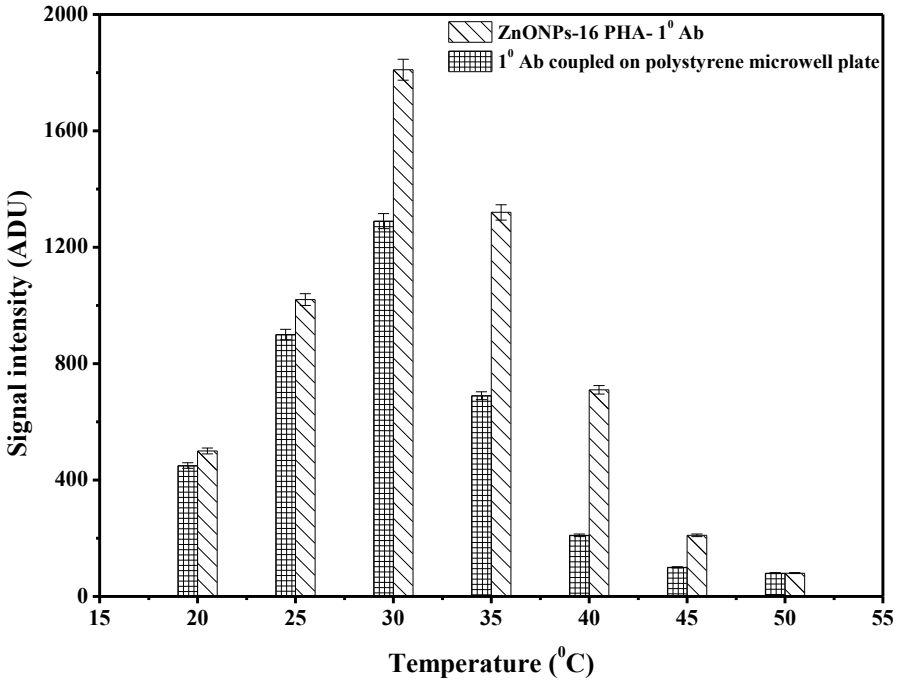

Figure 5.7 Optimization of temperature (20 – 50 °C) for CEA-ZnONPs immunoassay; in triplicate.

5.3.3 Optimization of assay parameters

The principle of the ZnONPs based immunoassay is based on a sandwich immunoassay as described in earlier section. Effective 3° Ab dilution is very much important to produce reproducible results and reduce non-specific bindings, which might produce false signals. To examine appropriate amount of 3° Ab-HRP, various 3° Ab-HRP dilutions were tested and data was plotted as shown in Figure 5.8. It is found that a 3° Ab-HRP dilution of 1:2000 produced better signal intensity against 1° Ab (0.2 μg mL^{-1}). Further, the amount of ZnONPs-CEA probe particles is also optimized as 2 mg mL^{-1}, having maximum signal intensity.

Various amounts of ZnONPs were tested in the range 0.5 – 5 mg mL^{-1}. The amount of particles is optimized as 2 mg mL^{-1}, having highest signal intensity (Figure 5.9).

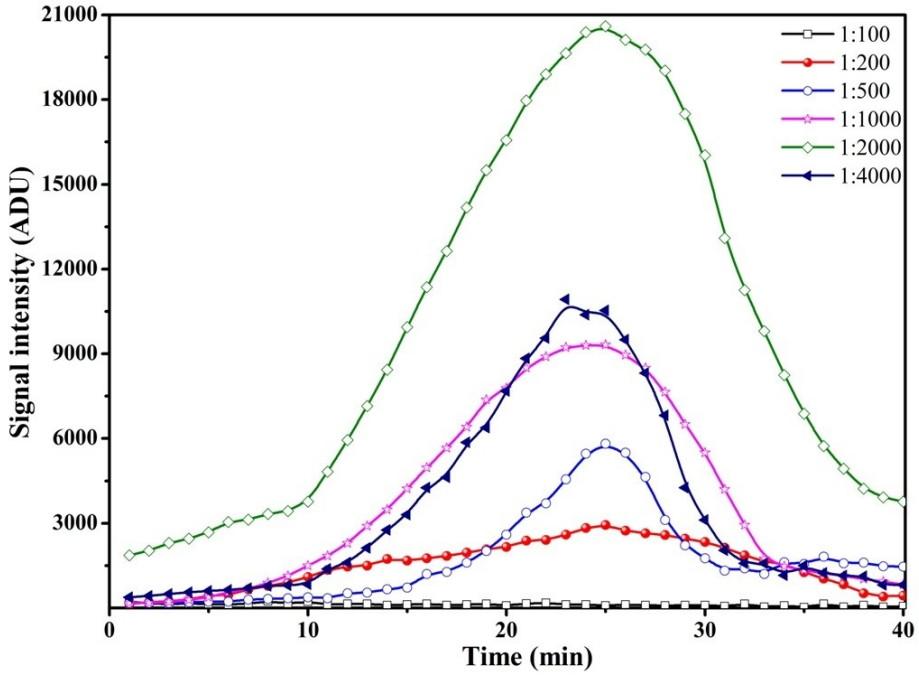

Figure 5.8 Optimization of 3° Ab-HRP (1:100 – 1:4000 dilutions) for CEA-ZnONPs immunoassay.

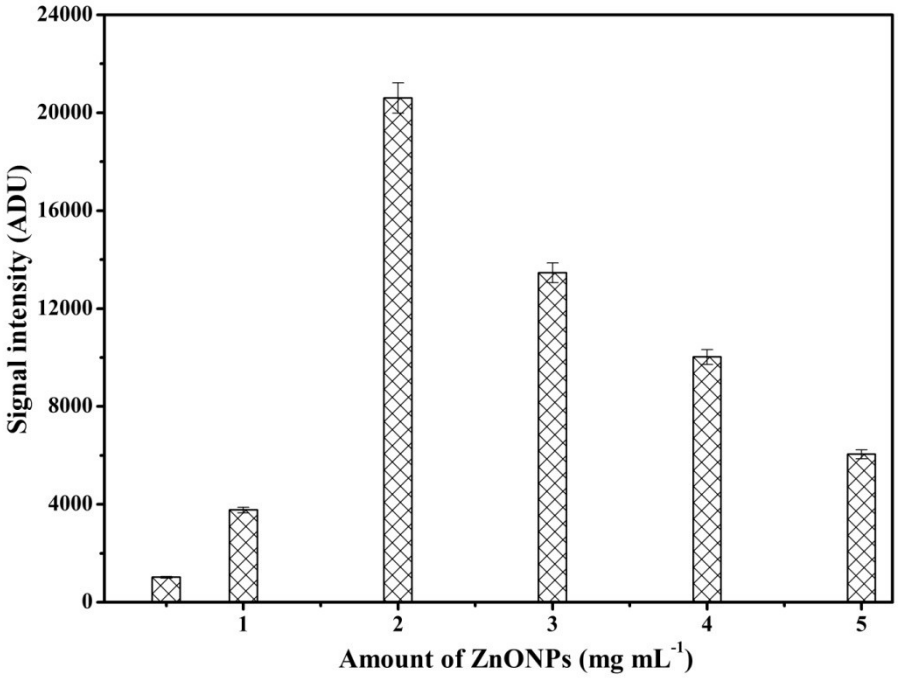

Figure 5.9 Optimization of amount of ZnONPs (1 – 5 mg mL^{-1}) for CEA-ZnONPs immunoassay.

5.3.4 Effect of surface modification

The performance of the 1° Ab coupled to the ZnONPs was evaluated against the 1° Ab immobilized on microwell plate using optimized condition. The kinetic intensity profile of the resulting signal intensity was recorded in Figure 5.10. The signal reached a stable value (95% of the steady state) after 25 min for 1° Ab-ZnONPs. The stable signal intensity was found at 30 min in case of 1° Ab coated on plate. The covalently attached 1° Ab showed significantly higher signal intensity over the 1° Ab coated on microwells. The order of the stable signal intensity recorded in absence of CEA for 1° Ab functionalized ZnONPs was found to be 20600 ADU (via phosphonation) and 6230 ADU for 1° Ab coated on microwells (*i.e.* non-specifically adsorbed 1° Ab) respectively (n = 5) (Inset of Figure 5.10). The signal intensities were found to 3 fold higher for phosphonated ZnONPs against 1° Ab coated on microwells. These observations are also found true for the inhibition studies. The control over biomolecules surface orientation suggests that SAMs play an important role in the construction of immuno recognition surfaces.

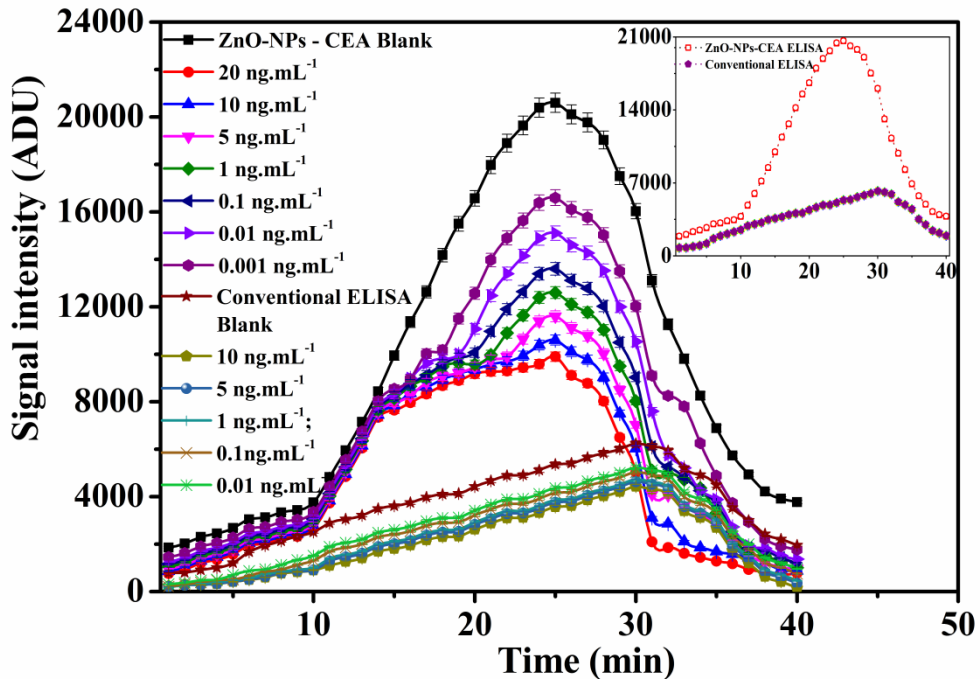

Figure 5.10 Comparison of signal intensity between 1° Ab immobilized through 16-PHA SAMs on ZnONPs and 1° Ab coated on polystyrene microwell plate.

5.3.5 Measurement for CEA in serum

To evaluate the analytical performance of sensor, calibration was obtained for CEA spiked serum samples under optimized conditions. The inhibition curve for CEA was obtained for different concentrations of CEA in the range 0.001 – 20 ng mL^{-1} by CL technique. The calibration curves were fitted by using Origin Pro 8 SR0 software. I % was calculated using equation 2.5.

The percentage of inhibited activity that results after exposure to the CEA is quantitatively related to the inhibitor concentration according to the equation. A calibration curve for various CEA concentration (0.001 – 20 ng mL^{-1}) is presented in Figure 5.11.

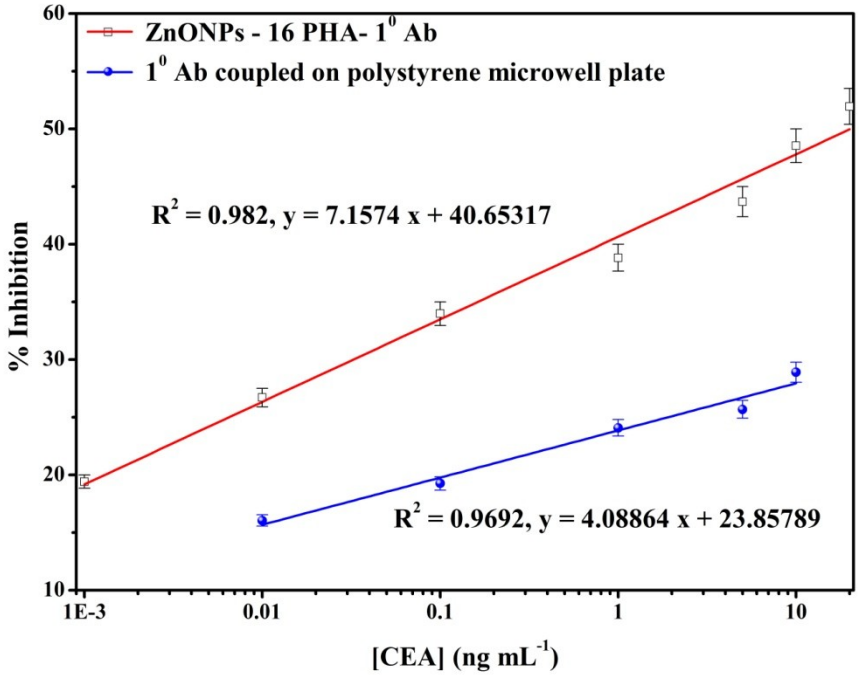

Figure 5.11 Calibration curve for various [CEA] using 1° Ab immobilized through 16-PHA SAMs on ZnONPs and 1° Ab coated on polystyrene microwell plate under optimized condition.

The calibration is found to be linear in the range 0.001 – 20 ng mL^{-1} (R^2 = 0.982, n = 5) with R.S.D of 3.21% ± 0.83 for the 1° Ab attached through 16-PHA modified ZnONPs. The linear equation is; y = 7.1574 x (ng mL^{-1}) + 40.65317. LOD and LOQ are found to be 0.001 ng mL^{-1} by analysing replicate sets of modified ZnONPs with good sensitivity about 7.86%. Whereas for conventional polystyrene plate ELISA, the linearity was found in the range 0.01 – 10 ng mL^{-1} (R^2 = 0.9692, n = 5) with RSD of 5.17% ± 0.69. The linear equation was; y = 4.08864 x

(ng mL^{-1}) + 23.85789. LOD and LOQ were determined as 0.01 ng mL^{-1} by analysing replicate sets with very low sensitivity about 3.7%. Lower values of LOD, LOQ, R^2 and sensitivity indicate that a surface-active head group binds strongly to a substrate; while an alkyl chain giving stability to the assembly that plays an important role in terms of coupling of a biomolecule to a monolayer. Although the developed immunoassay comprises of three antibodies, however, in view of prognosis of cancer this method might be a better choice over conventional microplate ELISA (Table 5.2).

Table 5.2 Comparison with recent reported immunosensors

Sensor configuration	**Transduction principle**	**Linear detection range (ng mL^{-1})**	**Limit of detection (pg mL^{-1})**	**References**
ZnONPs coupled 1° Ab on 384 microwell plate	Sandwich CL immunoassay	0.001 – 20	1.0	This work
Conventional ELISA	Sandwich CL immunoassay	0.01 – 10	10	This work
ZnONPs and glucose oxidase decorated graphene	Sandwiched luminol ECL immunosensing	0.01 – 80	3.3	Cheng *et al.*, 2012
Conjugated biotinylated anti-CEA Ab on streptavidin coated super-paramagnetic beads	Sandwich CL immunoassay	0.005 – 50	5.0	Qu *et al.*, 2013
Ab2-PdPt-Thi/Fc as probes	Electrochemical	0.05 – 200	1.4	Liu *et al.*, 2014
Fe_3O_4@C@CdTe QDs composite with CEA-mAb1 and the ZnO NWs	Sandwich fluorometric immunoassay	0.005 – 100	1.6	Wu *et al.*, 2015

5.3.6 Performance, recovery and real sample analysis

In the presence of possible interferences, such as glucose (Glu, 5 mM), ascorbic acid (AA, 10 µM), glycine (Gly), bovine serum albumin (BSA, 380 µg mL^{-1}) and mixture, the developed

immunosensor was studied for its selectivity in the incubation solution with 20 ng mL^{-1} CEA (Figure 5.12).

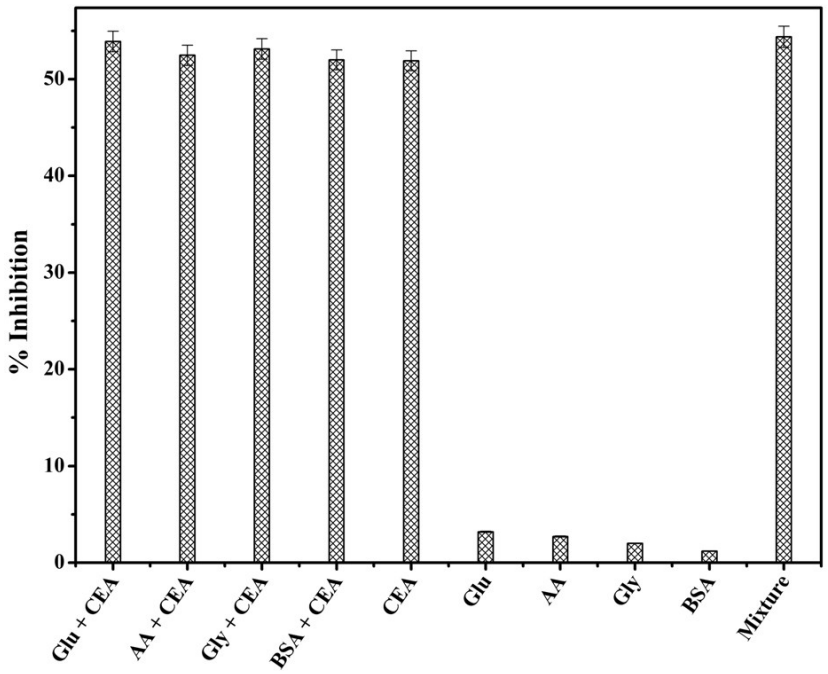

Figure 5.12 Interference study using glucose (Glu, 5 mM), ascorbic acid (AA, 10 μM), glycine (Gly), bovine serum albumin (BSA, 380 μg mL^{-1}) and mixture.

The I % was calculated from the signal intensity values in the presence of the interference and without interference. The results have shown that the interferences of relatively high concentrations only pose negligible effects on CEA detection, indicating that the selectivity of the proposed immunosensor is acceptable.

The stability of 1° Ab immobilized on ZnONPs was assessed over one month period at storage condition 4 °C in 10 mM PBS (pH 7.4) (Figure 5.13). No significant loss in the 1° Ab functional activity has been observed after four weeks. The response is found to be superior over microplate sandwich ELISA technique as the high surface area of ZnONPs plays an important role to retain the antibody orientation.

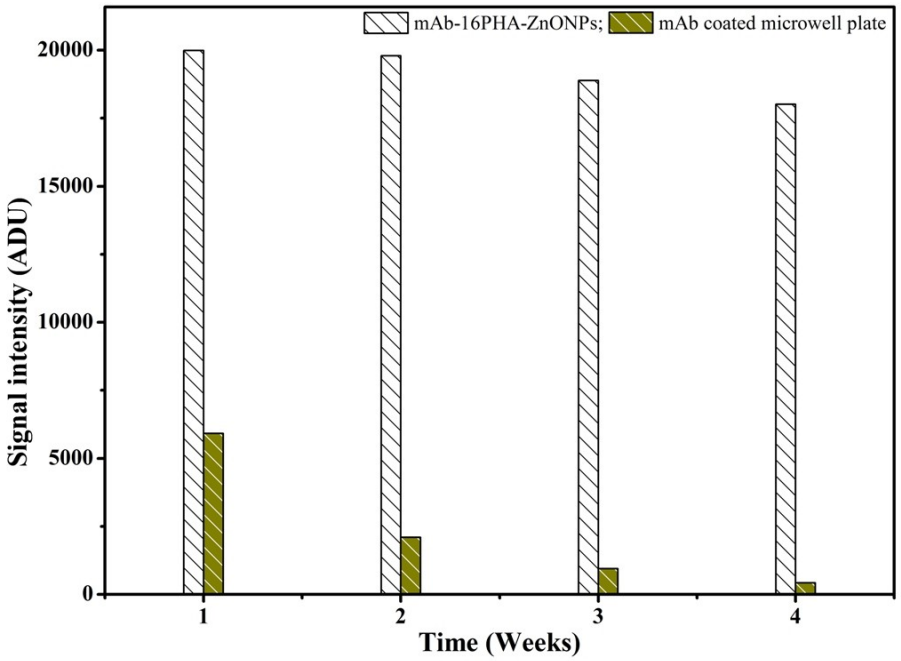

Figure 5.13 Comparison of stability of 1° Ab coated ZnONPs and microwell plate.

Recovery experiments were conducted to evaluate the accuracy and precision of the CEA-ZnO immunoassay. Known amount of CEA was spiked to seven serum samples in triplicate, and recovery experiments were performed for both formats. CEA was fortified at levels of 0.01. 0.05, 1, 2.5, 10, 15 and 20 ng mL^{-1}, the recoveries of CEA was found in range from 97 to 100% for CEA-ZnO immunoassay and 90 to 104% for microplate ELISA. The detection results of the accuracy and precision test are listed in Table 5.3.

Table 5.3 Recovery of [CEA] from different serum samples as determined by CEA – ZnONPs nano-immunosensor to assess the recovery efficiency

[CEA] added (ng mL^{-1})	ZnONPs – CEA immunoassay			Microplate ELISA		
	[CEA] Found (ng mL^{-1}) Mean ± S.D.	R.E. (%)	Recovery (%)	[CEA] Found (ng mL^{-1}) Mean ± S.D.	R.E. (%)	Recovery (%)
0.01	0.00988 ± 0.00019	1.2	98.8	0.0104 ± 0.0002	- 4.0	104
0.05	0.0487 ± 0.00252	2.6	97.4	0.0453 ± 0.00252	9.4	90.6
1	0.986 ± 0.007	1.4	98.6	1.1014 ± 0.0283	- 10.14	110.14

2.5	2.49 ± 0.0264	1.0	99.6	2.50 ± 0.0152	0.0	100.0
10	10.05 ± 0.02	- 0.5	100.5	10.47 ± 0.379	- 4.7	104.7
15	14.993 ± 0.041	0.047	99.95	N.D.#	-	-
20	19.81 ± 0.02	0.95	99.05	N. D.	-	-

not determined

Further, to demonstrate the applicability of the CEA-ZnONPs CL ELISA for the determination of CEA in real serum samples, eight different serum samples were collected. The samples were diluted in distilled water (3:7). The results were obtained using both CEA-ZnONPs ELISA and microplate ELISA. It was found that the results of the CEA-ZnONPs ELISA method were almost correlated with those of the microplate ELISA as shown in Table 5.4. The correlation between the developed method and the conventional ELISA was plotted. The correlation coefficient (r) has been obtained from the graph and as well as calculated theoretically i.e. 0.99998 and 0.999965 respectively. This indicates that both methods are highly correlated. However, the results obtained by the CEA-ZnONPs ELISA were highly correlated with those obtained by the microplate ELISA. These indicate that the CEA-ZnONPs ELISA can detect the presence of CEA in serum samples both qualitatively and quantitatively.

Table 5.4 Comparison of real sample analysis using 1° Ab attached via 16-PHA on ZnONPs and 1° Ab coated on microwell plate.

Sample	**ZnONPs - 16 PHA -1° Ab ELISA Mean ± S.D. (ng mL^{-1})**	**Conventional microwell plate ELISA Mean ± S.D. (ng mL^{-1})**
Sample-1	4.25 ± 0.022	4.382 ± 0.0471
Sample-2	1.784 ± 0.0151	1.81 ± 0.064
Sample-3	7.631 ± 0.14	7.393 ± 0.261
Sample-4	2.112 ± 0.0042	2.091 ± 0.0114
Sample-5	1.127 ± 0.0722	1.133 ± 0.0084
Sample-6	0.771 ± 0.0565	0.753 ± 0.00531
Sample-7	0.1564 ± 0.0192	0.1442 ± 0.0163
Sample-8	3.911 ± 0.0043	3.852 ± 0.05182

5.4 Conclusion

An ultrasensitive hybrid sandwich-immunoassay for the determination of CEA in human serum based on functionalized ZnONPs has been demonstrated. The immunoassay exhibits an excellent analytical performance in the range 0.001 – 20 ng mL^{-1} in terms of enhanced sensitivity as compared to polystyrene microplate ELISA. The developed assay is a promising technique over the conventional microwell plate ELISA with respect to LOD (1 pg mL^{-1}), LOQ (1 pg mL^{-1}), selectivity, sensitivity (three fold) and stability over a period of one month. Furthermore, the hybrid immuno-capture probe has exhibited an enhanced high thermal stability (1.39 fold). The most promising feature of this ZnONPs – ELISA is the high capture efficiency over other reported materials.

CHAPTER 6: CONCLUSION

The work incorporated in this thesis presents a systematic investigation of the physicochemical properties of various bio-functionalized nanoparticles and nanostructures such as Au, Fe_3O_4, HfO_2, ZnO nanoparticles and nanostructures, and SiO_2 porous material that allow their exploitation in the development of novel biosensing strategies to detect various environmental (AFM1, OPs, heavy metals) and clinical analytes (choline, glucose, CEA biomarker). Over the last two decades, the development and applications of nanoparticles based biosensors using optical transducers have been pursued with great interest by many researchers. Owing to the minimal signal interfere, the developed biosensing techniques in this thesis relies heavily on the use of optical transducer. Extensive experiments were carried out for optimizing influential parameters like pH, ionic strength, and temperature. Novel surface modification techniques were deployed to obtain suitable bio-functionalized surfaces. Based on optimized parameters, receptor biomolecules (such as enzymes and antibodies) were attached to the nanoparticles surface using physisorption and covalent immobilization techniques. During the course of study, significant observations were noted. The overall conclusions are summarized chapterwise (Chapter 1 to 5) below:

1. **Introduction (Chapter 1):** This chapter gives a detailed description of nanoparticles and various pathways for development of bio-functionalized nanoparticles. This chapter has presented an overview of various current biosensing technologies for the detection of environmental and clinical analytes. Attention has been given to identify the research gaps in the existing knowledge based on the survey of literature and thus identify the specific and objective for this doctoral thesis work.

2. **Development of nanoparticles based high-throughput immunoassay for aflatoxin M1 (Chapter 2):** This chapter has given a detailed account of the experiments to develop a fast, reliable and ultra sensitive NPs based sandwich ELISA for detection of AFM1 in milk. Various SAMs modified nanoparticles *e.g.* AuNPs, MNPs and HfO_2NPs were explored towards biosensor development using surface modification strategies such as thiolation, silanization and phosphonation. The surface modification was confirmed using magnetic measurement, XRD, UV-vis, SEM, HRTEM, FT-IR, particle size analysis and fluorescence microscopy in each steps. The miniaturised assay using chemiluminescence has enabled ultra trace analysis of AFM1 in milk with much improved lower limit of detection at 0.5 pg mL^{-1} as compared to other reported methods.

The total assay time to detect AFM1 was approximately 3 h. The novel hybrid assay has been developed comprising a micro column of 1° Ab immobilized on NPs coupled with microwell plate assay that has enabled simultaneous measurement of low (0.5 pg mL^{-1}) and high (200 pg mL^{-1}) AFM1 contamination in milk. The most promising feature of this NPs-ELISA is the small size, high capture efficiency and lower cost of AFM1 analysis over other reported materials.

3. **Nanostructured ZnO in biosensing and bio-catalysis (Chapter 3):** In this chapter, various ZnO nanostructures were studied towards biosensing applications. The novel self assembly technique *i.e.*, phosphonation on ZnO nanostructure imparted significant stability to the immobilized enzyme as against physisorbed enzyme. The stability of enzyme was confirmed by FT-IR. The ZnO nanostructures have been exploited for clinical analysis (choline, acetylcholine), environmental analysis (organophosphate residues) and bio- catalysis of *p*NPP using alkaline phosphatase enzyme.

   A choline nanobiosensor has been investigated using chemiluminescence technique over a wide range of choline from 0.0005 – 2 mM. For surface characterization, XRD, Raman and FT-IR were used. Importantly, the recovery of choline in milk samples was close to 99%. Using the developed biosensor, choline has been measurable even after 30 days with 60 repeated measurements proving the good stability of the sensor (Intraday R.S.D% = 2.83 and Interday R.S.D% = 3.51).

   Further, a biosensor has been developed for multiple analyte, a neurotransmitter (acetylcholine) and environmental contaminant (OPs) in a single chemiluminescence platform. It can save time, quantity of the sample and reduce the cost of analysis. The linear range for acetylcholine has been found in the range 0.01 mM to 10 mM (R^2 = 0.994). For OPs, the linear range is found in the range 0.01 – 5 ng mL^{-1} (R^2 = 0.99, n = 5) meeting the desired lavels of detection.

   Furthermore, a biochip based on ZnO-$ZnAl_2O_4$ composite nanostructures has been demonstrated successfully for bio-catalysis. The principle of *p*NPP bio-catalysis is based on the change of colour which is measured photometrically. The linear plot is obtained in the range of 0.001-10 mM for *p*NPP. Improved K_m of ALP activity, almost 0.6 time lower, has established enhanced bio-catalytic efficiency. The developed biochip has shown satisfactory reproducibility for whiskers having cross-linked immobilized enzyme over the physically adsorbed for analysis of *p*NPP. The results so obtained suggest that

the whisker based biosensor may be explored further as a platform for enhanced bio-catalysis and biosensor construction.

4. **Porous functional materials in bio and chemical sensing (Chapter 4):** In this chapter porous materials have been explored towards the development of bioassay for glucose and heavy metal such as Pb^{2+}. Biocompatible macroporous material (CPG) has been successfully constructed as an efficient capture probe and demonstrated for glucose sensing as a model analyte. The sensing probe has been tested simultaneously as duel read out system *i.e.* colorimetric and impedimetric detection. In both cases, glucose is measurable in the range from 0.001 – 10 mM. A prolonged retention of enzyme activity was observed for porous functional material even after multiple measurements. FEG-SEM, FT-IR and inverted fluorescence microscopy were applied to confirm the surface properties. The K_m obtained using colorimetric and EIS technique is found to be 0.013 mM and 0.0159 mM, respectively. The values of K_m indicates that enzyme retains its activity in the nano-sized porous functional materials.

   Furthermore, another sensing application has been developed using FITC functionalized mesoporous silica (SBA-15) and demonstrated for analysis of Pb^{2+} in water. TEM, surface area analysis, FT-IR and laser scanning confocal mocroscopy were applied for characterization of the SBA-15. So far as knowledge is concerned, this is the first report of a FITC coupled SBA-15 nano sensor for amplified fluorescence detection of Pb^{2+} using confocal microscopy. The developed sensor for Pb^{2+} has been found linear in the range 0.01 – 100 ng mL^{-1} with LOD 0.01 ng mL^{-1} and IC_{50} 0.94 ng mL^{-1}. An important feature of developed sensor is its low sample volume (1 μL) and short analysis time of 2 min.

5. **Development of nano-immunosensor for early stage cancer detection (Chapter 5):** In this chapter, a nano-immunosensor has been developed for sensitive detection of the biomarker for timely diagnosis of cancer which largely determines the survival rate of cancer patients. Using functionalized ZnONPs, a novel hybrid sandwich-type immunoassay has been developed for the determination of CEA labels in serum. The immunosensor exhibited an excellent analytical performance in terms of sensitivity, with a much lower detection limit, selectivity, reproducibility of the measurements and high throughput measurements (384 samples/ 25 min) as compared to conventional microwell plate ELISA. Furthermore, the hybrid immunosensor possessed a high thermal stability

as compared to microplate ELISA. Therefore, the immunosensor appears to be a useful analytical tool to face up relevant problems regarding obesity and related aspects with it.

In summary, the developed methods exploiting SAMs modified NPs and nanostructured materials might provide superiority over the conventional techniques in terms of sensitivity, selectivity, stability, broad range of detection, low cost of the materials, better analytical signal and no requirement to separate the reaction products.

Future scope of the work

- The developed hybrid immunoassay using low cost column technology may be further extended for routine monitoring of AFM1 in dairy industries and also for separation of AFM1 from the contaminated milk.
- The developed choline nanobiosensor may be extended for routine analysis in milk/milk powder and dietary supplements.
- Multiple analyte detection in a single platform using ZnO might be extended for commercialization.
- Based on successful development of sensitive bio-analysis and efficient bio-catalysis, ZnO-$ZnAl_2O_4$ composite nano-whiskers may act as a promising base for other enzyme immobilization and environmental analysis.
- The CPG based glucose sensor may be extended for continuous monitoring device.
- Functional SAB-15 may have biomedical applications with further alteration.
- The nano-immunosensor may be one of the promising technology in comparison to existing conventional techniques for prognosis of cancer.

REFERENCES

ATSDR, **2005**. U. ATSDR Toxicological profile for lead. (Draft for public comment). U.S. Department of health and human services. Public Health Service. Agency for toxic substances and Disease Registry, Atlanta, U.S.A.

Ahirwal, G.K., Mitra, C.K., **2010**. Gold nanoparticles based sandwich electrochemical immunosensor. *Biosensors and Bioelectronics* 25 (9), 2016-2020.

Ahmad, M., Zhu, J., **2011**. ZnO based advanced functional nanostructures: synthesis, properties and applications. *Journal of Materials Chemistry* 21 (3), 599-614.

Albanis, T.A., Hela, D.G., Lambropoulou, D.A., Vasilios, A.S., **2004**. Gas chromatographic–mass spectrometric methodology using solid-phase microextraction for the multiresidue determination of pesticides in surface waters. *International Journal of Environmental Analytical Chemistry* 84 (14-15), 1079-1092.

Al-Ogaidi, I., Gou, H., Al-kazaz, A.K.A., Aguilar, Z.P., Melconian, A.K., Zheng, P., Wu, N., **2014**. A gold@silica core–shell nanoparticle-based surface-enhanced Raman scattering biosensor for label-free glucose detection. *Analytica Chimica Acta* 811, 76-80.

Alvarez-Pérez, M., García-Hipolito, M., de La Fuente Hernández, J., Arzate, H., Carmona-Rodriguez, B., Ximenez-Fyvie, L., Juarez-Islas, J., Alvarez-Fregoso, O., **2009**. Biocompatibility of zinc aluminate nanostructured material. *Journal of Nano Research* 5, 169-176.

Ambrosi, A., Airò, F., Merkoçi, A., **2009**. Enhanced gold nanoparticle based ELISA for a breast cancer biomarker. *Analytical Chemistry* 82 (3), 1151-1156.

Anfossi, L., Calderara, M., Baggiani, C., Giovannoli, C., Arletti, E., Giraudi, G., **2008**. Development and application of solvent-free extraction for the detection of aflatoxin M1 in dairy products by enzyme immunoassay. *Journal of Agricultural and Food Chemistry* 56 (6), 1852-1857.

AOAC, AOAC official method, **2008**.08, Aflatoxin M1 in liquid milk.

Apostoli, P., Kiss, P., Porru, S., Bonde, J.P., Vanhoorne, M., **1998**. Male reproductive toxicity of lead in animals and humans. ASCLEPIOS Study Group. *Occupational and Environmental Medicine* 55 (6), 364-374.

Arduini, F., Amine, A., Moscone, D., Palleschi, G., **2009**. Reversible Enzyme Inhibition–Based Biosensors: Applications and Analytical Improvement Through Diagnostic Inhibition. *Analytical Letters* 42 (9), 1258-1293.

Ariga, K., Yamauchi, Y., Ji, Q., Yonamine, Y., Hill, J.P., **2014**. Research Update: Mesoporous sensor nanoarchitectonics. *APL Materials* 2 (3), 030701.

Arya, S.K., Saha, S., Ramirez-Vick, J.E., Gupta, V., Bhansali, S., Singh, S.P., **2012**. Recent advances in ZnO nanostructures and thin films for biosensor applications: Review. *Analytica Chimica Acta* 737, 1-21.

Asif, M.H., Ali, S.M.U., Nur, O., Willander, M., Brännmark, C., Strålfors, P., Englund, U.H., Elinder, F., Danielsson, B., **2010**. Functionalised ZnO-nanorod-based selective electrochemical sensor for intracellular glucose. *Biosensors and Bioelectronics* 25 (10), 2205-2211.

Bacher, G., Pal, S., Kanungo, L., Bhand, S., **2012**. A label-free silver wire based impedimetric immunosensor for detection of aflatoxin M1 in milk. *Sensors and Actuators B: Chemical* 168, 223-230.

Badea, M., Micheli, L., Messia, M.C., Candigliota, T., Marconi, E., Mottram, T., Velasco-Garcia, M., Moscone, D., Palleschi, G., **2004**. Aflatoxin M1 determination in raw milk using a flow-injection immunoassay system. *Analytica Chimica Acta* 520 (1–2), 141-148.

Bahrami, A., Besharati-Seidani, A., Abbaspour, A., Shamsipur, M., **2014**. A highly selective voltammetric sensor for sub-nanomolar detection of lead ions using a carbon paste electrode impregnated with novel ion imprinted polymeric nanobeads. *Electrochimica Acta* 118, 92-99.

Bai, Y., Yang, H., Yang, W., Li, Y., Sun, C., **2007**. Gold nanoparticles-mesoporous silica composite used as an enzyme immobilization matrix for amperometric glucose biosensor construction. *Sensors and Actuators B: Chemical* 124 (1), 179-186.

Barlési, F., Gimenez, C., Torre, J.-P., Doddoli, C., Mancini, J., Greillier, L., Roux, F., Kleisbauer, J.-P., **2004**. Prognostic value of combination of Cyfra 21-1, CEA and NSE in patients with advanced non-small cell lung cancer. *Respiratory medicine* 98 (4), 357-362.

Barth, S., Hernandez-Ramirez, F., Holmes, J.D., Romano-Rodriguez, A., **2010**. Synthesis and applications of one-dimensional semiconductors. *Progress in Materials Science* 55 (6), 563-627.

Beck, J.S., Vartuli, J.C., Roth, W.J., Leonowicz, M.E., Kresge, C.T., Schmitt, K.D., Chu, C.T.W., Olson, D.H., Sheppard, E.W., **1992**. A new family of mesoporous molecular sieves prepared with liquid crystal templates. *Journal of the American Chemical Society* 114 (27), 10834-10843.

Behera, B., Pal, S., Kanungo, L., Bhand, S., Chandra, S., **2015**. Synthesis and characterization of ZnO-$ZnAl_2O_4$ whiskers and their application in biosensors. *ScienceJet* 4, 102.

Bellinger, D.C., **2004**. Lead. *Pediatrics* 113(Supplement 3), 1016-1022.

Bellinger, D.C., **2008**. Very low lead exposures and children's neurodevelopment. *Current Opinion in Pediatrics* 20 (2), 172-177.

Beltrán, E., Ibáñez, M., Sancho, J.V., Cortés, M.Á., Yusà, V., Hernández, F., **2011**. UHPLC–MS/MS highly sensitive determination of aflatoxins, the aflatoxin metabolite M1 and ochratoxin A in baby food and milk. *Food Chemistry* 126 (2), 737-744.

Bernard, S.M., **2003**. Should the Centers for Disease Control and Prevention's Childhood Lead Poisoning Intervention Level Be Lowered? *American Journal of Public Health* 93 (8), 1253-1260.

Bhand, S.G., Soundararajan, S., Surugiu-Wärnmark, I., Milea, J.S., Dey, E.S., Yakovleva, M., Danielsson, B., **2010**. Fructose-selective calorimetric biosensor in flow injection analysis. *Analytica Chimica Acta* 668 (1), 13-18.

Biebuyck, H.A., Bain, C.D., Whitesides, G.M., **1994**. Comparison of Organic Monolayers on Polycrystalline Gold Spontaneously Assembled from Solutions Containing Dialkyl Disulfides or Alkanethiols. *Langmuir* 10 (6), 1825-1831.

Blusztajn, J.K., **1998**. Choline, a Vital Amine. *Science* 281(5378), 794-795.

Bontidean, I., Berggren, C., Johansson, G., Csöregi, E., Mattiasson, B., Lloyd, J.R., Jakeman, K.J., Brown, N.L., **1998**. Detection of heavy metal ions at femtomolar levels using protein-based biosensors. *Analytical chemistry* 70(19), 4162-4169.

Borras, G., Molina, R., Xercavins, J., Ballesta, A., Iglesias, J., **1995**. Tumor antigens ca 19.9, ca 125, and cea in carcinoma of the uterine cervix. *Gynecologic Oncology* 57(2), 205-211.

Bray, F., Jemal, A., Grey, N., Ferlay, J., Forman, D., **2012**. Global cancer transitions according to the human development index (2008–2030): a population-based study. *The Lancet Oncology* 13(8), 790-801.

Brown, W., **1993**. Dynamic light scattering: the method and some applications. Clarendon Press.

Bruni, S., Cariati, F., Casu, M., Lai, A., Musinu, A., Piccaluga, G., Solinas, S., **1999**. IR and NMR study of nanoparticle-support interactions in a Fe_2O_3-SiO_2 nanocomposite prepared by a Sol-gel method. *Nanostructured Materials* 11(5), 573-586.

Campbell, F.W., Compton, R.G., **2010**. The use of nanoparticles in electroanalysis: an updated review. *Analytical and bioanalytical chemistry* 396(1), 241-259.

Canfield, R.L., Henderson, C.R., Cory-Slechta, D.A., Cox, C., Jusko, T.A., Lanphear, B.P., **2003**. Intellectual impairment in children with blood lead concentrations below 10 μg per deciliter. *New England Journal of Medicine* 348(16), 1517-1526.

Caruntu, D., Caruntu, G., O'Connor, C.J., **2007**. Magnetic properties of variable-sized Fe_3O_4 nanoparticles synthesized from non-aqueous homogeneous solutions of polyols. *Journal of Physics D: Applied Physics* 40(19), 5801.

Carvalho, A., Geissler, M., Schmid, H., Michel, B., Delamarche, E., **2002**. Self-assembled monolayers of eicosanethiol on palladium and their use in microcontact printing. *Langmuir* 18(6), 2406-2412.

Casey, B.J., Kofinas, P., **2008**. Selective binding of carcinoembryonic antigen using imprinted polymeric hydrogels. *Journal of Biomedical Materials Research Part A* 87A(2), 359-363.

Cassiday, L., **2010**. Carbon nanotubes stretch the boundaries of biomarker detection. *Analytical Chemistry* 82(9), 3406-3406.

Chauhan, N., Pundir, C.S., **2012**. An amperometric acetylcholinesterase sensor based on Fe_3O_4 nanoparticle/multi-walled carbon nanotube-modified ITO-coated glass plate for the detection of pesticides. *Electrochimica Acta* 67, 79-86.

Chen, J., Zhang, W.-D., Ye, J.-S., **2008**. Nonenzymatic electrochemical glucose sensor based on MnO2/MWNTs nanocomposite. *Electrochemistry Communications* 10(9), 1268-1271.

Chen, P., Greenberg, B., Taghavi, S., Romano, C., van der Lelie, D., He, C., **2005**. An exceptionally selective lead(II)-regulatory protein from ralstonia metallidurans: Development of a fluorescent lead(II) probe. *Angewandte Chemie International Edition* 44(18), 2715-2719.

Chen, Y.Q., Zheng, X.J., Feng, X., **2010**. The fabrication of vanadium-doped ZnO piezoelectric nanofiber by electrospinning. *Nanotechnology* 21(5), 055708.

Chen, Z., Ren, X., Meng, X., Chen, D., Yan, C., Ren, J., Yuan, Y., Tang, F., **2011**. Optical detection of choline and acetylcholine based on H_2O_2-sensitive quantum dots. *Biosensors and Bioelectronics* 28(1), 50-55.

Cheng, Y., Yuan, R., Chai, Y., Niu, H., Cao, Y., Liu, H., Bai, L., Yuan, Y., **2012**. Highly sensitive luminol electrochemiluminescence immunosensor based on ZnO nanoparticles and glucose oxidase decorated graphene for cancer biomarker detection. *Analytica Chimica Acta* 745, 137-142.

Cheow, L.F., Ko, S.H., Kim, S.J., Kang, K.H., Han, J., **2010**. Increasing the sensitivity of enzyme-linked immunosorbent assay using multiplexed electrokinetic concentrator. *Analytical Chemistry* 82(8), 3383-3388.

Cho, W.C., **2014**. Proteomics in translational cancer research: biomarker discovery for clinical applications. *Expert Review of Proteomics* 11(2), 131-133.

Choi, Y.-E., Kwak, J.-W., Park, J.W., **2010**. Nanotechnology for early cancer detection. *Sensors* 10(1), 428-455.

Chon, H., Lee, S., Son, S.W., Oh, C.H., Choo, J., **2009**. Highly sensitive immunoassay of lung cancer marker carcinoembryonic antigen using surface-enhanced raman scattering of hollow gold nanospheres. *Analytical Chemistry* 81(8), 3029-3034.

Chung, T.D.Y., Sergienko, E., Millán, J.L., **2010**. Assay format as a critical success factor for identification of novel inhibitor chemotypes of tissue-nonspecific alkaline phosphatase from high-throughput screening. *Molecules* 15(5), 3010-3037.

Claeys, W.L., Van Loey, A.M., Hendrickx, M.E., **2002**. Intrinsic time temperature integrators for heat treatment of milk. *Trends in Food Science & Technology* 13(9–10), 293-311.

Clark Jr, L., Kaplan, S., Matthews, E., Edwards, F., Helmsworth, J., **1958**. Monitor and control of blood oxygen tension and pH during total body perfusion. *The Journal of thoracic surgery* 36(4), 488-496.

Comini, E., Baratto, C., Faglia, G., Ferroni, M., Vomiero, A., Sberveglieri, G., **2009**. Quasi-one dimensional metal oxide semiconductors: Preparation, characterization and application as chemical sensors. *Progress in Materials Science* 54(1), 1-67.

Creppy, E.E., **2002**. Update of survey, regulation and toxic effects of mycotoxins in Europe. *Toxicology Letters* 127(1–3), 19-28.

Dai, Z., Bao, J., Yang, X., Ju, H., **2008**. A bienzyme channeling glucose sensor with a wide concentration range based on co-entrapment of enzymes in SBA-15 mesopores. *Biosensors and Bioelectronics* 23(7), 1070-1076.

Dalui, S., Das, S.N., Roy, R.K., Gayen, R.N., Pal, A.K., **2008**. Aligned zinc oxide nanorods by hybrid wet chemical route and their field emission properties. *Thin Solid Films* 516(23), 8219-8226.

Daniel, M.-C., Astruc, D., **2004**. Gold nanoparticles: assembly, supramolecular chemistry, quantum-size-related properties, and applications toward biology, catalysis, and nanotechnology. *Chemical reviews* 104(1), 293-346.

de Oliveira, A.C.A., Assis, V.C., Matos, M.A.C., Matos, R.C., **2005**. Flow-injection system with glucose oxidase immobilized on a tubular reactor for determination of glucose in blood samples. *Analytica Chimica Acta* 535(1–2), 213-217.

Deshpande, K., Danielsson, B., Bhand, S., **2011a**. Flow injection analysis of choline in milk and dietary supplements using an enzyme thermistor. *Chemical Sensors* 1, 16.

Deshpande, K., Mishra, R., Bhand, S., **2011b**. Determination of methyl parathion in water and its removal on zirconia using optical enzyme assay. *Appl Biochem Biotechnol* 164(6), 906-917.

Dinçkaya, E., Kınık, Ö., Sezgintürk, M.K., Altuğ, Ç., Akkoca, A., **2011**. Development of an impedimetric aflatoxin M1 biosensor based on a DNA probe and gold nanoparticles. *Biosensors and Bioelectronics* 26(9), 3806-3811.

Dodeigne, C., Thunus, L., Lejeune, R., **2000**. Chemiluminescence as diagnostic tool. A review. *Talanta* 51(3), 415-439.

D'Orazio, P., **2003**. Biosensors in clinical chemistry. *Clinica Chimica Acta* 334(1), 41-69.

DRI, **1998**. Dietary Reference Intakes for Thiamin, Riboflavin, Niacin, Vitamin B6, Folate, Vitamin B12, Pantothenic Acid, Biotin, and Choline. The National Academies Press.

Du, D., Chen, A., Xie, Y., Zhang, A., Lin, Y., **2011**. Nanoparticle-based immunosensor with apoferritin templated metallic phosphate label for quantification of phosphorylated acetylcholinesterase. *Biosensors and Bioelectronics* 26(9), 3857-3863.

Dzyadevych, S.V., Soldatkin, A.P., Arkhypova, V.N., El'skaya, A.V., Chovelon, J.-M., Georgiou, C.A., Martelet, C., Jaffrezic-Renault, N., **2005**. Early-warning electrochemical biosensor system for environmental monitoring based on enzyme inhibition. *Sensors and Actuators B: Chemical* 105(1), 81-87.

EC, **1999**. (European Communities) Commission Directive 199/50/EC of 25 May 199 amending Directive 91/321/EEC on infant formulae and follow on formulae. Off. J. Eur. Commun. 139, 29-31.

EC, **2006**. European Commission (EC), **2006**. Commission Regulation (EC) No 1881/2006 of 19 December 2006 setting maximum levels for certain contaminants in foodstuffs. Official Journal of the European Union L. 364: 5-24.

Egmond, V., **1989**. Introduction to Mycotoxins in Dairy Products. Applied Science Publishers, London.

Enke, D., Janowski, F., Schwieger, W., **2003**. Porous glasses in the 21st century—a short review. *Microporous and Mesoporous Materials* 60(1–3), 19-30.

Fang, X., Zhai, T., Gautam, U.K., Li, L., Wu, L., Bando, Y., Golberg, D., **2011**. ZnS nanostructures: From synthesis to applications. *Progress in Materials Science* 56(2), 175-287.

Farhadi, S., Panahandehjoo, S., **2010**. Spinel-type zinc aluminate ($ZnAl_2O_4$) nanoparticles prepared by the co-precipitation method: A novel, green and recyclable heterogeneous catalyst for the acetylation of amines, alcohols and phenols under solvent-free conditions. *Applied Catalysis A: General* 382(2), 293-302.

Figa-Talamanca, I., Mearelli, I., Valente, P., Bascherini, S., **1993**. Cancer mortality in a cohort of rural licensed pesticide users in the province of Rome. *International Journal of Epidemiology* 22(4), 579-583.

Finsy, R., **1994**. Particle sizing by quasi-elastic light scattering. *Advances in Colloid and Interface Science* 52, 79-143.

Frens, G., **1973**. Controlled nucleation for the regulation of the particle size in monodisperse gold suspensions. *Nature* 241(105), 20-22.

FSSAI, **2006** Food Safety and Standards Act, Food Safety and Standards Regulations. (contaminants, toxins and residues) (34 of 2006) the Food Safety and Standards Authority of India, India.

Fulati, A., Ali, S.M.U., Asif, M.H., Alvi, N.u.H., Willander, M., Brännmark, C., Strålfors, P., Börjesson, S.I., Elinder, F., Danielsson, B., **2010**. An intracellular glucose biosensor based on nanoflake ZnO. *Sensors and Actuators B: Chemical* 150(2), 673-680.

Gan, N., Zhou, J., Xiong, P., Hu, F., Cao, Y., Li, T., Jiang, Q., **2013**. An ultrasensitive electrochemiluminescent immunoassay for Aflatoxin M1 in milk, based on extraction by magnetic graphene and detection by antibody-labeled CdTe quantumn dots-carbon nanotubes nanocomposite. *Toxins* 5(5), 865-883.

Gao, J., Gu, H., Xu, B., **2009**. Multifunctional magnetic nanoparticles: design, synthesis, and biomedical applications. *Accounts of chemical research* 42(8), 1097-1107.

Gao, Y., Cranston, R., **2010**. Polytyrosine as an electroactive label for signal amplification in electrochemical immunosensors. *Analytica Chimica Acta* 659(1–2), 109-114.

García Sánchez, F., Navas Díaz, A., Ramos Peinado, M.C., Belledone, C., **2003**. Free and sol–gel immobilized alkaline phosphatase-based biosensor for the determination of pesticides and inorganic compounds. *Analytica Chimica Acta* 484(1), 45-51.

Glunde, K., Bhujwalla, Z.M., Ronen, S.M., **2011**. Choline metabolism in malignant transformation. *Nature Reviews Cancer* 11(12), 835-848.

Godwin, H.A., **2001**. The biological chemistry of lead. *Current Opinion in Chemical Biology* 5(2), 223-227.

Goesmann, H., Feldmann, C., **2010**. Nanoparticulate functional materials. *Angewandte Chemie International Edition* 49(8), 1362-1395.

Gordon, C.J., Rowsey, P.J., **1998**. Experimental biology 1997 symposium on neurobiology of thennoregulation: Role of stress: Poisons and fever. *Clinical and experimental pharmacology and physiology* 25(2), 145-149.

Goriushkina, T.B., Soldatkin, A.P., Dzyadevych, S.V., **2009**. Application of Amperometric Biosensors for Analysis of Ethanol, Glucose, and Lactate in Wine. *Journal of Agricultural and Food Chemistry* 57(15), 6528-6535.

Groopman, J.D., Cain, L.G., Kensler, T.W., Harris, C.C., **1988**. Aflatoxin Exposure in Human Populations: Measurements and Relationship to Cancer. *Critical Reviews in Toxicology* 19(2), 113-145.

Grunnet, M., Sorensen, J.B., **2012**. Carcinoembryonic antigen (CEA) as tumor marker in lung cancer. *Lung Cancer* 76(2), 138-143.

Gu, B.X., Xu, C.X., Zhu, G.P., Liu, S.Q., Chen, L.Y., Li, X.S., **2008**. Tyrosinase Immobilization on ZnO Nanorods for Phenol Detection. *The Journal of Physical Chemistry B* 113(1), 377-381.

Guan, D., Li, P., Cui, Y., Zhang, Q., Zhang, W., **2011**. A competitive immunoassay with a surrogate calibrator curve for aflatoxin M1 in milk. *Analytica Chimica Acta* 703(1), 64-69.

Guan, D., Li, P., Zhang, Q., Zhang, W., Zhang, D., Jiang, J., **2011**. An ultra-sensitive monoclonal antibody-based competitive enzyme immunoassay for aflatoxin M1 in milk and infant milk products. *Food Chemistry* 125(4), 1359-1364.

Guo, X., Liang, B., Jian, J., Zhang, Y., Ye, X., **2014**. Glucose biosensor based on a platinum electrode modified with rhodium nanoparticles and with glucose oxidase immobilized on gold nanoparticles. *Microchimica Acta* 181(5-6), 519-525.

Gupta, S., Venkatesh, A., Ray, S., Srivastava, S., **2014**. Challenges and prospects for biomarker research: A current perspective from the developing world. *Biochimica et Biophysica Acta (BBA) - Proteins and Proteomics* 1844(5), 899-908.

Haghighi, B., Karimi, B., Tavahodi, M., Behzadneia, H., **2014**. Electrochemical behavior of glucose oxidase immobilized on Pd-nanoparticles decorated ionic liquid derived fibrillated mesoporous carbon. *Electroanalysis* 26(9), 2010-2016.

Hasanzadeh, M., Shadjou, N., Eskandani, M., Guardia, M.d.l., **2012a**. Mesoporous silica-based materials for use in electrochemical enzyme nanobiosensors. *TrAC Trends in Analytical Chemistry* 40, 106-118.

Hasanzadeh, M., Shadjou, N., de la Guardia, M., Eskandani, M., Sheikhzadeh, P., **2012b**. Mesoporous silica-based materials for use in biosensors. *TrAC Trends in Analytical Chemistry* 33, 117-129.

Hayden, K.M., Norton, M.C., Darcey, D., Østbye, T., Zandi, P.P., Breitner, J.C.S., Welsh-Bohmer, K.A., Investigators, F.t.C.C.S., **2010**. Occupational exposure to pesticides increases the risk of incident AD: The Cache County Study. *Neurology* 74(19), 1524-1530.

He, S.-B., Wu, G.-W., Deng, H.-H., Liu, A.-L., Lin, X.-H., Xia, X.-H., Chen, W., **2014**. Choline and acetylcholine detection based on peroxidase-like activity and protein antifouling property of platinum nanoparticles in bovine serum albumin scaffold. *Biosensors and Bioelectronics* 62, 331-336.

Heiney, P.A., Grüneberg, K., Fang, J., Dulcey, C., Shashidhar, R., **2000**. Structure and growth of chromophore-functionalized (3-aminopropyl)triethoxysilane self-assembled on silicon. *Langmuir* 16(6), 2651-2657.

Hood, L., Heath, J.R., Phelps, M.E., Lin, B., **2004**. Systems biology and new technologies enable predictive and preventative medicine. *Science* 306(5696), 640-643.

Hou, J.-Y., Liu, T.-C., Lin, G.-F., Li, Z.-X., Zou, L.-P., Li, M., Wu, Y.-S., **2012**. Development of an immunomagnetic bead-based time-resolved fluorescence immunoassay for rapid determination of levels of carcinoembryonic antigen in human serum. *Analytica Chimica Acta* 734, 93-98.

Hu, Q., Yang, G., Zhao, Y., Yin, J., **2003**. Determination of copper, nickel, cobalt, silver, lead, cadmium, and mercury ions in water by solid-phase extraction and the RP-HPLC with UV-Vis detection. *Analytical and Bioanalytical Chemistry* 375(6), 831-835.

Huang, I.Y., Lee, M.C., **2008**. Development of a FPW allergy biosensor for human IgE detection by MEMS and cystamine-based SAM technologies. *Sensors and Actuators B: Chemical* 132(1), 340-348.

IARC, **2002**. Monograph on the Evaluation of Carcinogenic Risk to Humans. Some Traditional Herbal Medicines, Some Mycotoxins, Naphtalene and Styrene. IARC: Lyon, France.

Inayat, A., Reinhardt, B., Uhlig, H., Einicke, W.-D., Enke, D., **2013**. Silica monoliths with hierarchical porosity obtained from porous glasses. *Chemical Society Reviews* 42(9), 3753-3764.

Iqbal, J., **2011**. An enzyme immobilized microassay in capillary electrophoresis for characterization and inhibition studies of alkaline phosphatases. *Analytical Biochemistry* 414(2), 226-231.

Israr, M.Q., Sadaf, J.R., Nur, O., Willander, M., Salman, S., Danielsson, B., **2011**. Chemically fashioned ZnO nanowalls and their potential application for potentiometric cholesterol biosensor. *Applied Physics Letters* 98(25), 253705.

IUPAC, **1997**. Compendium of Chemical Terminology, 2nd ed. (the "Gold Book"). Compiled by A. D. McNaught and A. Wilkinson. Blackwell Scientific Publications, Oxford (1997). XML on-line corrected version: http://goldbook.iupac.org (2006-) created by M. Nic, J. Jirat, B. Kosata; updates compiled by A. Jenkins. ISBN 0-9678550-9-8. doi:10.1351/goldbook.

Ivanova, E.P., Wright, J.P., Pham, D.K., Brack, N., Pigram, P., Alekseeva, Y.V., Demyashev, G.M., Nicolau, D.V., **2006**. A comparative study between the adsorption and covalent binding of human immunoglobulin and lysozyme on surface-modified poly(tert -butyl methacrylate). *Biomedical Materials* 1(1), 24.

Jain, K.K., **2005**. Nanotechnology in clinical laboratory diagnostics. *Clinica Chimica Acta* 358(1), 37-54.

Jeyapragasam, T., Saraswathi, R., **2014**. Electrochemical biosensing of carbofuran based on acetylcholinesterase immobilized onto iron oxide–chitosan nanocomposite. *Sensors and Actuators B: Chemical* 191, 681-687.

Jiang, J., Wang, Z., Zhang, H., Zhang, X., Liu, X., Wang, S., **2011**. Monoclonal antibody-based elisa and colloidal gold immunoassay for detecting 19-nortestosterone residue in animal tissues. *Journal of Agricultural and Food Chemistry* 59(18), 9763-9769.

Jiang, Y., Zhao, H., Lin, Y., Zhu, N., Ma, Y., Mao, L., **2010**. Colorimetric Detection of Glucose in Rat Brain Using Gold Nanoparticles. *Angewandte Chemie* 122(28), 4910-4914.

Kanungo, L., Pal, S., Bhand, S., **2011**. Miniaturised hybrid immunoassay for high sensitivity analysis of aflatoxin M1 in milk. *Biosensors and Bioelectronics* 26(5), 2601-2606.

Karnati, C., Du, H., Ji, H.-F., Xu, X., Lvov, Y., Mulchandani, A., Mulchandani, P., Chen, W., **2007**. Organophosphorus hydrolase multilayer modified microcantilevers for organophosphorus detection. *Biosensors and Bioelectronics* 22(11), 2636-2642.

Kavosi, B., Salimi, A., Hallaj, R., Amani, K., **2014**. A highly sensitive prostate-specific antigen immunosensor based on gold nanoparticles/PAMAM dendrimer loaded on MWCNTS/chitosan/ionic liquid nanocomposite. *Biosensors and Bioelectronics* 52, 20-28.

Khan, A.Y., Noronha, S.B., Bandyopadhyaya, R., **2014**. Glucose oxidase enzyme immobilized porous silica for improved performance of a glucose biosensor. *Biochemical Engineering Journal* 91, 78-85.

Kim, J., Yong, K., **2011**. Mechanism study of ZnO nanorod-bundle sensors for H_2S gas sensing. *The Journal of Physical Chemistry C* 115(15), 7218-7224.

Kim, M.S., Kim, G.W., Park, T.J., **2014**. A facile and sensitive detection of organophosphorus chemicals by rapid aggregation of gold nanoparticles using organic compounds. *Biosensors and Bioelectronics* doi:10.1016/j.bios.2014.08.073.

Kim, N., Park, I.-S., Kim, D.-K., **2007**. High-sensitivity detection for model organophosphorus and carbamate pesticide with quartz crystal microbalance-precipitation sensor. *Biosensors and Bioelectronics* 22(8), 1593-1599.

Kim, Y.J., Cho, Y.A., Lee, H.-S., Lee, Y.T., **2003**. Investigation of the effect of hapten heterology on immunoassay sensitivity and development of an enzyme-linked immunosorbent assay for the organophosphorus insecticide fenthion. *Analytica Chimica Acta* 494(1–2), 29-40.

Klopman, G., **1968**. Chemical reactivity and the concept of charge- and frontier-controlled reactions. *Journal of the American Chemical Society* 90(2), 223-234.

Krawczyński vel Krawczyk, T., Moszczyńska, M., Trojanowicz, M., **2000**. Inhibitive determination of mercury and other metal ions by potentiometric urea biosensor. *Biosensors and Bioelectronics* 15(11), 681-691.

Kremeskotter, J., Wilson, R., Schiffrin, D.J., Luff, B.J., Wilkinson, J.S., **1995**. Detection of glucose via electrochemiluminescence in a thin-layer cell with a planar optical waveguide. *Measurement Science and Technology* 6(9), 1325.

Kricka, L.J., **2003**. Clinical applications of chemiluminescence. *Analytica Chimica Acta* 500(1–2), 279-286.

Krstić, D.Z., Čolović, M., Bavcon kralj, M., Franko, M., Krinulović, K., Trebše, P., VASIĆ, V., **2008**. Inhibition of AChE by malathion and some structurally similar compounds. *Journal of Enzyme Inhibition and Medicinal Chemistry* 23(4), 562-573.

Kulasingam, V., Diamandis, E.P., **2008**. Strategies for discovering novel cancer biomarkers through utilization of emerging technologies. *Nature Clinical Practice Oncology* 5(10), 588-599.

Lai, G., Wu, J., Ju, H., Yan, F., **2011**. Streptavidin-functionalized silver-nanoparticle-enriched carbon nanotube tag for ultrasensitive multiplexed detection of tumor markers. *Advanced Functional Materials* 21(15), 2938-2943.

Lai, G., Yan, F., Ju, H., **2009**. Dual Signal Amplification of Glucose Oxidase-Functionalized Nanocomposites as a Trace Label for Ultrasensitive Simultaneous Multiplexed Electrochemical Detection of Tumor Markers. *Analytical Chemistry* 81(23), 9730-9736.

Laibinis, P.E., Hickman, J.J., Wrighton, M.S., Whitesides, G.M., **1989**. Orthogonal self-assembled monolayers: Alkanethiols on gold and alkane carboxylic acids on alumina. *Science* 245(4920), 845-847.

Laibinis, P.E., Whitesides, G.M., Allara, D.L., Tao, Y.T., Parikh, A.N., Nuzzo, R.G., **1991**. Comparison of the structures and wetting properties of self-assembled monolayers of n-alkanethiols on the coinage metal surfaces, copper, silver, and gold. *Journal of the American Chemical Society* 113(19), 7152-7167.

Lallès, J.-P., **2010**. Intestinal alkaline phosphatase: multiple biological roles in maintenance of intestinal homeostasis and modulation by diet. *Nutrition Reviews* 68(6), 323-332.

Lates, V., Yang, C., Popescu, I., Marty, J.-L., **2012**. Displacement immunoassay for the detection of ochratoxin A using ochratoxin B modified glass beads. *Analytical and Bioanalytical Chemistry* 402(9), 2861-2870.

Leandro, C.C., Hancock, P., Fussell, R.J., Keely, B.J., **2006**. Comparison of ultra-performance liquid chromatography and high-performance liquid chromatography for the determination of priority pesticides in baby foods by tandem quadrupole mass spectrometry. *Journal of Chromatography* A 1103(1), 94-101.

Li, D., Ackaah-Gyasi, N.A., Simpson, B.K., **2014a**. Immobilization of Bovine Trypsin onto Controlled Pore Glass. *Journal of Food Biochemistry* 38(2), 184-195.

Li, H., Guo, J., Ping, H., Liu, L., Zhang, M., Guan, F., Sun, C., Zhang, Q., **2011**. Visual detection of organophosphorus pesticides represented by mathamidophos using Au nanoparticles as colorimetric probe. *Talanta* 87, 93-99.

Li, K., Liu, G., Wu, Y., Hao, P., Zhou, W., Zhang, Z., **2014b**. Gold nanoparticle amplified optical microfiber evanescent wave absorption biosensor for cancer biomarker detection in serum. *Talanta* 120(0), 419-424.

Li, T., Wang, E., Dong, S., **2009**. Potassium−lead-switched g-quadruplexes: A new class of dna logic gates. *Journal of the American Chemical Society* 131(42), 15082-15083.

Li, Y., Huang, H., Shi, F., Li, Y., Su, X., **2013**. Optical choline sensor based on a water-soluble fluorescent conjugated polymer and an enzyme-coupled assay. *Microchimica Acta*, 1-6.

Li, Z., Chang, S.-C., Williams, R.S., **2003**. Self-assembly of alkanethiol molecules onto platinum and platinum oxide surfaces. *Langmuir* 19(17), 6744-6749.

Liang, H., Song, D., Gong, J., **2014**. Signal-on electrochemiluminescence of biofunctional CdTe quantum dots for biosensing of organophosphate pesticides. *Biosensors and Bioelectronics* 53, 363-369.

Liang, S., Wang, Y., Zhang, C., Liu, X., **2006**. Synthesis of amino-modified magnetite nanoparticles coated with Hepama-1 and radiolabeled with 188Re for bio-magnetically targeted radiotherapy. *Journal of Radioanalytical Nuclear Chemistry* 269(1), 3-7.

Limbut, W., Thavarungkul, P., Kanatharana, P., Asawatreratanakul, P., Limsakul, C., Wongkittisuksa, B., **2004**. Comparative study of controlled pore glass, silica gel and Poraver® for the immobilization of urease to determine urea in a flow injection conductimetric biosensor system. *Biosensors and Bioelectronics* 19(8), 813-821.

Lin, J., He, C., Zhang, S., **2009**. Immunoassay channels for α-fetoprotein based on encapsulation of biorecognition molecules into SBA-15 mesopores. *Analytica Chimica Acta* 643(1–2), 90-94.

Lin, J., Yan, F., Ju, H., **2004**. Noncompetitive enzyme immunoassay for carcinoembryonic antigen by flow injection chemiluminescence. *Clinica Chimica Acta* 341(1–2), 109-115.

Liu, C.-W., Huang, C.-C., Chang, H.-T., **2009a**. Highly selective DNA-based sensor for lead(II) and mercury(II) ions. *Analytical Chemistry* 81(6), 2383-2387.

Liu, D., Chen, W., Wei, J., Li, X., Wang, Z., Jiang, X., **2012a**. A highly sensitive, dual-readout assay based on gold nanoparticles for organophosphorus and carbamate pesticides. *Analytical Chemistry* 84(9), 4185-4191.

Liu, G., Lin, Y., **2006**. Biosensor based on self-assembling acetylcholinesterase on carbon nanotubes for flow injection/amperometric detection of organophosphate pesticides and nerve agents. *Analytical Chemistry* 78(3), 835-843.

Liu, J., Chen, H., Mao, X., Jin, X., **2000**. Determination of trace copper, lead, cadmium, and iron in environmental and biological samples by flame atomic absorption spectrometry coupled to flow injection on-line coprecipitation preconcentration using DDTC-nickel as coprecipitate carrier. *International Journal of Environmental Analytical Chemistry* 76(4), 267-282.

Liu, M., Liu, R., Chen, W., **2013**. Graphene wrapped Cu2O nanocubes: Non-enzymatic electrochemical sensors for the detection of glucose and hydrogen peroxide with enhanced stability. *Biosensors and Bioelectronics* 45, 206-212.

Liu, N., Feng, F., Liu, Z., Ma, Z., **2014**. Porous platinum nanoparticles and PdPt nanocages for use in an ultrasensitive immunoelectrode for the simultaneous determination of the tumor markers CEA and AFP. *Microchimica Acta*, 1-9.

Liu, Y., Wang, H., Huang, J., Yang, J., Liu, B., Yang, P., **2009b**. Microchip-based ELISA strategy for the detection of low-level disease biomarker in serum. *Analytica Chimica Acta* 650(1), 77-82.

Liu, Z., Kiessling, F., Gätjens, J., **2010**. Advanced Nanomaterials in Multimodal Imaging: Design, Functionalization, and Biomedical Applications. *Journal of Nanomaterials* 2010, 15.

Liu, Z., Wang, H., Li, B., Liu, C., Jiang, Y., Yu, G., Mu, X., **2012b**. Biocompatible magnetic cellulose-chitosan hybrid gel microspheres reconstituted from ionic liquids for enzyme immobilization. *Journal of Materials Chemistry* 22(30), 15085-15091.

Liu, Z.-M., Yang, H.-F., Li, Y.-F., Liu, Y.-L., Shen, G.-L., Yu, R.-Q., **2006**. Core–shell magnetic nanoparticles applied for immobilization of antibody on carbon paste electrode and amperometric immunosensing. *Sensors and Actuators B: Chemical* 113(2), 956-962.

López, C., Ramos, L., Ramadán, S., Bulacio, L., Perez, J., **2001**. Distribution of aflatoxin M1 in cheese obtained from milk artificially contaminated. *International Journal of Food Microbiology* 64(1–2), 211-215.

Love, J.C., Estroff, L.A., Kriebel, J.K., Nuzzo, R.G., Whitesides, G.M., **2005**. Self-assembled monolayers of thiolates on metals as a form of nanotechnology. *Chemical reviews* 105(4), 1103-1170.

Lu, A.H., Salabas, E.e.L., Schüth, F., **2007**. Magnetic nanoparticles: synthesis, protection, functionalization, and application. *Angewandte Chemie International Edition* 46(8), 1222-1244.

Lu, G.Q., Zhao, G.X.S., **2004**. Nanoporous Materials: Science and Engineering. Imperial College Press.

Ma, R., Van Mol, W., Adams, F., **1994**. Determination of cadmium, copper and lead in environmental samples. An evaluation of flow injection on-line sorbent extraction for flame atomic absorption spectrometry. *Analytica Chimica Acta* 285(1–2), 33-43.

Magliulo, M., Mirasoli, M., Simoni, P., Lelli, R., Portanti, O., Roda, A., **2005**. Development and validation of an ultrasensitive chemiluminescent enzyme immunoassay for aflatoxin M1 in milk. *Journal of Agricultural and Food Chemistry* 53(9), 3300-3305.

Malhotra, R., Patel, V., Vaqué, J.P., Gutkind, J.S., Rusling, J.F., **2010**. Ultrasensitive electrochemical immunosensor for oral cancer biomarker IL-6 using carbon nanotube forest electrodes and multilabel amplification. *Analytical chemistry* 82(8), 3118-3123.

Martínez, F.L., Toledano-Luque, M., Gandía, J.J., Cárabe, J., Bohne, W., Röhrich, J., Strub, E., Mártil, I., **2007**. Optical properties and structure of HfO_2 thin films grown by high pressure reactive sputtering. *Journal of Physics D: Applied Physics* 40(17), 5256.

Martín-Fernández, B., García Iñigo, F.J., Sánchez-Paniagua López, M., López-Ruiz, B., Cabanillas, G.F., **2008**. Amperometric enzyme biosensor based on the controlled pore glass. *Analytical Letters* 41(6), 1059-1073.

Mashhadizadeh, M.H., Talemi, R.P., **2014**. A novel optical DNA biosensor for detection of trace amounts of mercuric ions using gold nanoparticles introduced onto modified glass surface. *Spectrochimica Acta Part A: Molecular and Biomolecular Spectroscopy* 132, 403-409.

Mateo, C., Palomo, J.M., Fernandez-Lorente, G., Guisan, J.M., Fernandez-Lafuente, R., **2007**. Improvement of enzyme activity, stability and selectivity via immobilization techniques. *Enzyme and Microbial Technology* 40(6), 1451-1463.

Mayorga-Martinez, C.C., Pino, F., Kurbanoglu, S., Rivas, L., Ozkan, S.A., Merkoci, A., **2014**. Iridium oxide nanoparticle induced dual catalytic/inhibition based detection of phenol and pesticide compounds. *Journal of Materials Chemistry B* 2(16), 2233-2239.

McNeil, S.E., **2005**. Nanotechnology for the biologist. *Journal of Leukocyte Biology* 78(3), 585-594.

Meiser, F., Cortez, C., Caruso, F., **2004**. Biofunctionalization of fluorescent rare-earth-doped lanthanum phosphate colloidal nanoparticles. *Angewandte Chemie International Edition* 43(44), 5954-5957.

Michel, V., Yuan, Z., Ramsubir, S., Bakovic, M., **2006**. Choline transport for phospholipid synthesis. *Experimental Biology and Medicine* 231(5), 490-504.

Micheli, L., Grecco, R., Badea, M., Moscone, D., Palleschi, G., **2005**. An electrochemical immunosensor for aflatoxin M1 determination in milk using screen-printed electrodes. *Biosensors and Bioelectronics* 21(4), 588-596.

Mishra, G.K., Mishra, R.K., Bhand, S., **2010a**. Flow injection analysis biosensor for urea analysis in adulterated milk using enzyme thermistor. *Biosensors and Bioelectronics* 26(4), 1560-1564.

Mishra, R.K., Deshpande, K., Bhand, S., **2010b**. A High-Throughput Enzyme Assay for Organophosphate Residues in Milk. *Sensors* 10(12), 11274-11286.

Mishra, R.K., Dominguez, R.B., Bhand, S., Muñoz, R., Marty, J.-L., **2012**. A novel automated flow-based biosensor for the determination of organophosphate pesticides in milk. *Biosensors and Bioelectronics* 32(1), 56-61.

Mishra, R.K., Mishra, G.K., Dharma Teja, V., Danielsson, B., Bhand, S., **2013**. A visual colorimetric dual readout bioassay for determination of pesticide residues in drinking water. *Chemical sensors* 3(12).

Moschou, E., Sharma, B., Deo, S., Daunert, S., **2004**. Fluorescence Glucose Detection: Advances Toward the Ideal In Vivo Biosensor. *Journal of Fluorescence* 14(5), 535-547.

Mulchandani, A., Chen, W., Mulchandani, P., Wang, J., Rogers, K.R., **2001a**. Biosensors for direct determination of organophosphate pesticides. *Biosensors and Bioelectronics* 16(4–5), 225-230.

Mulchandani, P., Chen, W., Mulchandani, A., **2001b**. Flow Injection Amperometric Enzyme Biosensor for Direct Determination of Organophosphate Nerve Agents. *Environmental Science & Technology* 35(12), 2562-2565.

Murray, R.W., **2008**. Nanoelectrochemistry: metal nanoparticles, nanoelectrodes, and nanopores. *Chemical reviews* 108(7), 2688-2720.

Muskal, N., Turyan, I., Mandler, D., **1996**. Self-assembled monolayers on mercury surfaces. *Journal of Electroanalytical Chemistry* 409(1), 131-136.

Nagraj, N., Liu, J., Sterling, S., Wu, J., Lu, Y., **2009**. DNAzyme catalytic beacon sensors that resist temperature-dependent variations. *Chemical Communications* 27(27), 4103-4105.

Naik, B., Prasad, V.S., Ghosh, N.N., **2010**. A simple aqueous solution based chemical methodology for synthesis of Ag nanoparticles dispersed on mesoporous silicate matrix. *Powder Technology* 199(2), 197-201.

Nakano, K., Yoshitake, T., Yamashita, Y., Bowden, E.F., **2007**. Cytochrome c Self-Assembly on Alkanethiol Monolayer Electrodes as Characterized by AFM, IR, QCM, and Direct Electrochemistry. *Langmuir* 23(11), 6270-6275.

Navas-Acien, A., Guallar, E., Silbergeld, E.K., Rothenberg, S.J., **2007**. Lead Exposure and Cardiovascular Disease—A Systematic Review. *Environmental Health Perspectives* 115(3), 472–482.

Neagu, D., Perrino, S., Micheli, L., Palleschi, G., Moscone, D., **2009**. Aflatoxin M1 determination and stability study in milk samples using a screen-printed 96-well electrochemical microplate. *International Dairy Journal* 19(12), 753-758.

Needleman, H., **2004**. Lead poisoning. *Annual Review of Medicine* 55(1), 209-222.

Neouze, M.-A., Schubert, U., **2008**. surface modification and functionalization of metal and metal oxide nanoparticles by organic ligands. *Monatsh Chem* 139(3), 183-195.

Nguyen, B.H., Tran, L.D., Do, Q.P., Nguyen, H.L., Tran, N.H., Nguyen, P.X., **2013**. Label-free detection of aflatoxin M1 with electrochemical Fe_3O_4/polyaniline-based aptasensor. *Materials Science and Engineering: C* 33(4), 2229-2234.

Niemeyer, C.M., **2001**. Nanoparticles, Proteins, and Nucleic Acids: Biotechnology Meets Materials Science. *Angewandte Chemie International Edition* 40(22), 4128-4158.

Nikitin, P.I., Vetoshko, P.M., Ksenevich, T.I., **2007**. New type of biosensor based on magnetic nanoparticle detection. *Journal of Magnetism and Magnetic Materials* 311(1), 445-449.

Norouzi, P., Gupta, V.K., Faridbod, F., Pirali-Hamedani, M., Larijani, B., Ganjali, M.R., **2011**. Carcinoembryonic Antigen Admittance Biosensor Based on Au and ZnO Nanoparticles Using FFT Admittance Voltammetry. *Analytical Chemistry* 83(5), 1564-1570.

O'Malley, M., **1997**. Clinical evaluation of pesticide exposure and poisonings. *The Lancet* 349(9059), 1161-1166.

Pal, S., Sharma, M.K., Danielsson, B., Willander, M., Chatterjee, R., Bhand, S., **2014**. A miniaturized nanobiosensor for choline analysis. *Biosensors and Bioelectronics* 54, 558-564.

Paniel, N., Radoi, A., Marty, J.-L., **2010**. Development of an electrochemical biosensor for the detection of aflatoxin M1 in milk. *Sensors* 10, 9439-9448.

Park, J.-S., Cho, M.K., Lee, E.J., Ahn, K.-Y., Lee, K.E., Jung, J.H., Cho, Y., Han, S.-S., Kim, Y.K., Lee, J., **2009**. A highly sensitive and selective diagnostic assay based on virus nanoparticles. *Nature Nanotechnology* 4(4), 259-264.

Pathak, P., Katiyar, V., Giri, S., **2007**. Cancer research-nanoparticles, nanobiosensors and their use in cancer research. *Journal of Nanotechnology Online*, 14.

Pawsey, S., Yach, K., Reven, L., **2002**. Self-Assembly of Carboxyalkylphosphonic Acids on Metal Oxide Powders. *Langmuir* 18(13), 5205-5212.

Pearson, R.G., **1963**. Hard and soft acids and bases. *Journal of the American Chemical Society* 85(22), 3533-3539.

Peters, J., Schmidt-Gayk, H., Peters, B., Armbruster, F., Quentmeier, A., Mathias, D., **1989**. Immunoradiometric assay of carcinoembryonic antigen with use of avidin-biotin labeling. *Clinical chemistry* 35(4), 573-576.

Phillips, M., **2012**. Analytical approaches to determination of total choline in foods and dietary supplements. *Analytical and Bioanalytical Chemistry* 403(8), 2103-2112.

Piao, Y., Han, D.J., Seo, T.S., **2014**. Highly conductive graphite nanoparticle based enzyme biosensor for electrochemical glucose detection. *Sensors and Actuators B: Chemical* 194, 454-459.

Pison, U., Welte, T., Giersig, M., Groneberg, D.A., **2006**. Nanomedicine for respiratory diseases. *European Journal of Pharmacology* 533(1–3), 341-350.

Pocai, A., Lam, T.K.T., Obici, S., Gutierrez-Juarez, R., Muse, E.D., Arduini, A., Rossetti, L., **2006**. Restoration of hypothalamic lipid sensing normalizes energy and glucose homeostasis in overfed rats. *The Journal of Clinical Investigation* 116(4), 1081-1091.

Politi, J., Spadavecchia, J., Iodice, M., de Stefano, L., **2015**. Oligopeptide-heavy metal interaction monitoring by hybrid gold nanoparticle based assay. *Analyst* 140, 149-155.

Qie, Z., Ning, B., Liu, M., Bai, J., Peng, Y., Song, N., Lv, Z., Wang, Y., Sun, S., Su, X., Zhang, Y., Gao, Z., **2013**. Fast detection of atrazine in corn using thermometric biosensors. *Analyst* 138(17), 5151-5156.

Qin, X., Wang, H., Wang, X., Miao, Z., Chen, L., Zhao, W., Shan, M., Chen, Q., **2010**. Amperometric biosensors based on gold nanoparticles-decorated multiwalled carbon nanotubes-poly(diallyldimethylammonium chloride) biocomposite for the determination of choline. *Sensors and Actuators B: Chemical* 147(2), 593-598.

Qu, S., Liu, J., Luo, J., Huang, Y., Shi, W., Wang, B., Cai, X., **2013**. A rapid and highly sensitive portable chemiluminescent immunosensor of carcinoembryonic antigen based on immunomagnetic separation in human serum. *Analytica Chimica Acta* 766, 94-99.

Radoi, A., Targa, M., Prieto-Simon, B., Marty, J.L., **2008**. Enzyme-Linked Immunosorbent Assay (ELISA) based on superparamagnetic nanoparticles for aflatoxin M1 detection. *Talanta* 77(1), 138-143.

Ravindranath, S.P., Mauer, L.J., Deb-Roy, C., Irudayaraj, J., **2009**. Biofunctionalized Magnetic Nanoparticle Integrated Mid-Infrared Pathogen Sensor for Food Matrixes. *Analytical Chemistry* 81(8), 2840-2846.

Razola, S.S., Pochet, S., Grosfils, K., Kauffmann, J.M., **2003**. Amperometric determination of choline released from rat submandibular gland acinar cells using a choline oxidase biosensor. *Biosensors and Bioelectronics* 18(2–3), 185-191.

Richman, E.L., Kenfield, S.A., Stampfer, M.J., Giovannucci, E.L., Zeisel, S.H., Willett, W.C., Chan, J.M., **2012**. Choline intake and risk of lethal prostate cancer: incidence and survival. *The American Journal of Clinical Nutrition* 96(4), 855-863.

Rico, C.M., Majumdar, S., Duarte-Gardea, M., Peralta-Videa, J.R., Gardea-Torresdey, J.L., **2011**. Interaction of Nanoparticles with Edible Plants and Their Possible Implications in the Food Chain. *Journal of Agricultural and Food Chemistry* 59(8), 3485-3498.

Risveden, K., Dick, K.A., Bhand, S., Rydberg, P., Samuelson, L., Danielsson, B., **2010**. Branched nanotrees with immobilized acetylcholine esterase for nanobiosensor applications. *Nanotechnology* 21(5), 055102.

Rotiroti, L., Stefano, L.D., Rendina, I., Moretti, L., Rossi, A.M., Piccolo, A., **2005**. Optical microsensors for pesticides identification based on porous silicon technology. *Biosensors and Bioelectronics* 20(10), 2136-2139.

Rupa, D., Reddy, P., Reddi, O., **1989**. Chromosomal aberrations in peripheral lymphocytes of cotton field workers exposed to pesticides. *Environmental research* 49(1), 1-6.

Samanta, D., Sarkar, A., **2011**. Immobilization of bio-macromolecules on self-assembled monolayers: methods and sensor applications. *Chemical Society Reviews* 40(5), 2567-2592.

Sanvicens, N., Marco, M.P., **2008**. Multifunctional nanoparticles – properties and prospects for their use in human medicine. *Trends in Biotechnology* 26(8), 425-433.

Sayari, A., Hamoudi, S., **2001**. Periodic mesoporous silica-based organic−inorganic nanocomposite materials. *Chemistry of Materials* 13(10), 3151-3168.

Seeman, N.C., Belcher, A.M., **2002**. Emulating biology: building nanostructures from the bottom up. *Proceedings of the National Academy of Sciences of the United States of America* 99(Suppl 2), 6451-6455.

Shankaran, D.R., Miura, N., **2007**. Trends in interfacial design for surface plasmon resonance based immunoassays. *Journal of Physics D: Applied Physics* 40(23), 7187.

Sharma, M.K., Mishra, D.K., Ghosh, S., Kanjilal, D., Srivastava, P., Chatterjee, R., **2011**. Oxygen vacancy mediated large magnetization in chemically synthesized Ni-doped HfO_2 nanoparticle powder samples. *Journal of Applied Physics* 110(6), 063902.

Shephard, G., **2009**. Aflatoxin analysis at the beginning of the twenty-first century. *Analytical and Bioanalytical Chemistry* 395(5), 1215-1224.

Shimomura, T., Itoh, T., Sumiya, T., Mizukami, F., Ono, M., **2009**. Amperometric determination of choline with enzyme immobilized in a hybrid mesoporous membrane. *Talanta* 78(1), 217-220.

Shokry Hassan, H., Kashyout, A.B., Soliman, H.M.A., Uosif, M.A., Afify, N., **2013**. Effect of reaction time and Sb doping ratios on the architecturing of ZnO nanomaterials for gas sensor applications. *Applied Surface Science* 277, 73-82.

Shu, H., Wen, W., Xiong, H., Zhang, X., Wang, S., **2013**. Novel electrochemical aptamer biosensor based on gold nanoparticles signal amplification for the detection of carcinoembryonic antigen. *Electrochemistry Communications* 37, 15-19.

Singh, S., Gupta, B.D., **2013**. Fabrication and characterization of a surface plasmon resonance based fiber optic sensor using gel entrapment technique for the detection of low glucose concentration. *Sensors and Actuators B: Chemical* 177, 589-595.

Singh, S.P., Arya, S.K., Pandey, P., Malhotra, B.D., Saha, S., Sreenivas, K., Gupta, V., **2007**. Cholesterol biosensor based on rf sputtered zinc oxide nanoporous thin film. *Applied Physics Letters* 91(6), 063901.

Solanki, P.R., Kaushik, A., Agrawal, V.V., Malhotra, B.D., **2011**. Nanostructured metal oxide-based biosensors. *NPG Asia Materials* 3, 17-24.

Solanki, P.R., Kaushik, A., Ansari, A.A., Sumana, G., Malhotra, B.D., **2008**. Zinc oxide-chitosan nanobiocomposite for urea sensor. *Applied Physics Letters* 93(16), 163903.

Suárez-Franco, J.L., García-Hipólito, M., Surárez-Rosales, M.Á., Fernández-Pedrero, J.A., Álvarez-Fregoso, O., Juárez-Islas, J.A., Álvarez-Pérez, M.A., **2013**. Effects of surface morphology of $ZnAl_2O_4$ ceramic materials on osteoblastic cells responses. *Journal of Nanomaterials* 2013, 2.

Sulyok, M., Krska, R., Schuhmacher, R., **2010**. Application of an LC–MS/MS based multi-mycotoxin method for the semi-quantitative determination of mycotoxins occurring in different types of food infected by moulds. *Food Chemistry* 119(1), 408-416.

Syshchyk, O., Skryshevsky, V.A., Soldatkin, O.O., Soldatkin, A.P., **2015**. Enzyme biosensor systems based on porous silicon photoluminescence for detection of glucose, urea and heavy metals. *Biosensors and Bioelectronics* 66, 89-94.

Taherimaslak, Z., Amoli-Diva, M., Allahyary, M., Pourghazi, K., **2014**. Magnetically assisted solid phase extraction using Fe_3O_4 nanoparticles combined with enhanced spectrofluorimetric detection for aflatoxin M1 determination in milk samples. *Analytica Chimica Acta* 842(0), 63-69.

Takayama, M., Itoh, S., Nagasaki, T., Tanimizu, I., **1977**. A new enzymatic method for determination of serum choline-containing phospholipids. *Clinica Chimica Acta* 79(1), 93-98.

Tang, D., Hou, L., Niessner, R., Xu, M., Gao, Z., Knopp, D., **2013**. Multiplexed electrochemical immunoassay of biomarkers using metal sulfide quantum dot nanolabels and trifunctionalized magnetic beads. *Biosensors and Bioelectronics* 46, 37-43.

Tang, W., Li, L., Zeng, X., 2015. A glucose biosensor based on the synergistic action of nanometer-sized TiO2 and polyaniline. *Talanta* 131(0), 417-423.

Telting-Diaz, M., Bakker, E., **2002**. Mass-produced ionophore-based fluorescent microspheres for trace level determination of lead ions. *Analytical Chemistry* 74(20), 5251-5256.

Textor, M., Ruiz, L., Hofer, R., Rossi, A., Feldman, K., Hähner, G., Spencer, N.D., **2000**. Structural chemistry of self-assembled monolayers of octadecylphosphoric acid on tantalum oxide surfaces. *Langmuir* 16(7), 3257-3271.

Tiwari, A., Turner, A.P., **2014**. Biosensors Nanotechnology. John Wiley & Sons.

Topoglidis, E., Cass, A.E.G., O'Regan, B., Durrant, J.R., **2001**. Immobilisation and bioelectrochemistry of proteins on nanoporous TiO2 and ZnO films. *Journal of Electroanalytical Chemistry* 517(1–2), 20-27.

Ueland, P.M., **2011**. Choline and betaine in health and disease. *Journal of inherited metabolic disease* 34(1), 3-15.

Ulman, A., **1996**. Formation and structure of self-assembled monolayers. *Chemical Reviews* 96(4), 1533-1554.

Usman Ali, S.M., Alvi, N.H., Ibupoto, Z., Nur, O., Willander, M., Danielsson, B., **2011**. Selective potentiometric determination of uric acid with uricase immobilized on ZnO nanowires. *Sensors and Actuators B: Chemical* 152(2), 241-247.

Valgimigli, F., Mastrantonio, F., Lucarelli, F., **2014**. Blood Glucose Monitoring Systems. Security and Privacy for Implantable Medical Devices, pp. 15-82. Springer.

Van Dyk, J.S., Pletschke, B., **2011**. Review on the use of enzymes for the detection of organochlorine, organophosphate and carbamate pesticides in the environment. *Chemosphere* 82(3), 291-307.

Var, I., Kabak, B., Gök, F., **2007**. Survey of aflatoxin B1 in helva, a traditional Turkish food, by TLC. *Food Control* 18(1), 59-62.

Vashist, S.K., Marion Schneider, E., Lam, E., Hrapovic, S., Luong, J.H.T., **2014**. One-step antibody immobilization-based rapid and highly-sensitive sandwich ELISA procedure for potential in vitro diagnostics. *Nature Scientific Report* 4.

Veiseh, O., Gunn, J.W., Zhang, M., **2010**. Design and fabrication of magnetic nanoparticles for targeted drug delivery and imaging. *Advanced Drug Delivery Reviews* 62(3), 284-304.

Vo-Dinh, T., **2008**. Nanosensing at the single cell level. *Spectrochimica Acta Part B: Atomic Spectroscopy* 63(2), 95-103.

Walcarius, A., Minteer, S.D., Wang, J., Lin, Y., Merkoci, A., **2013**. Nanomaterials for bio-functionalized electrodes: recent trends. *Journal of Materials Chemistry B* 1(38), 4878-4908.

Wang, G., Huang, H., Zhang, G., Zhang, X., Fang, B., Wang, L., **2011**. Dual amplification strategy for the fabrication of highly sensitive interleukin-6 amperometric immunosensor based on poly-dopamine. *Langmuir* 27(3), 1224-1231.

Wang, J., Liu, G., Jan, M.R., **2004**. Ultrasensitive electrical biosensing of proteins and DNA: Carbon-nanotube derived amplification of the recognition and transduction events. *Journal of the American Chemical Society* 126(10), 3010-3011.

Wang, J., Munir, A., Li, Z., Zhou, H.S., **2009**. Aptamer–Au NPs conjugates-enhanced SPR sensing for the ultrasensitive sandwich immunoassay. *Biosensors and Bioelectronics* 25(1), 124-129.

Wang, J.X., Sun, X.W., Wei, A., Lei, Y., Cai, X.P., Li, C.M., Dong, Z.L., **2006**. Zinc oxide nanocomb biosensor for glucose detection. *Applied Physics Letters* 88(23), 233106.

Wang, L., Gan, X.-X., **2009**. Biomolecule-functionalized magnetic nanoparticles for flow-through quartz crystal microbalance immunoassay of aflatoxin B1. *Bioprocess Biosyst Eng* 32(1), 109-116.

Wang, S., Su, P., Yang, Y., **2012**. Online immobilized enzyme microreactor for the glucose oxidase enzymolysis and enzyme inhibition assay. *Analytical Biochemistry* 427(2), 139-143.

Wang, X., Lin, J.-M., Ying, X., **2007**. Evaluation of carbohydrate antigen 50 in human serum using magnetic particle-based chemiluminescence enzyme immunoassay. *Analytica Chimica Acta* 598(2), 261-267.

Wang, X., Niessner, R., Knopp, D., **2014**. Magnetic Bead-based colorimetric immunoassay for aflatoxin B1 using gold nanoparticles. *Sensors* 14(11), 21535-21548.

Wang, Z.L., **2008**. Towards Self-Powered Nanosystems: From Nanogenerators to Nanopiezotronics. *Advanced Functional Materials* 18(22), 3553-3567.

Weetall, H., **1993**. Preparation of immobilized proteins covalently coupled through silane coupling agents to inorganic supports. *Applied Biochemistry and Biotechnology* 41(3), 157-188.

Weetall, H.H., **1976**. Covalent coupling methods for inorganic support materials. In: Klaus, M. (Ed.), Methods in Enzymology, pp. 134-148. Academic Press.

Whitesides, G.M., **2005**. Nanoscience, Nanotechnology, and Chemistry. *Small* 1(2), 172-179.

WHO, **2011**. Diabetes. Fact Sheet: World Health Organization, Trans. Media Centre.

Wilkins, E., Atanasov, P., **1996**. Glucose monitoring: state of the art and future possibilities. *Medical Engineering and Physics* 18(4), 273-288.

Willander, M., Nur, O., ul Hasan, K., Amin, G., Soomro, M.Y., **2014**. Zinc Oxide Nanostructures: Synthesis, Characterization, and Device Applications on Nonconventional Substrates. Zinc Oxide Nanostructures: Advances and Applications, 185.

Wu, J., Fu, Z., Yan, F., Ju, H., **2007**. Biomedical and clinical applications of immunoassays and immunosensors for tumor markers. *TrAC Trends in Analytical Chemistry* 26(7), 679-688.

Wu, K., Chu, C., Ma, C., Yang, H., Yan, M., Ge, S., Yu, J., Song, X., **2015**. Immunoassay for carcinoembryonic antigen based on the Zn^{2+}-enhanced fluorescence of magnetic-fluorescent nanocomposites. *Sensors and Actuators B: Chemical* 206, 43-49.

Wu, P., Hwang, K., Lan, T., Lu, Y., **2013**. A DNAzyme-gold nanoparticle probe for uranyl ion in living cells. *Journal of the American Chemical Society* 135(14), 5254-5257.

Wu, Y., Chen, C., Liu, S., **2009**. Enzyme-functionalized silica nanoparticles as sensitive labels in biosensing. *Analytical chemistry* 81(4), 1600-1607.

Xian, Y., Xian, Y., Zhou, L., Wu, F., Ling, Y., Jin, L., **2007**. Encapsulation hemoglobin in ordered mesoporous silicas: Influence factors for immobilization and bioelectrochemistry. *Electrochemistry Communications* 9(1), 142-148.

Yakovleva, M., Buzas, O., Matsumura, H., Samejima, M., Igarashi, K., Larsson, P.-O., Gorton, L., Danielsson, B., **2012**. A novel combined thermometric and amperometric biosensor for lactose determination based on immobilised cellobiose dehydrogenase. *Biosensors and Bioelectronics* 31(1), 251-256.

Yang, C., Wang, Y., Marty, J.-L., Yang, X., **2011**. Aptamer-based colorimetric biosensing of Ochratoxin A using unmodified gold nanoparticles indicator. *Biosensors and Bioelectronics* 26(5), 2724-2727.

Yang, L., Qi, Y., Yuan, X., Shen, J., Kim, J., **2005**. Direct synthesis, characterization and catalytic application of SBA-15 containing heteropolyacid $H_3PW_{12}O_{40}$. *Journal of Molecular Catalysis A: Chemical* 229(1–2), 199-205.

Yang, X., Guo, Y., Wang, A., **2010**. Luminol/antibody labeled gold nanoparticles for chemiluminescence immunoassay of carcinoembryonic antigen. *Analytica Chimica Acta* 666(1–2), 91-96.

Yang, Y., Ji, H.-F., Thundat, T., **2003**. Nerve agents detection using a Cu^{2+}/l-cysteine bilayer-coated microcantilever. *Journal of the American Chemical Society* 125(5), 1124-1125.

Yang, Y.C., Song, C., Wang, X.H., Zeng, F., Pan, F., **2008**. Giant piezoelectric d33 coefficient in ferroelectric vanadium doped ZnO films. *Applied Physics Letters* 92(1), 012907.

Yezhelyev, M.V., Gao, X., Xing, Y., Al-Hajj, A., Nie, S., O'Regan, R.M., **2006**. Emerging use of nanoparticles in diagnosis and treatment of breast cancer. *The Lancet Oncology* 7(8), 657-667.

Yin, Y., Talapin, D., **2013**. The chemistry of functional nanomaterials. *Chemical Society Reviews* 42(7), 2484-2487.

Yu, H., **1998**. Comparative studies of magnetic particle-based solid phase fluorogenic and electrochemiluminescent immunoassay. *Journal of Immunological Methods* 218(1–2), 1-8.

Zeisel, S.H., **2000**. Choline: an essential nutrient for humans. Nutrition (Burbank, Los Angeles County, Calif.) 16(7), 669-671.

Zeisel, S.H., Blusztajn, J.K., **1994**. Choline and Human Nutrition. *Annual Review of Nutrition* 14(1), 269-296.

Zhang, B., Kong, T., Xu, W., Su, R., Gao, Y., Cheng, G., **2010a**. Surface functionalization of zinc oxide by carboxyalkylphosphonic acid self-assembled monolayers. *Langmuir* 26(6), 4514-4522.

Zhang, F., Wang, X., Ai, S., Sun, Z., Wan, Q., Zhu, Z., Xian, Y., Jin, L., Yamamoto, K., **2004**. Immobilization of uricase on ZnO nanorods for a reagentless uric acid biosensor. *Analytica Chimica Acta* 519(2), 155-160.

Zhang, J., Lei, J., Xu, C., Ding, L., Ju, H., **2010b**. Carbon nanohorn sensitized electrochemical immunosensor for rapid detection of microcystin-LR. *Analytical Chemistry* 82(3), 1117-1122.

Zhang, L., Goh, S., Hu, X., Crawford, R., Yu, A., **2012**. Removal of aqueous toxic Hg(II) by functionalized mesoporous silica materials. *Journal of Chemical Technology & Biotechnology* 87(10), 1473-1479.

Zhang, S., **2003**. Fabrication of novel biomaterials through molecular self-assembly. *Nature Biotechnology* 21(10), 1171-1178.

Zhang, Z., Lin, M., Zhang, S., Vardhanabhuti, B., **2013**. Detection of aflatoxin M1 in milk by dynamic light scattering coupled with superparamagnetic beads and gold nanoprobes. *Journal of Agricultural and Food Chemistry* 61(19), 4520-4525.

Zhao, H., Ji, X., Wang, B., Wang, N., Li, X., Ni, R., Ren, J., **2015**. An ultra-sensitive acetylcholinesterase biosensor based on reduced graphene oxide-Au nanoparticles-β-cyclodextrin/Prussian blue-chitosan nanocomposites for organophosphorus pesticides detection. *Biosensors and Bioelectronics* 65, 23-30.

Zhao, H., Ju, H., **2006**. Multilayer membranes for glucose biosensing via layer-by-layer assembly of multiwall carbon nanotubes and glucose oxidase. *Analytical Biochemistry* 350(1), 138-144.

Zhao, J., Xu, L., Zhang, T., Ren, G., Yang, Z., **2009**. Influences of nanoparticle zinc oxide on acutely isolated rat hippocampal CA3 pyramidal neurons. *NeuroToxicology* 30(2), 220-230.

Zhao, L.-H., Zhang, R., Zhang, J., Sun, S.-Q., **2012**. Synthesis and characterization of biocompatible ZnO nanoparticles. *CrystEngComm* 14(3), 945-950.

Zhao, X.-H., Kong, R.-M., Zhang, X.-B., Meng, H.-M., Liu, W.-N., Tan, W., Shen, G.-L., Yu, R.-Q., **2011**. Graphene–DNAzyme based biosensor for amplified fluorescence "Turn-On" detection of Pb^{2+} with a high selectivity. *Analytical Chemistry* 83(13), 5062-5066.

Zhao, X.S., **2006**. Novel porous materials for emerging applications. *Journal of Materials Chemistry* 16(7), 623-625.

Zhou, F., Yuan, L., Wang, H., Li, D., Chen, H., **2011**. Gold nanoparticle layer: A promising platform for ultra-sensitive cancer detection. *Langmuir* 27(6), 2155-2158.

Zhu, L., Wang, K., Lu, T., Xing, W., Li, J., Yang, X., **2008**. The direct electrochemistry behavior of Cyt c on the modified glassy carbon electrode by SBA-15 with a high-redox potential. *Journal of Molecular Catalysis B: Enzymatic* 55(1–2), 93-98.

Zou, B., Song, C., Xu, X., Xia, J., Huo, S., Cui, F., **2014**. Enhancing stabilities of lipase by enzyme aggregate coating immobilized onto ionic liquid modified mesoporous materials. *Applied Surface Science* 311, 62-67.

List of Patent applications and Publications

Patent applications counted in thesis

1. Bhand Sunil, **Pal Souvik**. A biosensor kit for detection and analysis of chemical pollutants, Indian Patent Application No. 3456/MUM/2013 Date of filing: 31 October 2013 (Output from chapter 3).

Manuscript published/accepted in peer-reviewed journal counted in thesis:

1. Kanungo, L.[*], **Pal, S**.[*], Bhand, S., **2011**. Miniaturised hybrid immunoassay for high sensitivity analysis of aflatoxin M1 in milk. *Biosensors and Bioelectronics* 26(5):2601-2606. ([*]Authors with equal contribution). (Output from chapter 2) (Impact Factor: 6.451; Citation: 22).

2. **Pal, S**., Sharma, M. K., Chatterjee, R., Bhand, S., **2015**. Multi-platform nano-immunosensor for aflatoxin M1 in milk. Accepted for publication in *Materials Research Express*. (Article I.D.: MRX/511510/PAP). (Output from chapter 2).

3. Behera, B.[*], **Pal, S**.[*], Kanungo, L., Bhand, S., Chandra, S., **2015**. Synthesis and characterization of ZnO-$ZnAl_2O_4$ whiskers and their application in biosensors. *ScienceJet* 4, 102. ([*]Authors with equal contribution). (Output from chapter 3).

4. **Pal, S**., Sharma, M. K., Danielsson, B., Willander, M., Chatterjee, R., Bhand, S., **2014.** A miniaturized nanobiosensor for choline analysis. *Biosensors and Bioelectronics* 54, 558-564. (Output from chapter 3) (IF: 6.451; Citation: 4).

5. **Pal, S**., Bhand, S., **2015**. Zinc oxide nanoparticle-enhanced ultrasensitive chemiluminescence immunoassay for CEA the carcinoma embryonic antigen. Accepted for publication in *Microchimica Acta*. (Article I.D.: MIAC-S-14-001010). (Output from chapter 5) (DOI 10.1007/s00604-015-1489-5) (Impact factor: 3.719).

Manuscript under preparation:

6. **Pal, S**., Singh, A., Bhand, S., Nano platform for multi-analyte detection of organophosphate residues. Manuscript under preparation. To be submitted. (Output from chapter 3).

7. **Pal, S**., Hazra, S., Ghosh, N. N., Millner, P., Bhand, S., **2015**. Functionalized mesoporous silica as fluorescence sensor for Pb^{2+} detection. Manuscript under preparation. (Output from chapter 4).

Patent applications not counted in thesis

8. Suri VK, Joshi DS, Balasubramaniam R, Rathore M, Mishra S, Bhand S, Ghildiyal S, **Pal S**, Pai G. Device for infectious disease. Indian Patent Application to be filed jointly with Department of Atomic Energy (DAE, India), BITS, Pilani and MGM Institute of Health Sciences.

Manuscript published in peer-reviewed journal not counted in thesis:

9. Bacher, G.*, **Pal, S**.*, Kanungo, L., Bhand, S., **2012**. A label-free silver wire based impedimetric immunosensor for detection of aflatoxin M1 in milk. *Sensors and Actuators B: Chemical* 168, 223–230. (*Authors with equal contribution).

10. Deshpande, K., Mishra, R. K., **Pal, S**., Danielsson, B., Willander, M., Bhand, S., **2010**. A novel on-chip analysis of dissolved Hg (II) in drinking water. *NSTI-Nanotech* 3, 133-136.

Conferences and workshop attended

1. National conference on Disperse Systems (NCDS), November 23-25, 2006. Silchar-788011.

2. National conference on Recent Advances in Magnetic Materials and Applications (MAGMA), January 20-21, 2010. Madurai-625015.

3. Fifth SERC School on "New Developments in Microfabrication with Focus on Synchrotron Radiation based Deep X-ray Lithography", October 29 – November 03, 2012. Raja Ramanna Centre for Advanced Technology, Indore, India.

4. International Conference on Emerging Technologies: Micro to Nano 2013 (ETMN-2013), February 23-24, 2013. BITS, Pilani-KK Birla Goa Campus, Goa-403726.

5. Interaction meeting on "X-ray lithography and micro fabrication research", December 5-6, 2013. Raja Ramanna Centre for Advanced Technology, Indore, India.

6. Indo - UK International Workshop on Advanced Materials and Their Applications in Nanotechnology (Aman 2014), May 17-19, 2014. BITS, Pilani-KK Birla Goa Campus, Goa-403726.

Abstract accepted in conferences

1. Abstract accepted for poster presentation: S. Pal and S. Bhand*, functionalized nanoparticle based assay for analysis of aflatoxin M1, Second International Conference on Multifunctional, Hybrid and Nanomaterials 6-10 March 2011, Strasbourg, France (Elsevier).

2. Abstract accepted for poster presentation: M. Kumar, S Pal, S Bhand* and R Chatterjee. Multifunctional zinc oxide nanorods as choline biosensor, Second International Conference on Multifunctional, Hybrid and Nanomaterials 6-10 March 2011, Strasbourg, France (Elsevier).

3. Abstract accepted for poster presentation: Lizy Kanungo, Souvik Pal and Sunil Bhand,* Miniaturized Immunoassays for High Sensitivity Analysis of Aflatoxin M1 in Milk, Poster No. : P1.1.098. 20th Anniversary World Congress on Biosensor, 26 – 28 May, 2010, Glasgow, UK (Elsevier).

4. Abstract accepted for poster presentation: Geetesh Mishra, Souvik Pal, Sunil Bhand. Gold Nanoparticle based Optical Biosensor for Monitoring Streptomycin in Milk Samples at 5th International Symposium on Recent Advances in Food Analysis (RAFA 2011) 1 – 4, November 2011, Prague, Czech Republic.

Brief Biography of the candidate

Name	Souvik Pal
Date of Birth	09-10-1982
Education	M.Sc. (Organic Chemistry), 2009
	Assam University, Silchar, Assam, India
	B.Sc. (Chemistry (H), Physics, Mathematics), 2006
	The University of Burdwan, Burdwan (W.B.) India
Email ID	p2010814@goa.bits-pilani.ac.in, souvipal@gmail.com,

Research experience (5 Years and 10 months)

1. Presently working as Senior Research Fellow in National Fund for Basic, Strategic and Frontier Application Research in Agriculture (NFBSFARA) Project sanctioned by ICAR at BITS, Pilani-K.K. Birla Goa Campus, Goa. PI: Prof. Sunil Bhand (November 2014 onwards).
2. Worked as Institute Research Scholar in the Department of Chemistry, BITS, Pilani-K. K. Birla Goa Campus, Goa. CPI: Prof. Sunil Bhand (July 2014 to October 2014).
3. Worked as Research Associate (National Agricultural Innovation Project, a consortium based project sponsored by ICAR, India and the World Bank at BITS, Pilani-K. K. Birla Goa Campus, Goa. CPI: Prof. Sunil Bhand (June 2011 to June 2014).
4. Worked as Senior Research Fellow (National Agricultural Innovation Project, a consortium based project sponsored by ICAR, India and the World Bank at BITS, Pilani-K. K. Birla Goa Campus, Goa. CPI: Prof. Sunil Bhand (May 2009 to May 2011).
5. Worked as Project Assistant at National Brain Research Centre, Haryana, India. Mentor: Dr. Pravat Mondal (November 2008 to January 2009).

Research Publications

01 Patent filed, 01 to be filed; 07 publications in international journal, 02 under preparation.

Brief Biography of the Supervisor

Name	Prof. Sunil Bhand
Date of Birth	17.03.1969
Present Position	Professor, Department of Chemistry, BITS, Pilani-KK Birla Goa Campus
Address	C-201 BITS, Pilani-KK Birla Goa Campus NH17B Bypass, Zuari Nagar Goa 403726 India
Email	sunilbhand@goa.bits-pilani.ac.in, sunil17_bhand@yahoo.com
Education	Ph.D., 1996 (Chemistry, Holkar Science College (DAVV) Indore,Thesis Title: Identification and analysis of cations and anions of industrial effluents) M.Sc., 1990 (School of Chemistry, D.A.V.V. Indore, First in University Merit)

Post-Doctoral Experience

Department of Pure and Applied Biochemistry
Lund University Sweden 2001-2002,
Short term visits 2003, 2004, 2005, 2007, 2008

No. of Sponsored Research Projects

(a) Completed projects

i. Joint Indo-Swedish Project on Biosensors for Environmental analysis 2003-2005 funded by Swedish Research Council (Prof. B. Danielsson and Prof. Sunil Bhand as joint PIs) 35 lakhs.

ii. CSIR Project 2006-2009 on biosensors for analysis of pesiticides in sea water 14.6 lakhs.

iii. Consortium PI for NAIP, ICAR New Delhi funded project on "Development of biosensors and micro techniques for analysis of pesticide residues, aflatoxin, heavy metals and bacterial contamination in milk. 30.01 Crores, in collaboration with IITD, NDRI and PU Patiala.

iv. Consortium Co-PI, NAIP project on "Detection and mitigation of dairy pathogens and detection of adulterants using chemical biology" 91 lakhs.

(b) Ongoing Project

i. Multi-institute Consortium Project entitled "Imprinted polymer for sensing and removal of selected antibiotic and pesticide residue" Project no. NFBSFARA/PHT-4007/2013-14. Funding Agency: National Funds for Basic and Strategic Research in Frontier Areas of Agricultural Science, ICAR, New Delhi, 125.25511 Lakh.

ii. Centre of Research Excellence in Water, Waste water and Energy Management (CORE WWEM) funded by BITS, Pilani. Subproject title: Development of Field Deployable biosensor for analysis of bacterial contaminant in potable water. Rs. 41 lakh

Honors and awards

i. Invited as Opponent to a Ph.D. Thesis for Linkoeping University Sept. 2011.

ii. Best Poster award "Biosensors for arsenic analysis" 7th Intl Conference on Biogeochemistry of trace elements 2003 Uppsala Sweden.

iii. UV Rao memorial awards for young scientists by Indian Chemical Society 1998.

Publications

i. 06 Patents (03 International including 02 PCT and 01 Australian and 03 Indian) and 38 publications in international journals.

ii. Membership of societies: Affiliate member IUPAC since 2000 IAEAC Switzerland, AAAS, USA, 2012.

Reviewer for international journals

Biosensors and Bioelectronics, Analytical Letters, Int Journal of Env Anal Chemistry, Applied Biochemistry and Biotechnology, J Agri food Chemistry.

No of Ph.D. Students

Awarded: 03, Registered 06 (03 Submitted),

No of Conferences organized: 04

Request for permission from authors

Whitesides, George <gwhitesides@gmwgroup.harvard.edu>
12/6/14
to Souvik Pal

Sure. You must, of course, for ethical reasons, explicitly acknowledge the paper.
George Whitesides

From: Souvik Pal [mailto:souvipal@gmail.com]
Sent: Friday, December 05, 2014 4:54 PM
To: Whitesides, George; clove@mit.edu
Subject: Request for permission

Dear Prof. George M. Whitesides & Dr. J. Christopher Love:
Greetings from India!!!
Myself, Souvik Pal, a Ph.D. scholar from BITS,Pilani-KK Birla Goa Campus. I am about to submit my doctoral thesis entitled "Nanoparticle based biosensor techniques for environmental and clinical analysis" under supervision of Prof. Sunil Bhand. Your article "Self-assembled monolayers of thiolates on metals as a form of nanotechnology" helped me a lot to understand about the inner details of self-assembly for nanotechnology.
In this regard, I want to reproduce partly the Table 1 (Combinations of Headgroups and Substrates Used in Forming SAMs on Metals, Oxides, and Semiconductors) from your article.
I would be highly obliged and thankful if you help me by giving your kind permission to reproduce the TABLE partially in my doctoral thesis. I have also attached an image file of the table that I wish to adopt from your article.
Thank you very much for your time.

Thanking you,
Sincerely,
Souvik Pal

Ratnamala Chatterjee <rmala@physics.iitd.ac.in>

12/8/14

to me, SUNIL

Dear Souvik,

With proper reference you are permitted to reproduce- just do not forget to refer to Manoj's reference.

Best,

Ratnamala Chatterjee

From: Souvik Pal [mailto:souvipal@gmail.com]

Sent: Sat, Dec 6, 2014 at 2:46 AM

To: Ratnamala Chatterjee rmala@physics.iitd.ac.in

Cc: SUNIL BHAND sgbhand@gmail.com

Respected Madam:

Hope you are fine.

I am about to submit my doctoral thesis. I need reproduce the attached files for supporting the data in my thesis. The description of figures are

listed below:

01. FESEM of ZnO nano-rod

02. XRD and Raman of ZnO nano-rod

03. HRTEM of HfO2 nanoparticles

In this context, I am seeking your kind permission to reproduce these data in my thesis.

Sincerely,

Souvik Pal

Appendix v

Reprints of Publications

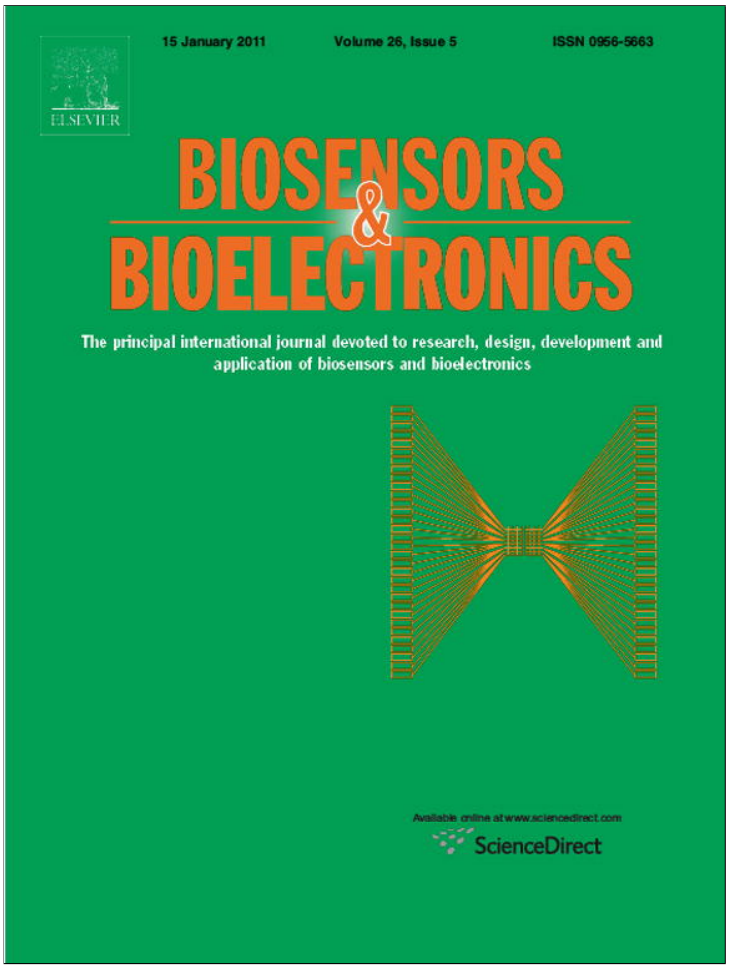

Biosensors and Bioelectronics 26 (2011) 2601–2606

Contents lists available at ScienceDirect

Biosensors and Bioelectronics

journal homepage: www.elsevier.com/locate/bios

Miniaturised hybrid immunoassay for high sensitivity analysis of aflatoxin M1 in milk☆

Lizy Kanungo[1], Souvik Pal[1], Sunil Bhand*

Biosensor Lab., Department of Chemistry, BITS, Pilani-KK Birla Goa Campus, Goa 403 726, India

ARTICLE INFO

Article history:
Received 4 September 2010
Received in revised form 26 October 2010
Accepted 9 November 2010
Available online 18 November 2010

Keywords:
ELISA
Chemiluminescence
Aflatoxin M1
Magnetic nanoparticles
Affinity capture
Milk

ABSTRACT

An ultra-sensitive sandwich ELISA was developed for detection of AFM1 in milk. The assay involved the immobilization of rat monoclonal antibody of AFM1 in 384 microtiter plate to capture AFM1 antigen. This was detected by tracer secondary rabbit poly-clonal antibody labelled with horseradish peroxidase upon addition of a luminol-based substrate. Milk samples with different fat percentage were analyzed after pre-treatment. Linear range of AFM1 detection 250–6.25 pg/mL was achieved in 3% fat milk. The miniaturised assay (10 μL) enabled ultra trace analysis of AFM1 in milk with much improved lower limit of detection at 0.005 pg/mL. A sensitive magnetic nanoparticles (MNPs) based ELISA was also developed and coupled with micro plate ELISA for analysis in milk. The hybrid-assay, by coupling the 1°Ab immobilized MNPs column with microwell plate assay enabled simultaneous measurement of low (0.5 pg/mL) and high AFM1 contamination (200 pg/mL). The most promising feature of this MNPs-ELISA is the small column size, high capture efficiency and lower cost over other reported materials. The proposed assay can be deployed for simultaneous analysis and monitoring of AFM1 in milk.

1. Introduction

Aflatoxins are highly toxic mycotoxins produced by *Aspergillus* species in a wide range of food and animal feedstuffs stored under temperature and humidity conditions favorable to mold growth. When aflatoxin B1 contaminated feed is ingested by cattle, it is transformed into its hydroxylated product, AFM1, which is then secreted in the milk. AFM1 is known for its hepatotoxic and carcinogenic effects. The toxic and carcinogenic effects of AFM1 recently lead WHO-IARC to change its classification from group 2 to group 1 (IARC, vol. 82, 2002). AFM1 is relatively stable during milk pasteurization, storage as well as during the preparation of various dairy products (Codex Committee, 2001; Badea et al., 2004). To date, aflatoxins are regulated in many countries worldwide. Due to the fact that milk intake in infants is high and when young they are vulnerable to toxins, the European Community legislation imposes maximum permissible levels AFM1 of 50 ng/L in milk and 25 ng/L for infant formulae (Henry et al., 2001). To minimize the occurrence of AFM1, it is essential to trace the sources of contamination using rapid, selective, sensitive and cost effective assays. Several methods for AFM1 determination have been developed. High-performance liquid chromatography (HPLC) (AOAC Official Method, 2000.08), thin layer chromatography (TLC) (Kamkar, 2006) and enzyme-linked immunosorbent assays (ELISA) (Rastogi et al., 2004) are mainly used in routine analysis. For an effective screening and monitoring of AFM1 in foodstuffs such as milk at ultra low level, analytical methods combining simplicity with high detectability and analytical throughput are required. This can be achieved by means of immunological methods in conjunction with a highly sensitive detection of the label (Magliulo et al., 2005). HPLC, TLC techniques require extensive sample preparation steps and well-trained personnel. Moreover, the reagents and instrumentation used are expensive (Thirumala-Devi et al., 2002). Immunochemical techniques are becoming very popular for mycotoxins analysis with many literatures reporting the use of a commercially developed ELISA (Thirumala-Devi et al., 2002; Lopez et al., 2003; Rodriguez et al., 2003; Rastogi et al., 2004). ELISA is not only suitable tool for quick and sensitive analysis with high sample throughput, but also cost-effective and requires only a small sample volume for analysis (Pei et al., 2009; Parker and Tothill, 2009). Among the established ELISA techniques, sandwich-type immunoassay is an effective bioassay due to the high specificity and sensitivity (Knopp, 2006).

Enzyme labels have experienced widespread popularity since their first use in 1971 in an ELISA (Van Weeman and Schuurs, 1971). Enzyme labels are not consumed, and their reactions can

☆ The paper was presented at the World Congress on Biosensors 2010.

* Corresponding author. Tel.: +91 832 2580332; fax: +91 832 2557030/33.
E-mail addresses: lizy_kanungo@yahoo.co.in (L. Kanungo), souvipal@gmail.com (S. Pal), sunil17_bhand@yahoo.com, sunilbhand@bits-goa.ac.in, sgbhand@gmail.com (S. Bhand).
[1] Authors with equal contribution.

0956-5663/$ – see front matter © 2010 Elsevier B.V. All rights reserved.
doi:10.1016/j.bios.2010.11.014

be initiated and stopped. Furthermore, enzymes amplify the signal because an enzyme can produce many detectable molecules, up to 10^7 molecules of substrate per minute per enzyme molecule, by its catalysis of a substrate product reaction. They can be used in both homogeneous and heterogeneous immunoassays. Enzymes are the most commonly used labels as they can produce colored, fluorescent, luminescent, and electroactive compounds enabling detection by a variety of techniques (Gracia et al., 2005). Enzyme labels detected by chemiluminescent (CL) substrates, such as the luminol (5-aminophthalyhydrazide)/peroxide/enhancer system for horseradish peroxidase (HRP) or dioxetane-based substrates for alkaline phosphatase represent the most sensitive detection system in immunoassay development. CL compounds produce light in response to chemical reactions and as labels in immunoassay, they can be more sensitive than radio labelled and fluorescent forms (Krick and Wild, 2001). In addition, the CL signal detection can be performed immediately after substrate addition, thus shortening the overall analytical procedure when compared with conventional colorimetric assays (Magliulo et al., 2005). Gracia et al. (2005) have reported that luminol could be used as an enzyme substrate for HRP that yield high sensitivity.

Owing to their high surface area, nano-materials can facilitate miniaturization and thereby provide enhanced number of binding sites. MNPs have special relevance in bio-analytical chemistry because of their larger surface to volume ratio, enhanced antibody–antigen kinetics, lower mass transfer resistance and easy separation of immobilized bio-molecules from reaction mixture using magnetic field (Yu, 1998). Recently, widespread use of MNPs in biosensors has been witnessed through a flurry of literature (Cheng et al., 2005; Nikitin et al., 2007; Ravindranath et al., 2009). Various antibody coupling strategies using nanoparticles have also been reported (Wang et al., 2006; Radoi et al., 2008; Wang and Gan, 2009; Ahirwal and Mitra, 2010). The covalent binding of antibody through self assembled monolayer is more suitable than the other conventional methods like physical adsorption and polymer entrapment (Liu et al., 2006; Shankaran and Miura, 2007). The advantages of using covalent binding over physical adsorption to anchor antibodies and other proteins to a substrate surface are well documented in the literature (Ivanova et al., 2006). Despite MNPs prevalent applicability in biosensor field, reports on MNPs being deployed for analysis of AFM1 have been scarce. In one such testimony, reported by Radoi et al. (2008), AFM1 detection was done using MNPs coated with protein G by physical adsorption.

In the present work, we report a novel approach where a highly sensitive microplate sandwich ELISA was developed and integrated with MNPs which could detect ultra trace amount of AFM1 in milk. The functionalized MNPs were used as an affinity capture column wherein antibodies immobilized on their surface could capture AFM1 from milk sample. To circumvent interference attributed to whey proteins and fat, the effect of pretreatment of milk sample with trichloro acetic acid (TCA) followed by centrifugation and filtration was investigated to assess the performance of integrated ELISA. The miniaturised assay was used for high throughput analysis of AFM1 which showed an astoundingly low detection limit 0.005 pg/mL as against other reported ELISA (Thirumala-Devi et al., 2002; Rastogi et al., 2004; Magliulo et al., 2005). Moreover the assay was validated by performing recovery studies in certified reference material for AFM1 (ERM-BD 282).

The proposed assay further demonstrated the use of functionalized MNPs as affinity capture material through a miniaturised column for AFM1. This gave better efficiency of capture and cost effectiveness when compared to materials like protein A and protein G (Fuentes et al., 2005; Radoi et al., 2008) in affinity column.

2. Materials and methods

2.1. Materials and instrumentation

AFM1, bovine serum albumin (BSA), Tween 20, luminol, protein A agarose fast flow, 50% (v/v), protein G sepharose 4B fast flow (recombinant protein G, in 20% ethanol) and iron oxide (Fe_3O_4, average particle size 15 nm), certified reference material ERM-BD282 (AFM1 in whole milk powder, <0.02 μg/kg) were purchased from Sigma–Aldrich (USA). Hydrogen peroxide (H_2O_2) 30% (w/v), acetonitrile (ACN) HPLC grade, trichloro acetic acid (TCA), sodium chloride (NaCl), methanol (99% pure) were purchased from Merck (Germany). Anti AFM1 fractionated antiserum primary antibody (1°Ab) raised from rat and HRP conjugated secondary antibody (2°Ab) raised from rabbit were purchased from Abcam (UK). 3-Aminopropyl-triethoxysilane (APTES) 99% pure and glycerol (99% pure) were purchased from Acros Organics (USA). Glutaraldehyde (GA) solution (25%) was purchased from Merck (India). Sodium hypochlorite (4%) solution was purchased from Fisher Scientific (India). Sonication of the sample was done in Toshcon ultrasonic cleaner (Toshniwal process instruments Pvt. Ltd., India). Centrifugation, shaking and filtration of the samples were done by Spinwin mini centrifuge, Spinix shaker and syringe filter, purchased from Tarsons (India). 0.22 μ filter papers (25 mm diameter) were obtained from Millipore (USA). White 384 well polystyrene microtiter plates were purchased from Nunc (Denmark). HybridSPE™ (30 mg/1 mL) SPE tubes were purchased from Supelco (USA). Flow analysis was done by a multi-channel pump, Gilson, Minipuls Evolution (France). For CL measurement, VictorX^4 2030 optiplate reader from Perkin Elmer (USA) was used. Glove box, Cole Parmer (USA) was used for the handling of AFM1 standard solution. Water produced in a Milli-Q system (Millipore, Beford, MA, USA) was used for preparing all the solutions. Certified ultra high pure nitrogen (99.9%), pH meter (Seven Multi Mettler Toledo, 8603, Switzerland) were used. Commercial milk samples of different fat content were purchased from the local supermarket of Goa, India.

2.2. Preparation of buffers

Buffers were made by the following method. For coating purpose, a 0.05 M carbonate buffer (CB) was prepared. The pH was adjusted to 9.6. As CB changes composition over time, it was made fresh each time. 0.01 M phosphate buffered saline (PBS) was used for incubation and washing purpose. The pH was adjusted to 7.4. Another washing buffer (PBST) was made by adding 0.05% Tween 20 (v/v) in PBS. All buffer solutions were stored at 4 °C when not in use. The blocking solution was prepared by adding 2.5% (w/v) BSA to PBS.

2.3. Preparation of AFM1 standard solutions

All the AFM1 solutions were prepared inside a Glove box in a maintained inert N_2 atmosphere. AFM1 stock solution was prepared by dissolving the AFM1 powder in 5% ACN (v/v) in PBS at a concentration of 5 μg/2 mL and stored at −20 °C. In order to develop the assay, meeting regulatory requirements of European Commission (50 ng/L), working standard solutions in the range of 250–0.005 pg/mL were prepared by diluting the stock with 5% ACN [safety note: aflatoxins are highly carcinogenic and should be handled with extreme care. Aflatoxin contaminated labware should be decontaminated with an aqueous solution of sodium hypochlorite (4%)].

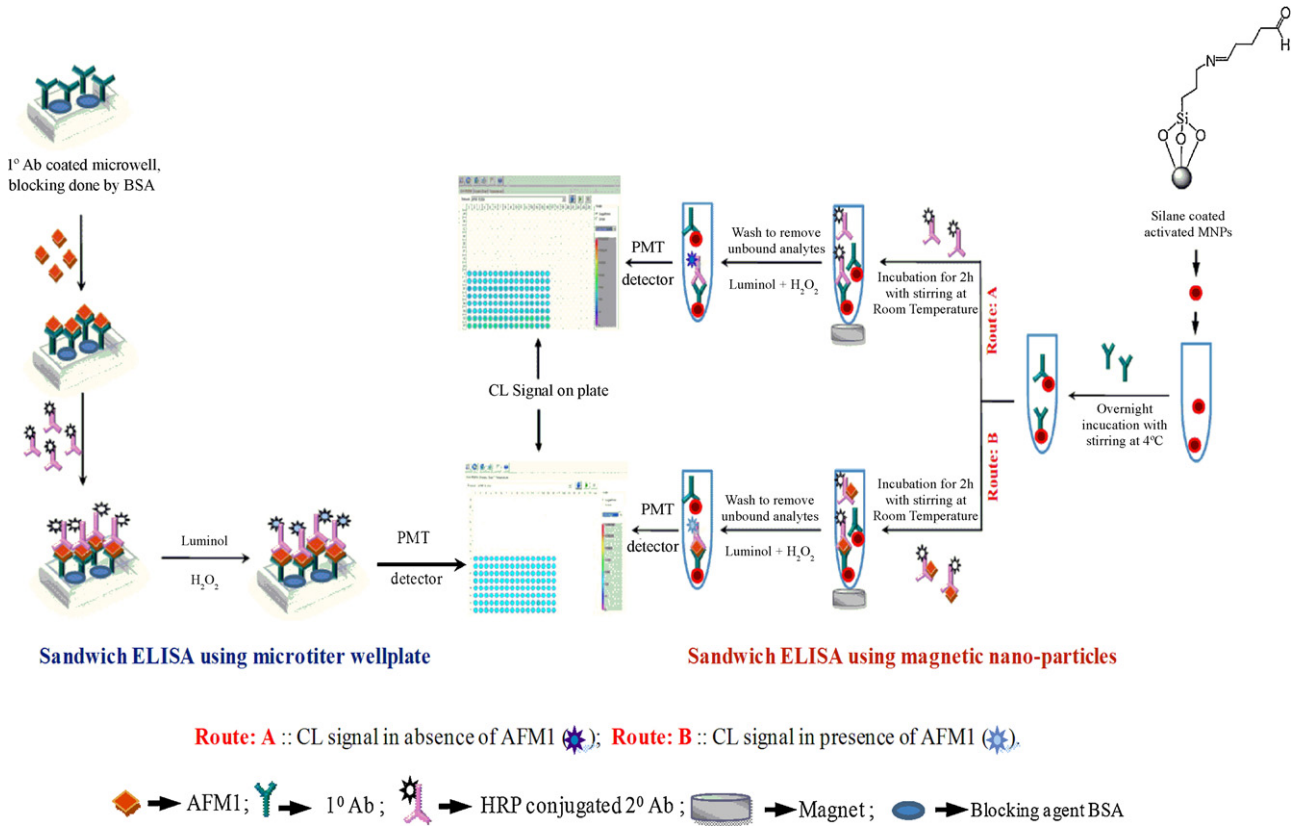

Fig. 1. Schematic diagram of microwell plate based sandwich ELISA and MNPs based sandwich ELISA for analysis of AFM1 in milk.

2.4. Preparation of AFM1 antibody solutions

The stock solution of rat monoclonal [1C6] 1°Ab, 100 μg (1 mg/mL) was diluted with 50 μL of de-ionized water. It was divided into 2 fractions. The first fraction containing 40 μL was stored at −20 °C. From the second fraction, working 1°Ab solution was prepared prior to the experiment by serial dilution in CB as 1:1000, 1:2000 etc. The stock solution of 1 mg (2 mg/mL) rabbit polyclonal to rat IgG-H & L (HRP) 2°Ab was diluted with 500 μL of de-ionized water. It was divided into 2 fractions. The first fraction containing 400 μL was stored in −20 °C. From the second fraction, working 2°Ab solution was prepared prior to the experiment by serial dilution in PBS.

2.5. Preparation of milk based buffer matrix

Commercial packaged milk samples containing 0.5%, 1.8% and 3% fat were divided into 4 fractions each. The first fraction was prepared by diluting 1 μL raw milk in 999 μL PBS making the final concentration to 1:1000. In the second fraction, 20% of 20 mM TCA was added to 1 mL of milk and kept for 20 min at 4 °C. This fraction was diluted in PBS as 1:1000. Similar to second fraction, third fraction was treated with TCA followed by centrifugation at 10,000 rpm for about 15 min. After centrifugation, the upper fat layer was completely removed, and the aqueous layer was directly used for the analysis. The decanted fraction was diluted in PBS as 1:1000. The fourth fraction was centrifuged at the 10,000 rpm for 15 min and filtered through a syringe filter using 0.22 μm filter paper and diluted to 1:1000 in PBS.

2.6. Immunoassay procedure

Sandwich ELISA was performed in 384 microwell plate as described in Fig. 1. Optimized 1°Ab was diluted to 1:16000 in CB and coated as 40 μL/well in triplicate. The plate was covered with parafilm and aluminium foil and kept at 4 °C for overnight; washed 3 times by rinsing the wells with 60 μL PBS. The remaining protein binding sites in the coated wells were blocked by adding 40 μL of blocking solution for about 1 h at room temperature. The plate was washed once with 40 μL PBST. Following this step, AFM1 standard solution in the range 250–0.005 pg/mL was added as 20 μL/well. The plate was incubated for about 2 h at room temperature. Then 1:1 mixture of optimized 2°Ab (diluted to 1:32,000 in PBS) and milk based buffer of each milk fraction was prepared. The final solution was added as 40 μL/well. The plate was kept for 2 h at room temperature. The excess label was removed by washing with PBS. The CL substrate 10 μL/well (1.2 μL of 0.5 M H_2O_2 + 8.8 μL luminol) was added. The signal intensity was kinetically measured at steady state and stability was found after 50 min.

2.7. Nanoparticles based immunoassay

2.7.1. Preparation of silane coated MNPs

All the glassware used for the preparation were soaked in freshly prepared HNO_3/HCl solution, rinsed thoroughly with distilled water and dried. APTES was used for the coating of MNPs as described by Liang et al. (2006). Briefly, 500 mg of MNPs, 0.135 μL water and 0.675 μL APTES were added into 50 mL methanol. After ultrasound treatment for 3 min, the mixture was added with 20 mL glycerol and then transferred to a 100 mL three-necked flask equipped with a mechanical stirrer. The temperature was maintained at 50 °C with rapid stirring for 12 h under N_2 environment. The resulting nanoparticles were washed with de-ionized water and methanol for several times using a magnet. This stock was used for further experiments.

2.7.2. MNPs-antibody conjugation and immunoassay

The NH_2 group of silane coated MNPs were activated by GA. The antibodies were immobilized via their carboxyl group onto activated MNPs as described by Liu et al. (2006). With some alteration, 0.7 mg of silane coated MNPs (from stock) were first activated by adding 500 μL of 2.5% GA in 0.01 M PBS and the resultant mixture was shaken at room temperature for 2 h. Unbound GA was washed from activated particles with PBS using a magnet.

1°Ab was freshly prepared by diluting in CB as 1:32,000 and 40 μL of this solution was added to activated-MNPs for coating. The resulting mixture was kept for overnight at 4 °C with occasional shaking to avoid aggregation and washed 3 times with 1000 μL PBS using magnet. A 1:1:1 mixture of optimized 2°Ab diluted to 1:32,000 in PBS, AFM1 standard solution and milk from first fraction was prepared. 40 μL of the final mixture was added to the coated MNPs and kept for 2 h at room temperature. Excess label was removed by washing with PBS using magnet. Subsequently, 2.4 μL of 0.5 M H_2O_2 was added and kept in dark for 5 min. Then the solution was transferred to micro well. Finally, 17.6 μL of luminol was added and the resulting signal was measured in VictorX4. The schematic of the MNPs-ELISA is presented in Fig. 1.

2.8. Preparation of affinity columns using protein A, G and MNPs

Five HybridSPE™ (30 mg/1 mL) SPE columns were prepared for capture and detection of AFM1. Among these columns, three were specifically customized for MNPs, protein A and protein G. The other two were used as control (blank) and PBS. The columns were tested for analysis of 50 pg/mL [AFM1].

The MNPs packed column was prepared by adding 3 mg MNPs functionalized with 1°Ab, whereas pre-swollen proteins A and G were washed with distilled water and packed in the SPE columns, as described in data file 18-1012-19 AC, GE Healthcare (Sweden). 20 μL of protein A was added to 40 μL of 1°Ab (1:16000) and allowed to bind overnight at 4 °C. Similarly protein G packed column was prepared.

The columns were washed 3 times with 60 μL PBS by applying 10 psi at 9.6 rpm using micro fluidic pump. The remaining protein-binding sites in the columns were blocked by adding 40 μL of blocking solution for about 1 h at room temperature. The columns were then washed in running buffer with 60 μL PBST. Subsequently, 40 μL of 2°Ab (1:32000) and AFM1 (1:1) was added to the columns, kept for 2 h at room temperature. The excess label was removed by washing with PBS in running buffer. 40 μL of the CL substrate was added to the columns. The final eluting solution was collected, added to the microwell plates and it was measured as described earlier.

3. Safety caution

All necessary precautionary measures must be taken while handling the highly toxic AFM1 to prevent contamination. As the substance is photosensitive (Rodriguez et al., 2003; AOAC Official Method, 2000), special care must be taken to ensure that solutions are not exposed to daylight. Safety goggles, respiratory mask and lab coats must be used throughout experiment. All laboratory glassware and consumables which had been contaminated with AFM1 were soaked in 4% sodium hypochlorite.

4. Results and discussions

4.1. AFM1 concentration and optimization of Abs

Generally, the principle of the sandwich ELISA is to incorporate a monoclonal antibody which is specific to analyte (AFM1) only.

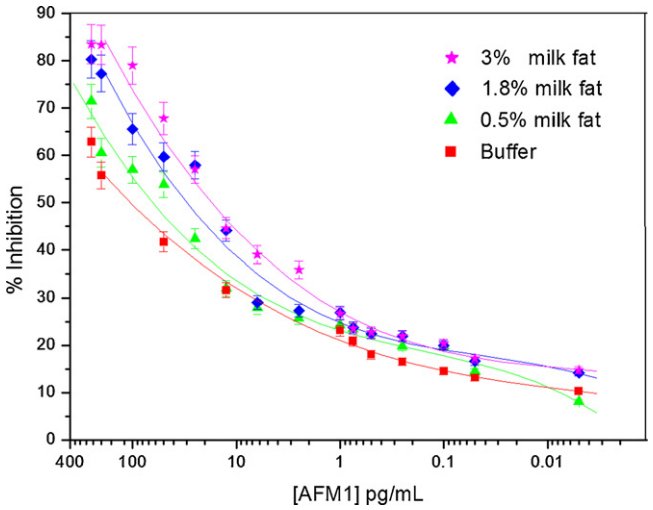

Fig. 2. Inhibition curves obtained for AFM1 spiked PBS buffer and AFM1 spiked pre-treated milk samples containing different fat %; 1°Ab diluted to 1:16000 in CB; 2°Ab diluted to 1:32000 in 0.01 M PBS, pH 7.4. S.D. = 1.1; r^2 = 0.99; IC_{50} = 122 pg/mL for AFM1 spiked PBS buffer. S.D. = 1.69; r^2 = 0.982; IC_{50} = 39.98 pg/mL for AFM1 spiked pre-treated milk samples containing 0.5% fat. S.D. = 1.95; r^2 = 0.965; IC_{50} = 17.7 pg/mL for AFM1 spiked pre-treated milk samples containing 1.8% fat. S.D. = 1.29; r^2 = 0.986; IC_{50} = 16.95 pg/mL for AFM1 spiked pre-treated milk samples containing 3.0% fat.

Either standards of known value or sample is added to immobilize antibodies. An additional 2°Ab with an attached enzyme or an enzyme conjugated analyte then binds to any surplus antibody sites and the excess 2°Ab with enzyme is then washed away. In our assay, the monoclonal antibody specifically captured AFM1 from the sample mixture and this was detected by a polyclonal HRP conjugated antibody upon addition of CL substrate. The method was optimized by determining the best values for parameters such as concentration of 1°Ab, immobilization procedure of antibody, tracer concentration and incubation time corresponding to immunoaffinity interaction. The dilution of 1°Ab and HRP conjugated 2°Ab should be a compromise between the high dilutions required achieving a low detection limit for AFM1 and that needed to produce a sufficiently high signal. We have tested various 1°Ab concentrations with 2°Ab concentration and found that, 1°Ab at a dilution 1:16,000 gave optimum signal intensity with 1:32,000 dilution of 2°Ab. The European Commission permissible limit for AFM1 in milk is 50 ng/L. We prepared AFM1 standard solutions in the range 250–0.005 pg/mL. For 0.7 mg of optimized MNPs, eight working solutions of AFM1 were prepared in the range 200–0.5 pg/mL.

4.2. Study of matrix effect in different fat percentage of milk

In milk, fat and proteins may act as interferents for analysis of AFM1. To study further, we pretreated milk sample by adding TCA and centrifuged, followed by filtration. The assay was performed in buffer as well as spiked milk samples with different fat percentage. Percentage inhibition (I %) was calculated as described by Arduini et al. (2009) in presence and absence of analyte

$$I\% = 100\left(\frac{I_0 - I_A}{I_0}\right)$$

I_0 = signal intensity of blank and I_A = signal intensity of spiked sample.

The mid-point value (IC_{50}) was evaluated as the [AFM1] at 50% inhibition. From Fig. 2, this was obtained as 122 pg/mL for AFM1 in PBS. The standard deviation (S.D.) was calculated as 1.1 and regression coefficient (r^2) was 0.99. The lower limit of detection (LOD) was calculated to be 0.005 pg/mL.

Calibrations were obtained using ELISA for AFM1 in milk samples having different fat percentage. To avoid interference attributed to whey proteins and fat, which is a major problem in measuring the signal intensity (Parker and Tothill, 2009); the effect of acid digestion using mild acid such as TCA was investigated. The performance of ELISA in milk samples was evaluated by different pre-treatment procedures as described in Section 2.5. Among the three tested pre-treatment procedures, milk treated with TCA, centrifuged and filtered (fourth fraction) in all cases showed best signal intensity. Milk samples having different fat content spiked with AFM1 were compared with assay in buffer and it was found that the milk sample containing 0.5% fat showed signal intensity close to that of buffer. From Fig. 2, it was observed that 3% fat milk showed highest inhibition than 1.8% than 0.5% fat milk. We found IC_{50} value for 3%, 1.8% and 0.5% fat milk as 16.95 pg/mL, 17.7 pg/mL and 39.88 pg/mL respectively. We observed two linear ranges in each calibration for instance, in 0.5% fat milk one linear range was from 250 to 6.25 pg/mL with higher sensitivity and another was from 6.25 to 0.005 pg/mL with a lower sensitivity. From calibration curves (Fig. 2), S.D. for 3%, 1.8% and 0.5% fat milk were obtained as 1.29, 1.95 and 1.69 and their r^2 values were 0.986, 0.965 and 0.982 respectively. Sensitivity of about 6–10% inhibition per decade change of AFM1 for 3% fat milk was observed. The LOD was found to be 0.005 pg/mL for 0.5% fat and 3% fat samples whereas a decrease in LOD for 1.8% fat sample was obtained as 0.05 pg/mL. In all the cases, signal suppression was found to be <10%.

4.3. MNPs-ELISA for AFM1 in milk

Calibration was obtained for milk samples having 0.5% milk fat for the MNPs based ELISA. The inhibition curve for AFM1 spiked milk samples in MNPs was obtained for eight different concentrations of AFM1 i.e. 0.5 pg/mL, 1 pg/mL, 6.25 pg/mL, 12.5 pg/mL, 25 pg/mL, 50 pg/mL, 100 pg/mL and 200 pg/mL by CL detection and presented as Fig. 3. The data points were fitted and unknown [AFM1] could be detected from mean standard deviation curve in MNPs based ELISA. We achieved a good assay sensitivity, about 6% with S.D. = 1.23; r^2 = 0.99. The LOD was found to be 0.5 pg/mL. The IC_{50} value for MNPs based ELISA was found at 95.73 pg/mL. Thus the MNPs-ELISA presented here is one of the sensitive methods for AFM1 analysis, comparable with other established methods (Table 1). The signal inhibited due to presence of AFM1 in milk was calculated and a significantly low detection limit 0.5 pg/mL could be achieved in case of MNPs based ELISA with analysis time of 45 min. This is the lowest ever LOD achieved by incorporating MNPs in ELISA for detection of AFM1.

4.4. MNPs as affinity capture column

Various approaches have been reported on affinity capture columns for pre-separation or enrichment of the analytes. Herein we have studied 1°Ab immobilized MNPs as affinity capture column and compared it with other reported columns such as protein

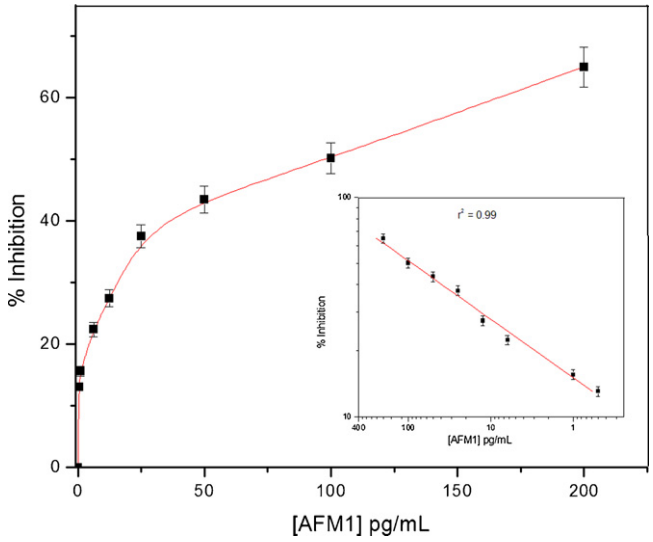

Fig. 3. Inhibition curve obtained for MNPs based sandwich ELISA. 1°Ab diluted to 1:32000 in CB; 2°Ab diluted to 1:32000 in PBS; S.D. = 1.23; r^2 = 0.99; IC_{50} = 95.73 pg/mL; inset: linear fit of inhibition curve.

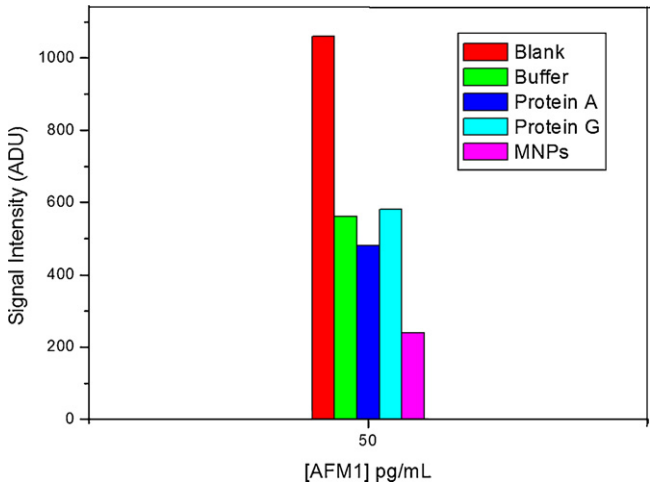

Fig. 4. Comparison of protein A, G and MNPs as affinity entrapment materials for [AFM1] = 50 pg/mL. 1°Ab = 1:16000; 2°Ab = 1:32000.

A & protein G for AFM1 (Badea et al., 2004; Radoi et al., 2008). For evaluation of the capacity of these three materials, affinity columns were prepared as described in section 2.8. A stock solution of 50 pg/mL AFM1 was eluted and the efficiency of the columns to capture AFM1 was determined. A significant binding was observed in functionalized MNPs as against protein A and G column. The signal intensity of ELISA by using these materials was plotted and presented as Fig. 4. Quantitative efficiencies for the three affinity capture columns were calculated by performing the inhibition

Table 1
Comparison of limit of detection in various established (reported) ELISA methods.

Assay type	Range	LOD achieved	Reference
Sandwich ELISA (wellplate)	0.005–250 pg/mL	0.005 pg/mL	Our work
(MNPs based assay)	0.5–200 pg/mL	0.5 pg/mL	Our work
Direct competitive ELISA (MNP)	4–250 ng/L	8 ng/L	Radoi et al. (2008)
Indirect competitive ELISA	10–100 ng/L	5 ng/kg	Anfossi et al. (2008)
Indirect competitive ELISA	10–0.01 ng/mL	0.24 ng/mL	Thirumala-Devi et al. (2002)
Flow-injection immunoassay	20–500 pg/mL	11 pg/mL	Badea et al. (2004)
Competitive ELISA	28–164 ng/kg	28 ng/kg	Rastogi et al. (2004)
Indirect competitive ELISA	0.1–3.2 ng/mL	0.04 ng/mL	Pei et al. (2009)
Competitive ELISA	0–1000 ng/L	39 ng/L	Parker and Tothill (2009)

Table 2
Recovery of AFM1 from certified reference material milk sample as determined by ELISA: BD282, zero level of AFM1 certified reference material was employed to asses the recovery efficiency using developed assay.

AFM1 added (pg/mL)	AFM1 found (pg/mL)	R.S.D (%)	R.E. (%)	Recovery (%)
1.00	0.96	1.56	−4.00	96.00
2.50	2.41	0.77	−3.40	96.40
6.25	6.02	1.12	−3.68	96.32
12.50	12.14	7.92	−2.88	97.10
25.00	24.72	5.77	−1.12	98.88
50.00	47.47	4.42	−5.06	94.94
100.00	89.46	2.04	−1.54	98.46

measurements. Inhibition as high as 73.5% was measured using MNPs packed columns as against protein A (54.71%) and protein G (45.28%) (Supplementary Table S1). These columns were deployed in an integrated fashion wherein after trapping the AFM1, the trace AFM1 were measured by deploying the ELISA in microplate. Thus, the MNPs affinity column was found to be most efficient in trapping of AFM1 from milk samples.

4.5. Recovery of AFM1 from spiked and CRM milk samples

The developed microplate ELISA was further validated with certified reference material (ERM-BD282, zero level of AFM1) for milk powder. The milk powder was reconstituted as indicated in the certification report supplied by the IRMM, Belgium. To test the accuracy of developed assay, AFM1 concentrations ranging from 1 to 100 pg/mL were added to the milk samples and assayed by ELISA. CRM milk samples known not to contain AFM1 were compared with samples deliberately contaminated with known amounts of AFM1.

Recovery was assessed by spiking AFM1 with the BD282 reconstituted material and presented as Table 2. The fortified (1, 2.5, 6.25, 12.5, 25, 50, 100 pg/mL of AFM1) milk samples (0.5% fat) were interpolated from the calibration curve performed using reconstituted CRM.

The precision and reliability of the developed assay is notable from the data presented in Table 2. The resultant data showed an excellent percentage of recovery, close to 100% for CRM. The precision was determined by calculating the relative standard deviation (R.S.D.%) for the replicate measurements and the accuracy (R.E.%) was calculated by assessing the agreement between measured and nominal concentration of the fortified samples.

$$\text{R.E. (relative error) } \% = \left[\frac{(\text{measured value} - \text{true value})}{\text{true value}}\right] \times 100$$

$$\text{R.S.D (relative standard deviation) } \% = \left[\frac{\text{standard deviation}}{\text{mean}}\right] \times 100; \quad n = 3$$

5. Conclusion

In the present work, a fast, reliable and ultra sensitive sandwich ELISA was developed for detection of AFM1 in milk. The miniaturised assay (assay volume 10 μL) enabled ultra trace analysis of AFM1 in milk with much improved lower limit of detection at 0.005 pg/mL. The total assay time to detect AFM1 by sandwich ELISA was approximately 4–5 h. Moreover, a sensitive MNPs-ELISA was also developed and coupled with micro plate ELISA for analysis in milk. The hybrid system by coupling the 1°Ab immobilized MNPs column with microwell plate assay enabled simultaneous measurement of low (0.5 pg/mL) and high AFM1 contamination (200 pg/mL). The most promising feature of this MNPs-ELISA is the small size, high capture efficiency and lower cost over other reported materials. It can be further extended for separation of AFM1 from the contaminated milk.

Acknowledgements

This work is funded by National Agriculture Innovation Project, (NAIP) No. C4/C10125, 2008-12, Indian Council of Agriculture & Research and The World Bank. LK and SP acknowledge to NAIP for the award of Senior Research Fellowship.

Appendix A. Supplementary data

Supplementary data associated with this article can be found, in the online version, at doi:10.1016/j.bios.2010.11.014.

References

Ahirwal, G.K., Mitra, C.K., 2010. Biosens. Bioelectron. 25 (9), 2016–2020.
Anfossi, L., Calderara, M., Baggiani, C., Giovannoli, C., Arletti, E., Giraudi, G., 2008. J. Agric. Food Chem. 56 (6), 1852–1857.
AOAC Official Method, 2000.08, Aflatoxin M1 in Liquid Milk.
Arduini, F., Amine, A., Moscone, D., Palleschi, G., 2009. Anal. Lett. 42, 1258–1293.
Badea, M., Micheli, L., Messia, M.C., Candigliota, T., Marconi, E., Mottram, T., Velasco-Garcia, M., Moscone, D., Palleschi, G., 2004. Anal. Chim. Acta 520, 141–148.
Cheng, Q., Peng, T.Z., Liu, A.L., 2005. Chin. Chem. Lett. 16 (8), 1059–1062.
Codex Committee on Food Additives and Contaminants, 2001. CL CX/FAC 01/20, Comments Submitted on the Draft Maximum Level for Aflatoxin M1 in Milk.
Fuentes, M., Mateo, C., Guisán, J.M., Fernández-Lafuente, R., 2005. Biosens. Bioelectron. 20, 1380–1387.
Gracia, G.L., Campana, A., Jorge, J., Chinchilla, S., Perez, J., Casado, G., 2005. TrAC 24 (11), 927–942.
Henry, S.H., Whitaker, T., Rabbani, I., Bowers, J., Park, D., Price, W., Bosch, F.X., Pennington, J., Verger, P., Yoshizawa, T., van Egmond, H., Jonker, M.A., Coker, R., 2001. Report 1012, Aflatoxin M1 (WHO Additives, series 47) Joint Expert Committee on Food Additives (JECFA).
IARC, International Agency for Research on Cancer, 2002. Monograph on the Evaluation of Carcinogenic Risk to Humans, vol. 82. World Health Organization, Lyon, France, p. 171.
Ivanova, E.P., Wright, J.P., Pham, D.K., Brack, N., Pigram, P., Alekseeva, Y.V., Demyashev, G.M., Nicolau, D.V., 2006. Biomed. Mater. 1, 24–32.
Kamkar, A., 2006. Food Control 17, 768–775.
Knopp, D., 2006. Anal. Bioanal. Chem. 3, 425–427.
Krick, L.J., Wild, D., 2001. The Immunoassay Handbook, 2nd ed. Nature Publishing Group, London.
Liang, S., Wang, Y., Zhang, C., Liu, X., Liu, Z., Xu, R., Yin, D., 2006. J. Radioanal. Nucl. Chem. 269 (1), 3–7.
Liu, Z.M., Yang, H.F., Li, Y.F., Liu, Y.L., Shen, G.L., Yu, R.Q., 2006. Sens. Actuators B 113, 956–962.
Lopez, C.E., Ramos, L.L., Ramadán, S.S., Bulacio, L.C., 2003. Food Control 14, 31–34.
Magliulo, M., Mirasoli, M., Simoni, P., Lelli, R., Portanti, O., Roda, A., 2005. J. Agric. Food Chem. 53, 3300–3305.
Nikitin, P.I., Vetoshko, P.M., Ksenevich, T.I., 2007. J. Magn. Magn. Mater. 311 (1), 445–449.
Parker, C.O., Tothill, I.E., 2009. Biosens. Bioelectron. 24 (8), 2452–2457.
Pei, S.C., Zhang, Y.Y., Eremin, A.S., Lee, W.J., 2009. Food Control 20, 1080–1085.
Ravindranath, S.P., Mauer, L.J., Deb-Roy, C., Irudayaraj, J., 2009. Anal. Chem. 81, 2840–2846.
Radoi, A., Targa, M., Prieto-Simon, B., Marty, J.-L., 2008. Talanta 77, 138–143.
Rodriguez, V.M.L., Calonge Delso, M.M., Ordonez Escudero, D., 2003. Food Addit. Contam. 20, 276–280.
Rastogi, S., Dwivedi, P.D., Khanna, S.K., Das, M., 2004. Food Control 15, 287–290.
Shankaran, D.R., Miura, N., 2007. J. Phys. D: Appl. Phys. 40, 7187–7200.
Thirumala-Devi, K., Mayo, M.A., Hall, A.J., Craufurd, P.Q., Wheeler, T.R., Waliyar, F., Subrahmanyam, A., Reddy, D.V., 2002. J. Agric. Food Chem. 50, 933–937.
Van Weeman, B.K., Schuurs, A.H.W.M., 1971. FEBS Lett. 15, 232–236.
Wang, F.C., Yuan, R., Chai, Y.Q., 2006. Appl. Microbiol. Biotechnol. 72, 671–675.
Wang, L., Gan, X.X., 2009. Bioprocess Biosyst. Eng. 32, 109–116.
Yu, H., 1998. J. Immunol. Methods 218, 1–8.

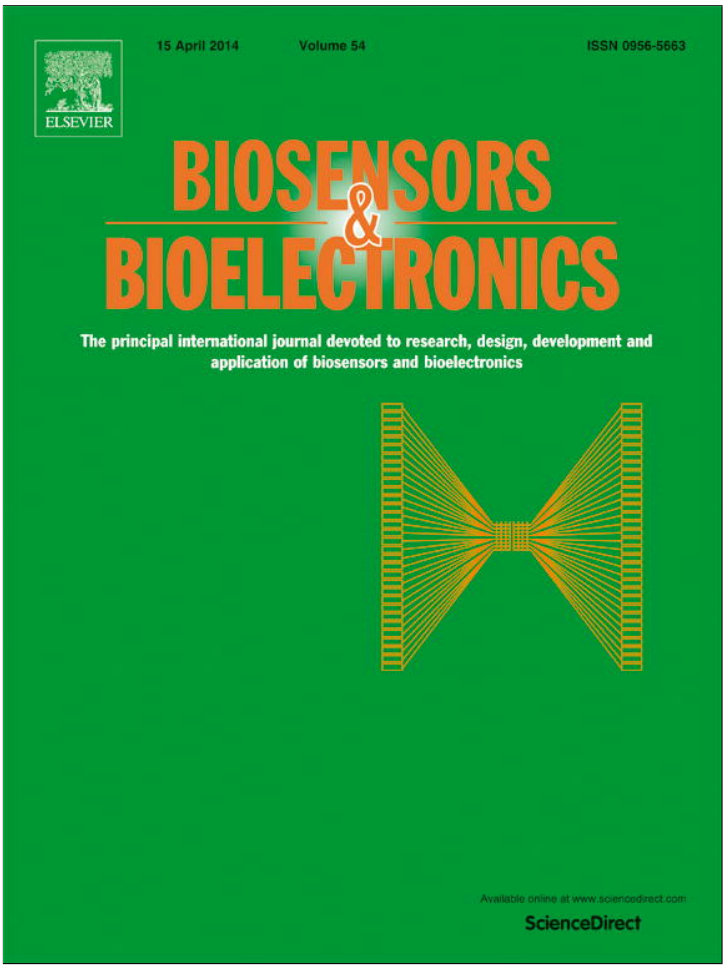

Biosensors and Bioelectronics 54 (2014) 558–564

Contents lists available at ScienceDirect

Biosensors and Bioelectronics

journal homepage: www.elsevier.com/locate/bios

A miniaturized nanobiosensor for choline analysis

Souvik Pal [a], Manoj Kumar Sharma [b], Bengt Danielsson [c], Magnus Willander [d], Ratnamala Chatterjee [b,*], Sunil Bhand [a,**]

[a] Biosensor Lab., Department of Chemistry, BITS, Pilani –KK Birla Goa Campus, Goa 403726, India
[b] Department of Physics, Indian Institute of Technology Delhi, New Delhi 110016, India
[c] Acromed Invest AB, Magistratsvagen 10, SE 226 43 Lund, Sweden
[d] Physical Electronics and Nanotechnology Division, Department of Science and Technology (ITN) Campus Norrköping, Linköping University, Norrköping SE-60174, Sweden

ARTICLE INFO

Article history:
Received 9 September 2013
Received in revised form
8 November 2013
Accepted 20 November 2013
Available online 28 November 2013

Keywords:
Choline
Nanobiosensor
Zinc oxide nanorod
Chemiluminescence
Phosphonation
Milk

ABSTRACT

A novel reusable chemiluminescence choline nanobiosensor has been developed using aligned zinc oxide nanorod-films (ZnONR). The chemically fashioned ZnONR were synthesized by hybrid wet chemical route onto glass substrates and used to fabricate a stable chemiluminescent choline biosensor. The biosensor was constructed by co-immobilization of the enzymes choline oxidase and peroxidase. The covalent immobilization of the enzymes on the ZnONR was achieved using 16-phosphonohexadecanoic acid as a cross-linker. The phosphonation of the ZnONR imparted significant stability to the immobilized enzyme as against physisorbed enzyme. A lower value of Michaelis–Menten constant (K_m), of 0.062 mM for the covalently coupled enzyme over the physisorbed enzymes facilitated enhanced stability of ZnONR nanobiosensor. The ZnONR-choline biosensor has been investigated over a wide range of choline from 0.0005 mM to 2 mM. Importantly, the recovery of choline in milk samples was close to 99%. Using the developed biosensor, choline was measurable even after 30 days with 60 repeated measurements proving the stability of the sensor (Intraday RSD%=2.83 and Interday RSD%=3.51).

1. Introduction

Milk, containing high level of choline, is an essential nutritional food for all age group (Phillips, 2012). Choline, as “vitamin-like”, is synthesized in the human body, but dietary supplementation is necessary to maintain proper function (Blusztajn, 1998; Zeisel, 2000). Choline has essential roles in brain development and memory function for infants as well as adults. It also has an important role to maintain the central nervous system and numerous metabolic functions in the body such as (a) methyl donor, (b) a precursor of the signaling lipids, platelet-activating factor and sphingosylphosphoryl choline and (c) as a precursor for acetylcholine, phosphatidyl choline and sphingomyelin biosynthesis (Dietary Reference Intakes, 1998). The adequate intake for choline ranges from 125 mg/day in infants to 550 mg/day in males over age 14 years and in breast-feeding women (Michel et al., 2006). Neurodegenerative disorders such as Alzheimer's, Parkinson's diseases and an increased risk of lethal prostate cancer have been implicated owing to abnormal metabolism of choline (Zeisel and Blusztajn, 1994; Richman et al., 2012). Since infant's nutritional intake is limited to a single source in general milk, choline supplementation is critically important. Therefore, the need for the development of a sensitive and efficient method for the estimation of the choline level in milk is extremely important.

Enzymatic choline biosensors based on thermal (Deshpande et al., 2011), colorimetric (Takayama et al., 1977), fluorimetric (Chen et al., 2011; Li et al., 2013) and electrochemical detection (Qin et al., 2010; Shimomura et al., 2009) have been reported for choline analysis. The reported choline biosensors use the enzyme choline oxidase (COD) that catalyzes choline in the presence of oxygen and produces hydrogen peroxide. Thus, one is able to measure choline by quantifying hydrogen peroxide using chemiluminescence technique. Owing to low background, high sensitivity, low cost of instrumentation and suitability for miniaturization in analytical chemistry, chemiluminescence (CL) has been recognized as one of the most useful analytical techniques (Dodeigne et al., 2000).

Recently, nanostructured metal oxides have been extensively reported for the construction of novel biosensors. The nanostructured materials provide upper limits in balancing the key factors that determine the efficiency of biocatalysts including surface area, mass transfer resistance and effective enzyme loading (Solanki et al., 2011). Among the reported nanostructured materials, zinc oxide (ZnO) has attracted considerable attention owing to wide band gap, strong excitation binding energy, esthetic morphologies

* Corresponding author. Tel.: +91 11 26591354; fax: +91 11 26581114.
** Corresponding author. Tel.: +91 832 2580332; fax: +91 832 2557030/33.
E-mail addresses: rmala@physics.iitd.ernet.in (R. Chatterjee), sunil17_bhand@yahoo.com, sunilbhand@goa.bits-pilani.ac.in (S. Bhand).

0956-5663/$ - see front matter © 2013 Elsevier B.V. All rights reserved.
http://dx.doi.org/10.1016/j.bios.2013.11.057

and multifunctional properties (Singh et al., 2007). The nanostructured ZnO also possesses several advantages for biosensing owing to the wide optical emission spectra, high aspect ratio, polar surface along on the top of the rods, good electron communication and nontoxicity. Notably, the isoelectric point (IEP) of ZnO is as high as about 9.5 i.e. suitable for immobilization of the enzymes and proteins (Topoglidis et al., 2001). So far, various ZnO nanostructures such as nanoparticles, porous films, nanocombs and nanorods have been deployed for development of biosensors (Ahmad and Zhu, 2011; Arya et al., 2012). ZnO nanostructures have also been demonstrated to detect cytochrome *c* (Topoglidis et al., 2001), protein (Huang and Lee, 2008), uric acid (Zhang et al., 2004), glucose (Wang et al., 2006; Wei et al., 2006), phenol (Gu et al., 2008), urea (Solanki et al., 2008) and cholesterol (Israr et al., 2011).

Enzyme immobilization on the transducer surface is a critical step in the design of biosensors as enzyme molecules must retain their activity after the immobilization in order to achieve enhanced stability and shelf life. Self-assembled monolayers (SAMs) provide versatility and novel properties to surfaces and interfaces by conjugating biomolecules to facilitate a low-cost method of fabricating miniaturized biosensor devices with improved enzyme activity, stability and selectivity (Ulman, 1996; Mateo et al., 2007; Samanta and Sarkar, 2011). A unique approach to utilizing CL technique for the detection of acetylcholine has been reported using enzyme coupled multiple-branched nanostructures (Risveden et al., 2010). Moreover, carboxylic acid, phosphonic acids, alkyl phosphonic acids and phosphoric acids (Laibinis et al., 1989; Textor et al., 2000; Pawsey et al., 2002) have been reported to form favorable functionalized surfaces of metal oxides. Alkyl phosphonates and phosphonic acid can form well-packed SAMs with excellent thermal and hydrolytic stability. Moreover, these SAMs are reported to exhibit much improved binding over carboxylic acids to a wide range of metal oxides (Zhang et al., 2010).

Herein, we present for the first time, construction of a sensitive chemiluminescence choline nanobiosensor using bi-enzyme coupled zinc oxide nanorod-films (ZnONR) via SAMs of 16-phosphonohexadecanoic acid (16-PHA). The developed choline nanobiosensor exhibited good selectivity, sensitivity, molecule capturing efficiency and stable output response over the other reported biosensors (Razola et al., 2003; Chen et al., 2011; Li et al., 2013). The remarkable feature of the presented biosensor is its excellent stability and reusability over the period of 30 days with 78% retention of enzyme activity. Moreover, the presented biosensor also provided a much broader working range for choline analysis (0.0005–2 mM). The application of the developed nanobiosensor for analysis of choline in milk is successfully demonstrated.

2. Materials and methods

2.1. Materials and instrumentation

Choline oxidase (EC 1.1.3.17) from Alkaligenes sp. (COD), peroxidase (EC 1.11.1.7) from Horseradish (HRP), choline chloride (ChCl), Zinc nitrate hydrate ($Zn(NO_3)_2$, xH_2O), Sodium hydroxide (NaOH) 99.99% trace metals basis, 16-phosphonohexadecanoic acid (16-PHA), 1-ethyl-3-[3-dimethylaminopropyl] carbodiimide hydrochloride (EDC), *N*-hydroxy succinimide (NHS) Tween-20 and luminol (5-amino-2,3-dihydro-1,4-phthalazinedione) were purchased from Sigma Chemical Co. (USA). Sodium phosphate dibasic, sodium phosphate monobasic and other chemicals were of GR grade, Merck (Germany). Centrifugation, shaking and filtration of the samples were done by Spinwin mini centrifuge, Spinix shaker purchased from Tarsons (India). White 384 well polystyrene microtiter plates were purchased from Nunc (Denmark). A Rigaku MiniFlex X-ray diffraction (XRD) using Cu K_α radiation was used to obtain the structural information. Raman spectra were recorded using Renishaw inVia micro-Raman spectrometer using 514 nm Argon laser. Fourier Transform Infrared (FT-IR) spectra were recorded using IRAffinity-1 (SHIMADZU, Japan) with attenuated total reflectance (ATR) attachment Specac Diamond ATR AQUA. For chemiluminescence measurement, Victor™ X4 2030 Opti-plate reader Perkin Elmer (USA) was used. Water produced in a reverse osmosis system (arium61316, Sartorius, Germany) was used for preparing all the solutions. Certified ultra-high pure nitrogen (99.9%), pH meter (Seven Multi Mettler Toledo, 8603, Switzerland) were used. Commercial milk samples of different fat contents were purchased from the local supermarket of Goa, India.

2.2. Sample preparation

Phosphate buffer (PB) 100 mM, pH 7.4 was prepared by mixing 100 mM of sodium di-hydrogen phosphate monohydrate and 100 mM of disodium hydrogen phosphate monohydrate in deionized (DI) water. PB was degassed before analysis. A stock solution of 100 mM ChCl was prepared by dissolving 0.139 g in 10 mL of PB (100 mM, pH 7.4). Working solution of ChCl was prepared freshly before daily use. Stock enzyme solutions were prepared in 100 mM PB (pH 7.4). Luminol solution was prepared by dissolving 4 mg of luminol in 2 mL 100 mM NaOH and making up the volume to 20 mL by 100 mM PB, pH 7.4.

For the determination of free choline a 5 mL aliquot of raw milk was added with 15 μL of Tween-20 (to give a final concentration of 0.3% v/v). To minimize the matrix effect, the solution was centrifuged for 10 min at 12 000 rpm at room temperature. A 1:4 (v/v) final dilution with PB was made prior to analysis so that the amount of choline lies in the calibration range. The developed protocol using dilution/centrifugation/filtration with 0.22 μM filter (Whatman, USA) we used to separate the milk fat.

2.3. Preparation of ZnONR film

Vertically aligned ZnONR films were deposited by hybrid wet chemical route at room temperature onto glass substrate by high pressure sputtering at ~30 Pa argon pressure with pre-deposited ZnO seed particles. The detailed method of preparation has been described elsewhere (Dalui et al., 2008). The ZnONR films thus produced were used in the construction of biosensor as shown in Fig. 1.

2.4. Fabrication of choline biosensor

Fabrication of choline biosensor is based on the efficient immobilization of bi-enzyme through SAMs. The glass containers used for monolayer preparation were cleaned with Piranha solution (a mixture of 98% H_2SO_4 and 30% H_2O_2, 7:3, v/v; caution: piranha solution reacts exothermally and strongly reacts with organics) for 1 h and rinsed exhaustively with deionized (DI) water and ethanol. ZnONR thin film was washed with ethanol, and dried under a stream of high purity nitrogen before use. These samples were immersed into 0.5 mM ethanolic solution of 16-PHA for 72 h to achieve self-assembly. The SAMs functionalized ZnONR were again rinsed in ethanol followed by DI water and dried under a stream of nitrogen. For enzyme immobilization, the carboxylic acid-terminated SAMs were modified using an aqueous equimolar solution of 100 mM EDC/100 mM NHS for 2 h at room temperature. The resultant NHS ester monolayers were reacted for 3 h in a solution of COD (1 IU/μL) and HRP (0.1 IU/μL) in PB (100 mM, pH~7.4). The covalently coupled bi-enzyme (COD/HRP) ZnONR thin film was taken out from solution and washed as described

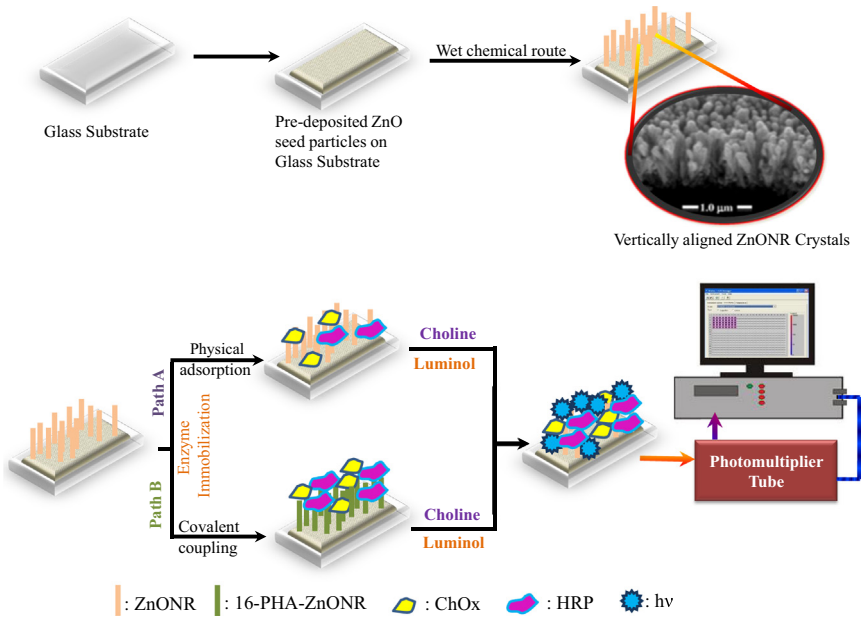

Fig. 1. Schematic pathway for construction along with working mechanism of the ZnONR choline biosensor during measurements for the attachment of bi-enzyme (COD/HRP) through physisorption (Path A) and covalent coupling (Path B) on ZnONR.

earlier. Similarly, same amount of the enzyme was also incubated on the ZnONR for 12 h to prepare physisorbed COD/HRP ZnONR films. The schematic of the enzyme immobilization procedure is shown in Fig. 1.

In the presented biosensor, COD provides the specificity and acts as a catalyst to initiate the bi-enzyme reaction. The enzyme catalytic reaction between COD and substrate ChCl solution produces the betaine aldehyde and hydrogen peroxide (H_2O_2) as product of this reaction. The produced H_2O_2 in the reaction is highly susceptible to undergo spontaneous reaction with second enzyme i.e. co-immobilized HRP. H_2O_2 thus produced was quantified using CL technique wherein, the numbers of photons emitted in presence of luminol were counted using a sensitive photomultiplier system Victor™ X4 2030.

3. Results and discussions

3.1. Characterization of ZnONR thin films

The XRD measurements (Supplementary Fig. S1) confirmed the polycrystalline nature of ZnONR with preferential [002] direction orientation. Raman spectroscopy offers a non-destructive tool for obtaining information about both the local and the non-local vibrational states related to the structure of ZnO. The reported Raman spectra of ZnONR film are shown in the inset of Supplementary Fig. S1. The spectrum is dominated by the presence of a strong sharp peak located at ~438 cm^{-1} identifying the good crystalline quality of our ZnONR films. The peak at ~438 cm^{-1} may be identified as high frequency branch of E_2 mode of ZnO. The broad and asymmetric nature of this peak is typical of the Raman active mode specially observed in wurtzite structure. The peak is preceded by peaks at ~332 cm^{-1} and ~378 cm^{-1} as reported [for ZnO films (Dalui et al., 2008). There is only one peak at ~577 cm^{-1} in the higher wave number region. The peak at ~577 cm^{-1} could be attributed to the A_1 longitudinal optical (LO) mode of ZnO. Origin of the above mode may be due to Zn interstitials present in the films. Raman spectroscopy results of ZnONR thus help us to conclude that these nanorod-films are of good crystalline quality with some Zn interstitials present in the film.

This technique is essentially a hybrid technique where we easily manipulate the size and distribution of the ZnO seed crystallites that in turn modulate the growth of ZnONRs. Thus, the ZnONR used in this work are [002] aligned polycrystalline as can be concluded from our XRD and Raman measurements.

3.2. Spectroscopic characterization by FT-IR

FT-IR spectroscopy was applied to measure the surface properties of the bi-enzyme COD/HRP coupling through SAMs via the carbodiimide cross-linking reaction on ZnONR surfaces. For the ZnONR samples, FT-IR ATR spectra were collected at a resolution of 2 cm^{-1} (128 scans). The FT-IR spectra recorded for ZnONR coupled enzyme (COD/HRP) via 16-PHA crosslinker are shown in Fig. 2(a). Fig. 2(a) (i), FT-IR spectrum of the bare ZnONR. Fig. 2(a) (ii), FT-IR spectra 16-PHA functionalized ZnONR. Fig. 2(a) (iii), FT-IR spectrum of covalently coupled enzyme on ZnONR.

Fig. 2(a) (ii) shows the asymmetric (ν_{as}(C–H)) and symmetric methylene stretches (ν_s(C–H)) of 16-PHA-modified ZnONR that appear at 2925 cm^{-1} and 2853 cm^{-1} respectively. These bands of 16-PHA modified ZnO suggest methylene chains during monolayer growth.

The C=O stretch at 1724 cm^{-1} on ZnONR associated with asymmetric and symmetric COO^- stretches at 1647 cm^{-1} and 1542 cm^{-1} respectively are characteristics of an organic carboxylic compound. The additional IR peaks at 1455 cm^{-1}, 1294 cm^{-1} and 1216 cm^{-1} are ascribed to C–H deformation and C–O stretch respectively. In the P–O stretching region (Fig. 2(a) (ii)), the binding mode information of phosphonic acids onto metal oxides is not easy to obtain. The peaks in the P–O stretching region appear between 1300 cm^{-1} and 800 cm^{-1} and the presence of several different binding modes in phosphonic acid monolayers is indicated by the presence of residual P=O and P–O–H sites. The peak located at 945 cm^{-1} in the spectrum of 16-PHA is assigned to a P–OH band that is observed only after binding to the ZnO surface. This indicates that the phosphonic acids bind to the surface Zn–OH group via condensation reactions. The linkage to the ZnO surface mode should be a tridentate chelating binding

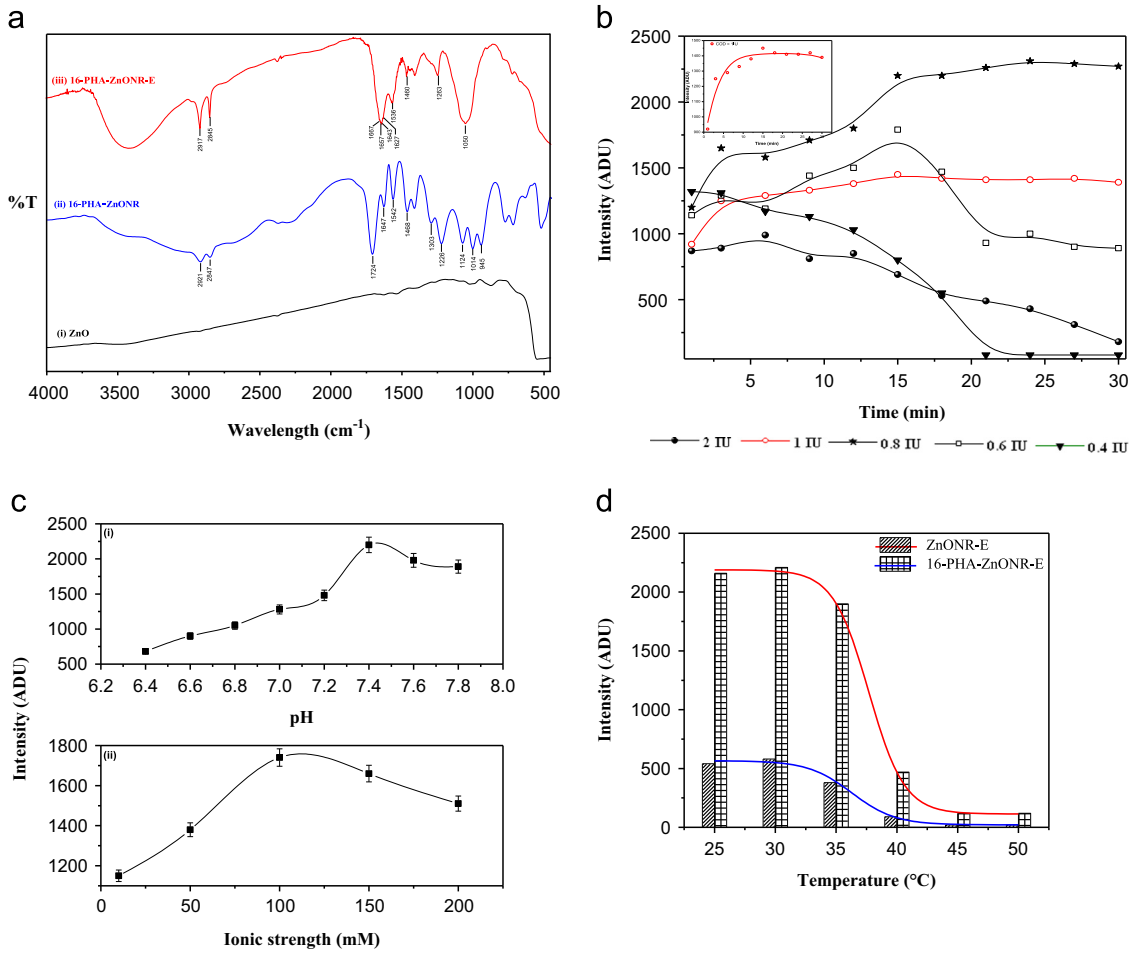

Fig. 2. (a) The ATR FT-IR spectrum of (i) the ZnONR film, (ii) ZnONR treated with 16-PHA, (iii) Enzyme (COD/HRP) coupled through 16-PHA functionalized ZnONR. Spectra were acquired using 128 scans at 2 cm^{-1} resolution collected under vacuum conditions. (b) Influence of COD concentration; 0.4 IU/μL, 0.6 IU/μL, 0.8 IU/μL, 1.0 IU/μL and 2 IU/μL (all solutions are in 100 mM, pH∼ 7.4 PB; [ChCl]=1 mM) (Inset: The intensity change for [COD]=1 IU/μL). (c) (i) Effect of ionic strength of the PB (10, 50, 100, 150 and 200 mM) on the response of ZnONR choline biosensor for 1 mM ChCl; (ii) influence of the PB pH (6.4–7.8) on the response of ZnONR choline biosensor for 1 mM ChCl. (d) Influence of temperature on physisorbed ZnONR and 16-PHA-ZnONR in the range of 25–50 °C; 100 mM, pH∼7.4 PB; 1 mM ChCl.

mode or a bidentate binding moiety rather than the monodentate surface binding mode. The existence of the peak at 1124 cm^{-1}, which is characteristic of the P=O stretching mode, is a possible evidence for bidentate binding modes. The observation of P–OH related modes indicates that the binding of 16-PHA on ZnONR occurs mainly through the PO_3H_2 groups. Similar coordination of binding modes of organic phosphonic acids on ZnO was also confirmed by Zhang et al., 2010.

The enzyme COD/HRP coupling through 16-PHA SAMs via the carbodiimide cross-linking reaction on ZnONR surfaces is presented as Fig. 2(a) (iii). Upon immobilization of COD/HRP in Fig. 2 (a) (iii) new absorption bands appeared; three IR bands at 1643 cm^{-1}, 1536 cm^{-1}, and 1263 cm^{-1} are ascribed to the absorption by the amide group that links COD/HRP to 16-PHA functionalized ZnONR. Also the bands at 1667 cm^{-1}, 1657 cm^{-1} and 1627 cm^{-1} are for the amide I region which is the common structural unit for all biomolecules (Nakano et al., 2007).

3.3. *Optimization of influential parameters of the choline biosensor system*

CL biosensors based on luminol involve appropriate enzymatic reaction between substrate and enzyme and the subsequent reaction between luminol and enzymatically produced H_2O_2. A minor change in enzyme concentration, pH, ionic strength and temperature can sometimes be responsible to lose the biological activity, as immobilized enzymes are very much sensitive towards environmental changes.

3.3.1. *Optimization of the COD units*

As COD is the main enzyme that imparts selectivity for choline, thus it is needed to optimize the amount of COD used in the construction of ZnONR biosensor. Various concentrations of COD were tested in order to get a stable response of ZnONR biosensor keeping other parameters like temperature, pH, ionic strength and amount of HRP constant.

The optimal concentration of COD used in the CL ZnONR biosensor system was investigated by measuring the CL intensities in the presence of different concentration of COD and same quantity of the other reagents. Immobilized COD amount on the biosensor response was studied by varying the concentration of COD from 0.4 to 2 IU/μL keeping the HRP units constant (0.1 IU/μL). From Fig. 2 (b), it was found that the effect was enhanced with the increasing quantity of COD up to 1 IU/μL. The inset figure clearly shows the stable CL intensity measured after 15 min. A stable intensity for the 0.8 IU/μL and 1 IU/μL COD was found using 1 mM ChCl. However, the stability of signal intensity extended to varying concentrations of ChCl only when 1 IU/μL COD was used. Thus, in order to realize the system effectively, 1 IU/μL COD was used for further experiment.

Further, the reaction time of COD on ZnONR choline biosensor was optimized (Fig. 2(b)). The CL intensity of the mixture gradually increased to a maximum value within 15 min. The result confirmed that the catalyzed oxidation process of choline was finished in 15 min. Thus, 15 min was adopted as the incubation time for further experiments.

3.3.2. Optimization of ionic strength and pH

The influence of the ionic strength and pH of PB on the activity of the enzyme was studied. Measurements were carried out on ZnONR system with various ionic strength (10, 50, 100, 150 and 200 mM PB) and pH (6.4–7.8) for 1 mM ChCl. The results are presented in Fig. 2(c). It is evident from Fig. 2(c) (i) that with increase in the ionic strength of PB, response signal increases up to 100 mM, and then decreases. Thus, further experiments were carried out with 100 mM PB. It is also clear from Fig. 2(c) (ii) that COD/HRP exhibit maximum activity at pH 7.4. On the other hand, it is known that the ideal pH balance for a healthy body is slightly more alkaline than acid measuring. Therefore, the pH of 7.4 was selected as a good compromise for our experiment. Milk and PB were mixed in different ratios (1:1–1:12) for the analysis of pH and ionic strength. The pH gets stabilized for milk:PB at 1:4 dilutions.

3.3.3. Optimization of temperature

The activities of free and immobilized enzyme were measured at different temperatures in the range 25–50 °C to determine optimal temperature for enzyme activity. The optimum temperature was determined for free and immobilized enzymes and presented as Fig. 2(d). While the physisorbed enzymes showed low signal response in the studied temperature range (25–50 °C), the co-immobilized enzymes exhibited significantly higher activity in the same temperature range. Enzymes immobilized through 16-PHA exhibited the highest change over the free enzyme activity. Both physisorbed and immobilized enzymes loose activities in the temperature range 40–50 °C. The residual activity was 3.7% for the physisorbed enzymes and 5.5% for enzymes immobilized at the same temperature (50 °C). Above 35 °C, the enzyme activity dropped significantly due to the thermal inactivation.

3.3.4. Kinetic parameters

The enzyme activities were determined at different substrate concentrations under the optimum conditions. Michaelis–Menten constant (K_m) (Eq. 1) values of the immobilized enzymes were determined using LineWeaver–Burk plot:

$$1/V = K_m/V_{max} \times 1/[S] + 1/V_{max} \quad (1)$$

where V, V_{max}, [S] and K_m are initial velocity, maximum velocity, initial substrate concentration and Michealis–Menten constant respectively.

3.4. Effect of surface modification

The stability of the bienzymes (COD/HRP) coupled to the ZnONR was evaluated when enzymes were attached on the surface via covalent coupling as against the physically adsorbed COD/HRP. The kinetic intensity profile of the resulting signal was recorded as shown inFig. 3(a). The signal reached a stable value (95% of the steady state) after 15 min (which is also supported by Fig. 2(b)). The covalently attached enzyme showed significantly higher signal intensity over the physically adsorbed enzymes. The order of the stable signal intensity recorded for COD/HRP functionalized ZnONR was found to be 7880 ADU (via phosphonation) and 1070 ADU (physisorbed i.e. non-specifically adsorbed COD/HRP) respectively. The signal intensities were found to be almost seven times higher for phosphonated ZnONR as against physisorbed COD/HRP nanorods.

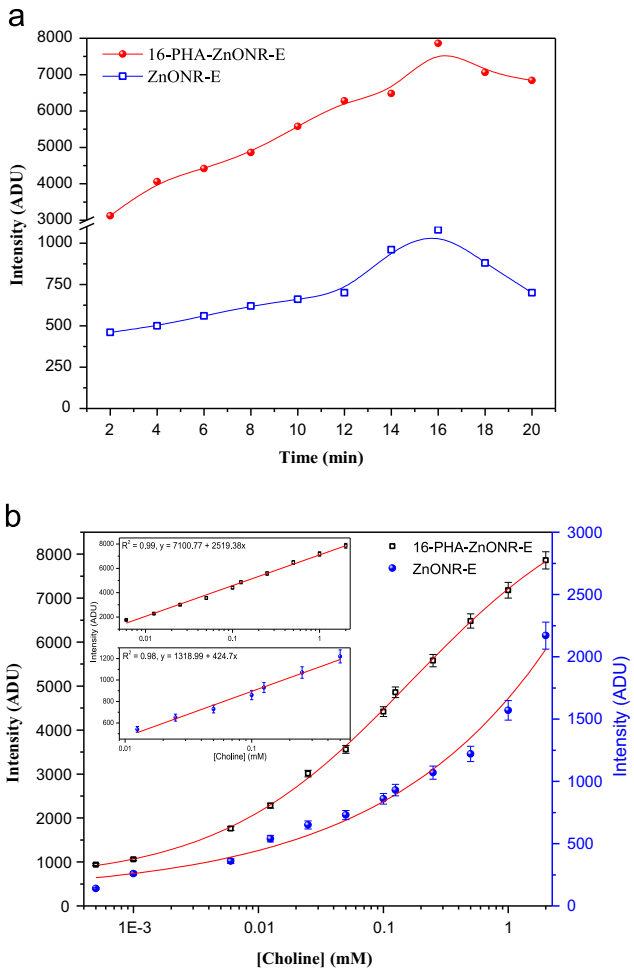

Fig. 3. (a) Comparison of the kinetic response of COD/HRP (covalently coupled against physically adsorbed) on ZnONR film. (b) Calibration curve for different choline concentrations obtained using 16-PHA-ZnONR coupled enzyme and physisorbed enzyme on ZnONR (Inset: the linear calibration graph).

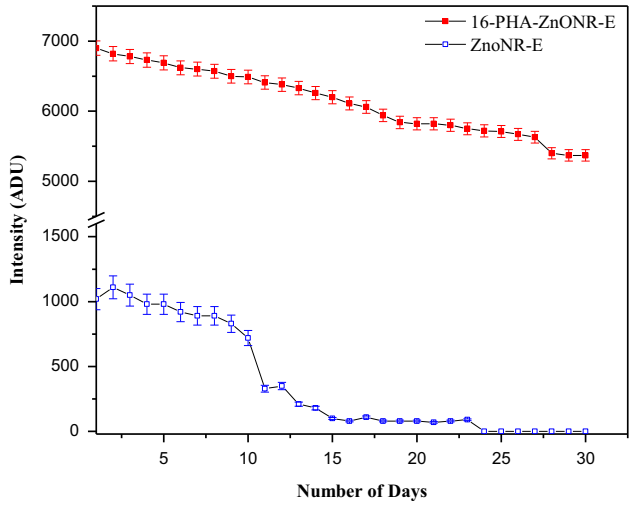

Fig. 4. The storage stability of ZnONR thin film modified with COD/HRP via16-PHA and physisorbed enzyme on ZnONR in a 100 mM, pH ~ 7.4 phosphate buffer solution over 30 days using choline biosensor each day showing its storages stability at 4 °C.

These important features of the presented biosensor play an important role to enhance efficacy and specificity towards the rapid signal transfer rate and bio-recognition properties.

3.5. Calibration of choline nanobiosensor

A calibration curve for choline (0.0005–2 mM), measured in triplicate, using ChCl as substrate is shown in Fig. 3(b). The calibration was found to be linear in the range 0.006–2 mM ($R^2=0.99$, $n=5$) with a relative standard deviation (RSD) of 4.1% $\pm$0.5 for the 16-PHA modified ZnONR (Fig. 3(b) Inset). The linear equation was $y=7100.77+2519.38x$ (mM). Limit of detection (LOD) was 0.0005 mM and limit of quantitation (LOQ) was 0.006 mM by analyzing replicate sets of 16-PHA modified ZnONR with good sensitivity about 193 ADU change per decade. Whereas for physisorbed enzyme ZnONR, the linearity was found in the range 0.5–0.0125 mM ($R^2=0.98$, $n=5$) with an RSD of 6.9% $\pm$ 0.8 (Fig. 3(b) Inset). The linear equation was $y=1318.99+424.7x$ (mM). LOD and LOQ were determined as 0.0125 mM by analyzing replicate sets with very low sensitivity about 19 ADU change per decade. Lower LOD, LOQ value, R^2 and sensitivity indicate that 16-PHA-ZnONR is much superior over physisorbed enzyme ZnONR. The reported linear range for the presented biosensor covers the free choline concentration (125 mg/day) found in infant formula, and thus the method can be adopted for routine measurements. Moreover, the method can also be easily applied to analyse the normal concentrations of dietary choline intake in milk by mere centrifugation and dilution of samples.

3.6. Operational stability

The stability and reusability of 16-PHA-ZnONR choline biosensor were evaluated against physically adsorbed choline biosensor by performing a series of repeated experiments over 30 days by using a single biosensor. The storage stability of developed biosensor was found excellent even after 60 measurements (Intraday RSD%=2.83 and Interday RSD%=3.51). The choline biosensor was stored under appropriate environmental conditions e.g. at 4 °C before and after the measurements. The response of the biosensor was found consistent for the first 10 days and after 30 days the biosensor response decreased to 78%. The decrease in response may be due to the reduction of enzyme activity and denaturation of the peroxidase. It was found that 16-PHA modified choline biosensor holds good storage stability, sensitivity and reusability for longer duration than physisorbed enzyme ZnONR surface as represented in Fig. 4.

The enhanced stability of the presented biosensor can be explained in terms of the stability imparted by SAM of 16-PHA crosslinker. The results of the experiment revealed good consistency in the calibration traces even as the surfactant residuals of the solution from 16-PHA-ZnONR choline biosensor was detached by washing in PB solution before each measurement. Repeated measurements on physically adsorbed choline biosensor revealed an unstable and non-reproducible response.

The ZnONR is coupled with the phosphate group of the 16-PHA chain on one side. The other end the 16-PHA is covalently coupled to the Enzyme COD/HRP via activation of the –COOH group. Thus, the 16-PHA SAMs provide strong binding to the either side of the chain. The improved stability was confirmed by washing the surface for both physisorbed and chemisorbed ZnONR sensor using PB. It was observed that the chemisorbed enzyme was held strongly even after 15 repeated wash as evident from the FT-IR spectra (Supplementary Figs. S2 and S3). The characteristic peaks present due to enzyme coupled SAMs were retained even after the multiple washing steps. In contrast, for the physisorbed enzyme, these peaks were found absent after the washing step in the FT-IR spectra.

The immobilization of enzyme is a well-accepted approach towards stabilization of enzyme (Mateo et al., 2007). An important feature that account for enzyme stability is the improvement obtained in the value of the Michaelis–Menten constant (K_m). The K_m value obtained using LineWeaver–Burk plot was estimated as 0.062 mM $\pm$ 0.06 for COD/HRP coupled via phosphonated ZnONR and 0.2 mM $\pm$ 0.09 for COD/HRP coupled via physisorbed enzyme ZnONR. The lower K_m value (almost 3.2 times) reflects higher enzymatic affinity of COD/HRP-coupled via phosphonated ZnONR towards choline as the affinity of phosphate group of 16-PHA is high with ZnO. The figures of merit of choline biosensor compared with other recent reported methods and presented in Table 1.

3.7. Recovery studies and real sample analysis

Recovery studies were performed on 16-PHA modified ZnONR for three different fat % milk samples (0.5, 1.5 and 3.5). The study was repeated with milk samples spiked with standard choline solution (1, 0.1 and 0.01 mM) to evaluate sensor performance for inter-batch and intra-batch reproducibility. The summaries of findings are tabulated in Table 2 with mean recovery intraday

Table 2
Recovery of choline from different fat % milk sample as determined by ZnONR choline biosensor to assess the recovery efficiency using developed assay.

Milk samples with different fat (%)	Choline spiked (mM)	Intraday		Interday	
		Recovery (%)	RSD (%)	Recovery (%)	RSD (%)
Milk-1 (0.5%)	1	98.1 $\pm$ 0.30	0.33	97.3 $\pm$ 0.21	0.64
	0.1	97.4 $\pm$ 0.65	0.49	94.0 $\pm$ 0.57	0.75
	0.01	101.0 $\pm$ 0.23	0.57	96.1 $\pm$ 0.60	1.04
Milk-2 (1.5%)	1	97.1 $\pm$ 0.60	0.70	93.3 $\pm$ 0.37	0.84
	0.1	103.1 $\pm$ 0.78	0.67	97.5 $\pm$ 0.41	0.93
	0.01	98.3 $\pm$ 0.43	0.42	96.0 $\pm$ 0.69	1.10
Milk-3 (3.5%)	1	95.2 $\pm$ 0.29	0.28	94.7 $\pm$ 0.47	0.92
	0.1	97.9 $\pm$ 0.71	0.78	91.3 $\pm$ 1.01	1.05
	0.01	98.6 $\pm$ 0.56	0.53	97.0 $\pm$ 1.09	1.07

Table 1
Comparison of various established biosensing techniques for the analysis of choline.

Biosensor configuration	Transducer	Linearity (mM)	Detection limit (mM)	K_m (mM)	Stability (biosensor response retained)	Reference
Chemiluminescence 16-PHA-ZnONR	Optical	0.006–2	0.0005	0.062 $\pm$ 0.06	78% after 1 month	Our work
Flow Injection Analysis-Enzyme immobilized on CPG support	Thermal	0.03–0.5	0.03	0.45	more than 85% after 15 months	Deshpande et al. (2011)
ChOx and different concentrations of choline solution in CdTe quantum dots	Optical	0.005–0.15	0.0001	0.20	n.r.	Chen et al. (2011)
Fluorescent conjugated polymer and an enzyme-coupled assay	Optical	0.0001–0.02	0.00005	n.r.	n.r.	Li et al. (2013)
Amperometric ChOx /HRP immobilized solid carbon paste electrode	Electrochemical	0.00005–0.007	0.00001	n.r.	1 month	Razola et al. (2003)

RSD% 0.53 ± 0.17 and mean interday RSD% was calculated as 0.93 ± 0.16.

4. Conclusion

In conclusion, vertically aligned ZnONR-films with an average diameter of ~80 nm and length ~780 nm (film thickness) has been successfully demonstrated for the construction of a stable and reproducible choline nanobiosensor. The developed biosensor is demonstrated for choline analysis in milk and it can be easily adopted for routine analysis of choline content in milk and infant formula. The conjugation with COD/HRP has been carried out to prepare a choline biosensor to harvest the substantial advantages of large surface area and smooth optical signal communication in ZnONR. Stability, reproducibility, sensitivity, and selectivity of the biosensor have been investigated over a large dynamic concentrations ranging from 0.0005 mM to 2 mM of choline solution and good sensitivity is achieved with total analysis time of 15 min at room temperature. The enhanced stability of the enzyme on ZnONR is achieved via phosphonation. The SAMs on the ZnONR also facilitates the protection of ZnO material in aqueous media. The presented biosensor could easily be extended for routine analysis in milk/milk powder and dietary supplements.

Acknowledgments

This work is funded in part by National Agriculture Innovation Project, (NAIP) No. C4/C10125, ICAR and The World Bank. SP acknowledges to NAIP for the award of Research Associate Fellowship.

Appendix A. Supporting information

Supplementary data associated with this article can be found in the online version at http://dx.doi.org/10.1016/j.bios.2013.11.057.

References

Ahmad, M., Zhu, J., 2011. J. Mater. Chem. 21, 599–614.
Arya, S.K., Saha, S., Ramirez-Vick, J.E., Gupta, V., Bhansali, S., Singh, S.P., 2012. Anal. Chim. Acta 737, 1–21.
Blusztajn, J.K., 1998. Science 281, 794–795.
Chen, Z., Ren, X., Meng, X., Chen, D., Yan, C., Ren, J., Yuan, Y., Tang, F., 2011. Biosensors Bioelectron. 28, 50–55.
Dalui, S., Das, S.N., Roy, R.K., Gayen, R.N., Pal, A.K., 2008. Thin Solid Films 516, 8219–8226.
Deshpande, K., Danielsson, B., Bhand, S., 2011. Chem. Sens. 1, 16.
Dietary Reference Intakes for Thiamin, Riboflavin, Niacin, Vitamin B6, Folate, Vitamin B12, Pantothenic Acid, Biotin, and Choline, 1998. The National Academies Press. Washington, D.C.
Dodeigne, C., Thunus, L., Lejeune, R., 2000. Talanta 51, 415–439.
Gu, B.X., Xu, C.X., Zhu, G.P., Liu, S.Q., Chen, L.Y., Li, X.S., 2008. J. Phys. Chem. B 113, 377–381.
Huang, I.Y., Lee, M.C., 2008. Sens. Actuators B: Chem. 132, 340–348.
Israr, M.Q., Sadaf, J.R., Nur, O., Willander, M., Salman, S., Danielsson, B., 2011. Appl. Phys. Lett. 98, 253705.
Laibinis, P.E., Hickman, J.J., Wrighton, M.S., Whitesides, G.M., 1989. Science 245, 845–847.
Li, Y., Huang, H., Shi, F., Li, Y., Su, X., 2013. Microchim. Acta 180, 135–1140.
Mateo, C., Palomo, J.M., Fernandez-Lorente, G., Guisan, J.M., Fernandez-Lafuente, R., 2007. Enzyme Microb. Technol. 40, 1451–1463.
Michel, V., Yuan, Z., Ramsubir, S., Bakovic, M., 2006. Exp. Biol. Med. 231, 490–504.
Nakano, K., Yoshitake, T., Yamashita, Y., Bowden, E.F., 2007. Langmuir 23, 6270–6275.
Pawsey, S., Yach, K., Reven, L., 2002. Langmuir 18, 5205–5212.
Phillips, M., 2012. Anal. Bioanal. Chem. 403, 2103–2112.
Qin, X., Wang, H., Wang, X., Miao, Z., Chen, L., Zhao, W., Shan, M., Chen, Q., 2010. Sens. Actuators B: Chem. 147, 593–598.
Razola, S.S., Pochet, S., Grosfils, K., Kauffmann, J.M., 2003. Biosensors Bioelectron. 18, 185–191.
Richman, E.L., Kenfield, S.A., Stampfer, M.J., Giovannucci, E.L., Zeisel, S.H., Willett, W.C., Chan, J.M., 2012. Am. J. Clin. Nutr. 96, 855–863.
Risveden, K., Dick, K.A., Bhand, S., Rydberg, P., Samuelson, L., Danielsson, B., 2010. Nanotechnology 21, 055102.
Samanta, D., Sarkar, A., 2011. Chem. Soc. Rev. 40, 2567–2592.
Shimomura, T., Itoh, T., Sumiya, T., Mizukami, F., Ono, M., 2009. Talanta 78, 217–220.
Singh, S.P., Arya, S.K., Pandey, P., Malhotra, B.D., Saha, S., Sreenivas, K., Gupta, V., 2007. Appl. Phys. Lett. 91, 063901.
Solanki, P.R., Kaushik, A., Ansari, A.A., Sumana, G., Malhotra, B.D., 2008. Appl. Phys. Lett. 93, 163903.
Solanki, P.R., Kaushik, A., Agrawal, V.V., Malhotra, B.D., 2011. NPG Asia Mater. 3, 17–24.
Takayama, M., Itoh, S., Nagasaki, T., Tanimizu, I., 1977. Clin. Chim. Acta 79, 93–98.
Textor, M., Ruiz, L., Hofer, R., Rossi, A., Feldman, K., Hähner, G., Spencer, N.D., 2000. Langmuir 16, 3257–3271.
Topoglidis, E., Cass, A.E.G., O'Regan, B., Durrant, J.R., 2001. J. Electroanal. Chem. 517, 20–27.
Ulman, A., 1996. Chem. Rev. 96, 1533–1554.
Wang, J.X., Sun, X.W., Wei, A., Lei, Y., Cai, X.P., Li, C.M., Dong, Z.L., 2006. Appl. Phys. Lett. 88, 233106.
Wei, A., Sun, X.W., Wang, J.X., Lei, Y., Cai, X.P., Li, C.M., Dong, Z.L., Huang, W., 2006. Appl. Phys. Lett. 89, 123902.
Zeisel, S.H., Blusztajn, J.K., 1994. Annu. Rev. Nutr. 14, 269–296.
Zeisel, S.H., 2000. Nutrition (Burbank, Los Angeles County, Calif.) 16, 669–671.
Zhang, B., Kong, T., Xu, W., Su, R., Gao, Y., Cheng, G., 2010. Langmuir 26, 4514–4522.
Zhang, F., Wang, X., Ai, S., Sun, Z., Wan, Q., Zhu, Z., Xian, Y., Jin, L., Yamamoto, K., 2004. Anal. Chim. Acta 519, 155–160.

Synthesis and characterization of ZnO-$ZnAl_2O_4$ whiskers and their application in biosensors

Bhagaban Behera[a,#], Souvik Pal[b,#], Lizy Kanungo[b], Sunil Bhand[b,*], Sudhir Chandra[a,*]

[a] *Centre for Applied Research in Electronics, Indian Institute of Technology, Delhi, New Delhi, 110016, India*
[b] *Biosensor Lab., Department of Chemistry, BITS, Pilani – K. K. Birla Goa Campus, Goa 403726, India*

[#] *Authors with equal contribution*
[*] *Authors for correspondence: Sunil Bhand, email: sunilbhand@goa.bits-pilani.ac.in*
Sudhir Chandra, email: schandra@care.iitd.ernet.in
Received 01 May 2014; Accepted 27 Jun 2014; Available Online 27 Jun 2014

Abstract

A simple and efficient technique to synthesize ZnO-$ZnAl_2O_4$ composite nano-whiskers has been reported. The application of developed nano-whiskers for sensitive bio-analysis and efficient bio-catalysis is demonstrated. For the synthesis of nanostructured ZnO-$ZnAl_2O_4$, Zn and Al in the form of thin films were taken as starting materials. To synthesize the composite nanostructured material, Zn thin film was deposited on oxidized silicon substrate using RF magnetron sputtering followed by Al film deposition by thermal evaporation. These layered metal films were thermally oxidized in a tube furnace at 400 - 550 ℃ in atmospheric environment for 1 h. The structural and crystal phase analysis was done using Scanning Electron Microscopy (SEM) and X-ray Diffraction (XRD). The effect of temperature, Al thickness and time of oxidation on whisker growth has been studied. The composite nanostructure formation is attributed to Kirkendall effect. In this study, alkaline phosphatase (ALP) was used as biocatalyst immobilized on nanostructured ZnO- $ZnAl_2O_4$ composite. The novel biochip was tested for bio-catalytic activity for analysis of p-nitro phenyl phosphate and p-nitro phenol. The performance of the covalently immobilized ALP nano whiskers was found to be almost double over the physically adsorbed ALP.

Keywords: Zinc Aluminates; Thin films; Nanostructures; Whiskers; Biochip; Bio-catalysis

1. Introduction

In recent years, several nanostructured metal oxides have achieved wide acceptability because of their high surface to volume ratio and excellent physical-chemical properties. Nanostructured materials have boosted applications in various fields such as energy, medicine and environment monitoring etc. Zinc oxide (ZnO) nanostructures have been used as gas sensing, piezoelectric and optical material [1-5]. It has been reported that the performances in applications can be improved by alloying ZnO [6, 7]. T. Santhaveesukand et al., A. Kashyout et al. have shown that ZnO gas sensing properties can be improved by alloying with titanium and antimony [8, 9]. Doping of vanadium in ZnO has improved piezoelectric properties [10]. ZnO doped with Al_2O_3 is known as Zinc aluminate ($ZnAl_2O_4$). It has been used as a catalytic and optical material [11, 12]. Several methods have been reported for synthesis of $ZnAl_2O_4$ such as sol-gel, solid-state reaction and wet chemical [13-15]. In most cases, $ZnAl_2O_4$ has been synthesized in the form of nanotubes, nanoparticles and hierarchical form. Only a few reports have been published on synthesis of composite ZnO/$ZnAl_2O_4$ nanoparticles [16, 17]. From biological application point of view, both ZnO and $ZnAl_2O_4$ are biocompatible [18-22]. One such testimony for biological application using enzyme coupled ZnO nanostructure biosensor technique has been reported recently [23].

Alkaline phosphatase (ALP), a nonspecific phosphomonoesterase found widely in many mammalian tissues [24], involves in various metabolic functions such as fat absorption, mucosal defense and skeletal mineralization. ALP catalyzes the hydrolysis of phosphomonoesters, releasing free inorganic phosphate and alcohol [25, 26]. In analytical chemistry, ALP is often used as a major target to probe causative disease mechanisms. In the milk industry, determination of ALP activity is a significant matter, since it is used as a parameter for pasteurization control and for disease diagnostic purposes [27, 28]. Studies of ALP activity and screening of its inhibitors are required to develop potential drug therapies for osteoarthritis, idiopathic infantile arterial calcification and end-stage renal diseases [29, 30]. Many ALP assays use free enzyme in a homogeneous solution, which may be susceptible to denaturation. It is difficult to reuse or recover enzyme in solution forms. Immobilized enzymes are reported to retain enzymatic activity and also contribute to improve its stability [31, 32]. Effectively, immobilized ALP has potential applications in the fields of biochemistry, food industry, clinical diagnosis and environmental engineering [33, 34]. Thus, the need for the development of a novel yet simple, efficient and economic immobilized biochip is extremely important.

Present study demonstrates preparation of novel ZnO-$ZnAl_2O_4$ composite whiskers and their application in bio-catalysis. We have demonstrated a novel route for synthesis of ZnO-$ZnAl_2O_4$ composite whisker growth. Thermal oxidation

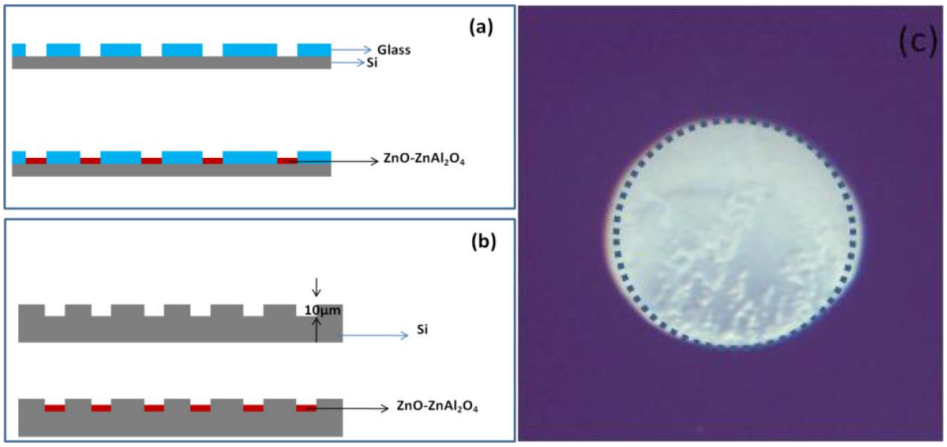

Figure 1. Schematic image of microwells (a) fabricated using Si-Glass anodic bonding (b) fabricated using Si bulk micromachining (c) 10 µm depth Si containing ZnO-$ZnAl_2O_4$.

of layered metallic films of Zn-Al has been followed for this growth. It has been explained by Kirkendall effect. The surface was tested for bio-catalysis using the enzyme alkaline phosphatase (ALP). The biosensor comprised of enzyme ALP, immobilized on the nanostructures materials using SAMs of 16-Phosphonohexadecanoic acid (16-PHA) and compared with simple physical adsorption. The catalytic efficiency of the ALP was evaluated by conversion of p-Nitrophenyl phosphate (pNPP) to p-Nitrophenol (p-NP). The catalytic efficiency of covalently immobilized enzyme on nanostructures was found to be more efficient than physisorped enzyme. The developed whiskers offer a good platform for application in biosensing and bio-catalysis.

2. Experimental Details

2.1. Preparation and characterization of nanostructured ZnO-$ZnAl_2O_4$

For the synthesis of nanostructured ZnO-$ZnAl_2O_4$ composite, Zn and Al metal films were deposited on oxidized Si substrate. One micron SiO_2 was grown on 2 inch diameter Si (100) substrate by wet thermal oxidation process at 1100 ^oC. RF magnetron sputtering was used for deposition of Zn film using a Zn (99.99%) target. For this purpose, base vacuum of 4.2×10^{-6} torr was created in the sputtering chamber using rotary pump and oil diffusion pump. Ar gas was then introduced in the chamber to establish a pressure of 5 mtorr for the sputtering process. Deposition was carried out by supplying 50 W RF (13.56 MHz) power to Zn target through an impedance matching network. The target-to-substrate spacing was 100 mm. Under these conditions of sputtering, the deposition rate of about 4.3 nm/min was achieved. The sputtering was carried out for 30 min to obtain 130 nm thickness of Zn film. Subsequently, Al film of different thickness (100-200 nm) was deposited on it using thermal evaporation in a separate system. After the depositions, the multilayer metal film appeared grey in color. The films were then subjected to thermal oxidation in a horizontal tube furnace at different temperatures (400-500 ^oC) for 1 h time. The morphologies and composition have been characterized by SEM and EDX (Zeiss, EVO-50). The structural information was analyzed using X-ray diffraction (XRD) pattern (X'pert).

2.2. Fabrication of the biochip

The application of the ZnO-$ZnAl_2O_4$ composite nanostructures for biochemical is presented. For the confinement of the bio-fluid, a microwell array was fabricated having ZnO-$ZnAl_2O_4$ composite nanostructures formed at the bottom of the well, schematically shown in Figure 1. Two different designs of micro-well array were conceptualized and realized. In the first version (Type-I), a 2-inch diameter Si wafer was anodically bonded to a Corning 7740$^{(®}$ glass plate of identical size. Prior to anodic bonding, holes were made in the glass plate at pre-determined locations using ultrasonic drilling process for making the wells. In the second version, the wells having a typical depth of 10 micron were made in silicon wafer itself by anisotropic etching in 40 wt. % aqueous solution of KOH at 65 ^oC. In both types of device, the Zn-Al double layer was then deposited selectively at the bottom of the well using a metal mask as per details given in previous sections. The oxidation process was subsequently carried out to convert the double layer of Zn-Al into $ZnAl_2O_4$. The Schematic image of the fabricated microwells is presented as Figure 1.

2.3. Materials and instruments used for bio-catalysis

Phosphatase, alkaline from calf intestine, grade 1, was purchased from Roche Diagnostics (Germany) and 4-Nitrophenyl phosphate disodium salt hexahydrate (pNPP) was purchased from Fluka (UK). 16-phosphonohexadecanoic acid (16-PHA), 1-Ethyl-3-[3-dimethylaminopropyl] carbodiimide hydrochloride (EDC) and N-hydroxy succinimide (NHS) were purchased from Sigma Chemical Co. (USA). Magnesium chloride, Glycine, Sodium hydroxide and other chemicals were of GR grade Merck (Germany). Micro pipettes (Eppendorf, Germany) were used to carry out enzyme assay. Corning, Costar 96 strip-well plates were obtained from Sigma (USA).

2.4. Biochemical solution and sample preparation

Glycine (0.1 M) was prepared by dissolving 1.875 g in 250 mL double distilled water. 25 mL of this solution was pipetted out and made to 250 mL. The pH was adjusted to 10.6 using NaOH solution at 27 ^oC. Glycine buffer (GB) was sonicated for 2 min to degas and to improve the homogeneity. 30 mg pNPP was dissolved in 10 mL GB to prepare the strength of 0.01 M substrate. $MgCl_2$ (0.01M) was prepared

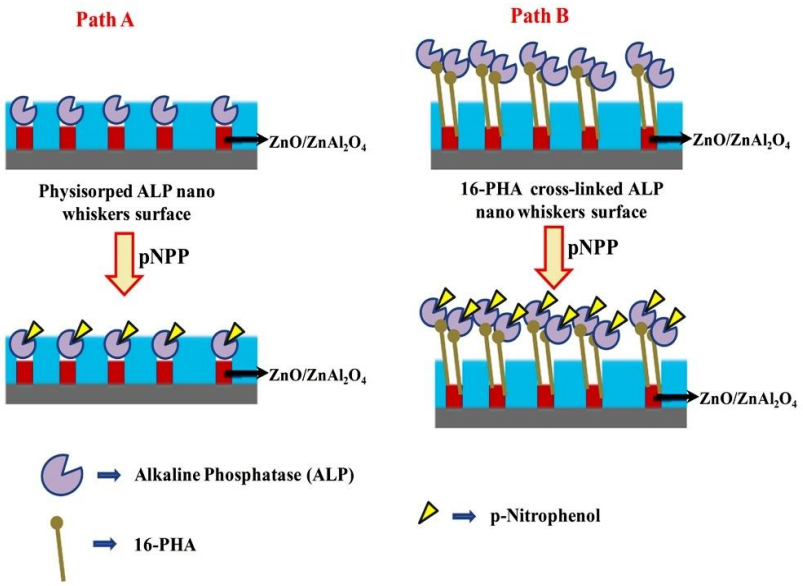

Figure 2. Schematic pathway for construction with working mechanism of the ZnO-$ZnAl_2O_4$ biochip during measurements for the attachment of enzyme (ALP) through Physisorption and Covalent coupling.

using 20 mg solids in 100 mL double distilled water (ddH_2O). pNPP working solution were prepared in GB ranging from 10 mM to 0.001 mM.

2.5. Testing of the biochip

Realization of ALP biochip is based on the efficient immobilization of enzyme through SAMs. The glass containers used for monolayer preparation were cleaned with Piranha solution (a mixture of 98% H_2SO_4 and 30% H_2O_2, 7:3, v/v; caution: piranha solution reacts exothermally and strongly reacts with organics) for 1 h and rinsed exhaustively with deionized (DI) water and ethanol. ZnO/$ZnAl_2O_4$ microwells was washed with ethanol, and dried under a stream of high purity nitrogen before use. These samples were immersed into 0.5 mM ethanolic solution of 16-PHA for 72 h to achieve self-assembly. The SAMs functionalized ZnO/$ZnAl_2O_4$ microwells were again rinsed in ethanol followed by double distilled H_2O and dried under a stream of nitrogen. For enzyme immobilization, the carboxylic acid-terminated SAMs were modified using an aqueous equimolar solution of 100 mM EDC /100 mM NHS for 2 h at room temperature. The resultant NHS ester monolayers were reacted for 3 h in a solution of ALP (0.045 IU/µL) in phosphate buffer (100 mM, pH ~ 7.4). The covalently coupled enzyme microwells (ALP/16-PHA/ZnO-$ZnAl_2O_4$) was taken out from solution and washed as described earlier. To prepare physisorped microwells (ALP/ZnO-$ZnAl_2O_4$), 0.44 IU/µL of the enzyme was also incubated on the microwells for 48 h.

In the presented biochip, ALP provides the specificity and acts as a catalyst to initiate the bio-catalysis reaction. The enzyme catalyzed reaction between ALP and substrate pNPP solution produces yellow colored water soluble p-NP as product of this reaction. The substrate (pNPP) is colorless but yellow colored p-NP has a strong absorbance at 405 nm. The rate of increased absorbance at 405 nm is proportional to the enzyme activity. Thus produced color was quantified using a sensitive photomultiplier system Victor™ X4 2030. The schematic of the enzyme catalyzed reaction is presented as Figure 2. Fourier Transform Infrared (FT-IR) spectra were recorded using IRAffinity-1 (SHIMADZU, Japan) with attenuated total reflectance (ATR) attachment Specac Diamond ATR AQUA. Colorimetric measurements were recorded using Victor™ X4 2030 Opti-plate reader Perkin Elmer (USA).

3. Results and Discussion

3.1. Morphological and structural characterization of nanostructured material

To investigate the morphological change, several sets of experiments were performed and parameters are summarized in Table 1. For these studies, Zn (130 nm) + Al films with different thicknesses (Sample # S2 =100 nm, S3=130 nm, S4=160 nm and S5=200 nm) were thermally annealed at 400 ^oC in atmospheric environment for 1 h. The SEM images for these samples are shown in Figure 3. The SEM images of as-deposited samples (before thermal oxidation) are nearly similar and a representative SEM image (S1) is shown in Figure 3 for 130 nm Zn + 160 nm Al film. It can be observed that sub-micron sized particles are grown on the surface, when Al thickness is 100 nm (Sample # S2). As the Al thickness increases, denser nanostructures are observed. Also, nanowires of 2-5 µm length are observed to grow on structures as shown in S3, S4 and S5. The diameter of nanowire is about 60-100 nm. From Figure 3 it can be concluded that Al thickness has an important role on structural growth.

In the next set of experiments, oxidation temperature was raised to 500 ^oC keeping all other parameters the same. The corresponding SEM images are shown in Figure 4. It is evident that growth is more uniform and dense, when Al thickness is 160 nm and nanostructures size is also observed to increase. The density increases with increase in annealing temperature. At this temperature, Zn is melted and Al is close to its melting point temperature. This is postulated to enhance oxidation. When growth temperature is further increased,

Table 1. Summary of parameters used for preparing nanostructured ZnO-$ZnAl_2O_4$ composite.

Sample no.	Zn film Thickness (nm)	Al film Thickness (nm)	Oxidation Time (h)	Oxidation Temperature (°C)
S1	130	160	0	No oxidation
S2	130	100	1	400
S3	130	130	1	400
S4	130	160	1	400
S5	130	200	1	400
S6	130	100	1	500
S7	130	130	1	500
S8	130	160	1	500
S9	130	200	1	500
S10	130	100	1	550
S11	130	130	1	550
S12	130	160	1	550
S13	130	200	1	550

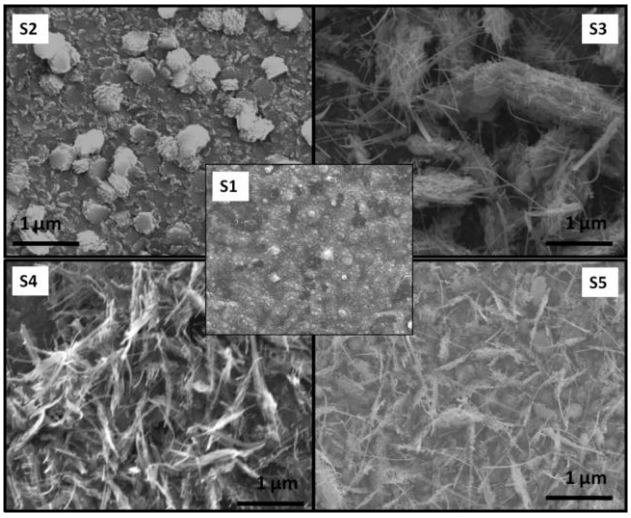

Figure 3. SEM images of ZnO-$ZnAl_2O_4$ composite nanostructures. (S2) 100 nm Al film over 130 nm Zn film and annealed at 400 °C for 1h. (S3) 130 nm Al film over 130 nm Zn film and annealed at 400 °C for 1 h. (S4) 160 nm Al film over 130 nm Zn film and annealed at 400 °C for 1 h. (S5) 200 nm Al film over 130 nm Zn film and annealed at 400 °C for 1 h. S1 is the SEM image of as-deposited 160 nm of Al film over 130 nm of Zn film.

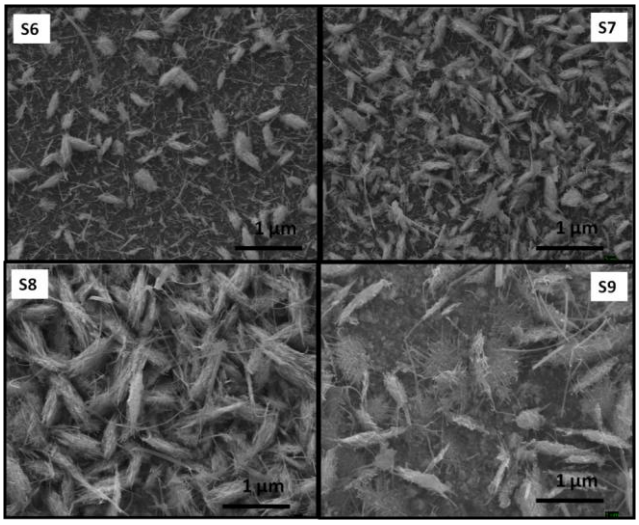

Figure 4. SEM images of ZnO+$ZnAl_2O_4$ composite nanostructures prepared from (S6) 100 nm Al film over 130 nm Zn film and annealed at 500 °C for 1h. (S7) 130 nm Al film over 130 nm Zn film and annealed at 500 °C for 1 h. (S8) 160 nm Al film over 130 nm Zn film and annealed at 500 °C for 1 h. (S9) 200 nm Al film over 130 nm Zn film and annealed at 500 °C for 1 h.

density of structure increases as shown in Figure 5. Thus, annealing temperature and Al thickness strongly determines optimal growth. At 550 °C, nanostructures grown from 160 nm Al have whisker growth and also nanowires are entangled with each other.

The chemical composition of the nanostructured material was evaluated using EDX spectra for 160 nm Al film annealed at 400 and 550 °C. The results are presented in Figure 6. It is evident that the structure consists of oxygen, aluminum and zinc. The atomic ratios of oxygen, zinc and aluminum for composite film annealed at 400 and 550 °C are 53.3-26.2-20.5 and 55.4-23.3-21.3. The oxygen percentage increased when annealing was performed at higher temperature. The zinc and aluminum percentages are nearly equal as expected, since corresponding thicknesses are 130 and 160 nm. Sample oxidized at 400 °C has shown a minor peak and its intensity is very small.

The crystalline phase of Al (160 nm) - Zn metal film and its corresponding oxide composite obtained by oxidation at 550 °C were investigated using XRD. The results are shown in Figure 7. As expected, the XRD peaks for the as-deposited metal film corresponds to Zn and Al. The peaks in oxidized sample are for hexagonal ZnO and spinal $ZnAl_2O_4$. From XRD results, it is evident that there are no peaks corresponding to Zn and Al in oxidized sample which confirms that the sample is completely oxidized. It is further observed that both $ZnAl_2O_4$ and ZnO phases are present in the sample. The dominant peak corresponds to (311) $ZnAl_2O_4$ phase but several small peaks corresponding to ZnO are also present.

To study the role of underlying Zn on nanostructures formation, one sharp step was created during Al (130 nm) film deposition and schematically shown in Figure 8(a). This film was oxidized at 550 °C and the SEM micrograph is shown in Figure 8(b). Several researchers have reported that Zn film turns into ZnO film/nanowire when oxidized at 400 - 600 °C

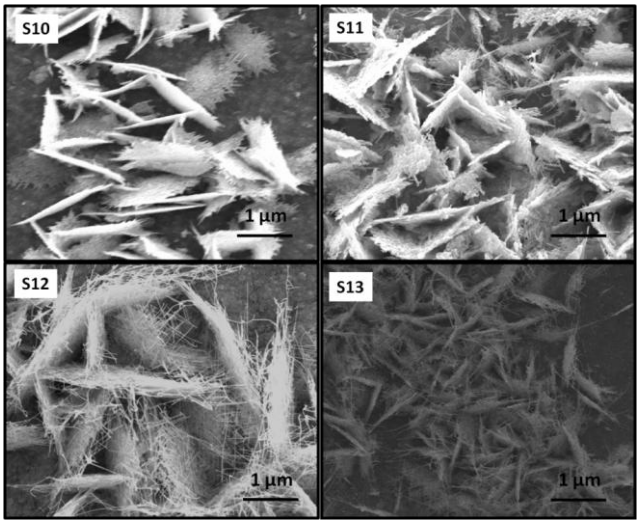

Figure 5. SEM images of $ZnO+ZnAl_2O_4$ composite nanostructures prepared from (S10) 100 nm Al film over 130 nm Zn film and annealed at 550 ^oC for 1 h. (S11) 130 nm Al film over 130 nm Zn film and annealed at 550 ^oC for 1 h. (S12) 160 nm Al film over 130 nm Zn film and annealed at 550 ^oC for 1 h. (S13) 200 nm Al film over 130 nm Zn film and annealed at 550 ^oC for 1h.

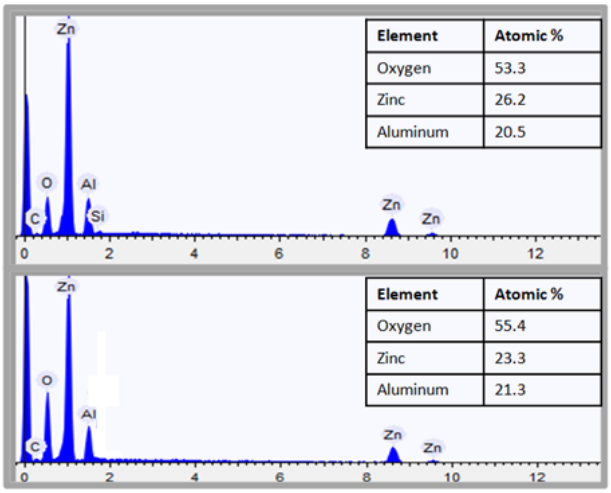

Figure 6. EDX spectra of composite nanostructures.

temperature [35]. In the present studies, it is observed that Zn film has turned into ZnO nanoneedles and nanowires whereas Al-Zn is converted into whiskers (Figure 8(c) and 8(d)). From XRD data, it is confirmed that the whiskers are composed of a mixture of ZnO and $ZnAl_2O_4$. It is postulated that Kirkendall effect is responsible for this growth. Kirkendall effect essentially states that two metals (layers), when heated, diffuse into each another at different rates. First top Al turns into Al_2O_3 and bottom Zn ion causes outward diffusion resulting in vacancies, which are known as Kirkendall voids. These voids enhance oxygen diffusion from ambient to form ZnO and $ZnAl_2O_4$. R. Nakamura et al. has proved that Kirkendall voids create nanoporous structure. Further annealing leads to direct reaction of oxygen with bottom Zn and hence ZnO nanowire/nanoneedle growth takes place [36, 37]. The nanowire/nanoneedle lengths will not be uniform since oxygen

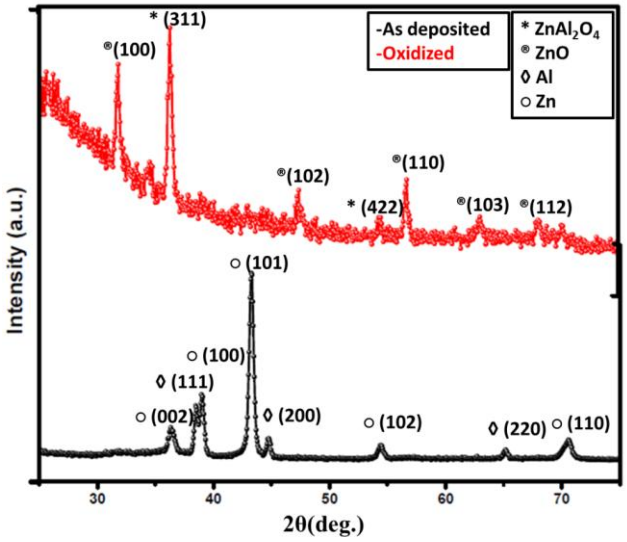

Figure 7. XRD patterns for (i) as-deposited 160 nm Al over Zn and (ii) after oxidation at 550 ^oC for 1 h.

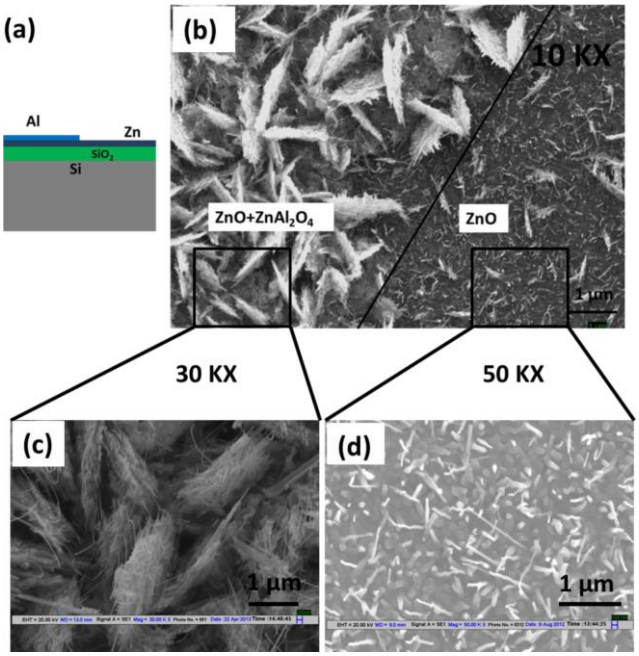

Figure 8. (a) Schematic diagram of multilayered metiallic film before oxidation (b) SEM images of ZnO-$ZnAl_2O_4$ composite nanostructures and ZnO nanoneedles/nanowires (c) Magnified SEM image of ZnO-$ZnAl_2O_4$ whisker (d) Magnified SEM image of ZnO nanoneedles/nanowires.

supply is not uniform. These nanowires/nanoneedles will cause stress on top porous structure and morphology will be in whisker form.

3.2. Spectroscopic characterization of biochip

FT-IR spectroscopy was applied to measure the surface properties of the enzyme ALP coupling through SAMs via the carbodiimide cross-linking reaction on ZnO-$ZnAl_2O_4$ surfaces. FT-IR ATR spectra were collected at a resolution of 4 cm^{-1} (128 scans). The FT-IR spectra recorded for ZnO-$ZnAl_2O_4$ coupled enzyme (ALP) via 16-PHA crosslinker are shown in Figure 9. Figure 9(a) is FT-IR spectrum of the bare

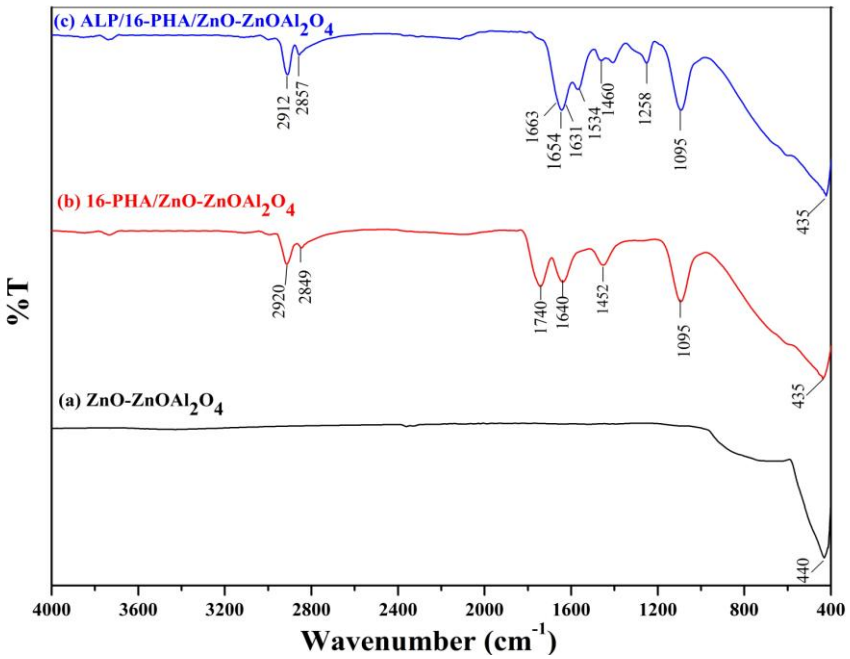

Figure 9. The ATR FT-IR spectrum of (a) the Bare ZnO-$ZnOAl_2O_4$ microwell (b) ZnO-$ZnOAl_2O_4$ treated with 16-PHA (c) Enzyme (ALP) coupled through 16-PHA functionalized ZnO-$ZnOAl_2O_4$. Spectra were acquired using 128 scans at 4 cm^{-1} resolution collected under vacuum conditions.

ZnO-$ZnAl_2O_4$. Figure 9(b) is FT-IR spectra 16-PHA functionalized ZnO-$ZnAl_2O_4$. Figure 9(c) is FT-IR spectrum of covalently coupled enzyme on ZnO-$ZnAl_2O_4$.

In Figure 9(a), the peaks appearing in the range of 440–510 cm^{-1} can be assigned to the stretching vibrations of Zn–O. Figure 9(b) showed the asymmetric (ν_{as}(C-H)) and symmetric methylene stretches (ν_s(C-H)) of 16-PHA-modified ZnO-$ZnAl_2O_4$ that appear at 2920 cm^{-1} and 2849 cm^{-1} respectively. These bands of 16-PHA modified ZnO whiskers suggest methylene chains during monolayer growth. The C=O stretch at 1740 cm^{-1} on ZnO-$ZnAl_2O_4$ associated with asymmetric and symmetric COO^- stretch at 1640 cm^{-1} is characteristics of an organic carboxylic compound. The additional IR peaks at 1452 cm^{-1} is ascribed to C-H deformation. The existence of the peak at 1095 cm^{-1}, which is characteristic of the P=O stretching mode, is a possible evidence for bidentate binding modes. The observation of P-OH related modes due to binding of 16-PHA was extensively reported elsewhere [23].

ALP coupling through 16-PHA SAMs via the carbodiimide cross-linking reaction on ZnO-$ZnAl_2O_4$ surfaces is presented as Figure 9(c). Upon immobilization of enzyme three new absorption bands appeared; IR bands at 1654 cm^{-1}, 1534 cm^{-1}, and 1258 cm^{-1} are ascribed to the absorption by the amide group that links enzyme to 16-PHA functionalized ZnO-$ZnAl_2O_4$. Also the bands at 1663 cm^{-1}, 1631 cm^{-1} and 1460 cm^{-1} are for all biomolecules' common structural unit i.e., the amide I region.

3.3. Biochip based bio-catalysis

Bio-catalysis reaction on biochip involves appropriate enzymatic reaction between substrate and catalyst enzyme. A minor change in pH, ionic strength and temperature can sometimes be responsible to lose the biological activity, as immobilized enzymes are very much sensitive towards environmental changes. Herein the optimized parameters have been adopted elsewhere [38].

The enzyme activity was tested on the novel biochip by addition of different concentration of pNPP. 6 µL of pNPP and $MgCl_2$ (2:1 ratio) was added to the wells of biochip. It was incubated for 1 h at room temperature. Then the yellow colored products were taken inside a 96 well optiplate and further diluted in 100 µL GB. The absorbance was measured at 405 nm for 0.1 s. The absorbance plot of different pNPP concentrations ranging 10 mM to 0.001 mM is presented in Figure 10. It was observed that, the absorbance values increased as the concentration of substrate increased resulting in production of more colored product by the catalyst (ALP). The calibration was found to be linear in the range 0.001 mM to 10 mM (R^2 = 0.99, n = 5) with a relative standard deviation (RSD) of 3.21% ± 0.27 for the ALP/16-PHA/ZnO-$ZnAl_2O_4$ (Figure 10(a) Inset). The linear equation was y = 0.4057 + 0.10673x (mM). Limit of detection (LOD) and limit of quantitation (LOQ) was 0.001 mM by analyzing replicate sets of ALP/16-PHA/ZnO-$ZnAl_2O_4$ with good sensitivity about 1.25 unit change per decade. Whereas for physisorbed enzyme ALP/ZnO-$ZnAl_2O_4$, the linearity was found in the range 0.01 mM to 10 mM (R^2 = 0.98, n = 5) with an RSD of 5.49% ± 0.61 (Figure 10(b) Inset). The linear equation was y = 0.11509 + 0.23882x (mM). LOD was determined as 0.01 mM and LOQ was 0.1 mM by analyzing replicate sets with very low sensitivity about 0.29 unit change per decade. Lower LOD, LOQ value, R^2 and sensitivity indicate that ALP/16-PHA/ZnO-$ZnAl_2O_4$ is much superior over physisorbed enzyme ZnO-$ZnAl_2O_4$.

In developing an enzyme based process, kinetic constants are the most important information. Simple enzyme kinetics is generally described by the Michaelis–Menten kinetics (Eq. (1)).

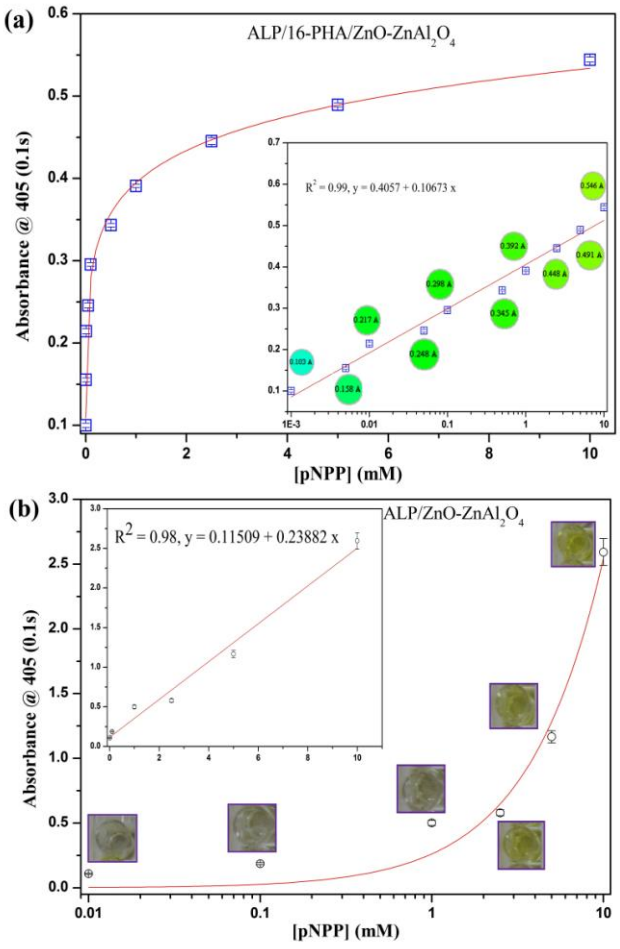

Figure 10. (a) Calibration curve for different pNPP concentration obtained using enzyme ALP coupled on 16-PHA modified ZnO-$ZnAl_2O_4$ biochip (Inset: the linear calibration graph) (b) Calibration curve for different pNPP concentration obtained using enzyme ALP physisorped on ZnO-$ZnAl_2O_4$ biochip (Inset: the linear calibration graph). pNPP diluted ranging from 0.001 mM to 10 mM in GB.

$$1/V = K_m/ V_{max} \times 1/[S] + 1/V_{max} \quad (1)$$

where V is the enzymatic reaction rate (mmol/min mg enzyme), S is the substrate concentration (mM), V_{max} is the maximum or limiting reaction rate (mmol/min mg enzyme) and K_m is the Michaelis–Menten constant (mM). The determination of numerical values of K_m was obtained by plotting 1/V versus 1/S (known as a Lineweaver–Burk plot).

An important feature that accounts for enzyme stability is the improvement obtained in the value of Michaelis–Menten constant (K_m). The K_m value obtained was estimated 0.63 mM for ALP/16-PHA/Zno-$ZnAl_2O_4$ whereas 1.04 mM for physisorped enzyme on Zno-$ZnAl_2O_4$. The lower K_m value (almost 1.65 times) reflects the covalently coupled enzyme over the physisorped enzymes facilitated enhanced stability of ZnO-$ZnAl_2O_4$ biochip. This confirmed that the catalyst (ALP) was successfully bound to the novel nanomaterials proving its efficiency in product formation. Thus the presented material provided a suitable substrate for development of high catalytic efficiency, miniaturized devices.

4. Conclusions

A simple and efficient technique to synthesize ZnO-$ZnAl_2O_4$ composite whiskers has been reported. The use of ZnO-$ZnAl_2O_4$ whiskers as novel biochip using immobilized ALP enzyme is demonstrated for bio-catalysis. The formation of ZnO-$ZnAl_2O_4$ whiskers were performed on oxidized Si using a simple route at low temperature. The optimal conditions for growth of uniform whisker are 160 nm Al film deposited over 130 nm Zn film and oxidized at 550 $^{\circ}$C for 1 h in atmospheric ambient. The measured lower LOD and LOQ for p-NPP, higher sensitivity and improved K_m of ALP activity confirmed enhanced bio-catalytic efficiency. The developed biochip presented satisfactory repeatability for whisker having cross-linked immobilized enzyme over physically adsorbed for analysis of p-NP.

Acknowledgements

This work is partly supported by National Funds for Basic& Strategic Research in Frontier Areas of Agricultural Sciences NFBSFARA of ICAR India. The research has been financially supported by NAIP, ICAR India through Project Number C10125 (Component-4). We also gratefully acknowledge Nanoscale Research Facility (NRF), IIT Delhi for providing assistance with thickness measurement.

References

1. L. Wang, Y. Kang, X. Liu, S. Zhang, W. Huang, and S. Wang, Sens. Actuat. B 162 (2012) 237.
2. M. J. S. Spencer, I. Yarovsky, J. Phys. Chem. C 114 (2010) 10881.
3. N. K. Hassan, M. R. Hashim, M. Bououdina, Superlattices Microstruct. 62 (2013) 182.
4. T. J. Athauda, P. Hari, R. R. Ozer, ACS Appl. Mater. Interfaces 5 (2013) 6237.
5. N. Zhang, K. Yu, Q. Li, C. Song, L. Zhu, Z. Zhu, Mater. Lett. 121 (2014) 231.
6. W. Liang, B. D. Yuhas, P. Yang, Nano Lett. 9 (2009) 892.
7. Y. Q. Chen, X. J. Zheng, X. Feng, Nanotechnology 21 (2010) 055708.
8. T. Santhaveesuk, D. Wongratanaphisan, S. Choopun, Sens. Actuat. B 147 (2010) 502.
9. H. Shokry Hassan, A. B. Kashyout, H. M. A. Soliman, M. A. Uosif, N. Afify, Appl. Surf. Sci. 277 (2013) 73.
10. Y. C. Yang, C. Song, X. H. Wang, F. Zeng, F. Pan, Appl. Phys. Lett. 92 (2008) 012907.
11. S. Farhadi, S. Panahandehjoo, Appl. Catal. A 382 (2010) 293.
12. S. K. Sampath, J. F. Cordaro, J. Am. Ceram. Soc. 81 (1998) 649.
13. M. Davis, C. Gümeci, R. Alsup, C. Korzeniewski, L. J. Hope-Weeks, Mater. Lett. 73 (2012) 139.
14. T. El-Nabarawy, A. A. Attia, M. N. Alaya, Mater. Lett. 24 (1995) 319.
15. D. P. Dutta, R. Ghildiyal, A. K. Tyagi, J. Phys. Chem. C 113 (2009) 16954.
16. X. Zhao, L. Wang, X. Xu, X. Lei, S. Xu, F. Zhang, Aiche J. 58 (2012) 573.
17. C. Aydın, M. Benhaliliba, A. A. Al-Ghamdi, Z. H. Gafer, F. El-Tantawy, F. Yakuphanoglu, J. Electroceramics 31 (2013) 265.
18. Li-Hua Zhao, Rui Zhang, Jing Zhanga, Shu-Qing Sun, Cryst. Eng. Commun. 14 (2012) 945.
19. M. A. Alvarez-Pérez, M. García-Hipolito, J. de La Fuente Hernández, H. Arzate, B. Carmona-Rodriguez, L. A. Ximenez-

Fyvie, J. A. Juarez-Islas, O. Alvarez-Fregoso, J. Nano Res. 5 (2009) 169.
20. J. L. Suárez-Franco, M. García-Hipólito, M. Á. Surárez-Rosales, J. A. Fernández-Pedrero, O. Álvarez-Fregoso, J. A. Juárez-Islas, M. A. Álvarez-Pérez, J. Nanomater. 2013 (2013) 1.
21. J. Zhao, L. Xu, T. Zhang, G. Ren, Z. Yang, Neurotoxicology 30 (2009) 220.
22. C. M. Rico, S. Majumdar, M. D-Gardea, J. R. P. Videa, J. L. G. Torresdey, J. Agric. Food. Chem. 59 (2011) 3485.
23. S. Pal, M. K. Sharma, B. Danielsson, M. Willander, R. Chatterjee, S. Bhand, Biosens. Bioelectron. 54 (2014) 558.
24. J. P. Lalles, Nutr. Rev. 68 (2010) 323.
25. T. D. Y. Chung, E. Sergienko, J. L. Millan, Molecules 15 (2010) 3010.
26. F. G. Sanchez, A. N. Diaz, M. C. R. Peinado, C. Belledone, Anal. Chim. Acta 484 (2003) 45.
27. W. L. Claeys, A. M. Van Loey, M. E. Hendrickx, Trends Food Sci. Tech. 13 (2002) 293.
28. V. F. Ximenes, A. Campa, W. J. Baader, L. H. Catalani, Anal. Chim. Acta 402 (1999) 99.
29. S. Sidique, R. Ardecky, Y. Su, S. Narisawa, B. Brown, J. L. Millan, E. Sergienko, N. D. P. Cosford, Bioorg. Med. Chem. Lett. 19 (2009) 222.
30. J. Iqbal, Anal. Biochem. 414 (2011) 226.
31. S. M. Wang, P. Su, Y. Yang, Anal. Biochem. 427 (2012) 139.
32. S. M. Wang, P. Su, E. Hongjun, Y. Yang, Anal. Biochem. 405 (2010) 230.
33. T. B. Goriushkina, A. P. Soldatkin, S. V. Dzyadevych, J. Agric. Food. Chem. 57 (2009) 6528.
34. Z. Liu, H. S. Wang, B. Li, C. Liu, Y. J. Jiang, G. Yu, X. D. Mu, J. Mater. Chem. 22 (2012) 15085.
35. D. Zappa, E. Comini, G. Sberveglieri, Nanotechnology 24 (2013) 444008.
36. R. Nakamura and H. Nakajim, Nanowires - Implementations Application, InTech (2011) pp. 101-116.
37. H. J. Fan, U. Gösele, M. Zacharias, Small 3 (2007) 1660.
38. R. K. Mishra, G. K. Mishra, Dharma Teja V, B. Danielsson, S. Bhand, Chem. Sens. 3 (2013) 12.

Cite this article as:

Bhagaban Behera *et al.*: **Synthesis and characterization of ZnO-$ZnAl_2O_4$whiskers and their application in biosensors.** ScienceJet 2015, **4**: 102

Microchim Acta
DOI 10.1007/s00604-015-1489-5

ORIGINAL PAPER

Zinc oxide nanoparticle-enhanced ultrasensitive chemiluminescence immunoassay for CEA the carcinoma embryonic antigen

Souvik Pal[1] · **Sunil Bhand**[1]

Received: 23 December 2014 / Accepted: 30 March 2015

Abstract An ultrasensitive enzyme-linked immunosorbent assay (ELISA) is reported for the determination of carcinoma embryonic antigen (CEA) in human serum. It was realized using a microplate reader using a 384-well plate. Monoclonal antibody (Ab) against CEA (1° Ab) acting as the capture probe was immobilized on zinc oxide nanoparticles (ZnO-NPs) in the form of self-assembled monolayers (SAMs). CEA captured by 1° Ab was quantified using a sandwich ELISA wherein a polyclonal second antibody against CEA (2° Ab) was used for detection and quantified using an HRP-labeled secondary antibody (3° Ab). The ZnO-NPs-CEA capture probe was deposited on the bottom of the wells in order to enhance capture of CEA. A 3-fold enhancement in the chemiluminescence (CL) signal of luminol is found (compared to a conventional ELISA). CEA can be quantified by this method in concentrations as low as 1 pg·mL^{-1}. The upper limit of detection is 20 ng·mL^{-1}. The use of ZnO-NPs also imparts improved thermal stability. When stored at 4 °C in phosphate-buffered saline of pH 7.4, the probe displays stability of up to 30 days.

Keywords Carcino embryonic antigen · Zinc oxide · Self-assembled monolayer · Sandwich ELISA · Serum · Chemiluminescence

Electronic supplementary material The online version of this article (doi:10.1007/s00604-015-1489-5) contains supplementary material, which is available to authorized users.

✉ Sunil Bhand
sunil17_bhand@yahoo.com; sunilbhand@goa.bits-pilani.ac.in

[1] Biosensor Lab. Department of Chemistry, BITS, Pilani –KK Birla Goa Campus, Goa 403726, India

Introduction

The determination of tumor makers is one of the important prognostic factors in clinical research and diagnosis. The levels of tumor markers in blood or tissue provide essential information for clinical cancer screening and disease diagnosis. Sensitive detection of the bio-markers is vitally important for timely diagnosis and treatment of early stage cancers, which largely determines the survival rate of cancer patients [1, 2]. Immunoassay is an easy and low-cost method in the detection of antigen or its specific antibody in clinical diagnostics [3]. Because of its adaptability, simplicity and sensitivity, enzyme-linked immunosorbent assay (ELISA) is one of the most extensively used analytical techniques in clinical research [4, 5]. Owing to their high sensitivity, preclusion of radiation damage and relatively simple instrumentation, chemiluminescence (CL) immunoassays have been commonly applied in the routine clinical analysis [6]. The sensitivity of conventional polystyrene plate ELISA for subsequent antibody (Ab) – Antigen (Ag) recognition and binding have been failed due to the low surface-to-volume ratio of the plate and the random orientation of the adsorbed Ab [7]. As the concentrations of cancer bio-markers are extremely low, i.e., ng·mL^{-1} or lower in vivo [8, 9], therefore, developing miniaturized ELISA for improved sensitivity, lower limit of detection and reproducibility is a paramount need in routine diagnosis. Sandwich-type immuno-sensors and immunoassay methods were developed for detection of Ag with more than one epitope due to the use of matched antibodies. High-affinity antibodies and appropriate labels were usually employed for the amplification of detectable signal. Use of nanoparticles (NPs) in the sandwich-type immuno-sensors and immunoassays has been increased recently as the innovative and powerful novel NPs labels developed with controlling and tailoring their properties in a very predictable manner to meet the requirements of specific applications by exploiting NPs labels [4].

Carcinoembryonic antigen (CEA), a polysaccharide–protein complex, is one of the most studied tumor markers due to its association with liver, colon, colorectal and breast cancer and existence in endoblast origin digestive system cancer [10]. Higher levels of CEA in serum were reported for individuals with colorectal, gastric, pancreatic, lung, and breast carcinomas, as well as individuals with medullary thyroid carcinoma than healthy individuals [11, 12]. The reported concentrations of CEA are 2.5 $ng \cdot mL^{-1}$ for non-smokers and 5.0 $ng \cdot mL^{-1}$ for smokers, respectively [13]. Thus, accurate determination of CEA is of significance for monitoring and prognosis of disease recurrence. The long-term survival of cancer patients can be improved by considering the levels of CEA in human organism, which reflects the disease progression or regression status [14]. As a result, there is an immense need for a sensitive immunoassay technique to detect a sub-nanogram per milliliter level.

Recently, we have demonstrated a novel enzymatic nanobiosensor for choline using ZnO nanorods (ZnONR) stabilized using 16-phosphonohexadecanoic acid (16-PHA) [15]. Herein, we report the development of ultra-sensitive NPs based ELISA for detection of CEA levels in human serum using zinc oxide nanoparticles based CEA probe (ZnO-NPs-CEA). The develop ZnO-NPs-CEA assay exhibited enhanced signal intensity, broader linear range and thermal stability over the conventional ELISA. A significant enhancement in sensitivity (about two fold per decade) was achieved with a lower limit of detection 1 $pg \cdot mL^{-1}$. The use of 1° Ab coupled ZnO-NPs as affinity capture material using a miniaturized microwell plate platform for CEA gave better efficiency of capture and stability over reported materials (Table 1).

Experimental

The materials and apparatus used are described in the Electronic Supplementary Material (ESM).

Preparation of buffers and samples

For coating purpose, a 50 mM carbonate buffer (CB) was prepared. The pH was adjusted to 9.6. As CB can change the composition over time, it was made fresh each time. 10 mM phosphate-buffered saline (PBS, pH 7.4) containing 137 mM NaCl, 2 mM KCl was used for incubation and washing purpose. Another washing buffer (PBST) was made by adding 0.05 % Tween 20 (*v/v*) in PBS. All buffer solutions were stored at 4 °C when not in use. The blocking solution was prepared by adding 2.5 % (*w/v*) BSA to PBS.

The stock 1° Ab (2 $mg \cdot mL^{-1}$) was diluted in 10 mM PBS to the final concentration (0.2 $\mu g \cdot mL^{-1}$). The stock 2° Ab (2 $mg \cdot mL^{-1}$) specifically to 1° Ab was diluted to 0.5 $\mu g\ mL^{-1}$ as indicated by manufacturer's protocol. 1 μL of the stock solution of 3° Ab-HRP (2 $mg \cdot mL^{-1}$) was diluted with 50 μL of de-ionized water. From the 1:50 dilution, working 3° Ab-HRP solution was prepared prior to the experiment by diluting 1:100, 1:500 and so on in PBS. The standard serum was used without any further dilution. CEA spiked serum solutions were prepared by standard addition method in the range 20–0.001 $ng \cdot mL^{-1}$.

CEA analysis using conventional ELISA

All liquid pipetting was performed using Eppendorf multichannel pipette in automatic mode. Conventional sandwich ELISA was performed in 384 microwell plate. An optimized 1° Ab was diluted to 0.2 $\mu g \cdot mL^{-1}$ in CB. Diluted 1° Ab (40 μL) was coated in each microwell. The plate was covered and kept at room temperature for 3 h. Each microwell was washed three times with 60 μL PBS. The remaining protein binding sites in the coated wells were blocked by adding 20 μL of 2.5 % BSA blocking solution for 1 h at room temperature. The plate was washed with 50 μL PBST. Following this step, CEA spiked serum samples in the range 20–0.001 $ng \cdot mL^{-1}$ were added as 20 μL in each well. The plate was incubated for about 2 h at room temperature. The unbound CEA antigen was removed by washing three times with 60 μL PBS. Then 1:1 mixture of optimized 2° Ab and 3° Ab-HRP was prepared. The excess label was removed by washing PBS. The final solution was added as 30 μL in each well. The plate was kept for 2 h at room temperature. The excess label was removed by washing three times with 60 μL PBS. The chemiluminescence (CL) substrate (1 μL of 0.05 M H_2O_2+ 4 μL of 0.5 mM luminol) was added. The signal intensity was kinetically measured at the steady state and stability was found after 30 min.

Construction of ZnO-NPs – CEA capture probe

Surface modification The development of CEA capture probe was based on the efficient immobilization of very specific anti-CEA 1° Ab through carboxy terminated SAMs on ZnO-NPs. The glass container used for monolayer preparation was cleaned with Piranha solution (a mixture of 98 % H_2SO_4 and 30 % H_2O_2, 7:3, *v/v*; caution: piranha solution reacts exothermally and strongly reacts with organics) for 1 h and rinsed exhaustively with de-ionized (DI) water and ethanol. 16-PHA modified ZnO-NPs were prepared as described in our previous report [15]. Briefly, 3 mg of ZnO-NPs was dispersed in 0.5 mM ethanolic solution of 16-PHA. The resulted suspension of particles was mechanically stirred for 72 h for SAMs formation.

Covalent coupling of 1° Ab onto ZnO-NPs For antibody immobilization, the carboxylic acid-terminated SAMs were modified using an aqueous equimolar solution of 100 mM

Q1

Q4 t1.1 **Table 1** Comparison of present assay with earlier reported immunosensors

t1.2 Sensor configuration	Transduction principle	Linear detection range (ng·mL-1)	Limit of detection (pg·mL-1)	References
t1.3 ZnO-NPs coupled 1° Ab on 384 microwell plate	Sandwich CL immunoassay	0.001 – 20	1.0	This work
t1.4 Conventional ELISA	Sandwich CL immunoassay	0.01 – 10	10	This work
t1.5 Ab2-PdPt-Thi/Fc as probes	Electrochemical	0.05 – 200	1.4	[25]
t1.6 Conjugated biotinylated anti-CEA Ab on streptavidine coated superparamagnetic beads	Sandwich CL immunoassay	0.005 – 50	5.0	[3]
t1.7 Fe3O4@C@CdTe QDs composit with CEA-mAb1 and the ZnO NWs	Sandwich fluorometric immunoassay	0.005 – 100	1.6	[26]
t1.8 ZnONPs and glucose oxidase decorated graphene	Sandwiched luminol electrochemiluminescence immunosensing	0.01 – 80	3.3	[27]

EDC /100 mM NHS for 2 h at room temperature. The resultant NHS ester monolayers were reacted in room temperature for 3 h in 1:1 solution of 1° Ab (0.2 μg·mL^{-1}) and CB. The 1° Ab coated ZnO-NPs (1° Ab-ZnO-NPs) were washed with PBS.

ZnO-NPs based ELISA The ZnO-NPs-CEA capture probe was coated in the bottom of the 384 well plates for enhanced capture of CEA antigen. The remaining protein binding sites in the ZnO-NPs were blocked by adding 20 μL of 2.5 % BSA blocking solution for about 1 h at room temperature. After washing step by PBST, CEA spiked serum samples (20 μL in each well) were incubated for 2 h at room temperature. The particles were washed again with 50 μL PBS to remove unbound CEA. The 2° Ab (15 μL) was incubated at room temperature for 2 h with the particles. Finally, for CL measurements, 15 μL of 3° Ab-HRP (1:2000) was incubated at room temperature for 1 h with the particles. The excess label was removed by washing with PBS. The CL substrate (1 μL of 0.05 M H_2O_2+4 μL of 0.5 mM luminol) was added. The signal intensity was kinetically measured at the steady state, and stability was found after 25 min.

The hybrid- immuno assay was realized in 384 micro well plates using anti CEA- monoclonal antibody (1° Ab) immobilized on ZnO-NPs via self-assembled monolayer as capture probes. The captured antigen was quantified using sandwich ELISA wherein a polyclonal anti CEA 2° Ab was used for detection and quantified using an enzyme labeled secondary antibody 3° Ab. The schematic of the detection procedure is shown in Fig. 1.

Results and discussions

Choice of materials

Bio-sensing techniques commonly rely upon the use of bio-functionalized NPs, inorganic-biological hybrid NPs, and signal tag-doped NPs [16]. The enormous signal enhancement associated to the use of NPs labels, and with the formation of nanoparticle-antibody-antigen assemblies provides the basis for sensitive detection of disease-related proteins or biomolecules [17]. Hybrid approaches involve noble metal NPs, carbon NPs, semiconductor NPs, metal oxide nano-structures, and hybrid nano-structures. Nano-structured metal oxides of zirconium, titanium, cerium, tin and zinc have gained much attention in bio-sensor and immuno-sensor application owing to their large surface to volume ratio, high surface reaction activity, high catalytic efficiency, and strong adsorption ability.

Choice of nano-structured oxide materials is crucial for immobilization of the desired biomolecule. The interface formed due to binding between an oxide nano-material and a

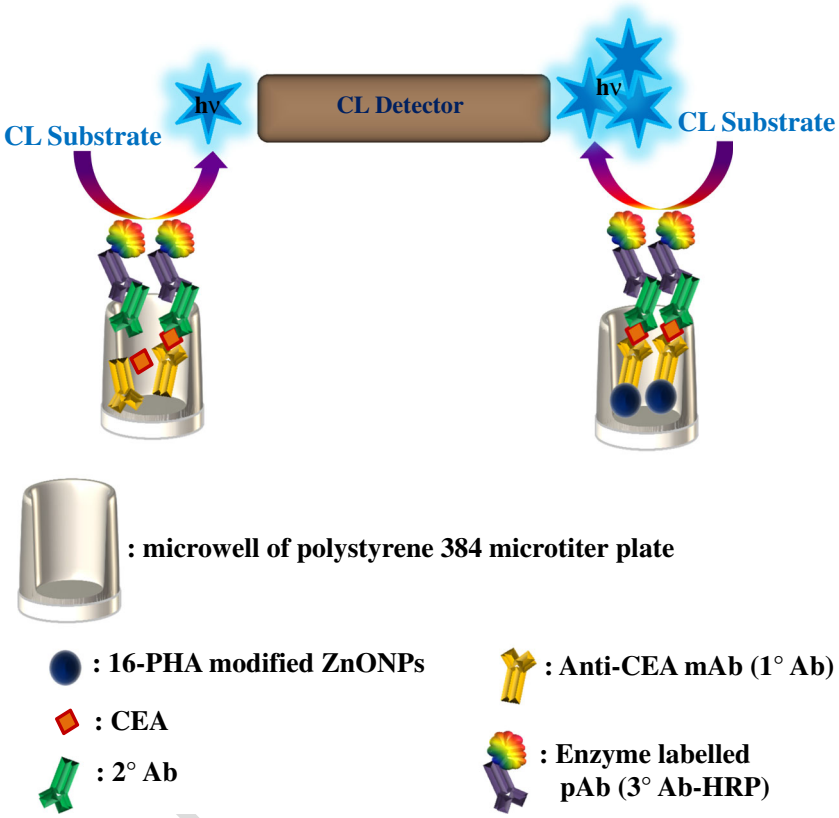

Fig. 1 Schematic representation of the CEA recognition process

biomolecule can influence the performance of an immunosensor. The formation and properties of a nano – bio interface depends upon the nature of nano-structure parameters like surface charge, valence/conductance states, functional groups, physical states and hygroscopic nature [16].

Among the other reported metal oxide nano-structures, ZnO is well known for its biocompatibility, high specific surface area, chemical and photochemical stability, excellent light transmission, strong electrochemical and electron communication response and lack of toxicity [18]. Owing to its non-toxicity, good bio-compatibility and high chemical stability, ZnO was used widely in construction of bio-sensors [19]. The high isoelectric point of ZnO, which is about 9.5, plays an important role in biological pH [20]. Due to lowering of isoelectric point in biological pH, the surface of ZnO has a positive charge; protein with a low isoelectric point (in case of CEA is 4.7) can be immobilized on it by an electrostatic force [21]. Furthermore, it was observed that ZnO-NPs based luminol-H_2O_2 system can also enhance the CL signals. The CL enhancement of ZnO-NPs may be attributed to the catalysis of ZnO-NPs on the radical generation and electron-transfer processes during the luminol CL reaction [22]. These observations indicate that the ZnO-NPs promote electron transport and thus improved the sensitivity and selectivity as compared to conventional ELISA.

Characterization of ZnO-NPs – CEA probe

Affinity analysis of ZnO-NPs – CEA capture probe

Real time binding analysis using QCM was performed to confirm the CEA binding on the 16-PHA modified ZnO surface. The functionalized quartz crystal ZnO-16PHA (10 MHz, non-bonded) was placed in a plexiglass flow cell in static mode, sandwiched between two O-rings and connected to the frequency-measuring unit. The direct mass change was recorded using Voltascan 5 software. The data was plotted and presented as Fig. 2a. The 16-PHA modified ZnO quartz crystals were prepared for the QCM study as described earlier. The binding of 1° Ab, CEA, 2° Ab and 3° Ab-HRP were performed in static mode using the optimized condition as earlier. The mass change was recorded after each step. The increasing change in mass confirms the stepwise binding of (i) 1° Ab (anti-CEA), (ii) CEA-Ag, (iii) 2° Ab and (iv) 3° Ab-HRP. The 1° Ab attached on SAMs modified ZnO crystal showed the initial mass of 121 ng. Subsequent mass changes of 91 ng, 303 ng, 331 ng and 223 ng were observed for the attachment of 1° Ab, CEA, 2° Ab and 3° Ab-HRP respectively as shown in Fig. 2a. Upon using 2° Ab for CEA recognition, a mass change of 28 ng was observed. Whereas, with the 3° Ab as recognition probe, a negligible mass change (0.048563 ng).was observed.

Q1

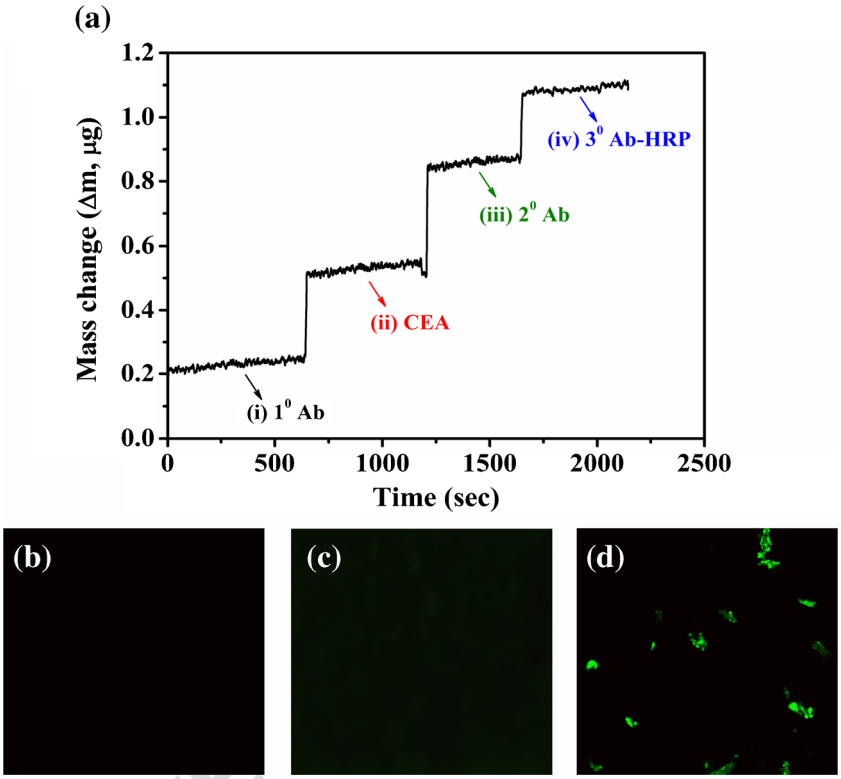

Fig. 2 **a** Stepwise mass change response on SAMs modified ZnO crystal after the attachment of (i) 1° Ab (anti-CEA); (ii) CEA-Ag; (iii) 2° Ab, and (iv) 3° Ab-HRP; Fluorescence image of **b** reference 1° Ab-ZnO-NPs without 3° Ab-FITC, **c** sample 1° Ab-ZnO-NPs directly coupled with labelled 3° Ab (3° Ab-FITC), **d** sample 1° Ab-ZnO-NPs coupled with unlabelled 2° Ab and 3° Ab-FITC at 20× magnification; incubated with 3° Ab-FITC (1:8000) (λ_{ex} 480 nm / λ_{em} 520 nm)

Thus, it can be concluded that 2° Ab was working as recognition of CEA. Further, the significant mass change observed for CEA capture using the ZnO-16PHA-anti CEA (about 212 ng) provided a strong evidence of the enhanced surface to volume ratio available for successful construction of a ZnO-NPs based immuno-sensor.

Fluorescence binding studies of 3° probe

The specificity of the 3° Ab was further confirmed by fluorescence microscopy. Microscopy slides were prepared as (a) reference 1° Ab-ZnO-NPs without 3° Ab-FITC, (b) sample 1° Ab-ZnO-NPs directly coupled with labelled 3° Ab (3° Ab-FITC) and (c) sample 1° Ab-ZnO-NPs coupled with unlabelled 2° Ab and 3° Ab-FITC. During measurement, suspended 1° Ab-ZnO-NPs (3 μL) were spotted onto three glass slide that were dried by keeping in a humidity chamber at room temperature. One of the spotted 1° Ab-ZnO-NPs glass microscopy slides was named as reference (1° Ab-ZnO-NPs without 3° Ab-FITC). Another glass slide among the three was incubated with 3° Ab-FITC (1:8000) for 2 h at room temperature in dark. This slide was designated as sample (1° Ab-ZnO-NPs directly coupled with labelled 3° Ab). The remaining glass slide was incubated with 2° Ab (15 μL) at room temperature for 2 h. Finally, for fluorescence measurements, 15 μL of 3° Ab-FITC (1:8000) was incubated at room temperature for 2 h in dark. This slide was also assigned as sample (1° Ab-ZnO-NPs coupled with unlabelled 2° Ab and 3° Ab-FITC). Before excitation the sample slides were rinsed with 10 mM PBS to remove unbound 3° Ab-FITC. The reference 1° Ab-ZnO-NPs without 3° Ab-FITC and sample 1° Ab-ZnO-NPs directly coupled with labeled 3° Ab (3° Ab-FITC) showed negligible fluorescence signal as the binding is non-specific (Fig. 2b and c). The binding between 1° Ab on ZnO-NPs and 1° Ab specific unlabelled 2° Ab, 3° Ab-FITC were demonstrated by a bright fluorescence signal from the agglomerated spots (Fig. 2d). These observations proved that the 1° Ab on ZnO-NPs preserved the excellent biological recognition of antibody to their targets.

Development of immunoassay

Optimization of experimental conditions

The optimum results for the ionic strength and pH of PBS were found at 10 mM, pH 7.4 (Supplementary Figure S1 and S2). It was found that a 3° Ab-HRP dilution of 1:2000 produced better signal intensity against 1° Ab (0.2 $\mu g \cdot mL^{-1}$) (Supplementary Figure S3). Further, the amount of ZnO-NPs – CEA probe particles was also optimized as 2 $mg \cdot mL^{-1}$, having maximum signal intensity (Supplementary Figure S4).

Thermal stability of ZnO-NPs – CEA probe

The thermal stability was compared for the 1° Ab coupled of ZnO-NPs and 1° Ab immobilized on the microwell plate. The

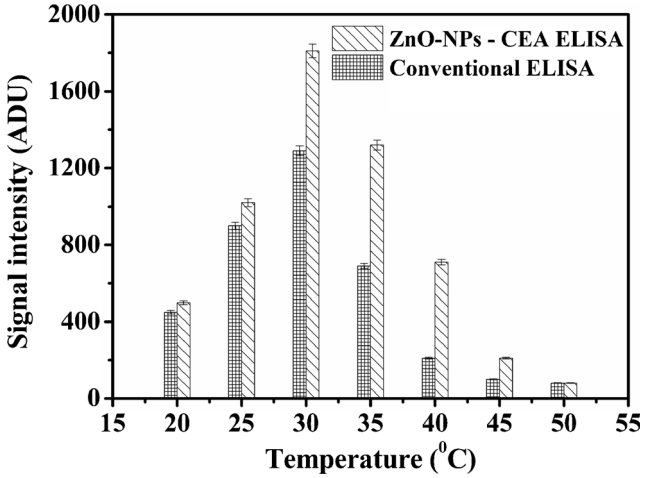

Fig. 3 Comparison of signal intensity for thermal stability of developed immunosensor

effect of temperature on the immunoassay was evaluated in the range 20 °C to 50 °C and presented as Fig. 3. In both cases i.e., 1° Ab immobilized on plate and 1° Ab immobilized on ZnO-NPs showed similar behavior. However, enhance signal intensity was found in the range 26 °C to 35 °C for the 1° Ab-ZnO-NPs over the 1° Ab immobilized on plate. Above 40 °C, the signal intensity was decreased and reached to the blank value i.e., signal intensity without any pAb-HRP. Thus, all experiments were carried out at 30 °C. So, the 1° Ab on modified ZnO-NPs exhibited good thermal stability compared to the 1° Ab immobilized on polystyrene plate.

Effect of surface modification

The performance of the 1° Ab coupled to the ZnO-NPs was evaluated as against the 1° Ab immobilized on microwell plate using optimized condition. The kinetic intensity profile of the resulting signal intensity was recorded as Fig. 4. The signal reached a stable value (95 % of the steady state) after 25 min for 1° Ab-ZnO-NPs. The stable signal intensity was found at 30 min in case of 1° Ab coated on plate. The covalently attached 1° Ab showed significantly higher signal intensity over the 1° Ab coated on microwells. The order of the stable signal intensity recorded in absence of CEA for 1° Ab functionalized ZnO-NPs was found to be 20600 ADU (via phosphonation) and 6230 ADU for 1° Ab coated on microwells (i.e., non-specifically adsorbed 1° Ab) respectively (n=5) (Inset of Fig. 4). The signal intensities were found to 3 fold higher for phosphonated ZnO-NPs against 1° Ab coated on microwells. These observations were also found true for the inhibition studies. The control over bio-molecule's surface orientation suggests that SAMs played an important role for the construction of immuno recognition surfaces.

Immunoassay for CEA in serum

To evaluate the analytical performance of sensor, calibration was obtained for CEA spiked serum samples under optimized conditions. The inhibition curve for CEA was obtained at different concentrations of CEA in the range 0.001 – 20 ng·mL^{-1} using CL technique. The calibration curves were fitted by using Origin Pro 8 SR0 software. Percentage inhibition (%I) was calculated as described by Arduini et al., [23] in presence and absence of analyte.

$$I\,\% = \frac{I_0 - I_A}{I_0} \times 100 \quad (1)$$

Where, I_0=Signal Intensity of blank; I_A=Signal Intensity of spiked sample

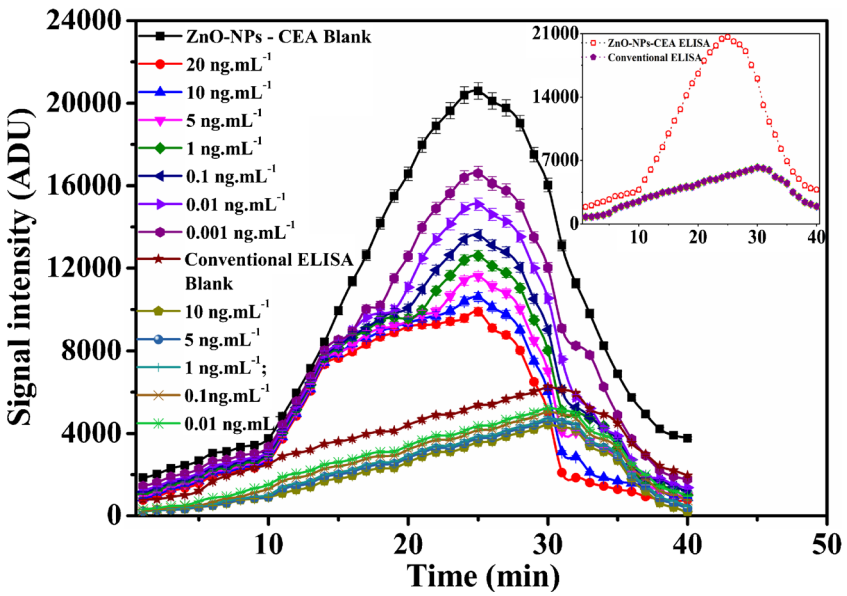

Fig. 4 Comparison of signal intensity under optimized condition between ZnO-NPs-CEA ELISA and conventional microwell plate ELISA for CEA in the range 0.001 – 20 ng mL^{-1}. (Inset: kinetics plot for the both method in absence of CEA)

JrnlID 604_ArtID 1489_Proof# 1 - 03/04/2015

The percentage of inhibited activity that results after exposure to the CEA is quantitatively related with the inhibitor concentration according to the equation. The limit of detection (LOD) was defined as the lowest concentration of analyte that exhibits a signal of 15 % inhibition [24].

A calibration curve for various CEA concentration (0.001–20 ng·mL^{-1}) is presented as Fig. 5. The calibration was found to be linear in the range 0.001–20 ng·mL^{-1} (R^2=0.982, n=5) with a relative standard deviation (RSD) of 3.21 %±0.83 for the 1° Ab attached through 16-PHA modified ZnO-NPs (Fig. 5). The linear equation was y=7.1574×(ng·mL^{-1})+40.65317. Limit of detection (LOD) was 0.001 ng·mL^{-1} and limit of quantitation (LOQ) was 0.001 ng·mL^{-1} by analyzing replicate sets of modified ZnO-NPs with good sensitivity about 7.86 %. Whereas for conventional polystyrene plate ELISA, the linearity was found in the range 0.01 – 10 ng·mL^{-1} (R^2=0.9692, n=5) with an RSD of 5.17 %±0.69 (Fig. 5). The linear equation was y=4.08864×(ng·mL^{-1})+23.85789. LOD and LOQ were determined as 0.01 ng·mL^{-1} by analyzing replicate sets with very low sensitivity about 3.7 %. Lower LOD, LOQ value, R^2 and sensitivity indicate that a surface-active head group which binds strongly to a substrate, an alkyl chain giving stability to the assembly that plays an important role in terms of coupling of biomolecules to self assembled monolayers. Although the developed immunoassay comprises of three antibodies, however, in view of prognosis of cancer, this method could be a better choice over conventional microplate ELISA (Table 1).

Selectivity, recovery and real sample analysis

The developed immunosensor was studied for its selectivity in the incubation solution with 0.2, 2 and 20 ng·mL^{-1} CEA. The

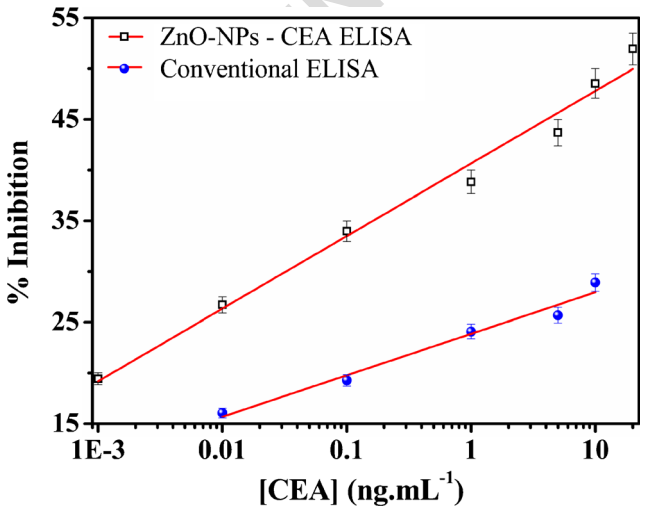

Fig. 5 Calibration curve for various [CEA] using 1° Ab immobilized through 16-PHA SAMs on ZnO-NPs and 1° Ab coated on polystyrene microwell plate under optimized condition (Inset: linear calibration curve)

Table 2 Comparison of real sample analysis using ZnO-NPs – CEA ELISA and conventional 1° Ab coated on microwell plate

Technique	Sample-1 (ng·mL-1) Mean±S.D.	Sample-2 (ng·mL-1) Mean±S.D.	Sample-3 (ng·mL-1) Mean±S.D.	Sample-4 (ng·mL-1) Mean±S.D.	Sample-5 (ng·mL-1) Mean±S.D.	Sample-6 (ng·mL-1) Mean±S.D.	Sample-7 (ng·mL-1) Mean±S.D.	Sample-8 (ng·mL-1) Mean±S.D.
ZnO-NPs - 16 PHA –1° Ab	4.25±0.022	1.784±0.0151	7.631±0.14	2.112±0.0042	1.127±0.0722	0.771±0.0565	0.1564±0.0192	3.911±0.0043
on polystyrene microwell plate	4.382±0.0471	1.81±0.064	7.393±0.261	2.091±0.0114	1.133±0.0084	0.753±0.00531	0.1442±0.0163	3.852±0.05182

% I was calculated from the signal intensity values in the presence of the interference and without interference (Supplementary Figure S5, S6 and S7). The results showed that the interferences of relatively high concentrations only posed negligible effects on CEA detection, indicating that the selectivity of the developed immunosensor was acceptable.

The stability of 1° Ab immobilized on ZnO-NPs was assessed over one month period at storage condition 4 °C in 10 mM PBS (pH 7.4). No significant loss in the 1° Ab functional activity was observed even after four weeks (Supplementary Figure S8). The response was found to be superior over microplate sandwich ELISA technique.

Recovery experiments were conducted to evaluate the accuracy and precision of the ZnO-NPs – CEA immunoassay. Known amounts of CEA were spiked to four serum samples in triplicate. Recovery experiments were performed for both formats. CEA was fortified at levels of 0.05, 2.5, 10 and 15 ng·mL^{-1}; the recoveries of CEA were found in range 97 to 100 % for ZnO-NPs – CEA immunoassay and 90 to 104 % for microplate ELISA. The results of the accuracy and precision test are listed in Supplementary Table S1.

Further, to demonstrate the applicability of the ZnO-NPs – CEA CL ELISA for the determination of CEA in real serum samples, seven different serum samples were collected. The serum samples were diluted in distilled water (3:7). The results were obtained using both ZnO-NPs – CEA ELISA and microplate ELISA. We found that the results of the ZnO-NPs – CEA ELISA method correlated well with those of the microplate ELISA as shown in Table 2, showing that the ZnO-NPs – CEA ELISA can detect the presence of CEA in serum samples both qualitatively and quantitatively. The correlation between the developed method and the conventional ELISA was plotted. The correlation coefficient (r) was obtained from the graph and as well as calculated theoretically i.e., 0.99998 and 0.999965 respectively (Supplementary Figure S9, S10). This indicates that both methods are highly correlated.

Conclusions

In this endeavor, we have demonstrated an ultrasensitive hybrid sandwich-immunoassay for the determination of CEA in human serum based on functionalized ZnO-NPs. The immunoassay exhibits an excellent analytical performance in terms of linearity, enhanced selectivity over polystyrene micro-plate conventional ELISA. ZnO-NPs facilitated the catalysis during H_2O_2-luminol reaction, and also the 16-PHA modified ZnO-NPs exhibited an enhanced thermal stability (1.39 fold). The enhancement in CL intensities facilitated improved assay performance in sensitivity and stability. Moreover, the higher isoelectric point of ZnO-NPs than CEA allows toward novel bio – nano interface by immobilizing high amount of capture probes. The developed method showed better selectivity in presence of other interfering elements. The most promising feature of ZnO-NPs – ELISA is the low-cost and high capture efficiency over other reported materials.

References

1. Choi Y-E, Kwak J-W, Park JW (2010) Nanotechnology for early cancer detection. Sensors 10:428–455
2. Cheow LF, Ko SH, Kim SJ, Kang KH, Han J (2010) Increasing the sensitivity of enzyme-linked immunosorbent assay using multiplexed electrokinetic concentrator. Anal Chem 82:3383–3388
3. Qu S, Liu J, Luo J, Huang Y, Shi W, Wang B, Cai X (2013) A rapid and highly sensitive portable chemiluminescent immunosensor of carcinoembryonic antigen based on immunomagnetic separation in human serum. Anal Chim Acta 766:94–99
4. Zhou F, Yuan L, Wang H, Li D, Chen H (2011) Gold nanoparticle layer: a promising platform for ultra-sensitive cancer detection. Langmuir 27:2155–2158
5. Ambrosi A, Airò F, Merkoçi A (2009) Enhanced gold nanoparticle based ELISA for a breast cancer biomarker. Anal Chem 82:1151–1156
6. Pei X, Zhang B, Tang J, Liu B, Lai W, Tang D (2013) Sandwich-type immunosensors and immunoassays exploiting nanostructure labels: a review. Anal Chim Acta 758:1–18
7. Park J-S, Cho MK, Lee EJ, Ahn K-Y, Lee KE, Jung JH, Cho Y, Han S-S, Kim YK, Lee J (2009) A highly sensitive and selective diagnostic assay based on virus nanoparticles. Nat Nanotechnol 4:259–264
8. Wang G, Huang H, Zhang G, Zhang X, Fang B, Wang L (2011) Dual amplification strategy for the fabrication of highly sensitive Interleukin-6 amperometric immunosensor based on poly-dopamine. Langmuir 27:1224–1231
9. Cassiday L (2010) Carbon nanotubes stretch the boundaries of biomarker detection. Anal Chem 82:3406
10. Borras G, Molina R, Xercavins J, Ballesta A, Iglesias J (1995) Tumor antigens CA 19.9, CA 125, and CEA in carcinoma of the uterine cervix. Gynecol Oncol 57:205–211
11. Grunnet M, Sorensen JB (2012) Carcinoembryonic antigen (CEA) as tumor marker in lung cancer. Lung Cancer 76:138–143
12. Hammarström S (1999) The carcinoembryonic antigen (CEA) family: structures, suggested functions and expression in normal and malignant tissues. Semin Cancer Biol 9:67–81
13. Chon H, Lee S, Son SW, Oh CH, Choo J (2009) Highly sensitive immunoassay of lung cancer marker carcinoembryonic antigen using surface-enhanced Raman scattering of hollow gold nanospheres. Anal Chem 81:3029–3034
14. Kulasingam V, Diamandis EP (2008) Strategies for discovering novel cancer biomarkers through utilization of emerging technologies. Nat Clin Pract Oncol 5:588–599
15. Pal S, Sharma MK, Danielsson B, Willander M, Chatterjee R, Bhand S (2014) A miniaturized nanobiosensor for choline analysis. Biosens Bioelectron 54:558–564
16. Solanki PR, Kaushik A, Agrawal VV, Malhotra BD (2011) Nanostructured metal oxide-based biosensors. NPG Asia Mater 3:17–24
17. Vashist SK, Marion Schneider E, Lam E, Hrapovic S, Luong JHT (2014) One-step antibody immobilization-based rapid and highly-sensitive sandwich ELISA procedure for potential in vitro diagnostics. Sci Rep 4:4407

Q1

18. Willander M, Khun K, Ibupoto Z (2014) Metal oxide nanosensors using polymeric membranes, enzymes and antibody receptors as ion and molecular recognition elements. Sensors 14:8605–8632
19. Arya SK, Saha S, Ramirez-Vick JE, Gupta V, Bhansali S, Singh SP (2012) Recent advances in ZnO nanostructures and thin films for biosensor applications: Review. Anal Chim Acta 737:1–21
20. Norouzi P, Gupta VK, Faridbod F, Pirali-Hamedani M, Larijani B, Ganjali MR (2011) Carcinoembryonic antigen admittance biosensor based on Au and ZnO nanoparticles using FFT admittance voltammetry. Anal Chem 83:1564–1570
21. Casey BJ, Kofinas P (2008) Selective binding of carcinoembryonic antigen using imprinted polymeric hydrogels. J Biomed Mater Res A 87:359–363
22. Li S-F, Zhang X-M, Du W-X, Ni Y-H, Wei X-W (2008) Chemiluminescence reactions of a luminol system catalyzed by ZnO nanoparticles. J Phys Chem C 113:1046–1051
23. Arduini F, Amine A, Moscone D, Palleschi G (2009) Reversible enzyme inhibition–based biosensors: Applications and analytical improvement through diagnostic inhibition. Anal Lett 42:1258–1293
24. Jiang J, Wang Z, Zhang H, Zhang X, Liu X, Wang S (2011) Monoclonal antibody-based ELISA and colloidal gold immunoassay for detecting 19-Nortestosterone residue in animal tissues. J Agric Food Chem 59:9763–9769
25. Liu N, Feng F, Liu Z, Ma Z (2014) Porous platinum nanoparticles and PdPt nanocages for use in an ultrasensitive immunoelectrode for the simultaneous determination of the tumor markers CEA and AFP. Microchim Acta 1–9
26. Wu K, Chu C, Ma C, Yang H, Yan M, Ge S, Yu J, Song X (2015) Immunoassay for carcinoembryonic antigen based on the Zn^{2+}-enhanced fluorescence of magnetic-fluorescent nanocomposites. Sensors Actuators B Chem 206:43–49
27. Cheng Y, Yuan R, Chai Y, Niu H, Cao Y, Liu H, Bai L, Yuan Y (2012) Highly sensitive luminol electrochemiluminescence immunosensor based on ZnO nanoparticles and glucose oxidase decorated graphene for cancer biomarker detection. Anal Chim Acta 745:137–142

Q6

APP Template V1.00 Article id: mrx511510 Typesetter: MPS Date received by MPS: 24/03/2015 PE: MAC003313 CE: LE: UNCORRECTED PROOF

IOP Publishing *Mater. Res. Express* **00** (2015) 000000

Materials Research Express

PAPER

Multi-platform nano-immunosensor for aflatoxin M1 in milk

Souvik Pal[1], **Manoj Kumar Sharma**[2], **Ratnamala Chatterjee**[2,3] **and Sunil Bhand**[1,3]

[1] Biosensor Lab. Department of Chemistry, BITS, Pilani –KK Birla Goa Campus, Goa 403726, India
[2] Department of Physics, Indian Institute of Technology Delhi, New Delhi 110016, India
[3] Author to whom any correspondence should be addressed.

E-mail: souvipal@gmail.com, manojphy@gmail.com, rmala@physics.iitd.ernet.in, sunil17_bhand@yahoo.com and sunilbhand@goa.bits-pilani.ac.in

RECEIVED
18 November 2014

REVISED
23 February 2015

ACCEPTED FOR PUBLICATION
9 March 2015

PUBLISHED
DD MM 2014

Keywords: hafnia nanoparticles, self-assembled monolayer, immunosensor, chemiluminescence, photometry, aflatixin M1, milk

Supplementary material for this article is available online

Abstract

A multi-platform detection based on hafnia nanoparticles (HfO_2NPs) has been developed for immunosensing of aflatoxin M1 (AFM1) as a model analyte. The fine-grained nanocrystal ceramic powder samples of HfO_2NPs were prepared using a solution based chemical method by easily available laboratory reagents. Highly specific monoclonal antibody was immobilized on HfO_2 surface using novel chemical modification and crosslinking chemistry. The nano-immunosensor was investigated using the chemiluminescent sandwich enzyme-linked immunosorbent assay in the range 200–0.5 pg mL^{-1}. Simultaneously, the particles were also investigated photometrically. The developed immuno-sensor exhibited good linearity with a limit of detection 6.25 pg mL^{-1}, sensitivity, selectivity and stability. The IC_{50} value was obtained at 61.48 pg mL^{-1}. Moreover, recovery of milk samples was close to 100%. Using the developed immuno-sensor, AFM1 was measurable even after 30 days at storage condition of 4 °C and as well as room temperature (at 28 °C). The miniaturised nano-immunosensor was used for high-throughput analysis (384 individual samples/40 min) of AFM1. To the best of our knowledge, this is the first report in which HfO_2NPs are used for the fabrication of a multi-platform immuno-sensor system for AFM1 in milk.

1. Introduction

Hybrid functional nanomaterials combined with multiple-platform diagnostic nanotechnologies are emerging day by day due to their properties like high sensitivity, stability, detectability and bio-compatibility [1, 2]. Nanomaterials e.g., nanoparticles, nanorods and nanotubes have been explored in many applications, e.g., biosensing [3, 4], biological separation [5], molecular imaging [6] because of their novel properties and functions differ drastically from the bulk counterparts. Owing to their high volume to surface ratio, surface tailorability and multifunctionality with intrinsic optical, magnetic and electrical properties of nanomaterials offer remarkable opportunities to detect and monitor the objects in complex biological environments for ultrasensitive biosensing. The integrated nanoprobe systems, including metals, metal oxides with polymers, enzymes, antibody or other components give the system required functionality and specificity [7]. Widespread use in a variety of daily applications, such as food colouring agents, transistors, photocatalysts, dental implants, sunscreens, paints, thermal barrier coatings, oxide of the group 4 metals have gained much attention [8]. Among them, hafnium oxide (hafnia, HfO_2) is of interest because it has high thermal, chemical and mechanical stability, as well as a high refractive index and dielectric constant [9]. This combination of properties makes it a valuable material for many applications in optical coatings [10], gate dielectric [11, 12] and sensors [13, 14]. In view of the material compatibility with silicon, HfO_2 is already under active consideration as gate dielectrics for next-generation devices in semiconductor technology due to the high-*k* dielectric [15, 16].

The aflatoxins (AFs), a group of toxic metabolites consisting of a coumarin and a double furan ring, causes extremely serious human health disorders such as hepatocellular carcinoma, aflatoxicosis, Reye's syndrome and chronic hepatitis [17]. Among the other AFs, Aflatoxin M1 (AFM1) which is often present in milk and dairy

products designated as a class I carcinogen by the International Agency for Research on Cancer [18]. The European Union, Food Safety and Standards Authority of India have set strict limits for AFM1 in milk products. The maximum residue level for AFM1 has been set in milk and dried or processed milk products intended for adults at 50 pg mL^{-1}, and at 25 pg mL^{-1} for milk intended for infants or for baby-food [19]. Several studies have provided evidence of potential hazardous human exposure to AFM1 through milk and milk products [20]. As infants' nutritional intake is limited to a single source in general milk, so the need for the development of sensitive, efficient method is an outcome of the thrust to estimate of the AFM1 level in milk.

Several methods, including thin layer chromatography, chromatography–mass spectrometry, immunological methods, including enzyme-linked immunosorbent assay (ELISA) and the electro-chemical immuno-sensor method have been developed for AFM1 determination [5, 21–24]. The well-proven chromatographic methods are having drawbacks in terms of labour, time, expensive equipment and materials. On the other hand, immunochemical methods based on high affinity antibody can provide excellent sensitivity. The sensitivity of ELISA depends upon the key factors like stability of antibody, composition of the medium and the operating conditions. Among the established ELISA techniques, sandwich-type immunoassay is an effective technique due to the high specificity and sensitivity [25]. ELISA in combination of the chemiluminescent (luminol/ peroxide) system for horseradish peroxidase (HRP) has the advantages of high sensitivity of chemiluminescence (CL) and high specificity with characteristics of simplicity and rapidity, high throughput and low-cost equipment [26]. Furthermore, the optical signal is not influenced by electrical, magnetic or ionic fields. The advantage that optical transducers have over other methods is the use of visible radiation that allows versatile detection in many different areas and also accommodates miniaturization.

In the present work, we report, for the first time, a novel approach to develop and integrated hafnia nanoparticles (HfO_2NPs) based sandwich immuno-sensor. The self-assembled monolayer (SAMs) of 16-phosphonohexadecanoic acid (16-PHA) was utilized to modify the surface of HfO_2NPs. A multi-sensing platform, exploiting sensitive CL and also fluorescence (FL) and colorimetric techniques, was developed for analysis of AFM1 using SAMs modified HfO_2NPs. Particle size analyzer and Fourier transform InfraRed spectroscopy (FT-IR) were applied towards the construction of multi-platform HfO_2 nano-immunosensor for AM1 in milk. The presented immuno-sensor investigated in the range 0.5–200 pg mL^{-1}. The application of the developed immuno-sensor for analysis of AFM1 in milk has been demonstrated. The miniaturised nano-immunosensor was used for high-throughput analysis (384 individual samples/40 min) of AFM1, which showed a limit of detection (LOD) at 0.5 pg mL^{-1} and limit of quantification (LOQ) at 6.25 pg mL^{-1}. Moreover, the developed immuno-sensor based on synthesized HfO_2NPs showed better performance than commercially available HfO_2NPs.

2. Materials and methods

2.1. Chemicals and biochemicals

Anti AFM1 fractionated antiserum primary antibody (mAb) raised from rat, anti AFM1 HRP conjugated secondary antibody (pAb–HRP) raised from rabbit and Anti-rabbit (Rat) Fluorescein isothiocyanate (FITC) conjugated secondary antibody (pAb–FITC) were purchased from AbCam (UK). Spec-pure powders of hafnium chloride ($HfCl_2$) (99.99%), nickel (II) nitrate hexahydrate $Ni(NO_3)_2.6H_2O$, AFM1, 16-PHA, 1-Ethyl-3-[3–dimethylaminopropyl]carbodiimide hydrochloride (EDC), N-Hydroxy succinimide (NHS), O-phenylenediamine dihydrochloride (OPD), certified reference material ERM-BD282 (AFM1 in whole milk powder <0.02 μg kg^{-1}), tween 20 were purchased from Sigma-Aldrich, USA. Black 384 well polystyrene microtiter plates were purchased from Nunc (Denmark). Ethyl Alcohol 200 proof has been purchased from TEDIA, USA. Triethanol amine, Di-Sodium hydrogen phosphate (Na_2HPO_4), Sodium di-hydrogen phosphate (NaH_2PO_4), Sodium bi-carbonate ($NaHCO_3$), and Sodium Carbonate (Na_2CO_3) has been purchased from MERCK, Germany. Sodium hypochlorite (4%) solution was purchased from Fisher Scientific (India). Centrifugation, shaking and filtration of the samples were done by eppendrof minispin centrifuge and Spinix shaker, syringe filter from Tarsons (India). Glove box, Cole Parmer (USA) was used for the handling of AFM1 standard solution. Water produced in a Milli-Q system (Millipore, Beford, MA, USA) was used for preparing all the solutions. Certified ultra high pure nitrogen (99.9%), pH meter (Seven Multi Mettler Toledo, 8603, Switzerland) were used.

2.2. Preparation of HfO_2NPs

The fine-grained nanocrystal ceramic powder samples of HfO_2NPs were prepared using a solution based chemical method by easily available laboratory reagents as described elsewhere [27]. The method involves the complete dehydration of the metal ion ligand complex precursor solution, which is accompanied by the decomposition of the metal complexes.

2.3. Preparation of solutions

Carbonate buffer (CB; 0.05 M, pH ~ 9.6), phosphate buffer (PB; 0.01 M, pH ~ 7.4), phosphate-buffered saline (PBS) were prepared. All the AFM1 solutions were prepared inside a Glove box in a maintained inert N_2 atmosphere. AFM1 stock solution was prepared by dissolving the AFM1 powder in 5% ACN (v/v) in PBS at a concentration of 5 μg/2 mL and stored at−20 °C. (**Safety Note**: *AFs are highly carcinogenic and should be handled with extreme care. AF contaminated labware should be decontaminated with an aqueous solution of sodium hypochlorite* (4%).)

The stock solution of rat monoclonal [1C6] Ab, 100 μg (1 mg mL^{-1}) was diluted with 50 μL of de-ionized water. Working mAb solution was prepared prior to the experiment by serial dilution in CB as 1:1000, 1:2000, etc. The stock solution of 1 mg (2 mg mL^{-1}) rabbit polyclonal to rat IgG-H and L pAb–HRP was diluted with 500 μL of de-ionized water. Working pAb solution was prepared prior to the experiment by serial dilution in PBS.

To assess the performance of the immuno-sensor, milk samples milk samples with spiked AFM1 were prepared by standard addition method with a fixed amount of AFM1 (ranging from 200–0.5 pg mL^{-1}). The preparation of buffers, standard solutions of AFM1and standard milk samples were reported earlier in details [24].

2.4. Preparation of AFM1 capture probe

2.4.1. Surface modification

The AFM1 capture probe is based on the efficient immobilization of capture efficient very specific mAb through carboxy terminated SAMs on HfO_2NPs. The glass containers used for monolayer preparation was cleaned with Piranha solution (a mixture of 98% H_2SO_4 and 30% H_2O_2, 7:3, v/v; **caution**: piranha solution reacts exothermally and strongly reacts with organics) for 1 h and rinsed exhaustively with deionized (DI) water and ethanol. HfO_2NPs were dispersed in 0.5 mM ethanolic solution of 16-PHA and sonicated for 5 min to obtain well dispersed solution. These samples were stirred on a Spinx shaker for 48 h (self-assembly time). The SAMs functionalized HfO_2NPs were centrifuged for 15 min at 6000 rpm and rinsed in ethanol followed by DI water and dried under a stream of dry nitrogen.

2.4.2. mAb immobilization

For antibody immobilization, the carboxylic acid-terminated SAMs were modified using an aqueous equimolar solution of 100 mM EDC/100 mM NHS for 2 h at room temperature. The resultant NHS ester monolayers were reacted for 3 h at 1:1 solution of 1:16000 mAb and CB. The mAb coated HfO_2NPs (mAb–HfO_2NPs) were washed with PB.

2.4.3. pAb incubation and measurements

AFM1 spiked milk samples were incubated for 2 h at room temperature. The particles were washed again with PBS to remove unbound AFM1. For CL and optical measurements, pAb–HRP (1:32000) was incubated at room temperature for 2 h with the particles. For FL measurements, the AFM1 bound mAb coated particles were incubated with pAb–FITC (1:64000) at room temperature in the dark for 3 h. The excess label was removed by washing with PBS.

The sensing principle of the sensor relies on the effective binding of mAb and label pAb antibody. The signal intensity is higher when the binding is perfect. In presence of analyte very specific to mAb, the binding with label pAb is influenced drastically and lowering of optical signal intensity is observed. By measuring the signal intensity difference between reference and contaminated samples, one can detect the presence of analyte in the sample. The schematic of capture probe development is presented as figure 1.

For CL measurements, VictorX^4 2030 optiplate reader from Perkin Elmer (USA) was used. CL substrate (1.2 μL of 0.5 M H_2O_2 + 8.8 μL luminol) was added to each microwell of the 384 microtiter well plate. The signal intensity was kinetically measured at the steady state and stability was found after 40 min.

For colorimetric assay, the washed particles were incubated in presence of 0.5 M H_2O_2 and OPD chromogen for 35 min in the dark. After 35 min, stop solution was introduced to stop the reaction. The signal intensity was measured by the VictorX^4 2030 optiplate reader.

FL images were acquired on inverted microscope (IX-71 Olympus, Japan) coupled with charged coupled device (CCD), Hamamatsu Orca-ER (Japan). For FL measurement, 2 μL of the final nanoparticles suspension was placed on a microscopic slide. The optical images were viewed under FL microscope and captured by CCD. The FL intensity was acquired by VictorX^4 2030 optiplate reader.

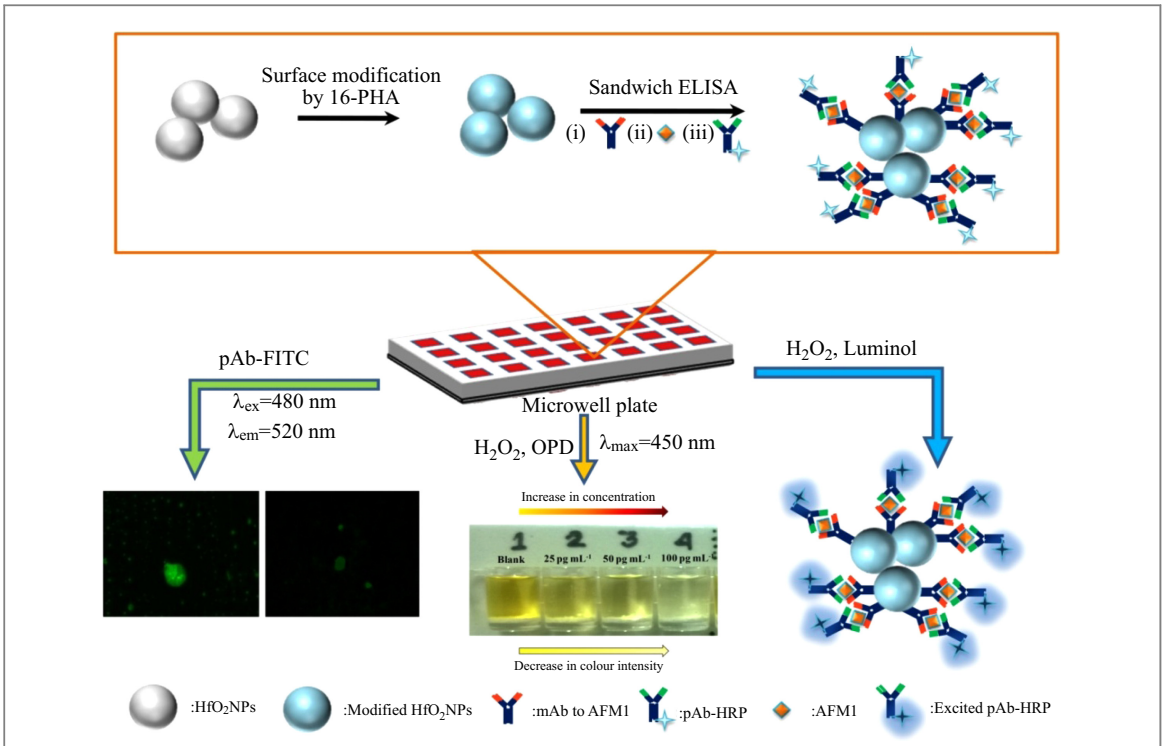

Figure 1. Schematic pathway for construction along with working mechanism of the HfO_2NPs based multi-platform nano-immunosensor during measurements.

2.5. Particle size measurement

DELSA Nano dynamic light scattering (DLS) Particle size analyzer from Beckmann-Coulter, USA was used for measuring particle size. The operation principle of the instrument is based on DLS technique. Due to both its wide spectrum of particles and dispersion media and its ease of use, DLS technique is a popular for determining particle size. The average hydrodynamic diameter of a particle suspension can be measured by deflection of scattered light produced by particles due to Brownian motion.

During the particle movement in Brownian motion, short time delays in τ the intensities will be highly correlated, while there is decay for long delays. The measured diffusion coefficient for a monodisperse system can then be related to the hydrodynamic diameter using the Stokes–Einstein's equation (1).

$$D = \left(K_B T\right) / \left(3\pi\eta_0 d\right), \tag{1}$$

Where, d is the particle's hydrodynamic diameter; D is diffusion coefficient; K_B is the Boltzmann constant; T is the absolute temperature and η_0 is the viscosity of the medium. The correlation function of a polydisperse system can be described by the sum of the exponential decays of different populations of particles present in the sample. A more detailed analysis of DLS has been reported elsewhere [28].

3. Results and discussions

3.1. Surface characterization by FT-IR

FT-IR was applied to measure the surface properties of HfO_2NPs modified mAb through SAMs via carbodiimide cross-linking reaction. FT-IR spectra were recorded using IRAffinity-1 (SHIMADZU, Japan) with attenuated total reflectance (ATR) attachment Specac Diamond ATR AQUA. For the samples, FT-IR ATR spectra were collected at a resolution of 2 cm^{-1} (68 scans). The recorded FT-IR spectra are shown in figure 2.

FT-IR spectrum of the bare HfO_2NPs is presented as figure 2(i). In the mid-infrared region there is only one strong absorption peak at 510 cm^{-1}. The feature at 660 cm^{-1} is the characteristic of a HfO_2 longitudinal-optical phonon mode. The peak at 753 cm^{-1} is assigned for an A_u mode (atomic displacement parallel to the c-axis of the unit-cell). This is in agreement with the report by Martínez F L, 2007 [29].

Figure 2(ii) shows FT-IR spectrum of 16-PHA functionalized HfO_2NPs. Asymmetric (ν_{as}) and symmetric methylene stretches (ν_s) of 16-PHA-modified HfO_2NPs appear at 2974 cm^{-1} and 2880 cm^{-1} respectively. These bands of SAMs modified HfO_2NPs suggest methylene chains during monolayer growth. The C=O stretch at 1736 cm^{-1} on HfO_2NPs associated with ν_{as} COO^- stretch at 1650 cm^{-1} is characteristics of an organic carboxylic

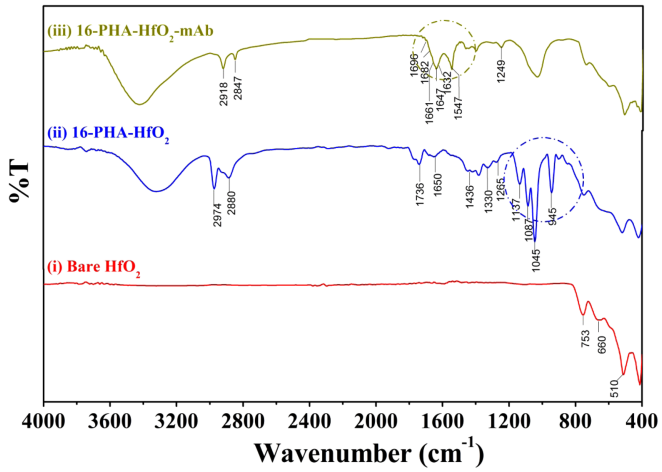

Figure 2. The ATR FT-IR spectrum of (i) the bare HfO_2NPs (ii) HfO_2NPs treated with 16-PHA (iii) anti-AFM1 mAb coupled through 16-PHA functionalized HfO_2. Spectra were acquired using 68 scans at 2 cm^{-1} resolution collected under vacuum conditions.

compound. The additional IR peaks at 1436 cm^{-1}, 1330 cm^{-1} and 1265 cm^{-1} are ascribed to C–H deformation and C–O stretch respectively.

It is very difficult to obtain the P–O stretching region information due to the binding of phosphonic acids onto metal oxides. The presence of several different binding modes for residual P=O and P–O–H sites in phosphonic acid monolayers appear between 1300 cm^{-1} and 800 cm^{-1} in the P–O stretching region. The peak located at 945 cm^{-1} in the spectrum assigned to a P–OH band that is observed only after binding of 16-PHA on HfO_2. This indicates that the phosphonic acids bind to the surface Hf–OH group via condensation reactions. The linkage between HfO_2NPs and 16-PHA should be a tridentate chelating binding mode or a bidentate binding moiety rather than the monodentate surface binding mode. The existence of the peak at 1137 cm^{-1}, which is characteristic of the P=O stretching mode, is a possible evidence for bidentate binding modes. The observation of P–OH related modes indicates that the binding of 16-PHA on HfO_2NPs occurs mainly through the PO_3H_2 groups.

Figure 2(iii) is the FT-IR spectrum of covalently coupled mAb on HfO2NPs. The C=O peak, however, completely vanished as mAb introduced. The existence of amide region in the samples was confirmed by presence of intense and broad absorption bands at 1647 cm^{-1}, 1547 cm^{-1} and 1249 cm^{-1}. Further new associated absorption bands at 1696, 1682, 1661 and 1632 cm^{-1} confirms the presence of amide group, which is also the evidence for -COOH of 16-PHA and -NH_2 of mAb linkage.

3.2. Particle size analysis

The differential intensity related to particle size distributions was obtained from DLS study at 30 °C. A normalized particle size distribution is presented in figure 3 for the stepwise surface modification. Instrument performance was first evaluated using particle standards (20 and 100 nm) supplied in solution by the manufacturer.

Samples were prepared by dispersing 1 mg of sample into 100 mL of PB. Figure 3(i) depicts the particle size distribution of bare HfO_2NPs particles. The cumulant mean diameter of the particles was found 12.91 nm with PDI 0.221. The particle size was increased upon the treatment with 16-PHA. From figure 3(ii), the cumulant diameter of the modified particles was found 22.6 nm with PDI 0.397. Further increment was observed for the particles modified with mAb (figure 3(iii)). The particle size was 48.62 nm with PDI 0.567. The increment in particle size about 10 nm after surface modification and about 26 nm after mAb attachment confirms the successful fabrication of AFM1 capture probe.

3.3. Microscopy study

The binding of mAb to functionalized HfO_2NPs was also confirmed by FL microscopy. Two microscopy slides were prepared as reference mAb–HfO_2NPs without pAb–FITC and sample mAb–HfO_2NPs coupled with pAb–FITC NPs. The sample mAb–HfO_2NPs was incubated with pAb–FITC (1:64000) for 2 h at room temperature in dark. Before excitation the sample was rinsed with 0.01 M PBS to remove unbound pAb–FITC. The reference mAb–HfO_2NPs without pAb–FITC was showed negligible FL signal (figure 4(a)). The binding between mAb on HfO_2NPs and pAb–FITC was demonstrated by a bright FL signal (figure 4(b)). These observations proved that the mAb on HfO_2NPs preserved the excellent biological recognition of antibody to their targets.

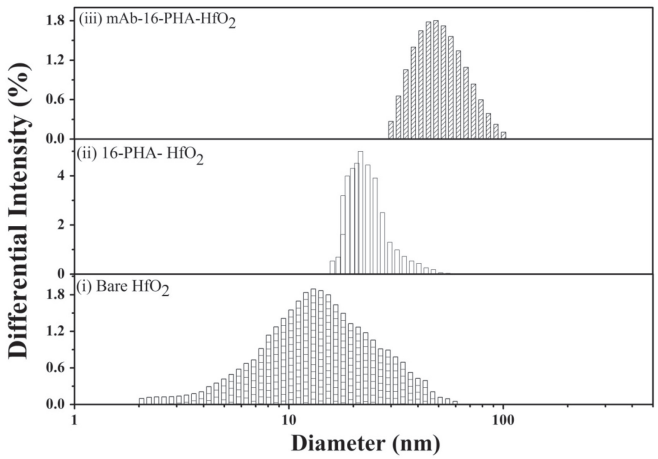

Figure 3. Particle size distribution curve of (i) the bare HfO_2NPs; (ii) HfO_2NPs treated with 16-PHA; (iii) anti-AFM1 mAb coupled through 16-PHA functionalized HfO_2. NPs were dispersed and diluted in PB of 0.01 M, pH ~ 7.4.

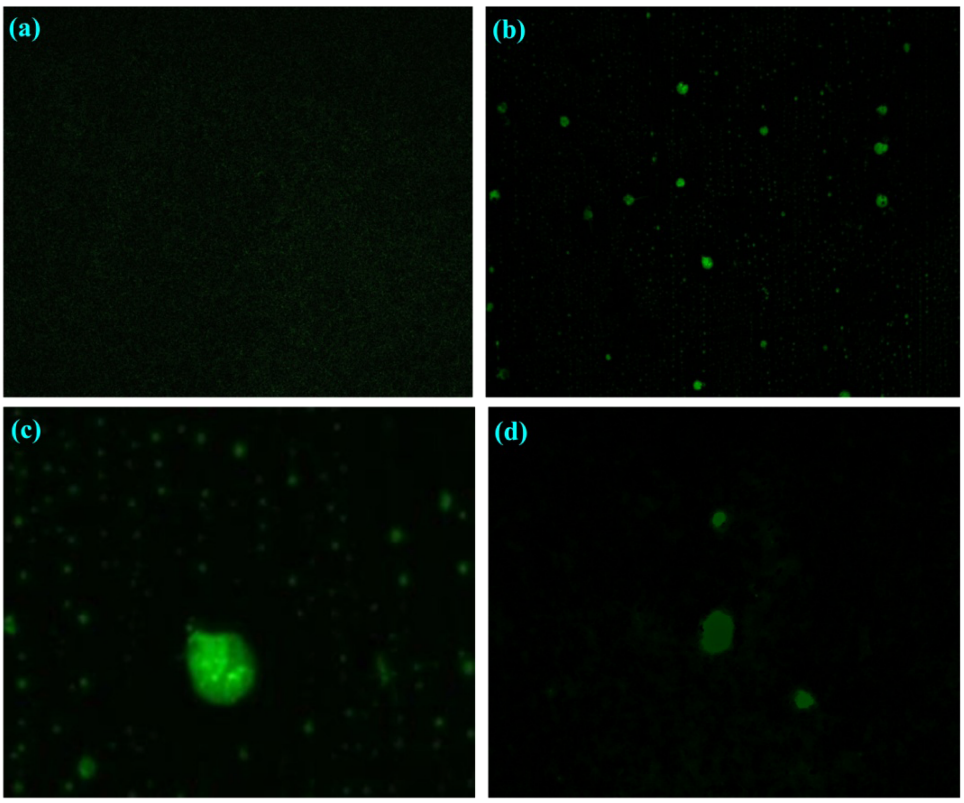

Figure 4. Fluorescence image of (a) reference mAb–HfO_2NPs without pAb–FITC (b) sample mAb–HfO_2NPs coupled with pAb–FITC at 10× magnification (c) reference mAb–HfO_2NPs coupled with pAb–FITC at 40× magnification in absence of AFM1 (d) sample mAb–HfO_2NPs coupled with pAb–FITC at 40× magnification in presence of AFM1; mAb (1:32000) incubated with pAb–FITC (1:64000); captured using pAb-FITC (λ_{ex} 480 nm/λ_{em} 520 nm).

Further, the samples were prepared to study the inhibition caused by AFM1. Like earlier two microscopic slides were prepared. The reference slide was incubated with pAb–FITC in absence of AFM1 as described earlier conditions. Another slide, sample, was prepared by incubating mAb–HfO_2NPs with AFM1 (50 pg mL^{-1}). The sample slide was washed and incubation process was performed using pAb–FITC as described earlier condition. Before excitation both reference and sample were rinsed with 0.01 M PBS to remove unbound pAb–FITC. The intense signal from the reference again confirms the attachment of pAb–FITC on mAb–HfO_2NPs (figure 4(c)).

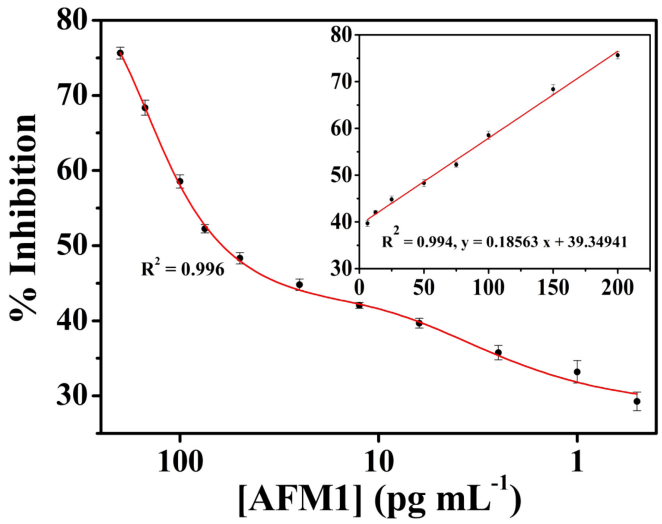

Figure 5. Calibration curve for different [AFM1] obtained using 16-PHA–HfO_2 coupled mAb (Inset: the linear calibration graph).

The signal intensity of sample slide was drastically quenched in presence of AFM1 (figure 4(d)). The observations confirm that the signal intensity decreased due to binding of AFM1 to mAb. Thus, the sensor exhibits as an excellent bio-recognition towards AFM1.

3.4. Optimization of the factors affecting sensing probe

In order to optimize buffer parameters, first assays were performed with free mAb. The ionic strength and pH of PB and PBS was optimized as 0.01 M, pH ~ 7.4. The developed sensor relies on the amount of mAb on the HfO_2NPs. Amount of mAb was optimized by coupling different amount of mAb on the NPs surface against fixed amount of label pAb. A mAb dilution of 1:32000 was optimized after analysing data (supplementary figure S1).

Amount of NPs also was optimized. Different amount of NPs were analysed using optimized mAb dilution. The signal intensity was unchanged from 1.5 mg to 3.0 mg and after 3.0 mg, the signal intensity was decreased (supplementary figure S2). The introduction of more particles could afford lower intensity due to self aggregation of mAb at nano-platform.

Further, pAb amount was optimized to select the final sensing probe. Using optimized mAb on optimized particles, different dilutions of pAb–HRP was tested. A pAb dilution of 1:32000 was adopted to assess the rest of the sensor performance (supplementary figure S3). The blocking step was also studied, since this is central point in immunoassays, to avoid non specific adsorption of antibodies. BSA (1%) and whole milk powder (5%) were assessed as blocking solutions and similar results were found with both types of reagents.

To access the stability of mAb–HfO_2, the modified NPs were stored at 4 °C for two weeks. Results obtained were similar to those obtained with freshly prepared mAb–HfO_2, indicating no loss of the activity. Also thermal stability of the mAb–HfO_2 was evaluated by performing experiments in temperature ranging from 20 °C to 50 °C (supplementary figure S4). Immobilized mAb through 16-PHA exhibited the highest signal intensity at 25 °C. But the signal intensity was almost stable upto 35 °C. The immobilized mAb loose activities in the temperature range 40–50 °C. The residual activity was 2.9% for immobilized mAb at temperature 50 °C. Above 35 °C, the mAb activity dropped significantly due to the thermal inactivation.

3.5. Calibration curve for AFM1 immunosensor

Using the optimized parameters, the calibrations curves were performed with mAb immobilized on HfO_2NPs. The inhibition curve for AFM1 spiked milk samples in HfO_2NPs was obtained for eleven different concentrations of AFM1 (200 pg mL^{-1}, 150 pg mL^{-1}, 100 pg mL^{-1}, 75 pg mL^{-1}, 50 pg mL^{-1}, 25 pg mL^{-1}, 12.5 pg mL^{-1}, 6.25 pg mL^{-1}, 0.25 pg mL^{-1}, 1 pg mL^{-1} and 0.5 pg mL^{-1}) by CL detection. The calibration curves were fitted by the sigmoidal bidoseresp equation (Origin Pro 8 SR0). The inhibition curve obtained using CL technique was shown in figure 5.

The data points were fitted and unknown [AFM1] could be detected from mean standard deviation (S.D.) curve in HfO_2NPs based ELISA. We achieved a good assay sensitivity, about 2.068% with S.D. = 0.85; coefficient of determination (R^2) = 0.996. The detection of limit (LOD) was defined as the lowest concentration of AFM1 that exhibits a signal of 15% inhibition [30]. The LOD was found to be 0.5 pg mL^{-1}. The half maximal inhibitory

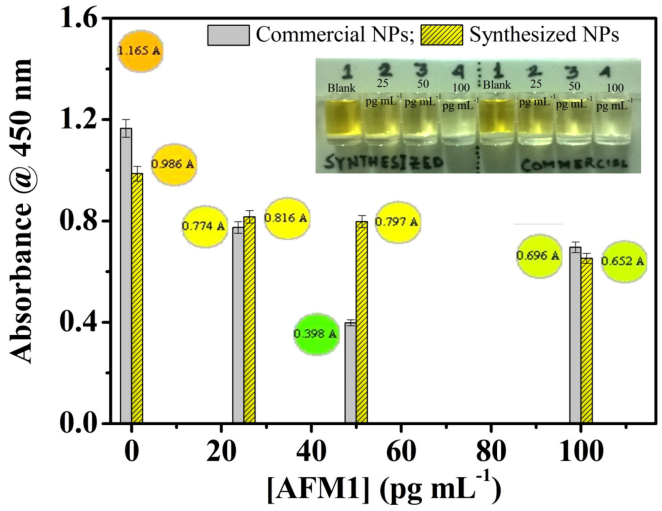

Figure 6. Comparison of signal intensity associated with real time images obtained using mAb coupled on synthesized and commercial HfO_2NPs for different [AFM1].

concentration (IC_{50}) value for developed immuno-sensor based on sandwich ELISA was found at 61.48 pg mL^{-1}.

The signal inhibited due to presence of AFM1 in milk was calculated and a significantly low detection limit 0.5 pg mL^{-1} could be achieved in case of HfO_2NPs based sandwich ELISA with analysis time of 40 min. The curve was also fitted linear in the concentration range from 6.25 pg mL^{-1} to 200 pg mL^{-1} and presented as figure 5 (Inset). The plot shows a good linear relationship with regression equation $y = 0.185\ 63\ x$ (pg mL^{-1}) + 39.349 41 and $R^2 = 0.994$. The LOQ was found to be 6.25 pg mL^{-1}.

3.6. Photometry study and comparison with commercial particles

Simultaneously, the immuno-sensor was examined colorimetrically using OPD chromogen suitable for use in ELISA procedures which utilize HRP conjugates. This substrate produces a soluble end product that is orange-brown in colour and can be read spectrophotometrically at 450 nm. The OPD reaction can be stopped with 3 N HCl and read at 492 nm. Also, the immuno-sensor based on synthesized HfO_2NPs was compared visually as well as photometrically with commercially available HfO_2 particles (figure 6).

The percentage inhibition (%*I*) for the both cases was calculated and plotted for the AFM1 concentration above, near and below IC_{50} values (100 pg mL^{-1}, 50 pg mL^{-1} and 25 pg mL^{-1}) obtained from the CL data (supplementary figure S5)). At lower concentration of AFM1 i.e., 25 pg mL^{-1}, the %*I* values were almost equal for both synthesized and commercial particles. But the AFM1 concentrations near and above IC_{50} were showed almost 46.67% and 23.01% higher %*I* values respectively using the immuno-sensor based on synthesized HfO_2NPs. The large binding surface area of the synthesized HfO_2NPs could allow the proper orientation of the antibody binding sites, improving the sensitivity of immunoassays.

3.7. Specificity of sensing probe

The specificity of mAb is one of the most important factors and is usually represented by cross-reactivity (CR). The reliability and specificity of mAb can be determined by lowering of CR value. AFM1, aflatoxin M2 (AFM2), aflatoxin B1 (AFB1) and aflatoxin G1 (AFG1) have similar structures. Thus the capture antibody may recognize its specific analyte but also may recognize partly the other structural analogues. Bearing this concept in mind, we have carried out CR studies in our for AFM1, AFB1, AFG1, and AFM2 recognition by the mAb. The results showed high specificity of AFM1 towards mAb and partial recognition towards AFM2 and AFB1 and showed negligible towards AFG1 (the results are not shown here).

3.8. Recovery studies and real sample analysis

Recovery studies were performed on mAb immobilized via 16-PHA modified HfO_2NPs for three different milk samples. The study was repeated with milk samples spiked with AFM1 solution (50, 20 and 10 pg mL^{-1}) to evaluate sensor performance for inter-batch and intra-batch reproducibility. The summaries of findings are tabulated in table 1. It was calculated that mean recovery intra-day RSD% 0.83 ± 0.50 whereas mean inter-day RSD% was calculated as 0.70 ± 0.61 for AFM1 concentration in the range 10–50 pg ml^{-1}.

Table 1. Recovery of [AFM1] from different milk samples as determined by HfO_2NPs AFM1 nano-immunosensor to assess the recovery efficiency.

	Intraday				Interday			
[AFM1] added (pg mL^{-1})	[AFM1] Found (pg mL^{-1})	RSD (%)	R.E. (%)	Recovery (%)	[AFM1] Found (pg mL^{-1})	RSD (%)	R.E. (%)	Recovery (%)
50	50.23	0.22	0.42	100.46	49.65	0.26	−0.48	99.30
50	20.14	0.50	0.85	100.70	18.87	1.08	−6.55	94.35
10	9.36	1.40	−6.1	93.60	9.51	1.17	−5.1	95.10

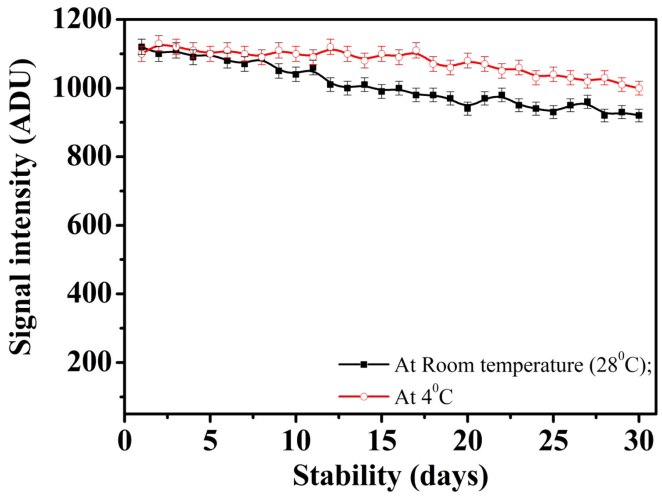

Figure 7. The storage stability comparison of HfO_2NPs based nano-immunosensor at 4 °C and room temperature (28 °C).

Along with other features, the storage stability of immuno-sensor was investigated with a series of repeated experiments over 30 days (figure 7). The storage stability of developed immuno-sensor was examined at two different temperatures (i) at 4 °C and (ii) at room temperature (28 °C). The response was found excellent even after 30 measurements (Intraday RSD% = 3.13 and Interday RSD% = 2.19). Under both conditions, the immuno-sensor exhibited good stability. The environmental condition e.g. at 4 °C was produced better response. The response of mAb modified NPs at 4 °C was constant for the first 15 days and after 30 days the response was decreased to 89% of its original response. The mAb modified NPs at room temperature were retained 82% of its original response after 30 days. The decrease in response may be due to the reduction of antibody activity. It was found that 16-PHA modified HfO_2NPs based immuno-sensor holds good storage stability, sensitivity and reusability for longer duration.

4. Conclusion

In this endeavour, we have reported a novel approach to exploit HfO_2NPs towards nano-immunosensing platform using 16-PHA for AFM1 in milk. To the best of our knowledge, this is the first report on 16-PHA modified HfO_2NPs surface and its application in specific, selective and multi-platform nano-immunosensor. HfO_2NPs with an average particle size of 12.91 nm deployed for AFM1 ranging from 0.5 pg mL^{-1} to 200 pg mL^{-1}. The developed sensor showed a broader linear range (6.25–200 pg mL^{-1}) with $R^2 = 0.994$ ($n = 5$) and IC_{50} value 61.48 pg mL^{-1}. Another advantage of this method is reduced analysis time and sample preparation in comparison with the conventional methods. In conclusion, this proposed immunosensor can facilitate the development of screening methods for AFM1 in milk products.

Acknowledgments

This work is funded by National Agriculture Innovation Project (NAIP) No. C4/C10125, ICAR and The World Bank. SP acknowledges to NAIP for the award of Research Associate Fellowship.

References

[1] Sanchez C, Belleville P, Popall M and Nicole L 2011 Applications of advanced hybrid organic–inorganic nanomaterials: from laboratory to market *Chem. Soc. Rev.* **40** 696–753
[2] Lei J and Ju H 2012 Signal amplification using functional nanomaterials for biosensing *Chem. Soc. Rev.* **41** 2122–34
[3] Risveden K, Dick K A, Bhand S, Rydberg P, Samuelson L and Danielsson B 2010 Branched nanotrees with immobilized acetylcholine esterase for nanobiosensor applications *Nanotechnology* **21** 055102
[4] Pal S, Sharma M K, Danielsson B, Willander M, Chatterjee R and Bhand S 2014 A miniaturized nanobiosensor for choline analysis *Biosens. Bioelectron.* **54** 558–64
[5] Kanungo L, Pal S and Bhand S 2011 Miniaturised hybrid immunoassay for high sensitivity analysis of aflatoxin M1 in milk *Biosens. Bioelectron.* **26** 2601–6
[6] Depan D and Misra R D K 2012 Hybrid nanoparticle architecture for cellular uptake and bioimaging: direct crystallization of a polymer immobilized with magnetic nanoparticles on carbon nanotubes *Nanoscale* **4** 6325–35

Q3

[7] de Dios A S and Díaz-García M E 2010 Multifunctional nanoparticles: analytical prospects *Anal. Chim. Acta* **666** 1–22
[8] Boyle T J, Steele L A M, Burton P D, Hoppe S M, Lockhart C and Rodriguez M A 2012 Synthesis and structural characterization of a family of modified hafnium tert-butoxide for use as precursors to hafnia nanoparticles *Inorg. Chem.* **51** 12075–92
[9] Brezesinski T, Smarsly B, Iimura K-I, Grosso D, Boissière C, Amenitsch H, Antonietti M and Sanchez C 2005 Self-assembly and crystallization behavior of mesoporous, crystalline HfO_2 thin films: a model system for the generation of mesostructured transition-metal oxides *Small* **1** 889–98
[10] Kim D H, Park J W, Chang Y M, Lim D and Chung H 2010 Electrical properties and structure of laser-spike-annealed hafnium oxide *Thin Solid Films* **518** 2812–5
[11] Lin Y-S, Puthenkovilakam R and Chang J P 2002 Dielectric property and thermal stability of HfO_2 on silicon *Appl. Phys. Lett.* **81** 2041–3
[12] Ying Z, Tang W, Hu Z, Li W, Sun J, Xu N and Wu J 2010 Annealing behaviors of structural, interfacial and optical properties of HfO_2 thin films prepared by plasma assisted reactive pulsed laser deposition *J. Mater. Res.* **25** 680–6
[13] Takashi U, Greg N A, David C S, John L H, Groot C H D and Peter A 2010 Growth of carbon nanotubes on HfO_2 towards highly sensitive nano-sensors *Japan. J. Appl. Phys.* **49** 04DN11
[14] Sufi Z, Christopher D E, Ali A, Benjamin F, Zhu Y and Tak N 2011 Optimization of pH sensing using silicon nanowire field effect transistors with HfO_2 as the sensing surface *Nanotechnology* **22** 405501
[15] Cho M-H, Roh Y S, Whang C N, Jeong K, Nahm S W, Ko D-H, Lee J H, Lee N I and Fujihara K 2002 Thermal stability and structural characteristics of HfO_2 films on Si (100) grown by atomic-layer deposition *Appl. Phys. Lett.* **81** 472–4
[16] Triyoso D H *et al* 2005 Impact of titanium addition on film characteristics of HfO_2 gate dielectrics deposited by atomic layer deposition *J. Appl. Phys.* **98** 054104
[17] van Egmond H, Schothorst R and Jonker M 2007 Regulations relating to mycotoxins in food *Anal. Bioanal. Chem.* **389** 147–57
[18] International Agency for Research on Cancer (IARC) 1993 Aflatoxins. Some naturally occurring substances: food items and constituents, heterocyclic aromatic amines and mycotoxins *IARC Monograph on the Evaluation of Cardnogenic Risks to Humans* vol 56 (Lyon, France: IARC, World Health Organization) pp 245–395
[19] European Commission Regulation (2004) No. 683/2004/EC Amending Regulation (EC) No. 466/2001 as Regards Aflatoxins and Ochratoxin A in Foods for Infants and Young Children (13 April 2004) O.J.E.C. L106 3–5
[20] Pei S C, Zhang Y Y, Eremin S A and Lee W J 2009 Detection of aflatoxin M1 in milk products from China by ELISA using monoclonal antibodies *Food Control* **20** 1080–5
[21] Turner N W, Subrahmanyam S and Piletsky S A 2009 Analytical methods for determination of mycotoxins: a review *Anal. Chim. Acta* **632** 168–80
[22] Wang Y, Liu X, Xiao C, Wang Z, Wang J, Xiao H, Cui L, Xiang Q and Yue T 2012 HPLC determination of aflatoxin M1 in liquid milk and milk powder using solid phase extraction on OASIS HLB *Food Control* **28** 131–4
[23] Jiang W, Wang Z, Nölke G, Zhang J, Niu L and Shen J 2013 Simultaneous determination of aflatoxin B1 and aflatoxin M1 in food matrices by enzyme-linked immunosorbent assay *Food Anal. Methods* **6** 767–74
[24] Bacher G, Pal S, Kanungo L and Bhand S 2012 A label-free silver wire based impedimetric immunosensor for detection of aflatoxin M1 in milk *Sensors Actuators* B **168** 223–30
[25] Knopp D 2006 Immunoassay development for environmental analysis *Anal. Bioanal. Chem.* **385** 425–7
[26] Kricka L J 2003 Clinical applications of chemiluminescence *Anal. Chim. Acta* **500** 279–86
[27] Sharma M K, Mishra D K, Ghosh S, Kanjilal D, Srivastava P and Chatterjee R 2011 Oxygen vacancy mediated large magnetization in chemically synthesized Ni-doped HfO_2 nanoparticle powder samples *J. Appl. Phys.* **110** 063902
[28] Finsy R 1994 Particle sizing by quasi-elastic light scattering *Adv. Colloid Interface Sci.* **52** 79–143
[29] Martínez F L, Toledano-Luque M, Gandía J J, Cárabe J, Bohne W, Röhrich J, Strub E and Mártil I 2007 Optical properties and structure of HfO_2 thin films grown by high pressure reactive sputtering *J. Phys. D: Appl. Phys.* **40** 5256
[30] Jiang J, Wang Z, Zhang H, Zhang X, Liu X and Wang S 2011 Monoclonal antibody-based ELISA and colloidal gold immunoassay for detecting 19-nortestosterone residue in animal tissues *J. Agric. Food Chem.* **59** 9763–9

Q1